

FINAL REPORT

**EXPERIMENTAL EVALUATION OF  
FULL DEPTH  
PRECAST/PRESTRESSED CONCRETE  
BRIDGE DECK PANELS**

**Project IB-H1, FY 98**

Report No. ITRC FR 98-5

Prepared by

Mohsen Issa, Ph.D., P.E., S.E.  
Department of Civil and Materials Engineering  
University of Illinois at Chicago  
Chicago, Illinois

February 2002

**Illinois Transportation Research Center**  
Illinois Department of Transportation

# **ILLINOIS TRANSPORTATION RESEARCH CENTER**

This research project was sponsored by the State of Illinois, acting by and through its Department of Transportation, according to the terms of the Memorandum of Understanding established with the Illinois Transportation Research Center. The Illinois Transportation Research Center is a joint Public-Private-University cooperative transportation research unit underwritten by the Illinois Department of Transportation. The purpose of the Center is the conduct of research in all modes of transportation to provide the knowledge and technology base to improve the capacity to meet the present and future mobility needs of individuals, industry and commerce of the State of Illinois.

Research reports are published throughout the year as research projects are completed. The contents of these reports reflect the views of the authors who are responsible for the facts and the accuracy of the data presented herein. The contents do not necessarily reflect the official views or policies of the Illinois Transportation Research Center or the Illinois Department of Transportation. This report does not constitute a standard, specification, or regulation.

Neither the United States Government nor the State of Illinois endorses products or manufacturers. Trade or manufacturers' names appear in the reports solely because they are considered essential to the object of the reports.

## **Illinois Transportation Research Center Members**

**Bradley University**  
**DePaul University**  
**Eastern Illinois University**  
**Illinois Department of Transportation**  
**Illinois Institute of Technology**  
**Lewis University**  
**Northern Illinois University**  
**Northwestern University**  
**Southern Illinois University Carbondale**  
**Southern Illinois University Edwardsville**  
**University of Illinois at Chicago**  
**University of Illinois at Urbana-Champaign**  
**Western Illinois University**

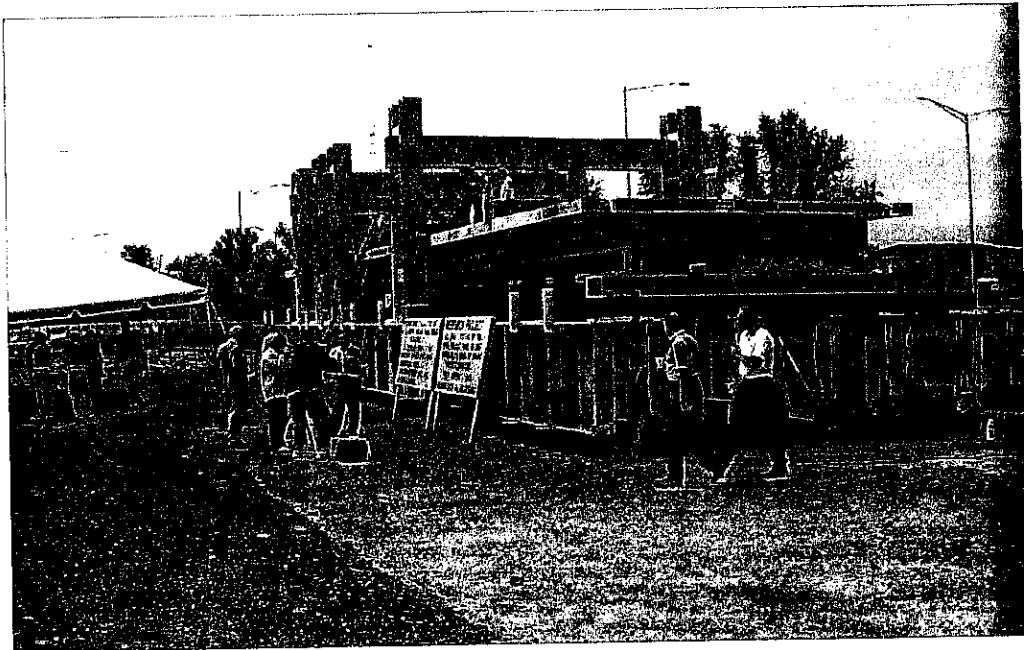
Reports may be obtained by writing to the administrative offices of the Illinois Transportation Research Center at Southern Illinois University Edwardsville, Campus Box 1803, Edwardsville, IL 62026 [telephone (618) 650-2972], or you may contact the Engineer of Physical Research, Illinois Department of Transportation, at (217) 782-6732.

<b>1. Report No.</b> ITRC FR 98-5	<b>2. Government Accession No.</b>	<b>3. Recipient's Catalog No.</b>	
<b>4. Title and Subtitle</b> Experimental Evaluation of Full Depth Precast/Prestressed Concrete Bridge Deck Panels		<b>5. Report Date</b> February 2002	<b>6. Performing Organization Code</b>
<b>7. Author(s)</b> Mohsen Issa, Ph.D., P.E., S.E.		<b>8. Performing Organization Report No.</b>	
<b>9. Performing Organization Name and Address</b> University of Illinois at Chicago Department of Civil and Materials Engineering 2095 Engineering Research Facility, M/C 246 842 West Taylor Street Chicago, IL 60607		<b>10. Work Unit No. (TRAVIS)</b>	
<b>12. Sponsoring Agency Name and Address</b> Illinois Transportation Research Center, Administrative Office, Southern Illinois University at Edwardsville Engineering Building, Room 3026, Edwardsville, IL 62026		<b>11. Contract or Grant No.</b> IB-H1, FY 98	<b>13. Type of Report and Period Covered</b> Final Report July 1998 through October 2001
<b>15. Supplementary Notes</b>			
<b>16. Abstract</b> A literature review concerning the objectives of the project was completed. A significant number of published papers, reports, etc. were examined to determine the effectiveness of full depth precast panels for bridge deck replacement. A detailed description of the experimental methodology was developed which includes design and fabrication of the panels and assembly of the bridge. The design and construction process was carried out in cooperation with the project Technical Review Panel. The major components of the bridge deck system were investigated. This includes the transverse joints and the different materials within the joint as well as composite action. The materials investigated within the joint were polymer concrete, non-shrink grout, and set-45 for the transverse joint. The transverse joints were subjected to direct shear tests, direct tension tests, and flexure tests. These tests exhibited the excellent behavior of the system in terms of strength and failure modes. Shear key tests were also conducted. The shear connection study focused on investigating the composite behavior of the system based on varying the number of shear studs within a respective pocket as well as varying the number of pockets within a respective panel. The results indicated that this shear connection is extremely efficient in rendering the system under full composite action. Finite element analysis was conducted to determine the behavior of the shear connection prior to initiation of the actual full scale tests. In addition, finite element analysis was also performed with respect to the transverse joint tests in an effort to determine the behavior of the joints prior to actual testing. The most significant phase of the project was testing a full-scale model. The bridge was assembled in accordance with the procedures developed as part of the study on full-depth precast panels and the results obtained through this research. The system proved its effectiveness in withstanding the applied loading that exceeded eight (8) times the truck loading in addition to the maximum negative and positive moment application. Only hairline cracking was observed in the deck at the maximum applied load. Of most significance was the fact that full composite action was achieved between the precast panels and the steel supporting system, and the exceptional performance of the transverse joint between adjacent panels.			
<b>17. Key Words</b> Full Depth, transverse joints, composite action, joint materials, post-tensioned, shear studs, truck loading		<b>18. Distribution Statement</b> No restrictions. This document is available to the public through the National Technical Information Service (NTIS), Springfield, Virginia 22161.	
<b>19. Security Classification (of this report)</b> Unclassified	<b>20. Security Classification (of this page)</b> Unclassified	<b>21. No. of Pages</b> 265	<b>22. Price</b>

**FINAL REPORT**

**EXPERIMENTAL EVALUATION OF FULL DEPTH  
PRECAST/PRESTRESSED CONCRETE  
BRIDGE DECK PANELS**

**Project IB-H1, FY 98**



**Prepared by**

**Mohsen A. Issa, Ph.D., P.E., S.E.  
Professor of Civil Engineering  
Department of Civil and Materials Engineering  
University of Illinois at Chicago  
Chicago, Illinois**

**February 2002**

**Illinois Transportation Research Center**

## **DISCLAIMER**

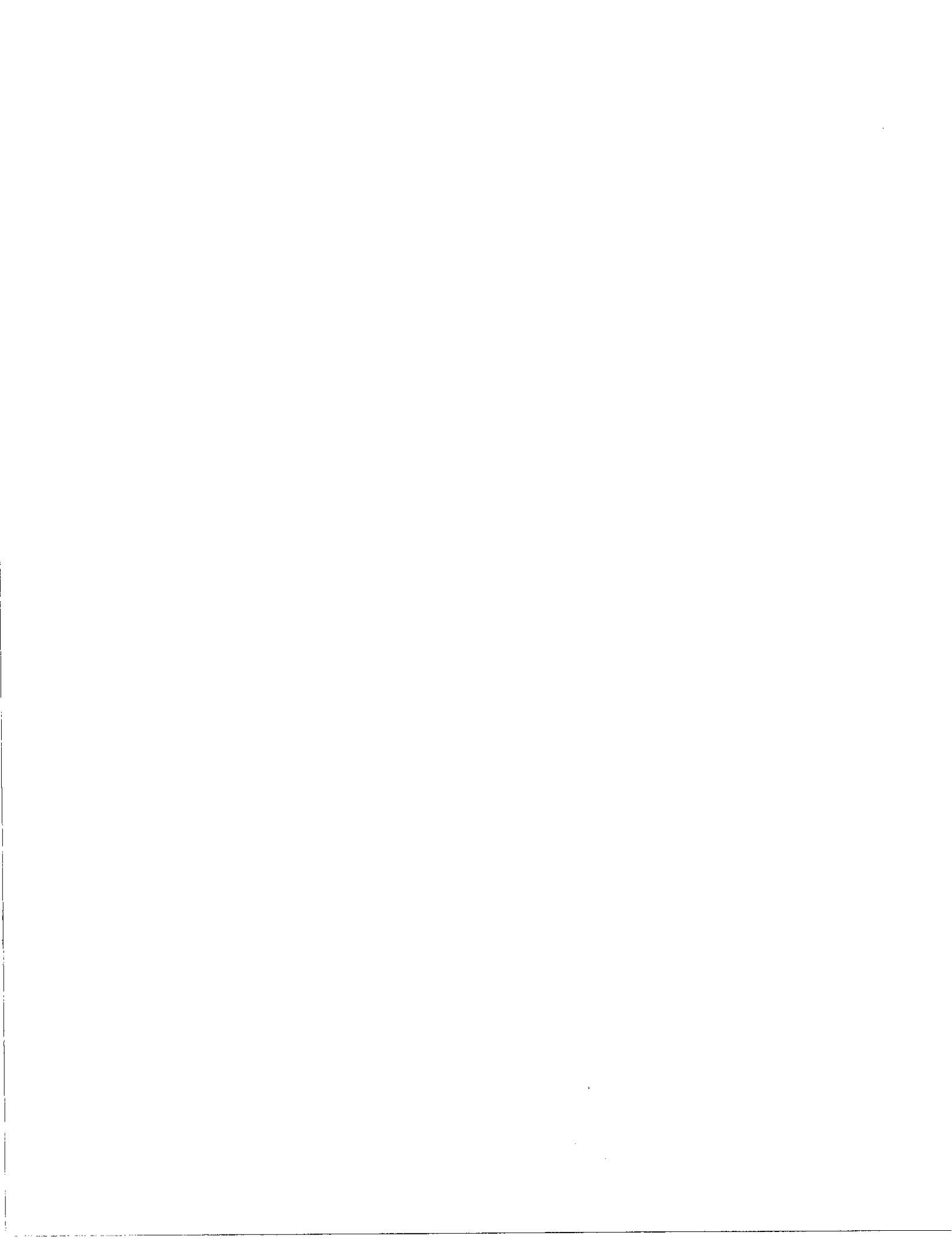
This document is disseminated under the sponsorship of the Illinois Department of Transportation in the interest of information exchange. Neither the United States Government nor the State of Illinois assumes liability for its contents or use thereof. The contents of this report reflect the views of the authors who are responsible for the facts and the accuracy of the data presented herein. The contents do not necessarily reflect the policy of the Department of Transportation or the Illinois Department of Transportation. This report does not constitute a standard, specification, or regulation. Neither the United States Government nor the State of Illinois endorses products or manufacturers. Trade or manufacturers' names appear herein only because they are considered essential to the objective of this document.

## CONVERSION FACTORS, US CUSTOMARY TO METRIC UNITS

<b>Multiply</b>	<b>by</b>	<b>to obtain</b>
in.	25.4	mm
ft	0.3048	m
in. <sup>2</sup>	645	mm <sup>2</sup>
yd <sup>3</sup>	0.765	m <sup>3</sup>
pound (lb)	4.448	newtons (N)
kip (1000 lb)	4.448	kilo newtons (kN)
kip/ft	14.59	kN/m
psi	0.0069	MPa
ksi	6.895	MPa
ft-kip	1.356	kN m
in.-kip	0.113	kN m

## PREFACE

This study is funded by a contract awarded to the University of Illinois at Chicago (UIC) by the Illinois Transportation Research Center (ITRC) and the Illinois Department of Transportation (IDOT). Their financial support is gratefully acknowledged. Thanks are due to the members of the Technical Review Panel. Thanks are due to Master Builders for providing all the grouting materials for the transverse joints and the shear pockets. Thanks are also due to Dywidag-Systems International USA, Inc. (DSI) for providing the prestressing steel, anchorage system, jacking system, and the grouting pump. Thanks are due to Industrial Steel for providing most of the needed steel sections for the project. Furthermore, the continuous support of Steven Hanna, ITRC Center Administrator is acknowledged. Thanks are due to Alfred Yousif, Mahmoud Issa, Moussa Issa, Mohamed El-Metwally, Visiting Professor, Md. Shahidul Islam and graduate students Thomas Patton, Cyro Luiz Ribeiro do Valle, Adugna Fanuel, Hiba Abdalla, and Mohamad Faraj for their valuable contributions.



## PROJECT SUMMARY

A literature review concerning the objectives of the project was completed. A significant number of published papers, reports, etc. were examined to determine the effectiveness of full depth precast panels for bridge deck replacement. This review included published and unpublished reports, ILDOT final report conducted here at the University of Illinois at Chicago "Structural Behavior of Full Depth Precast Prestressed Concrete Bridge Deck Replacement" and the NCHRP final report "Rapid Replacement Bridge Decks".

A detailed description of the experimental methodology was developed which includes design and fabrication of the panels and assembly of the bridge. The design and construction process was carried out in cooperation with the project Technical Review Panel. The major components of the bridge deck system were investigated. This includes the transverse joints and the different materials within the joint as well as composite action. The materials investigated within the joint were polymer concrete, non-shrink grout, and set-45 for the transverse joint. The transverse joints were subjected to direct shear tests, direct tension tests, and flexure tests. These tests exhibited the excellent behavior of the system in terms of strength and failure modes. Shear key tests were also conducted. These shear connection study focused at investigating the composite behavior of the system based on varying the number of shear studs within a respective pocket as well as varying the number of pockets within a respective panel. The results indicated that this shear connection is extremely efficient in rendering the system under full composite action.

Finite element analysis was conducted to determine the behavior of the shear connection prior to initiation of the actual full scale tests. In addition, finite element analysis was also performed with respect to the transverse joint tests in an effort to determine the behavior of the joints prior to the actual tests. Non-linear finite element analysis of the full-scale model was also conducted. The final report includes comparisons to experimental work pertaining to the load-deflection behavior for each load case, i.e., maximum positive and negative service loading, overloads, and ultimate loading.

The most significant phase of the project is testing of the full-scale bridge in Biesterfield (Elk Grove), Illinois. The bridge was assembled in accordance with the procedure developed as part of the earlier study on full-depth precast panels and the results obtained through this research. The system proved its effectiveness in withstanding the applied loading that exceeded 8 times truck loading in addition to the maximum negative and positive moment application. Only hairline cracking was observed in the deck at the maximum loading applied. Of most

significance, was the fact that full composite action was achieved between the precast panels and the steel supporting system, and the exceptional performance of the transverse joint between adjacent precast panels.

## TABLE OF CONTENTS

<u>CHAPTER</u>	<u>PAGE</u>
<b>1. INTRODUCTION.....</b>	<b>1</b>
1.1 General.....	1
1.2 Objective and scope of Study .....	3
<b>2. LITERATURE REVIEW .....</b>	<b>5</b>
2.1 Early Research .....	5
2.2 Selected Applications.....	7
2.2.1 State of Illinois.....	7
2.2.2 Connecticut Department of Transportation .....	8
2.2.3 Commonwealth of Virginia Department of Transportation.....	9
2.2.4 Maryland Department of Transportation .....	10
2.2.5 Maryland Transportation Authority .....	11
2.2.6 Iowa Department of Transportation.....	11
2.2.7 California Department of Transportation.....	12
2.2.8 New York State Thruway Authority (NYSTA).....	13
2.2.9 New York State Department of Transportation (NYSDOT).....	15
2.2.10 Alaska Department of Transportation and Public Facilities .....	17
2.2.11 Ohio Department of Transportation.....	18
2.2.12 Pennsylvania Turnpike Commission .....	19
2.2.13 State of Maine Department of Transportation .....	20
2.2.14 Massachusetts Turnpike Authority .....	21
2.2.15 Texas Department of Highways and Public Transportation .....	21
2.2.16 Ministry of Transportation of Ontario, Canada .....	22
2.3 Recent Research.....	23
2.4 Shear Connection Test .....	28
<b>3. FINITE ELEMENT ANALYSIS .....</b>	<b>37</b>
3.1 Push-Out Specimens .....	37
3.1.1 Elastic Finite Element Analysis .....	37
3.1.2 Non-Linear Finite Element Analysis .....	39
3.2 Direct Shear Test.....	42
3.3 Finite Element Analyses of Full-Depth Bridge Deck System .....	43
3.3.1 Geometry of the Prototype Model .....	43
3.3.2 Static Analysis Procedure .....	49
<b>4. EXPERIMENTAL PROGRAM.....</b>	<b>54</b>
4.1 Shear Connection Tests.....	63
4.1.1 Quarter-Scale Shear Connection Tests .....	63
4.1.1.1 Specimen Description and Material Properties.....	65
4.1.1.2 Test Setup.....	70
4.1.1.3 Push-out Test Procedure .....	71
4.1.2 Full-Scale Shear Connection Tests .....	73

## TABLE OF CONTENTS (Continued)

<u>CHAPTER</u>	<u>PAGE</u>
4.1.2.1 Specimen Description and Material Properties.....	73
4.1.2.2 Full-Scale Push-out (Shear Connection) Test Setup and Procedure.....	81
4.2 Transverse Joint Tests.....	83
4.2.1 Set 45 and Set 45 Hot Weather.....	84
4.2.1.1 Mixing and Placing Procedure.....	84
4.2.2 Set Grout.....	84
4.2.2.1 Mixing and Placing Procedure.....	85
4.2.3 Polymer Concrete.....	85
4.2.3.1 Mixing and Placing Procedure.....	85
4.3 Direct Shear Test.....	86
4.4 Direct Tension Test.....	89
4.5 Flexural Testing.....	91
<b>5. TEST RESULTS.....</b>	<b>92</b>
5.1 Test Results for Quarter-Scale Shear Connection.....	92
5.2 Test Results for Full-Scale Shear Connection.....	118
5.3 Correlation between Quarter-Scale and Full-Scale Shear Connection Testing.....	131
5.4 Comparison of Experimental and Finite Element Analysis Results for Push-Out Test.....	133
5.5 Test Results for Transverse Joint.....	136
5.5.1 Direct Shear Results.....	136
5.5.2 Direct Tension Results.....	138
5.5.3 Flexural Results.....	141
5.5.4 Strength, Permeability and Shrinkage Measurement.....	144
5.6 Comparison of Material Behavior in Transverse Joints.....	147
5.7 Comparison of Finite Element Analysis.....	147
<b>6. FULL-SCALE BRIDGE TESTING.....</b>	<b>151</b>
6.1 Description of Full-Scale Bridge.....	151
6.2 Construction Procedure.....	151
6.2.1 Panel Fabrication.....	152
6.2.2 Casting and Curing of Panels.....	153
6.2.3 Abutment.....	153
6.3 Bridge Assembly.....	165
6.3.1 Preparation of Testing Bed.....	165
6.3.2 Panel Preparation.....	165
6.3.3 Placement of Panels.....	165
6.3.4 Forming for Transverse Joints.....	165
6.3.5 Placement of Longitudinal Post-Tensioning Strands and Bars.....	166
6.3.6 Grouting of the Transverse Joints.....	166
6.3.7 Post-Tensioning of Strands and Dywidag Bars.....	166

## TABLE OF CONTENTS (Continued)

<u>CHAPTER</u>	<u>PAGE</u>
6.3.8 Installation of Shear Studs .....	168
6.3.9 Grouting of Shear Pockets and Haunches.....	168
6.3.10 Grouting of Longitudinal Ducts.....	168
6.4 Bridge Testing.....	188
6.4.1 Testing Setup .....	188
6.4.1.1 Loading Frame .....	188
6.4.1.2 Truck Load Simulation .....	188
6.4.1.3 Instrumentation of Bridge .....	189
6.4.1.4 Data Recording .....	189
6.4.2 Load Tests.....	189
6.4.2.1 Service Load Tests.....	190
6.4.2.2 Overload Tests .....	191
6.4.2.3 Ultimate Load Tests.....	191
<b>7. TEST RESULTS OF FULL-SCALE BRIDGE .....</b>	<b>206</b>
7.1 Introduction.....	206
7.2 Test Results.....	206
7.2.1 Service Loads.....	206
7.2.1.1 Maximum Negative Service Load Test .....	206
7.2.1.2 Maximum Positive Service Load Test.....	206
7.2.2 Overloads .....	207
7.2.2.1 Maximum Positive Over Load Test.....	207
7.2.2.2 Maximum Negative Over Load Test .....	207
7.2.3 Ultimate Positive Load Test.....	208
7.2.4 Ultimate Negative Load Test.....	208
<b>8. SPECIFICATIONS FOR PRECAST CONCRETE BRIDGE DECK PANELS.....</b>	<b>229</b>
8.1 Introduction.....	229
<b>9. CONCLUSIONS .....</b>	<b>237</b>
<b>REFERENCES.....</b>	<b>240</b>



## LIST OF TABLES

<u>TABLE</u>		<u>PAGE</u>
4.1	Quarter scale shear connection test configuration .....	55
4.2	Full scale shear connection test configuration .....	56
4.3	Transverse joint test specimen configuration .....	56
4.4	Aggregate gradation for model concrete.....	66
4.5	Mix proportions of concrete for quarter-scale specimens.....	66
4.6	Specimen designation .....	70
4.7	Mix proportions .....	76
4.8	Full-scale specimen designation .....	81
5.1	Test results for quarter-scale specimens .....	94
5.2	Full-scale test results.....	130
5.3	Test results (¼-scale vs full-scale).....	132
5.4	Full-scale test results and predictions .....	133
5.5	Comparison of experimental and finite element analysis results.....	134
5.6	Direct shear test results .....	138
5.7	Direct tension test results .....	141
5.8	Flexural test results .....	143
5.9	Strength development of grouting material .....	145
5.10	Coulomb permeability test results .....	145
6.1	Mix proportions of concrete for full-scale bridge deck panels.....	154



## LIST OF FIGURES

<u>FIGURE</u>		<u>PAGE</u>
2.1	Quarter-scale HS20 truck loading beams .....	33
2.2	Test setup .....	33
2.3	Vibrating wire strain gages .....	34
2.4	Placement of panels .....	34
2.5	Deflected bridge.....	36
2.6	Crack in beam at central support .....	36
3.1	Mesh generation for single pocket configuration .....	38
3.2	Mesh generation for double pocket configuration .....	38
3.3	Typical finite element mesh for pushout test model with one pocket .....	41
3.4	Typical finite element mesh for pushout test model with two pockets.....	41
3.5	Finite element mesh and boundary conditions.....	42
3.6	SOLID65 (3-D reinforced concrete solid) .....	45
3.7	SOLID45 (3-D solid) .....	46
3.8	BEAM188 (3-D line element) .....	47
3.9	LINK10 (Tension-only or compression-only spar) .....	48
3.10	LINK8 (3-D Spar) .....	49
3.11	Finite element meshing of the full-depth deck system .....	50
3.12	Steel beams and precast deck meshing .....	51
3.13	Grouted shear key meshing.....	51
3.14	Loading arrangement for positive service loading.....	52
3.15	Top strain distribution due to positive service loading .....	52
3.16	Bottom strain distribution due to positive service loading .....	52

## LIST OF FIGURES (Continued)

<u>FIGURE</u>		<u>PAGE</u>
3.17	Loading arrangement for negative service loading.....	53
3.18	Top strain distribution due to negative service loading .....	53
3.19	Bottom strain distribution due to negative service loading .....	53
4.1	Typical two-span continuous prototype bridge on steel girders .....	57
4.2	Typical layout of precast slab on steel girders.....	57
4.3	Typical cross section for slab on steel stringers.....	58
4.4	Plan and section views of a typical precast panel.....	58
4.5	Shear stud pocket connector details.....	59
4.6	Typical female to female type joint between precast panels .....	59
4.7	Test setup for shear connection.....	60
4.8	Precast panel forming for shear connection test .....	60
4.9	Typical test setups for transverse joints .....	61
4.10	Precast panel forming for transverse joint tests .....	62
4.11	Stud configurations .....	63
4.12	Beam specimens with different stud configurations.....	64
4.13	Beam specimens used in push-out testing program.....	64
4.14	Specimen configuration for push-out test.....	67
4.15	Steel wire mesh, 25 x 25 mm.....	67
4.16	Pocket pouring .....	68
4.17	Pocket curing .....	69
4.18	Push-out specimens with different number of pockets.....	69
4.19	Slip instrumentation for one-pocket specimen .....	71
4.20	Slip instrumentation for two-pocket specimen .....	72
4.21	Uplift measurements in specimen with one pocket .....	73

## LIST OF FIGURES (Continued)

<u>FIGURE</u>	<u>PAGE</u>
4.22 Forming of the one-pocket precast panel.....	75
4.23 Forming of the two-pocket precast panel.....	75
4.24 Casting of precast panels for full-scale shear connection test .....	76
4.25 Full-scale panel configuration for one-pocket specimen .....	77
4.26 Full-scale panel configuration for two-pocket specimen.....	78
4.27 Steel forming used to create haunch .....	80
4.28 Curing of shear pocket after set grout casting .....	80
4.29 Test setup for full-scale shear connection specimen (two pockets).....	82
4.30 Typical female to female type joint between precast panels .....	83
4.31 Direct shear test specimen with sandblasted surface .....	87
4.32 First direct shear test model .....	87
4.33 New specimen wrapped with carbon fiber for direct shear test.....	88
4.34 Direct tensile test specimen with sandblasted surface .....	89
4.35 Direct tension test setup .....	90
4.36 Specimen configuration for flexural testing .....	91
5.1 Mode of failure for QS1P1S .....	93
5.2 Mode of failure for QS1P2S .....	93
5.3 Load-slip curves for specimen with 1 shear pocket and 1 stud per pocket.....	100
5.4 Load-slip curves for specimen with 1 shear pocket and 2 studs per pocket.....	101
5.5 Load-slip curves for specimen with 1 shear pocket and 3 studs per pocket.....	102
5.6 Load-slip curves for specimen with 1 shear pocket and 4 studs per pocket.....	103
5.7 Load-slip curves for specimen with 2 shear pockets and 1 stud per pocket.....	104
5.8 Load-slip curves for specimen with 2 shear pockets and 2 studs per pocket.....	105
5.9 Load-slip curves for specimen with 2 shear pockets and 3 studs per pocket.....	106

## LIST OF FIGURES (Continued)

<u>FIGURE</u>	<u>PAGE</u>
5.10 Load-slip curves for specimen with 2 shear pockets and 4 studs per pocket.....	107
5.11 Load-slip curves for specimen with 3 shear pockets and 1 stud per pocket.....	108
5.12 Load-slip curves for specimen with 3 shear pockets and 2 studs per pocket.....	109
5.13 Load-slip curves for specimen with 4 shear pockets and 1 stud per pocket.....	110
5.14 Load-slip curves for specimen with 4 shear pockets and 2 studs per pocket.....	111
5.15 Load-slip curves for specimen with one pocket .....	112
5.16 Load-slip curves for specimen with two pockets.....	113
5.17 Load-slip curves for specimen with three pockets.....	114
5.18 Load-slip curves for specimen with four pockets .....	115
5.19 Ultimate load versus number of studs.....	116
5.20 Ultimate load versus number of pockets.....	117
5.21 Mode of failure for typical full-scale shear connection specimen.....	120
5.22 Shearing of studs and the grouting material in typical full-scale specimen.. .....	120
5.23 Load-slip behavior for one pocket specimen and two studs per pocket .....	121
5.24 Load-slip behavior for one pocket specimen and three studs per pocket .....	122
5.25 Load-slip behavior for one pocket specimen and four studs per pocket.....	123
5.26 Load-slip behavior for two pocket specimen and two studs per pocket .....	124
5.27 Load-slip behavior for two pocket specimen and three studs per pocket .....	125
5.28 Load-slip behavior for one pocket, various number of studs.....	126
5.29 Load-slip behavior for two pockets, various number of studs.....	127
5.30 Load-slip behavior for two studs, various number of pockets.....	128
5.31 Load-slip behavior for three studs, various number of pockets.....	129
5.32 Stress intensity distribution in a typical haunch of quarter-scale specimen .....	134
5.33 Comparison of experimental and FEM results for a typical quarter-scale specimen.....	135

## LIST OF FIGURES (Continued)

<u>FIGURE</u>	<u>PAGE</u>
5.34 Failure in polymer concrete specimen .....	137
5.35 Failure mode in set grout direct tension specimen.....	139
5.36 Failure mode in set 45 direct tension specimen.....	140
5.37 Failure mode in polymer concrete direct tension specimen.....	140
5.38 Failure mode in set grout flexural specimen.....	142
5.39 Failure mode in set 45 flexural specimen .....	142
5.40 Failure mode in polymer concrete flexural specimen.....	143
5.41 Shrinkage test results of joint materials .....	146
5.42 Crack pattern in polymer concrete model.....	148
5.43 Shear stress distribution in polymer concrete .....	149
5.44 Crack pattern in set grout model.....	149
5.45 Shear stress distribution in set grout.....	150
5.46 Shear stress distribution in set 45.....	150
6.1 Plan and cross section of the prototype bridge .....	155
6.2 Forming of typical precast panel.....	156
6.3 Typical layout of steel reinforcement in full-scale panel.....	157
6.4 Arrangements of Dywidag bars and strands in full-scale bridge.....	158
6.5 Post-tensioning duct configuration .....	159
6.6 Leveling screw configuration .....	159
6.7 Instrumentation for precast panel .....	160
6.8 Instrumentation for precast panel.....	160
6.9 Typical panel after forming and instrumentation .....	161
6.10 Finished precast concrete panel .....	161
6.11 Unloading of cured precast concrete panels in the field .....	162

## LIST OF FIGURES (Continued)

<u>FIGURE</u>		<u>PAGE</u>
6.12	Set of cured precast concrete panels .....	162
6.13	Abutment arrangement .....	163
6.14	Reinforcement details of abutment .....	164
6.15	Assembly of testing bed .....	169
6.16	Placement of precast panels .....	170
6.17	Placement of precast panels .....	170
6.18	Transverse joint configuration .....	171
6.19	Forming of transverse joints .....	172
6.20	Forming of transverse joints .....	172
6.21	Curing of transverse joints .....	173
6.22	Grouted transverse joints .....	173
6.23	Post-tensioning details .....	174
6.24	Arrangement of Dywidag bars prior to post-tensioning .....	175
6.25	Strain gages mounted on prestressing steel and placed inside concrete deck.....	176
6.26	Post-tensioning of Dywidag bars .....	177
6.27	End plates of post-tensioned Dywidag bars.....	177
6.28	Load-strain calibration curve for Post-tensioned Dywidag bars.....	178
6.29	Block-out for coupling of Dywidag bars .....	179
6.30	Coupling of Dywidag bars .....	179
6.31	Instrumentation of prestressing strands .....	180
6.32	Post-tensioning sequence for strands .....	180
6.33	Post-tensioned panels.....	181
6.34	Load-strain calibration curve for prestressing strands .....	182
6.35	Cleaning of flange tops for stud welding .....	183

## LIST OF FIGURES (Continued)

<u>FIGURE</u>	<u>PAGE</u>
6.36 Layout of shear studs in pockets .....	183
6.37 Stud welding .....	184
6.38 Close-up view of shear pocket with welded stud.....	184
6.39 Forming of haunches and shear pockets .....	185
6.40 Grouting of shear pockets .....	185
6.41 Finished pockets.....	186
6.42 Haunch after grouting .....	186
6.43 Overview of assembled bridge.....	187
6.44 Overview of assembled bridge.....	187
6.45 Beam-column connection of the loading frame.....	192
6.46 Elevation view of the loading frame .....	192
6.47 Test Setup.....	193
6.48 Simulated AASHTO truck loading.....	194
6.49 Simulated single axle .....	195
6.50 Close-up view of hydraulic cylinder.....	195
6.51 Spread beams used to distribute the load at contact points.....	196
6.52 Layout of electrical resistance strain gauges and vibrating wire strain gages on concrete bridge deck (top and bottom surface).....	197
6.53 Strain gages across the depth of the steel beam.....	198
6.54 LVDT used to measure the deflection of the steel beams and deck .....	199
6.55 Slippage measurement .....	200
6.56 Layout of LVDT's for deflection and slip measurement in full-scale bridge.....	201
6.57 CMOD gage to measure the concrete strain over middle support and transverse joint.....	202
6.58 Data acquisition system used in collecting data .....	203

## LIST OF FIGURES (Continued)

<u>FIGURE</u>	<u>PAGE</u>
6.59 Overall view of the loading arrangement for maximum positive moment.....	204
6.60 Overall view of the loading arrangement for maximum negative moment.....	205
7.1 Location of top and bottom concrete strain gages .....	210
7.2 Location of steel strain gages .....	211
7.3 Location of LVDTs for deflection and slippage measurement .....	212
7.4 Load-deflection response at 14 ft from middle support for service negative Loading .....	213
7.5 Load-slippage response of the composite section for service negative loading ..	213
7.6 Load-strain response of central steel beam (bottom) for service negative loading	214
7.7 Load-deflection response at 0.4L from left support for service positive loading .	214
7.8 Load-slippage response of composite section for service positive loading .....	215
7.9 Load-strain response of central steel beam (bottom) for service positive loading	215
7.10 Variation of strain along depth of composite section for positive service loading	216
7.11 Load-deflection response at 0.4L from left support for positive overloading ....	216
7.12 Load-slippage response of composite section for positive overloading .....	217
7.13 Load-strain response of central steel beam (bottom) for positive overloading ...	217
7.14 Variation of strain along depth of composite section for positive overloading ...	218
7.15 Cracks underneath deck during positive overloading .....	218
7.16 Load-deflection response at 14 ft from middle support for negative overloading	219
7.17 Load-slippage response of composite section for negative overloading .....	219
7.18 Load-strain response of central steel beam (bottom) for negative overloading ...	220
7.19 Load-deflection response at 0.4L from left support for ultimate positive loading	220

## LIST OF FIGURES (Continued)

<u>FIGURE</u>	<u>PAGE</u>
7.20 Load-slippage response of composite section for ultimate positive loading .....	221
7.21 Load-strain response of central steel beam (bottom) for ultimate positive loading	221
7.22 Load-strain response of concrete at 0.4L from left support for ultimate positive loading .....	222
7.23 Variation of strain along depth of composite section for ultimate positive loading	222
7.24 Close-up view of hairline cracking at haunch at 386 kips load for positive bending	223
7.25 Cracking of bottom deck at ultimate positive loading .....	223
7.26 Uplift of steel beam due to positive bending of other span .....	224
7.27 Close-up view of steel beam deflection for ultimate positive bending .....	224
7.28 Comparison of deflections for positive loading at different load levels .....	225
7.29 Load-deflection response at 14 ft from middle support for ultimate negative Loading .....	225
7.30 Load-slippage response of composite section for ultimate negative loading .....	226
7.31 Load-strain response of central steel beam (bottom) for ultimate negative loading	226
7.32 Load-strain response of concrete at critical locations for ultimate negative loading	227
7.33 Opening of transverse joint near central support during ultimate negative loading	227
7.34 Cracks at bottom of deck at 14 ft from central support at load of 552 kips during negative bending .....	228
7.35 Measuring of crack width after ultimate negative loading .....	228
8.1 Typical layout of precast slab on steel stringers .....	229
8.2 Leveling device .....	230
8.3 Typical transverse joint .....	231
8.4 Sequence of post-tensioning .....	234

**LIST OF FIGURES (Continued)**

<u>FIGURE</u>		<u>PAGE</u>
8.5	Shear stud breakout details .....	235

# 1. INTRODUCTION

## 1.1 General

The scope of this research is to investigate the structural behavior of full-depth precast prestressed concrete bridge deck panels under static loading. The investigation entails a detailed evaluation of system components, particularly the joints between adjacent precast panels as well as the connection between the slab and its supporting system, and adequacy of prestressing force provided to secure the tightness of the transverse joints. This investigation will also encompass the materials included within such as grout and shear stud connectors. The proposed system provides a very effective and economic design concept, and can be implemented for the rehabilitation of existing highway bridges as well as new bridge construction in order to shorten the time of reconstruction and bridge closures, and to minimize interference with traffic flow.

This system combines high strength tendons and good quality concrete to produce durable deck panels that are effective in aggressive environments. The panels are connected to the steel stringers through shear pockets to provide composite action. The deck panels can either be precast or precast prestressed, and post-tensioned in the longitudinal direction to provide continuity and secure tightness in the joints between adjacent precast elements. In this type of construction, the entire bridge deck is of precast concrete to enable the rapid replacement of deteriorated decks, and render the rehabilitation process extremely cost effective. There is no additional field cast-in-place concrete acting structurally, except that used in the connections and slab closures.

The objective of the experimental phase of the study is to test the proposed full scale bridge; two-span continuous with full-depth precast panels installed on steel girders including fabrication, instrumentation and testing for service, and ultimate loads; analysis of the experimental data; linear and non-linear finite element analysis; and provide ultimate design and construction recommendations on the full depth precast deck system. Full scale laboratory testing of the proposed shear connection was conducted to assure the effectiveness of the slab-to-beam connections. The dimensions and details of all the structural elements are based on the

selected prototype bridge. The precast panels were fabricated and instrumented using all the necessary materials.

The complete erection and installation of the bridge was performed including erection of the supporting system in its final position under the testing machine. The bridge was assembled in accordance with the construction procedure established in the previous study (Issa et al. 1995a,b,c,d, 1998, 2000). Recently, an experimental program was carried out on three quarter-scale bridge models of composite construction to predict the actual structural behavior of the system for the same prototype bridge. Design of the models was directly obtained from the present continuous two-span prototype bridge by using scale factors that comply with geometric similitude so that the test results can be used to determine the corresponding quantities in the prototype bridge. The model bridge length was 6.2 m (20.5 ft). The first model was not post-tensioned, while the second and third bridge models were post-tensioned using a direct prestress level of 1379 and 2758 kPa (200 and 400 psi), respectively. The main objective in testing the  $\frac{1}{4}$  scale bridge models was to determine the optimum amount of post-tensioning needed to secure the tightness of the joints and render them in compression. As expected, first cracking was observed at the transverse joint in the vicinity of the central support. The results obtained from the three bridge models will serve as an indication in the behavior of the joints, shear pockets, materials used, and the amount of post-tensioning necessary for the proposed full scale testing.

To assess the structural performance of the proposed deck, the bridge will be instrumented to monitor; applied loads and reactions, deflections, end rotations, strain changes on concrete and steel, detection and measurement of cracks, performance of the joints between precast panels, and relative displacement (slippage) between the supporting system and precast deck. The variables affecting the adverse conditions will be weighed in terms of magnitude and impact on the structure in an effort to confirm the source of the problems. The results of the laboratory study will be compared to the analytical study as well as the recent  $\frac{1}{4}$ -scale bridge model testing in order to validate the major factors influencing the design and construction of the proposed system. Finite element modeling procedures will be developed for the structure mentioned earlier in order to predict the stress level and distribution in the concrete. As a result

of completing the analytical and experimental phases of the project, a recommendation plan will be provided for implementing the construction design specifications and procedures.

In the past, structural beams needed enough contact area to provide the necessary friction between the steel and concrete slab for complete interaction. With the advent of shear connectors, the area that is necessary to transmit the shear loads to both materials was reduced, making composite design economically attractive. Composite systems permit savings of steel up to 20%. The push-out test has been performed countless times since the early 1950's to measure composite action in cast-in-place concrete slabs. This test is a non-standard method for measuring the strength of shear-connectors. Therefore, many versions of the push-out test exist in which certain parameters are varied, all of which yield different results. Some of the parameters of the push-out test that influence the results include: (1) different construction systems adopted in different regions of the United States, (2) types of shear connectors used, and (3) placement of the test instrumentation and respective range of precision. Shear connectors are important since they provide connections and points of interaction between the steel beams and the concrete slab. The goal is to have the neutral axes for both materials coincident so that the combination of the concrete slab with the steel beam act as a single composite material.

The keyway joint is the structural element of a bridge that connects the ends of precast concrete units. The joint is subjected to several types of loads during bridge life such as flexure, tension and shear. The results of these events generate cracks that allow infiltration of water that is an important factor in steel corrosion. The materials that filled the joints and conditions at time of casting were variables in this study. The selected materials to fill the joints were set 45, hot weather set 45, set grout, and polymer concrete. The qualities for each material and their limitation are reported in this study.

## **1.2 Objectives and Scope of Study**

The structural performance of the most critical components of full depth precast concrete bridge deck systems under static loading conditions is the focus of the proposed research. Particularly, this research aims at investigating the joints between adjacent precast panels as well

as the connection between the slab and its supporting system (shear pockets), and determining the adequacy of prestressing force provided to secure the tightness of the transverse joints. As revealed from the previous study (Issa et al. 1995d), it is essential to examine the performance of these joints and connections and the materials included within such as grout and shear stud connectors. The investigation of problems such as cracking, stiffness degradation, and deterioration is vital in order to conclude what part of the system is not appropriate and needs to be replaced or modified. An experimental program is proposed herein which consists of testing a full scale prototype bridge, two-span continuous over one support incorporating precast concrete panels on steel stringers via shear pocket connections.

The specific tasks and objectives of the proposed research are as follows:

1. Full scale laboratory testing of the proposed shear connections under static conditions to determine the effectiveness of the slab-to-beam connections.
2. Full scale testing of the transverse joint for negative and positive moments.
3. Design of full scale two-span continuous bridge with full-depth precast panels installed on steel stringers for use in laboratory testing.
4. Experimental program that includes fabrication, instrumentation and testing of the bridge under static loading to obtain optimal performance data.
5. Analysis of experimental data to assess system response under various loading conditions.
6. Provide ultimate design and construction procedure recommendations on the full depth precast deck system.

## 2. LITERATURE REVIEW

### 2.1 Early Research

Previous literature indicated that many states have experimented with precast concrete slabs for deck replacements offering a wide variety of design and construction methods. The first trials were started in the early 70's in New York, Alabama, and Indiana. The spans did not have any skew or superelevation. More projects involved new construction rather than rehabilitation, so that, fewer geometric fit up problems were experienced rather than with deck replacement. The deck-stringer system was primarily noncomposite, although some composite action was noticed.

Significant advances have been made since the mid-70's through the beginning of 80's. Many of the spans were composite and some involved complex geometries. Major structures were constructed nationwide by New York State Thruway Authority (NYSTA), Pennsylvania Turnpike Commission, Massachusetts Turnpike Authority, New York State DOT (NYSDOT), California DOT, Maryland State Highway Administration, Federal Highway Administration, Delaware River Joint Toll Bridge Commission, Pennsylvania DOT, Connecticut DOT, Virginia DOT, Iowa DOT, Alaska DOT and Public Facilities, Ohio DOT, and ILDOT.

The connecting system between the slab and the stringers was of great importance. The way the deck acts is entirely controlled by the type of connection system used. The New York Thruway projects were examples of assuring composite action. The design was based on mechanical connectors providing full horizontal shear ties between the slabs and the girders. On the Oakland Bridge in California, composite behavior was established by using welded studs in the grout pockets. Conversely, the Santa Fe Railroad Bridge used epoxy mortar without any mechanical ties except spring clips, which cannot be counted upon for significant shear resistance. Field tests indicated that satisfactory composite action was accomplished with just epoxy bonding.

Construction using full depth precast panels has been accomplished prior to 1973. Many bridges were constructed using this concept in such states as Alabama, New York, and Indiana. In addition, two bridges were built in Hannover, Germany using precast decks on steel box girders. These early applications were used for both permanent and temporary construction. These structures have generally performed well, with minor problems attributed to partial failure of the joints at the slab-to-slab interfaces.

The knowledge obtained from these early applications provided guidance for further construction of a large number of bridges after 1973. Major bridges have been constructed over the past two decades. The research revealed that some states have experimented with precast/precast prestressed concrete panels for deck replacements using a wide variety of design and construction methods.

In 1969 a research project at Purdue University was initiated to determine the feasibility of using precast, prestressed concrete deck members on steel stringers. The research consisted of comprehensive prototype testing in the laboratory, and two other bridges constructed by the Indiana State Highway Commission. The test bridge deck consisted of narrow precast pre-tensioned planks placed transversely on the stringers. The planks were connected together with a tongue and groove joint, and post-tensioned longitudinally.

Three different shapes of joints were photoelastically investigated. As a result of this study, the flat shape was found superior to the others. A common form (match-cast) was used to insure good male-female fitting in that joint test. Since it was commercially impractical to use such a type of casting, additional tests were conducted on slabs which were cast using long-line forms in the precasting yard. The slabs underwent more than 10 million cycles of simulated 80 kN (18 kips), single-axle load application on adjacent sides of a joint without any apparent deterioration. A 0.4 mm ( $1/16$  in.) V60 neoprene sheet was placed in the joint for the tests on the plant-cast specimens to reduce stress concentration and prevent water leakage through the joints in the field applications. One of the significant conclusions of the researchers was that nearly full composite action between the deck and the stringers was achieved. This composite behavior

did not change after a period of two years. Successful laboratory testing resulted in two experimental decks being constructed on the Indiana Highway System.

The construction aimed at removing the two-lane timber deck and replacing it with 1.2 m (4 ft) wide, precast prestressed concrete panels with a tongue-and-groove joint. The slabs were secured to the stringers with railroad tie-down clips and post-tensioned together in the longitudinal direction. The post-tensioning provided approximately 620 kPa (90 psi) compression after all losses.

The construction was accomplished in 47 days, including 5 no-work days (4 days due to delivery delays and 1 day due to weather conditions). A detailed inspection of the Bloomington bridge was made after five years of service. The major problems observed were cracking, spalling, and leakage at the panel joints. The elevation between slabs varied by 6 mm (¼ in.) and under repeated wheel loads the slabs were damaged. Cracking, spalling, improper materials, and application techniques were all reasons for joint leakage. A second inspection in May 1980, revealed that cracking and spalling had been repaired and the deck appeared to work satisfactorily. However, water leakage appeared to be a continuous problem. Some of the tie-down clips had corroded extensively, and some were completely destroyed.

## **2.2 Selected Applications**

The selected bridges are briefly described in terms of system components. However, details pertaining to these bridge including sketches and photographs are reported in the ILDOT final report (Issa et al. 1995c).

### **2.2.1 State of Illinois**

The Quincy structure is a two-lane, nearly 670 m (2200 ft) long, cable-stayed bridge. Full width, full depth, precast deck panels were supported on a system of steel stringers, floor-beams, and welded girders. The full width of the panel was 14.2 m (46 ft-6 in.). The lengths of the panels varied from 2.7 to 3.4 m (9 to 11 ft). Three to five panels were post-tensioned to form a group. The groups were connected to each other by splicing the post-tensioning tendons and

grouting the intervening space. The panels were elevated by using a leveling device. The deck was designed to act compositely with the stringers, where composite action was achieved by the use of welded studs placed in shear pockets in the panels. A polymer grout was used to fill the pockets.

The Seneca bridge was built in 1932 and consisted of thirteen total spans. The four truss spans along with the approach spans had the existing concrete deck removed and replaced with a 165 mm (6½ in.) precast prestressed slab deck. All precast planks are match set, with the replacement being performed in sections. Full two way traffic was maintained throughout construction in accordance with outlined special provisions. Bridge closure was permitted in a ten hour period, Sunday through Thursday, from 7:00 PM to 5:00 AM.

### **2.2.2 Connecticut Department of Transportation**

During the early 1990's, the Connecticut Department of Transportation undertook a \$7 billion Infrastructure Renewal Program. Part of this program involved the rehabilitation of approximately 1640 bridges at an estimated cost of \$1.6 billion. Many of these bridges involved complete deck replacements requiring complicated stage construction sequences and occasional bridge closures during construction. In an attempt to expedite the construction process, a design using precast concrete deck slabs was incorporated for one of the structures (Waterbury bridge).

This six span bridge has a total length of 213 m (700 ft) consisting of straight composite plate girders running on tangents from pier to pier. Three of the spans are continuous with a hung span supported by pins and hangers. In order to account for the curvature, each slab was designed as a trapezoid. One end of the slab would be 2.4 m (8 ft) wide and the other slightly less depending on the curvature. Two different shapes were chosen since there are two different curves on the structure. Since the bridge is only 8.4 m (27 ft-6 in.) wide, it was decided to use full width precast panels with 2.4 m (8 ft) width, 8.1 m (26 ft-8 in.) length, and 203 mm (8 in.) depth. Since the slabs had to be composite, blockouts were required to allow for the installation of shear connectors. This would mean that the transverse location of the blockouts would be different for each slab.

The shear connector blockouts for the Seymour bridge were rectangular 457 x 127 mm (18 x 5 in.) at the top and trapezoidal from top to bottom. The spacing of these blockouts was 600 mm (2 ft) on center for each slab. Three 22 mm (7/8 in.) welded stud shear connectors were placed in each blockout. A minimal amount of prestressing was a necessity to prevent cracking during handling and installation. A leveling bolt system was used to provide for grade adjustment in the field. The bolt would be cut below the surface of the slab and the void grouted.

A standard shear key configuration filled with high strength non-shrink grout was chosen for the transverse joints. Longitudinal post-tensioning was designed to provide continuity. The strands were run through plastic ducts that were spliced at each transverse joint through small blockouts. An arbitrary stress of 1034 kPa (150 psi) was chosen for the simple spans and significantly increased to 2068 kPa (300 psi) in the three span continuous portion of the bridge in order to account for the significant composite dead load and live load stresses. After the strands were installed and tensioned, the ducts were completely grouted.

At the end of each span, a small cast-in-place pour closure was used to account for the dimensional growth problem in the precast slabs and to protect the post-tensioning system. In order to properly seal the deck, the finished slab was topped with a membrane waterproofing system and a 64 mm (2½ in.) bituminous wearing surface.

### **2.2.3 Commonwealth of Virginia Department of Transportation**

The Culpeper bridge is a simple span structure, 16.5 m (54 ft) long and 9.1 m (30 ft) wide. The existing steel rolled beams are 1.9 m (6 ft-3 in.) center to center. The two exterior beams, spaced 900 mm (3 ft) from end, are W33x125, while the interior beams are W33x132. Two phases of construction were carried out to maintain traffic flow. Six precast panels at 2.4 m (8 ft) were installed. The joints between adjacent panels were of type female-female. The connection system between the slab and the beams consisted of shear studs. The stud voids were filled with high early strength concrete and a non-shrink additive.

The Fairfax bridge consisted of four 11.5 m (38 ft) spans and a width of 11 m (36 ft) face-to-face of rails. The bridge was originally built in January, 1932. In January, 1969 some minor repairs were performed on the structure, however, in February, 1981 the bridge was redecked with precast deck panels. The panel dimensions were 2.1 m (7 ft) wide and 5.5 m (17 ft-11 in.) long for the end panels, and 2.3 m (7 ft-6 in.) wide and 5.5 m (17 ft-11 in.) long for interior panels. The existing interior steel rolled beams (W28x104) were preserved and cleaned, while new beams (W27x102) were installed at the ends. The beams are spaced 1.9 m (6 ft-4 in.) center to center, with the exterior beams at 940 mm (3 ft-1 in.) from the ends. A two phase construction process was used to maintain traffic flow. The joints between the precast panels were similar to those used in the Culpeper bridge, i.e., female-female. These joints were filled with non-shrink mortar. Twenty-two mm (7/8 in.) stud shear connectors were used between the precast slab and beams.

#### **2.2.4 Maryland Department of Transportation**

The Woodrow Wilson Memorial Bridge is the major crossing of Interstate 95 on Potomac River, south of Washington, D.C. This bridge was constructed in 1962 for the Federal Highway Administration. The bridge is 1798 m (5900 ft) long consisting of 18 steel deck girder approach units, 8 on the Virginia side and 10 on the Maryland side. Most approach units are four-girder continuous multi-span units. Floor-beams between girders are spaced approximately 4.9 to 7.9 m (16 to 26 ft) on centers and carry five rolled beam stringers per roadway continuously over the floor-beams.

The deck provided a six-lane roadway 23 m (76 ft) wide. The original 27 m (89 ft) width was subdivided by a longitudinal centerline roadway joint. Because of the heavy volume of traffic (110,000 vehicles per day), the study called for uninterrupted traffic flow. Six lanes of traffic during peak hours, four or five lanes during off-peak daytime hours, and one lane in each direction during the night time periods were essential. Due to the above restrictions, it was decided to replace the deck part-by-part with precast prestressed lightweight concrete panels. These panels were installed transversely to cover the full roadway width. The new deck system

provides 13.4 m (44 ft) roadways to permit space for disabled vehicles that previously had caused commuter traffic delays.

The typical lightweight concrete panel was 14.2 m (46 ft-7¼ in.) wide, 3.0 to 3.6 m (10 to 12 ft) long, and a 127 mm (5 in.) haunch at the exterior girder. A total of 1,026 panels were utilized for the construction of the bridge. The panels were transversely post-tensioned at the fabrication plant. The 12.7 mm (½ in.) diameter transverse strands were in pairs at approximately 305 mm (12 in.) on centers in the planes of the top and bottom reinforcing steel. These panels were installed transversely to cover a half width of the bridge and post-tensioned in the longitudinal direction to provide sufficient compression to keep the transverse joints between panels closed. This was provided by 13 groups of four 15.24 mm (0.6 in.) diameter strands at the slab mid-depth. The post-tensioning connected segments in lengths of 42.7 to 86.9 m (140 to 285 ft), averaging 17 panels. To ensure full bearing between deck panels under longitudinal post-tensioning, and to provide for construction tolerances, the plans called for a 32 mm (1¼ in.) joint between panels to be filled with polymer concrete immediately prior to post-tensioning.

Since the construction work sequence required many steps and the need to open all lanes for traffic in the rush hours, it was necessary to use polymer concrete based on methylmethacrylate monomer that gives the required strength in one hour to hold the new panels in place under normal traffic. Two-coat epoxy-sand membrane was applied to the top surface of the panels at the fabrication plant. Rehabilitation was completed 8 months ahead of schedule, \$6 million under budget, and without disrupting the flow of traffic.

### **2.2.5 Maryland Transportation Authority**

The Bay bridge was built in 1952 and consisted of two lanes in each direction. The deck for most of the spans were replaced with precast panels that varied in sizes in order to fit the geometric necessities. The bridge was completely closed to traffic for six months in order for the replacement process to commence. The overlay for the deck consisted of a two inch layer of Latex Modified Concrete in addition to the 152 mm (6 in.) deck. The panels were post-tensioned in the longitudinal direction to secure the tightness in the joints.

### **2.2.6 Iowa Department of Transportation**

The Burlington bridge was rehabilitated using full depth precast prestressed concrete deck panels which were designed to act compositely with the steel floor-beams and girders. This cable stayed bridge over the Mississippi river at Burlington, Iowa is 26.7 m (87.5 ft) wide and 325 m (1065 ft) long with two spans; 201 and 123 m (660 and 405 ft). The supporting system consists of transverse floor-beams with a spacing of 4.5 m (15 ft) carried by two girders at the north and south bounds. The precast panels were 254 mm (10 in.) thick, 4.1 m (13 ft-9 in.) long, and 14.4 or 11.7 m (47 ft-3 in. or 38 ft-3 in.) wide.

Post-tensioning in the transverse direction was applied to the panels for handling and erection. The entire post-tensioning system (thread bars, nuts, couplers, and anchor plates) except the ducts, was epoxy coated. The initial post-tensioning force was 396 kN (89 kips) for the 25 mm (1 in.) diameter thread bar and 738 kN (166 kips) for the 35 mm (1 in.) diameter thread bar. Cast-in-place concrete was used to fill the 600 mm (2 ft) wide longitudinal and 381 mm (1 ft-3 in.) wide transverse joints.

The shear connector pockets were 229 mm (9 in.) long and 76 mm (3 in.) wide. All these pockets were distributed on the edge girders with a spacing of 229 mm (9 in.). A non-shrink grout was used to fill the pockets and the space between the precast panels and girder flanges. Leveling screws were used to adjust the level of the precast panels. A layer of 51 mm (2 in.) low-slump dense concrete was used as protection for the precast deck.

### **2.2.7 California Department of Transportation**

The nearly 533 m (1750 ft) long High Street structure consisted of twin (left and right) bridges on an extremely busy urban freeway. This structure was widened on the left in 1955, while in 1963, the structure was widened on the right. The structure currently consists of four lanes of which the fourth lane on spans one through twenty nine of the 30 plus spans bridge were replaced with precast concrete deck panels in 1978. This project was a good example of replacing a deteriorated deck while maintaining traffic on the freeway. Precast panels were used

to rehabilitate only the outside southbound lane of the "left bridge". By using precast panels, it was possible to maintain full peak period traffic during the evening rush hours.

Eighteen to 24 m (60 to 80 ft) of the old concrete deck, 3.6 m (12 ft) wide, was removed each day, leaving the girders bare. The new precast panels, 165 mm (6½ in.) thick 9 to 12 m (30 to 40 ft) long, and about 4.3 m (14 ft-2 in.) wide, were installed over two steel I-beam girders spanning a distance of 2.4 m (8 ft) on center with 600 mm (2 ft) overhangs on both sides. Oblong holes, 305 mm (12 in.) long and 102 mm (4 in.) wide, were formed in the panels. Four shear connector studs were welded to the girders through each hole. The studs were 22 mm (in.) diameter and 152 mm (6 in.) long. Leveling devices were placed on girder lines at 2.4 m (8 ft) maximum spacing. No post-tensioning was provided between the precast elements to secure the tightness of the joints between adjacent panels. A 229 mm (9 in.) closure pour was provided between every two adjacent panels while stud connection pockets are available for providing composite action between the slab deck and its supporting system (girders). The closure pours as well as the shear stud pockets were grouted with the same material (high alumina cement concrete).

The double deck Oakland-San Francisco bridge was originally built to accommodate trucks and trains on the lower deck and regular cars on the upper deck. The bridge design includes cable stayed spans in addition to truss spans. In 1960-61, the bridge underwent rehabilitation. As a result, the bridge now accommodates traffic to San Francisco on the upper deck and the other way to Oakland on the lower deck. Trains are no longer accessible on the bridge as the right two lanes of the lower deck were rehabilitated for regular traffic. These two lanes were replaced with precast concrete deck panels (light weight concrete). The bridge deck was originally paved with Epoxy Asphalt pavement in 1964 as part of the reconstruction of the bridge. The deck was resurfaced in 1974 (upper deck) and 1977 (lower deck) with Epoxy Asphalt due to wear.

In 1989, an earthquake hit the area and the bridge. As a result, a small section of the lower deck fell through and the entire width in that section was replaced with precast panels.

However, that area has not been overlaid. Three-hundred mm (12 in.) closure pours are provided between adjacent precast elements. The bridge was closed for a period of one month, while construction took place on the deck as well as other aspects related directly or indirectly to the bridge.

### **2.2.8 New York State Thruway Authority (NYSTA)**

The New York State Thruway Authority has used full-depth precast concrete decks for rehabilitation in three different locations. The Krum Kill Road bridge is a 15.2 m (50 ft) long single-span, six-lane mainline throughway structure in Albany County. The bridge consists of two structurally separate spans supported on common abutments. Each structure carries two active traffic lanes. The remaining lane is expected to be used in the case where widening is needed. This extra lane was effectively used to detour traffic during construction. To make the deck fully composite with the structural steel, welded headed studs were provided. Precast panels, 190 mm (7½ in.) thick and 1.6 m (5 ft-2 in.) long, of two different widths, were used. The 12.8 m (42 ft) wide panels were placed over six stringers, and the 6.4 m (21 ft) wide panels were placed over three stringers. A 900 mm (3 ft) wide cast-in-place longitudinal joint was provided over continuous reinforcing bars extending from the adjacent panels. The deck is overlain with a membrane and 152 mm (6 in.) of asphalt. Cracks over the reinforcing bars were detected in the precast panels during construction, that were subsequently sealed with epoxy.

The Amsterdam Interchange bridge was set up as an experimental project in 1954, constructed during the Fall of 1973 and the Spring of 1974. The objective of this prototype project was to evaluate the effectiveness of both welded and bolted connections, that were designed to accomplish composite action with the steel girders. This bridge is a two-lane bridge consisting of four spans; 10, 18, 20, and 18 m (33, 59, 66, and 60 ft) long, respectively. Precast panels were installed on only one-half of span two due to constraints on the availability of resources and weather. Seven panels were placed in each lane, three of them using bolted connections, and four with welded connections. A staged construction sequence was used to maintain at least one-lane of traffic open during construction. The overall width of the deck is 13.7 m (45 ft). The full depth precast panels were 203 mm x 1.2 m x 6.7 m (8 in. x 4 ft x 22 ft).

The slabs were poured in an open air casting bed built by NYSTA maintenance forces. The deck was water-proofed with a sheet membrane and overlaid with asphaltic concrete.

The transverse keyways were filled with a low modulus epoxy mortar, mixed one part resin and two parts aggregate. The blockouts for the welded shear connectors were filled with epoxy mortar, one part resin and three parts aggregate. The epoxy mortar in the shear pockets set in about one or two hours, while the mortar in the transverse key took about five hours to set due to the low mass of material in the long thin joint.

The Harriman Interchange bridge is a three-span (each 23 m (75 ft) long), two-lane ramp. The connection details are similar to those of the Krum Kill Road Bridge. The roadway is on both vertical and horizontal curves. Since this is a curved, super-elevated bridge, the precast panels are not level on the beam flanges. Therefore, the epoxy mortar bed is thicker on one edge of the flange than the other.

### **2.2.9 New York State Department of Transportation (NYSDOT)**

NYSDOT probably enjoys the distinction of having built the largest number of bridges as well as the most different types of bridges using full depth precast concrete deck panels. At least six bridges have been built over a period of 8 years.

The Vischer Ferry Road bridge was originally designed for H15 loading due to the fact that this bridge is a means of transportation for four homes in the town. The cost of replacing the deck was \$300,000 as the rehabilitation process took approximately one season, i.e., six months. The residents were transported back and forth prior to and after each day's work which consisted of replacing two panels per day (full width panels). During construction, the bridge was closed to traffic between 10:00 AM and 7:00 PM. The existing deck was removed and the top of the structural steel cleaned and primed. A 12.7 mm (½ in.) stiff grout was then placed on top of the structural steel stringers and supports. Half inch bolts were then installed in the corners of the precast panels to act as spacers as well as to allow the lifting of the panels via a crane.

The Batchellerville bridge spans 937 m (3075 ft). The bridge was significant since it was the only direct route to a remote community. The community was given the option of a staged construction with a long complete construction time or closing the bridge completely for 6 months. The community opted for the 6 month bridge closing, with a provision for ferry service during that time. The design called for full width precast panels placed over newly installed floor-beams. The crown of the roadway was built into the panels by using curved panels. Since the transverse slab joints are located over the floor-beams, the panel length varies from 3.6 to 4 m (11 ft-8 in. to 13 ft) depending on the spacing of the floor-beams. Construction started on April 30, 1982 and ended on October 8, 1982, a week ahead of schedule. This project demonstrated the combined cost and time effectiveness which was achievable through the application of precast concrete slabs in large scale bridge deck replacement.

The Normanskill bridge was built in 1928 in the town of Guilderland. Two previous contracts were accomplished, the first was the original bridge construction in 1931 and the second was the bridge deck resurfacing in 1972. The replaced area was 31 m (101 ft-10 in.) long and 7.8 m (25 ft-5½ in.) wide. The construction process consisted of a Stage I to close 4.3 m (14 ft-3 in.) of the full width of the bridge leaving 3 m (9 ft-9 in.) as a traveling lane. In Stage II the work commenced on the other side of the roadway keeping 3 m (9 ft-11 in.) for traffic. Two types of precast panels were used as intermediate and end panels with the same width of 1.9 m (6 ft-4 in.) and two different lengths of 1.3 and 4 m (12 ft-4 in. and 13 ft-4 in.), respectively. These panels were installed on the framing system (transverse girders with a spacing of 3.8 m (12 ft-6 in.) held by two trusses at the north and south bounds). The typical 12.7 mm (½ in.) female-female longitudinal joint is filled with non-shrink cement grout. Every panel has four leveling bolt sleeves at the four corners to accomplish the required position of the panel. 19 mm (¾ in.) no-head shear studs were installed in the 51 mm (2 in.) transverse joints. They are 102 mm (4 in.) long for the intermediate panels and 25 mm (1 in.) long for the end panels with a typical spacing of 381 mm (1 ft-3 in.).

The Kingston structure is a three-span, two-lane suspension bridge with a 213 m (700 ft) long main suspended middle span. Typically, about 2.7 m (9 ft) long panels with full roadway

widths of about 7.3 m (24 ft) were used. Panel thickness varies from 152 mm (6 in.) at the edges to 178 mm (7 in.) at the crown. This type of deck reconstruction was chosen for two reasons. First, to allow rapid construction and second, to control dead weight effects by selective sequential placement. The panels were transversely prestressed to accommodate handling stresses. The prestressing steel used was 12.7 mm (½ in.), 1860 MPa (270 ksi) strands with an initial force of 128.5 kN (28.9 kips) per strand. A simple V male-female joint, with no grouting or caulking, except at the connections to the steel stringers, was used. The slabs were bolted together longitudinally with tie rods.

The Cochection structure is a three-span, two-lane truss bridge with a total span length of 206 m (675 ft). The panels are 190 mm (7½ in.) thick, 2.3 m (7 ft-6 in.) long and about half of the roadway width. A bituminous wearing surface along with a waterproofing membrane system were provided. The transverse joints were filled with mortar having one part Type II Portland cement to two parts mortar sand. Traffic was maintained by way of staged construction. Reflected cracks appeared along the longitudinal joint that were batched later.

The Southwestern Boulevard structure is a two-lane, 167.6 m (550 ft) long, three-span truss bridge, with span lengths of 54.9 m (180 ft) each. The spans are at a skew of about 22 degrees. Typically, 190 mm (7½ in.) thick, 2.4 m (8 ft) long, and about 6.4 m (21 ft) wide trapezoidal slab panels were used to accommodate the skewed span ends. The transverse and longitudinal slab joints were similar to those used on the Cochection Bridge.

#### **2.2.10 Alaska Department of Transportation and Public Facilities**

The rehabilitation program includes two main projects that had to be finished by October 1992: The Dalton Highway Bridge Rehabilitation and Chulitna River Bridge redecking. The second project was the rehabilitation of Chulitna River Bridge. The bridge has a total span length of 241 m (790 ft) and a total width of 10.4 m (34 ft). The existing structure has a concrete deck on steel trusses and stringers. The new construction required the removal of the 10.4 m (34 ft) wide cast-in-place deck and replacing it with 12.9 m (42 ft-2 in.) wide full-depth precast concrete deck panels. A stage construction was adopted in order to maintain the traffic flow

during the rehabilitation process. Mag-phosphate grout was used to fill the pockets. Two types of connections between the panels and the supporting system were used; a grouted pocket connection on the steel stringers and a bolted connection on truss elements. The design called for the use of two different types of connections for two reasons. First, the truss flanges were very narrow for a grouted connection, and second, the bolted connection provided some support for the structure prior to grouting.

The first project contained 18 bridges in one contract. The existing bridges had timber decks supported on either steel stringers or timber floor-beams depending on the bridge span length. Steel stringers were used for spans of 18.3 m (60 ft) long, and timber stringers were used for spans of 9.1 m (30 ft) long. The rehabilitation process was to remove the existing timber decks, railings, stringers, and pile caps, and to install permanent full-width full-depth precast prestressed concrete deck panels on new steel "W" shape stringers and pile caps.

Stage construction was adopted to maintain traffic flow during construction. The primary stage consisted of removing a half-width of the superstructure and pile caps, and installing a temporary railing at the free end. The new steel pile caps and stringers were installed and covered by a temporary timber or concrete deck. At the end of this stage, one half of the bridge width was ready to support traffic flow. The second stage was to work on the other half width of the bridge, where new pile caps and stringers were installed. Finally the temporary deck was removed, field splices between the separated pile caps assembled, and permanent full-width precast prestressed concrete panels installed.

All precast panels were 241 mm (9½ in.) thick at the center line of the roadway and 190 mm (7½ in.) thick at the edges with one typical length of 8.4 m (27 ft-5 in.) and two typical widths of 1.5 to 1.7 m (4 ft-10 in. and 5 ft-7 in.). Normal weight concrete was used with a strength of 34 MPa (5,000 psi) at transfer and 45 MPa (6,500 psi) at 28 days. The prestressing strands were 12.7 mm (½ in.) diameter seven wire strands low relaxation with an ultimate strength of 1860 MPa (270 ksi). The jacking stress for the pretensioning strands was 1303 MPa (189 ksi) and the effective stress after all losses was 1027 MPa (149 ksi). A typical female-

female joint was chosen between the adjacent panels and an elastomeric compression joint seal was used as an expansion joint. Two sizes of shear pockets were used. The first pocket size was 178 x 127 mm (7 x 5 in.) with two studs 22 x 152 mm ( x 6 in.) installed in each pocket for a 9.1 m (30 ft) span length. The second pocket size was 305 x 127 mm (12 x 5 in.) with three studs of the same size installed for a 18.3 m (60 ft) span length.

### **2.2.11 Ohio Department of Transportation**

The State of Ohio Department of Transportation reported the rehabilitation of 5 bridges. Construction started on the Dublin skew bridge in 1986. The bridge consists of six spans; 22, 29, 30.5, 30.5, 29, and 22 m (73, 95, 100, 100, 95, and 73 ft), with a bridge width of 17 m (56 ft) from the face of railings, and a bridge clearance of 15+ m (50+ ft). The bridge has a concrete arch with cross beams as its deck supporting system. The full depth precast panels consisted of panel lengths; 3.7, 3.0, 2.9, 2.9, and 3.1 m (12 ft-1½ in., 9 ft-10½ in., 9 ft-6½ in., 9 ft-5½ in., and 10 ft-1 in.), panel width of 8.5 m (28 ft), along with a varying depth.

Non-prestressed steel was furnished as panel reinforcement for handling and erection stresses, and post-tensioned tendons for service load stresses. The concrete stress level for the post-tensioning was about 6895 kPa (1000 psi). Panels are supported on elastomeric bearings and are anchored down to floor-beams using dowel bars. All of the mild reinforcement was epoxy coated, and the prestressing strands were polymer coated. The unit stress for the precast post-tensioned deck panels was 15 MPa (2200 psi) compression (service load), and 3061 kPa (444 psi) tension (construction phase II). Epoxy mortar material was used for the joints between the adjacent precast panels.

### **2.2.12 Pennsylvania Turnpike Commission**

The Somerset structure is a simple span bridge exit ramp for the Pennsylvania Turnpike. This narrow, one lane bridge is simply supported. The deck is in good condition due to the fact that the bridge is only used by a private community. The bridge was designed for low volume traffic. The precast panels are connected to the structural steel via a tie down.

The Quakertown Interchange bridge is a suspended cantilever system with a composite deck in the suspended span and a non-composite deck in the cantilever span. The bridge serves as an interchange exit for the Pennsylvania Turnpike. The precast panels were 165 mm (6½ in.) thick, with a varying haunch thickness, 2.3 m (7 ft-7½ in.) long, and 5.3 m (17 ft-6 in.) wide, and covered one-half the width of the structure. Existing bulb angle shear connectors were left in place as the old slab was removed in 1981. The slab panels with shear pockets were cast with sufficient precision so that the precast slab fitted properly when set in place. The transverse joints were pulled together by using nominal longitudinal post-tensioning. In addition to providing rapid erection, construction of the bridge proved to be cost effective compared to conventional deck replacement methods.

The Clark Summit bridge is a ten-span, 496 m (1627 ft) long bridge consisting of two parallel structures carrying two lanes each way and a clearance of 15 m (49 ft). In 1980, precast panels were chosen for the replacement of the deteriorated deck. They were chosen because it was necessary to maintain traffic on half of the bridge while redecking the other half. It was also feared that vibrations from the traffic could interfere with the proper concrete setting, especially at the juncture of the new decks. The panels were typically 171 mm (6¾ in.) thick, 2.1 m (7 ft) long with a full roadway width of 8.8 m (29 ft), and weighing 8167 kg (18,000 lbs) each. Non-shrink cement grout was placed at the transverse joints and nominal longitudinal post-tensioning was used.

### **2.2.13 State of Maine Department of Transportation**

The Deer Isle-Sedgwick Bridge is located over Eggemoggin Reach between Little Deer Isle & Sedgwick. This bridge consists of 9 spans; 4 at 20 m (65 ft), 1 at 147.5 m (484 ft), 1 at 329 m (1080 ft), 1 at 147.5 m (484 ft), and 2 at 20 m (65 ft), with a total width of 7.2 m (23.5 ft) centerline to centerline of the suspended girders. The supporting deck system consisted of two types of suspended transverse girders, WF14x42 (for approach spans) and WF24x74 (for suspended spans), with floor beams in between. The work started in May 1987 and concluded in October 1987, without major traffic interruption. The light weight precast concrete panels were designed to cover a half-width of the bridge to maintain traffic flow during construction. The

panels were 152 mm (6½ in.) thick, 3 m (9 ft-11 in.) wide, and had a variable length depending on the spacing of the suspended girders.

A typical female-female transverse joint was chosen. Joints and blockouts were filled with epoxy mortar after the shear connectors and plate connections were welded. No prestressing was applied to the slabs. All the panels had 12.7 mm (½ in.) epoxy waterproofing overlaid prior to erection. The overlay covered the entire top surface of the panels within 152 mm (6 in.) of any blockout or shear key. After the shear keys and blockouts were filled, the epoxy waterproofing overlay was placed over these areas. Elastomeric compression joints were adopted to absorb the cyclic movement of the bridge.

#### **2.2.14 Massachusetts Turnpike Authority**

The Connecticut River bridge was built in 1957 and rehabilitated in 1982. It carries traffic through the Massachusetts Turnpike over the Connecticut River. This structure is a 373 m (1224 ft) long, four-lane divided highway. A typical interior span is 68 m (224 ft) long. The rehabilitation process started with the east bound roadway, and was opened to traffic before the target date. The west bound roadway was completed in 1982. Lightweight concrete was used for the precast concrete slabs and cast-in-place parapets. The lifting weight of each panel was 11 tons. The precast slabs were transversely pre-tensioned and longitudinally post-tensioned. Four lifting inserts were provided for each panel.

The precast panels were set in proper elevation by using a system of leveling bolts. Welded studs in grouted pockets were used to hold down the slab to prevent buckling during post-tensioning. Each typical panel was provided with 24, 12.7 mm (½ in.), 1860 MPa (270 ksi) prestressing strands. The 12.7 mm (½ in.) strands were pretensioned so that after transfer, the initial stress would equal 70 percent of the strength, i.e., 1303 MPa (189 ksi). These panels also included 42, 57 x 102 mm (2¼ x 4 in.) conduit connection blockouts and 21, 32 mm (1¼ in.) intermediate metal conduits for the 15.24 mm (0.6 in.), 1860 MPa (270 ksi) post-tensioning strands.

The Chicopee River bridge, like the Connecticut River bridge, is on the same four-lane, divided highway and had twin separate east and west bound roadway structures. Each had five spans with a total span length of 255 m (837 ft). Encouraged by the success of the Connecticut River bridge deck rehabilitation project, the turnpike authority used essentially the same technique. The east bound roadway was completed in 1983, and the west bound roadway was finished by the target date of July 4, 1984. The panel sizes as well as all design details were identical to those of the Connecticut River bridge. The thickness of deck slab used for this bridge deck was 203 mm (8 in.).

#### **2.2.15 Texas Department of Highways and Public Transportation**

The Department of Highways and Public Transportation of the State of Texas reported the reconstruction of a bridge (A.T. & S.F. Railway Overpass). The span length for this bridge is 15 m (50 ft) and the width 13.7 m (45 ft). The bridge deck is supported on W36x150 I-beams. The project was to replace the deck with a precast concrete deck as well as replacing the two end beams with new W36x135 I-beams. These two beams were replaced and new diaphragms installed. The remaining four beams (W36x150) were preserved. Two types of panels were used in this construction. The end panels have a width of 1.8 m (6 ft- in.), and the interior panels 1.9 m (6 ft-2¾ in.). The beams are spaced; 2 spaces at 2.1 m (7 ft) and 3 spaces at 2.4 m (8 ft). The distance from the end where the new beams were installed is 900 mm (3 ft), and the distance from the other end is 1.2 m (4 ft). The shear connector openings were of beveled shape, 127 x 279 mm (5 x 11 in.). 22 x 152 mm ( x 6 in.) headed studs were end welded after all deck panels were placed. A female-female type joint was used between the deck panels.

#### **2.2.16 Ministry of Transportation of Ontario, Canada**

The structure selected for redecking was the eighteen span Welland River bridge, carrying two southbound lanes near the City of Niagra Falls. The bridge was built in 1939 and consists of five units of continuous spans. The structure was non-composite prior to the rehabilitation. For comparison purposes, four of the five units were rehabilitated using cast-in-place concrete decks and only one unit of three spans at the south end with precast concrete

decks. The three spans were; 14.859, 14.63, and 14.63 m. The bridge width is 13.26 m with a variable bridge clearance, and panel depth of 225 mm.

The deck supporting system consisted of four lines of steel girders with sizes; 33WF125 for the exterior girders, and 33WF150 for the interior girders. The full-depth precast panels consisted of a length of 24.28 m for the end panels and 24.18 m for the remaining panels. Non-prestressed steel was used as reinforcement for the panels. The steel sizes were 15 @ 250 mm longitudinally and 15 @ 230 mm transversely (with 340 mm spacing at the openings for stud connectors). The tendons consisted of 11 (four 16 mm diameter strands) tendons in the panels near the ends to 20 (four 16 mm diameter strands) tendons over the piers and center span. The strands were 16 mm with a strength of 260 kN. The joints between the adjacent precast panels were key joints with a non-shrink grout. Longitudinal prestressing was increased by about 33% to prevent the occurrence of any cracks. As a result, no problems were encountered during actual installation. A waterproofing membrane w/Class I (bituminous surfacing) was used as a protection system.

### **2.3 Recent Research**

A comprehensive study was conducted by the University of Nebraska (1997), jointly with HDR Engineering Inc. and Kiewit Construction Company to evaluate existing rapid bridge deck replacement methods and develop better procedures and new superstructure designs for future rapid deck replacement. Three main areas were investigated where modifications could be made to make deck systems more suitable for rapid replacement. These three areas correspond to the demolition process and equipment, the bridge deck system itself, and the bridge girder-to-deck connection. The cost of removal has a major influence on the selection of the method of rehabilitation. The second of three areas to improve the speed of deck replacement dealt with the deck system itself. The new AASHTO LRFD Specifications require a significantly reduced amount of reinforcement in the deck and should be used wherever applicable. Also, the use of welded wire fabric (WWF) as a replacement for conventional reinforcing bars can considerably reduce the amount of construction time. The third area to improve the speed of deck replacement examined the connection system of concrete decks and concrete or steel girders. Two new

connection systems were developed, one for concrete girder/concrete deck connections and the other for steel girder/concrete deck connections. For concrete girders, a debonded shear key system was developed. For steel girder/concrete deck connections, a new 32 mm (1¼ in.) diameter shear stud was developed to replace the popular 19 mm (¾ in.) and 22 mm (7/8 in.) shear studs. The new 32 mm (1¼ in.) stud, which provides approximately twice the capacity of a 22 in. (7/8 in.) stud, would allow positioning in a single row over the girder web. Also, it was found that alternating headed and headless studs was adequate for anchorage to the concrete deck. This further facilitates deck removal.

A two-year research project entitled "Structural Behavior of Full Depth Precast/Precast Prestressed Concrete Bridge Deck Replacement" was recently completed (Issa et al. 1995a,b,c,d, 1998). This project was funded by the Illinois Department of Transportation. The aim of this study was to evaluate the durability, performance, and cost effectiveness of full depth precast concrete bridge decks, that can be installed on steel stringers, in order to formulate an optimum bridge deck system. This optimum design can help in further establishing the effectiveness of precast and prestressed concrete components in the design and construction of the bridges and highway systems across the country. The proposed bridge deck systems will introduce improved features to the construction and rehabilitation procedures employed by the transportation industry. The findings indicate that the potential to adopt the proposed design system is very promising, and could be of great interest throughout the nation. A major advantage in using the precast system is the minimum interference with traffic resulting from a reduction in construction time. In most cases, traffic is maintained in both directions during the rehabilitation process by either employing a two-phase construction plan or weekend and/or night closures of the bridge under construction. The advantages of such systems have also been reported by others (e.g., Knudsen 1980, Slavis 1983, Berger 1983).

A comprehensive survey was conducted to identify bridge decks rehabilitated or built using full depth precast concrete decks for the rehabilitation of deteriorated bridges as well as new bridge construction (Issa et al. 1995c). Fifty-three questionnaires were sent to all departments of transportation in the United States as well as Ontario, Canada. The response was

excellent as the collected data was analyzed. The results revealed that this concept has been used for two decades in a few parts of the United States and recently in Ontario, Canada. Results of the survey also indicated that several states had problems with some aspects of the system. These problems included improper design, inadequate configuration of the structural components of the system (i.e., joint between the panels and connection at shear pockets), poor construction procedures, and unsatisfactory materials. However, once these issues were addressed, the rehabilitation process was efficient and proved to be economical in terms of time and resources. It was obvious that there was no code criteria governing this concept of rehabilitation or new bridge construction. As a result, this study determined the necessity for establishing code specifications for new bridge construction and rehabilitation using full depth precast and precast prestressed, concrete bridge deck panels.

The survey was complemented with a comprehensive field investigation to collect the data from several selected bridges in the United States and Canada in order to evaluate their durability and performance. The field investigation was carried out in different states including Illinois, Connecticut, Virginia, Maryland, California, Iowa, New York, Alaska, Washington, Ohio, Pennsylvania, and Washington, D.C. Valuable information was collected with respect to the systems using precast or precast prestressed concrete bridge deck panels. Bridge engineers from each state were very helpful and cooperative. The field observations were helpful in assessing the performance of the bridge deck system.

The ultimate goal of the proposed research is to achieve an optimum design incorporating the best aspects of using full depth precast prestressed slab panels for the rehabilitation or replacement processes as well as to determine the cost effectiveness of the proposed system to conventional cast-in-place systems. In order to verify the effectiveness of these structural systems, particularly to evaluate the critical system components under static and fatigue loads, an experimental study was deemed necessary. The experimental study will facilitate the overall optimal design and construction features in order to attain the best possible replacement system.

A recent quarter-scale experimental program was conducted on three bridge models at the University of Illinois at Chicago. Three bridge models were fabricated and tested in accordance with the guidelines set forth in the earlier study. The first bridge model was a two-span continuous structure without post-tensioning. Due to an overdesign in the steel stringers for the first bridge, the size of the beams was reduced for the remaining two bridge models. This was accomplished in order to obtain more deflections in the structure and to reduce the stiffness provided by the steel stringers. Furthermore, the second bridge was post-tensioned at a direct prestress level of 1434 kPa (208 psi) to determine the effect of post-tensioning on the behavior of the transverse joints between adjacent precast panels. The third bridge was identical to the second bridge, however, a larger prestressing force of 2620 kPa (380 psi) was provided to determine the effect of amount of post-tensioning.

The equivalent service load moments produced by an HS20 AASHTO truck were used. The spread beam providing the truck loading simulated a quarter-scale of an actual HS20 truck on each span (Fig. 2.1). The loading beams were stiffened to guard against any premature failure. The wheel area was in accordance with AASHTO specifications. The overall test setup and instrumentation are presented in Fig. 2.2. LVDTs were used to monitor the bridge vertical deflections, while clip gages were used to monitor for any movement and slippage between the precast panels and supporting system, i.e., the magnitude of full composite action. The deflections were monitored for the two stringers at critical sections and along the length of the beams. In addition, vibrating wire strain gages and crack displacement transducers were used to monitor any movement in the transverse joint between adjacent precast panels to predict adequacy of the joint configuration and the material within the joint (Fig. 2.3).

A general view of the loading beams and panels is shown in Fig. 2.4. The post-tensioning ducts were grouted through the extension passages. The studs were welded on the top flanges of the stringers and the panels were placed atop the stringers by allowing for a 9.5 mm (3/8 in.) haunch. The deflected bridge is shown in Fig. 2.5.

The first cracking in the non-post-tensioned bridge model occurred in the transverse joints near the vicinity of the central support at 49 kN (11 kips), which ultimately lead to the failure of the bridge through complete splitting between the central panel and the joints. Cracking in the first bridge model only occurred in the two transverse joints at the central support. The second and third bridges experienced cracking at the central support at 156 and 178 kN (35 and 40 kips), respectively. However, more cracking developed away from that region within the central panel as the load was increased. The first cracking load was three times higher for the post-tensioned bridge models than the non-post-tensioned bridge.

During fatigue loading, the load cycles were carried out at predetermined intervals. During fatigue, no cracking developed, hence the stress range was increased in order to examine the behavior of the panels. Even as the fatigue cycles were increased, the crack over the central support was controlled due to the post-tensioning. Furthermore, a crack developed in the steel beam that extended from the top flange down to the bottom flange as shown in Fig. 2.6. This plot depicts the static and fatigue intervals from the testing, where the fatigue stress range cycles were increased. The crack over the central support would open as a result of increased loading and close during unloading, hence confirming the effect of post-tensioning in closing the crack. In addition, a nonlinear finite element analysis was performed which reasonably predicted the load-deflection behavior of the three bridge models.

Full composite action was also evident since no slippage occurred at the concrete-steel interface until the load reached approximately 445 kN (100 kips) for the second bridge model. When the load reached 445 kN (100 kips), cracking was observed in the haunches at both ends of the bridge model. Furthermore, readings from the clip and strain gages across the depth of the beam indicated that a noticeable amount of slippage occurred after a load of 445 kN (100 kips). Finally, this bridge model failed at a load of 480 kN (108 kips), which is approximately nine times that of the service loading based on the two quarter-scale HS20 trucks.

## 2.4 Shear Connection Tests

In the past, channels, spirals and studs were widely accepted as the choice for shear connectors. However, because of their ease of installation and low cost, welded shear studs are the most economic and popular shear connector of our time. The use of mechanical shear connectors in composite construction was proposed in the early 1920's. Research on the utilization of simple shear connectors in composite construction dates back to 1933. However, testing of welded studs as shear connectors in composite design was first demonstrated in 1955. Since the load carried per connector cannot be quantitatively measured directly from a beam test (Slutter and Driscoll 1965), some investigators used the pushout test to evaluate the ultimate strength characteristics of the shear connectors. It can be argued that the loading on a connector in a pushout specimen is not identical to that in a beam since the presence of direct stresses causes bending in the beam slab (Slutter and Driscoll 1965). The distribution of these stresses in a pushout specimen causes the slabs to uplift at the top of the steel beam. This combined with eccentric loading and minor fabrication errors have been known to lower the ultimate load capacity of shear studs in pushout specimens. However, if constructed and tested in a precise manner, the ultimate strength of these connectors can be successfully evaluated.

Early tests consisted of fatiguing bare studs without encasement in concrete. A significant number of stress ranges were investigated in order to develop an appropriate S-N curve. The results of this investigation were rather conservative since there would be inherently little danger of fatigue failure of shear stud connectors in composite beams (Sinclair 1955). At Lehigh University, King et al. (1963) incorporated Sinclair's (1955) research on the fatigue testing of bare studs and compared it to his their pushout and beam tests. The general objective of their investigation was to determine if the design of composite beams could in fact be based on data from the static and fatigue testing of shear studs in pushout specimens. To make this comparison, the appropriate S-N curves for both pushout specimens and beam tests containing 12.7 mm ( $\frac{1}{2}$  in.) shear studs needed to be developed. However, the task of determining shear stud failure in composite beam tests was an issue that had not been addressed in prior studies. After considerable investigation and research it was found that the use of local distortion strain gages directly underneath the shear stud on the bottom side of the top flange was the best way to

determine shear stud failure. The high readings on the distortion gages showed large localization of stresses in the base metal. This combined with equivalent shear stresses on the connectors may have been the reason for typical failure in the heat-affected zone of the base metal. Generally, the results of the push-out tests fell below that of the beam test. However, it appears that the push-out test can be a fast, efficient, and cost effective way to forecast the behavior of mechanical shear connectors in composite beams (King et al. 1963). The difference between the pushout and beam specimen could be associated with what is commonly known as the “size-effect.”

One of the first tests in fatigue behavior took place at Lehigh University in the earlier 60's, where Driscoll et al. (1963) tested twelve beams with 12.7 mm ( $\frac{1}{2}$  in.) diameter stud connectors. The objective of these tests was to verify if design of the shear studs was reliable. Previous tests such as the push-out test were used to compare with their experiment. The stud failures were generally located at the heat-affected zone, i.e., the studs failed by shear. After bond failure, the loss of interaction was directly proportional to the decrease of the stud horizontal section during application of the load.

The main issue in the past was to determine if the push-out test was an accurate and reproducible procedure for determining the shear capacity of different types of connectors. Prior to 1965, the comparison between the two types of tests, the push-out test versus tests on composite beam specimens, was not possible for determining a relationship between the strength results of the shear studs. Therefore, this correlation could not be used in bridge design. After further studies by Slutter and Driscoll (1965), the comparison proved to be effective and was accepted by many researchers in the country, allowing designers to base their bridge design calculations on this knowledge.

The push-out test was originally a static test. However, researchers later began using dynamic or fatigue tests, which allowed for a better estimation of the time-dependence strength of the material. In the same year, Lehman et al. (1965) performed push-out tests on 14 specimens using studs of 19 mm ( $\frac{3}{4}$  in.) diameter and light-weight concrete. They tested

specimens under static and fatigue conditions to investigate the effect of shear stress range and maximum stress in each stud. The studs were placed in pairs, 152 mm (6 in.) on center. The bottom of the specimen was fixed to prevent lateral movement of the slab during testing. The instrumentation was located in such a way as to measure stud deterioration during the fatigue test. Fracture of the stud connectors normally took place at the bottom of the steel beam flange. Shearing occurred at different instances and different frequencies for each stud position in the same group of four stud connectors. They concluded that fatigue strength is independent of the maximum applied load, and that stress range plays an important role in the fatigue life of the stud. The slip was found to be independent of the fatigue life and fatigue values were higher once the test lasted less than one million cycles.

Toprac (1965) also analyzed 7 beams for composite action. He divided the beams into two distinct groups with three and four beams in each group. All groups had 19 mm ( $\frac{3}{4}$  in.) diameter headed steel studs and ready-mix concrete for the slabs. A thin layer of oil was applied on the steel beam surface to reduce the friction between the steel and concrete forcing the stud connectors to resist the shear load. The mode of failure of the specimens was by shearing of the studs. Analysis was based on the instant that the load suffered a considerable decrement. The results proved that the 19 mm ( $\frac{3}{4}$  in.) diameter studs had a lower fatigue life than the 12.7 mm ( $\frac{1}{2}$  in.) diameter studs. He concluded that studs have a progressive loss in their performance, while slip and deflection are not analogous to stud failure. The comparison between the 12.7 and 19 mm ( $\frac{1}{2}$  and  $\frac{3}{4}$  in.) studs showed that there was in fact a significant "size-effect" on the order of 20.7 MPa (3 ksi), with the 19 mm ( $\frac{3}{4}$  in.) studs having a shorter fatigue life than the 12.7 mm ( $\frac{1}{2}$  in.) studs.

Mainstone and Menzies (1967) performed push-out tests on three different types of shear connectors, studs, channels and bars. The shear studs were configured in two studs parallel to the shorter dimension of the steel bar with dimensions of 19 mm ( $\frac{3}{4}$  in.) in diameter by 102 mm (4 in.) in length. Two different tests were implemented; the push-out test and the beam test. Initially, the specimens were 152 mm (6 in.) thick, however, within the progress of the project these dimensions were changed to 229 mm (9 in.). The concrete was cast-in-place (CIP). The

specimens were tested in fatigue, and static with and without reverse load. Cracking in the slabs occurred at 60 to 85 percent of the ultimate load. However, separations appeared well below the ultimate load in the majority of the cases. In a specific case, the base of one specimen was fixed to study the slab behavior for this type of condition. The relationship established by Mainstone and Menzies between load and mode of failure indicated that if the ultimate load is high, the stud fails in shear and respectively if it is low, shear and tension generate failure. Proportionality of the slip increment and separation was verified by these tests. The results showed that slabs without fixity at the base had stud strengths 10 percent less than the strength indicated in the code (CP 117 19). The authors reported that the percentage of static strength is not a useful parameter when it is compared with the fatigue strength, once the mode of failure in the static method tests occurs in the stud and not in the weld.

In the late 1970's, the Metropolitan Atlanta Rapid Transit Authority system organized a program managed by Rabbat and Hanson (1979) to perform push-out tests. Their study was initiated with interest in analyzing the viability of using bolted connections with precast slab units. The load was applied initially as static load, then fatigue and finally static testing until failure. The conclusions indicated that once the pre-load increased, the slip measurements decreased.

In 1983, Dedic conducted a study at the Research Institute of Iowa State University involving the testing of conventional mechanical shear connectors commonly used today, and the feasibility of strengthening pre-existing composite, single span bridges by use of high strength bolt connectors. Push-out tests were performed on 22 specimens to explore the behavior and ultimate strength of different types of connectors. The specimens were divided into two group sizes; one full-scale and the other half scale. The studs were fixed to the beam by two different methods, bolting and welding. The slabs were cast in two different manners; direct contact with the beam and separate from the beam. His measurements revealed an excellent agreement in ultimate strength and load-slip, while addition of shear connectors affected the load slip behavior. Pushout specimens consisted half-scale and full-scale specimens. Four beams were also fabricated by cutting up sections of a previously constructed half-scale bridge model. The

shear capacities of the beams were less than that required by AASHTO bridge standards. Thus, additional shear connectors in the form of high strength bolts double-nutted to the top flange of the beam were added. The test results showed that there was a deviation in the ultimate strength characteristics of the bolted connectors compared to those of the welded studs. This was attributed to the large difference in tensile strengths between the two connectors, as well as the friction, which had to be overcome since the slab was fastened to the beam by the bolt. It was concluded that high-strength bolts attain a higher ultimate strength than welded shear studs and can be used as shear connectors with little or no difference in the strength or behavior from that of welded shear stud.

In 1993, the Ministry of Transportation of Ontario selected precast concrete deck panels for the reconstruction of a portion of the Queen Elizabeth Way Welland River Bridge in order to minimize the time of bridge closure. To establish a design criteria and ensure an acceptable performance of the full-scale slabs, an extensive research and test program was conducted. The design of the shear connections in this case was governed by fatigue considerations. Therefore, a cyclic load testing program was conducted to determine the fatigue characteristics of the shear connections being used. This test program consisted of static and fatigue testing of shear connections which varied in height, spacing, and configuration. The various patterns were used to determine the relative effectiveness of shear transfer of the stud configurations in a group. The test results show that in a dense configuration of shear studs, studs of non-uniform lengths prove to be more effective by eliminating the potential of having a plane of weakness in a slab fabricated by having all of the connector heads in one plane.

Farago et al. (1993) related their experiment with shear studs for evaluating the performance of future installation of precast panels in the Welland River Bridge in Canada. The precast system was adopted since it was a viable alternative in terms of shortening the time of construction as well as its economic impact. Their objectives focused particularly on the effectiveness of closely spaced shear studs and composite action in comparison to widely spaced groups of studs. As a result, static and fatigue loading were applied on several push-out specimens. A 60 mm haunch filled by grout was used between the steel and precast concrete

slab. However, the number of studs and respective height as well as their configuration were variables in the experiments. They concluded that the variation of shear stud height in a particular group improved the performance of the group, hence composite action.

In 1995, Gulyas et al. reported their evaluation of precast panel keyways. The experiments consisted of shear and tensile tests. The results showed moderate advantages for the use of set 45 in hot weather. The keyways were submitted to different types of environmental exposures. The performance was reduced for the set 45 hot weather specimens with carbonated surfaces. They concluded that systematic bond failure exists in carbonated surfaces and that composite testing is more practical than testing the physical properties of each material.

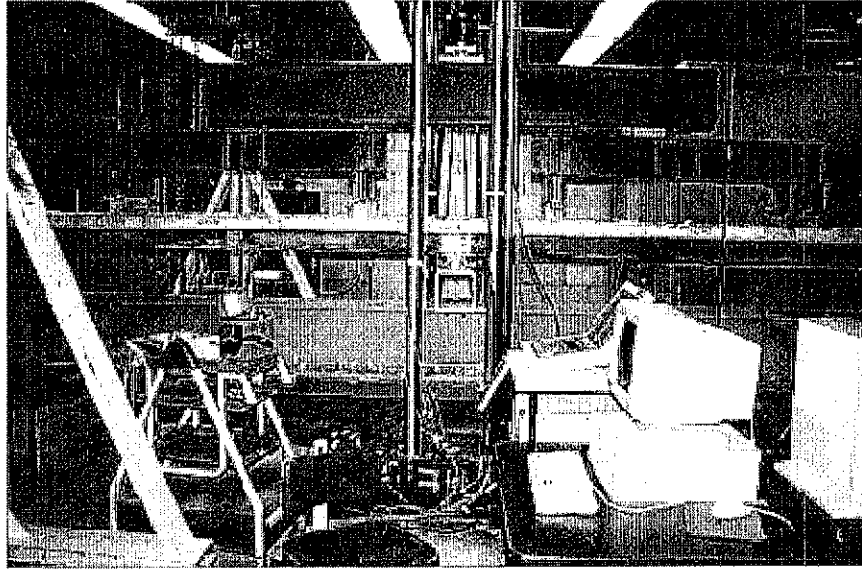


Fig. 2.1 Quarter-scale HS20 truck loading beams

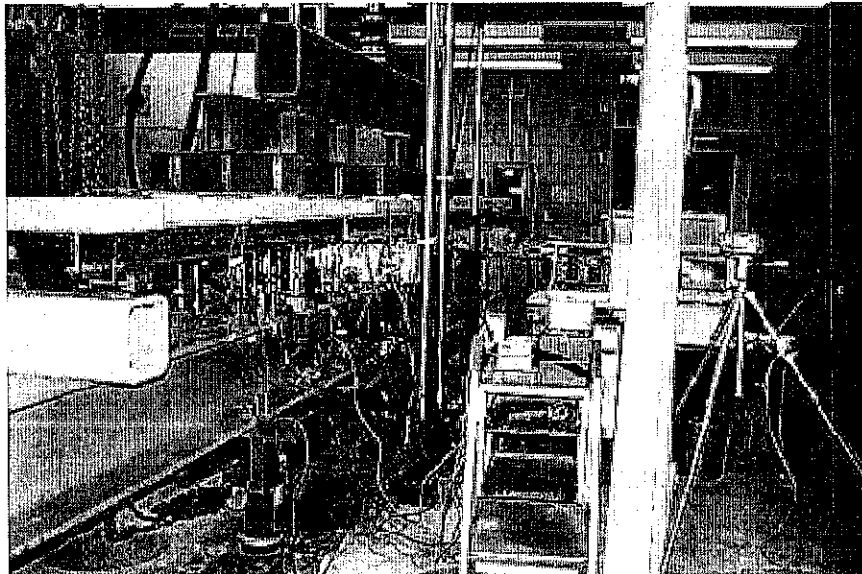


Fig. 2.2 Test setup

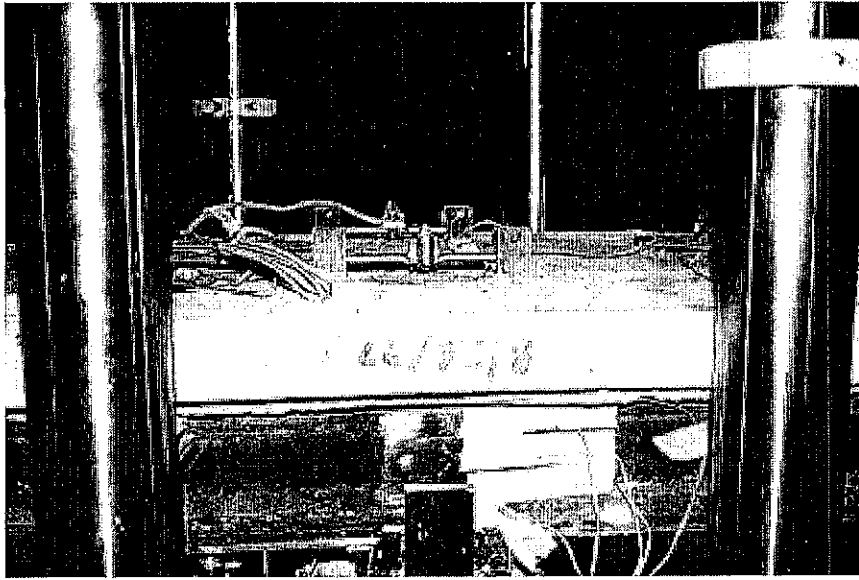


Fig. 2.3 Vibrating wire strain gages



Fig. 2.4 Placement of panels

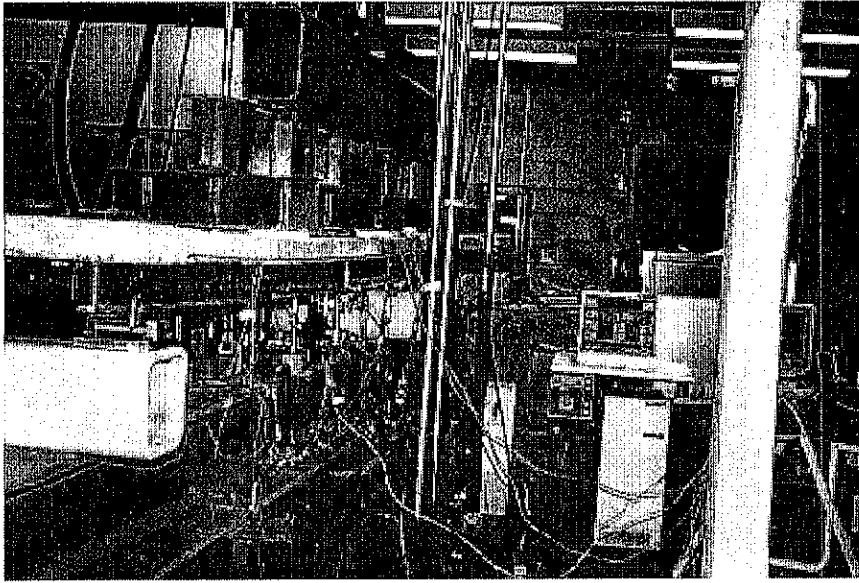


Fig. 2.5 Deflected bridge

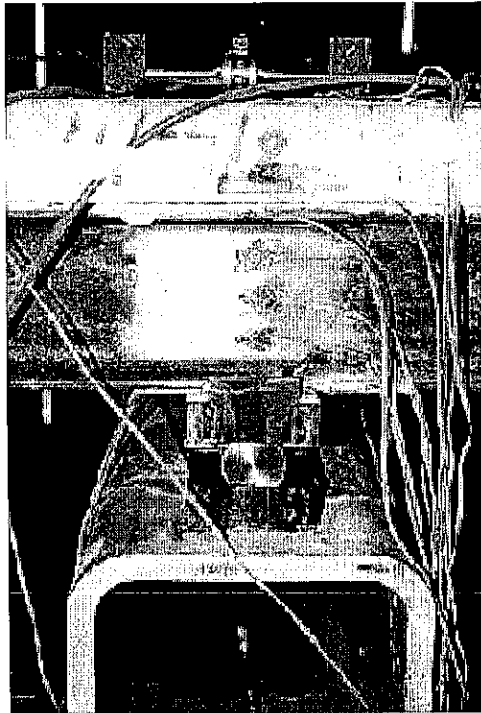


Fig. 2.6 Crack in beam at central support

### **3. FINITE ELEMENT ANALYSIS**

Finite element analysis provides a valuable tool in the prediction of the performance of structures as well as in the detection and evaluation of damage and failure mechanisms of the different components comprising the structure. A structural system is an assemblage of a number of elements with different material properties, and their combined action results in an improved performance. Finite element analyses were carried out for the composite behavior of the deck, for the direct shear behavior of grouting materials, and for the complete bridge deck system incorporating the material and structural non-linearities.

#### **3.1 Push-Out Specimens**

Elastic and non-linear finite element analyses were conducted to determine the composite behavior of the shear connection. Details of the modeling for elastic analysis by using ALGOR and non-linear analysis by using ANSYS are explained in the following section.

##### **3.1.1 Elastic Finite Element Analysis**

Two configurations of the shear connection test were modeled as shown in Figs. 3.1 and 3.2 using finite element analysis software ALGOR. The mesh generation depicting one pocket and two pockets are shown in these two figures, respectively. Symmetry was used to model these two configurations, where only half of the beam and one panel are modeled. However, appropriate boundary conditions were imposed on the models to simulate exact conditions for the full scale configurations. Figs. 3.1 and 3.2 also depict the applied loading on the beam. This loading was distributed on the top of the beam since it is simulating a plate between the applied loading and beam. Separate models were prepared for the beam, panel, haunch, pockets, studs, and reinforcing steel since the materials used are different for each component.

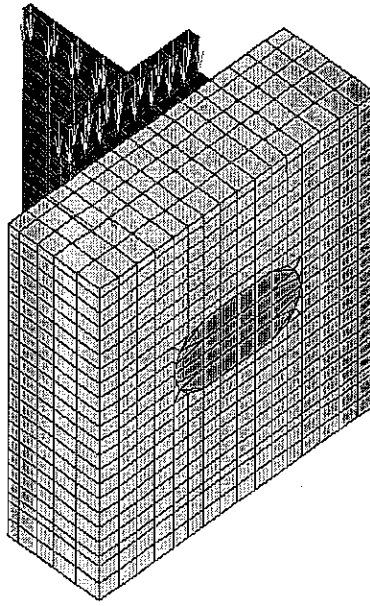


Fig. 3.1 Mesh generation for single pocket configuration

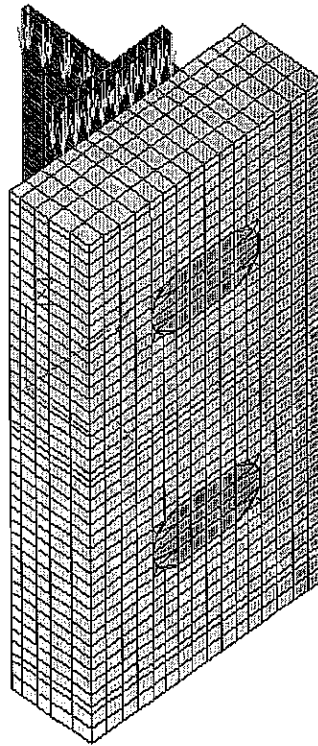


Fig. 3.2 Mesh generation for double pocket configuration

### 3.1.2 Non-Linear Finite Element Analysis

Three-dimensional non-linear finite element analyses were performed to simulate the push-out tests. The models consist of concrete slabs, shear pockets, haunch grouting materials, steel beams, shear connectors, as well as mild steel reinforcing bars. The materials comprising each of these components display non-linear behavior, and in order to achieve the desired performance, material properties had to be accurately modeled.

Modeling of the push-out specimens was performed using the structural analysis software, ANSYS. Six element types were used for the finite element discretization of the models. The concrete slabs were meshed using a special solid element type that is capable of depicting the failure of concrete in cracking or crushing. The same element type was used for modeling the grout used in the shear pockets and the haunches. Beam elements were used for modeling the shear connectors, and reinforcement bars were meshed using truss elements. The interface between the steel beam and concrete haunch was modeled using contact and target elements.

#### Geometry of the Specimen and Elements Used

Geometry of the push-out model was modeled with the actual dimensions of the specimen. For the full-scale model, the mesh size ranged between 6.6 mm (0.259 in.) element edge width in regions where a finer mesh was required and 50.8 mm (2.0 in.) edge width in regions where a coarser mesh was used. For the quarter-scale model, the mesh size ranged between 4.3 and 38 mm (0.168 and 1.5 in.). This was an optimum size to accommodate the model in the most efficient manner. Due to symmetry, only half of the specimen was modeled in order to minimize run time requirements. The model was restrained against lateral translations in all three directions at the bottom of the slab, while symmetry boundary conditions were imposed at the cut section of the steel beam. Load was applied in uniform distribution on the top surface of the web and flange thickness. Figures 3.3 and 3.4 show typical mesh for the push-out test specimens with one- and two-pocket specimens, respectively.

Basic input parameters for the concrete material include uniaxial compressive strength, and shear transfer coefficients for open and closed cracks. Compressive strength for the concrete slab was 7000 psi with an elastic modulus of 4,700 ksi, and Poisson's ratio of 0.15. Grout for the haunch and shear pocket had a compressive strength of 8100 psi, an elastic modulus of 5,100 ksi and Poisson's ratio of 0.15. Shear transfer coefficients for an open crack was assumed to be 0.6, and for a closed crack it was assumed to be 0.75 for both materials. Steel yield strength was 36 ksi with an elastic modulus of 29,000 ksi and Poisson's ratio of 0.3, while for shear connectors, yield strength of 72 ksi and an elastic modulus of 29,000 ksi was used. For modeling the slab-beam interface, the surface of the slab was considered to be the target surface and the adjacent surface of the beam flange was the contact surface. A standard contact option is used in which sliding is permitted and controlled by friction.

#### Analysis Procedure

Analysis was performed using a step-wise procedure tracing the load-displacement response throughout its complex path. A Full Newton-Raphson Method was used for the solution process. In this method, the stiffness of the model is updated at the beginning of every iteration within the load step, to reflect element status based on the previous converged solution. Load is applied in a step-wise process to smoothly depict the structural response of the pushout test specimen. Displacements, stresses, strains, and reactions were obtained at each load step.

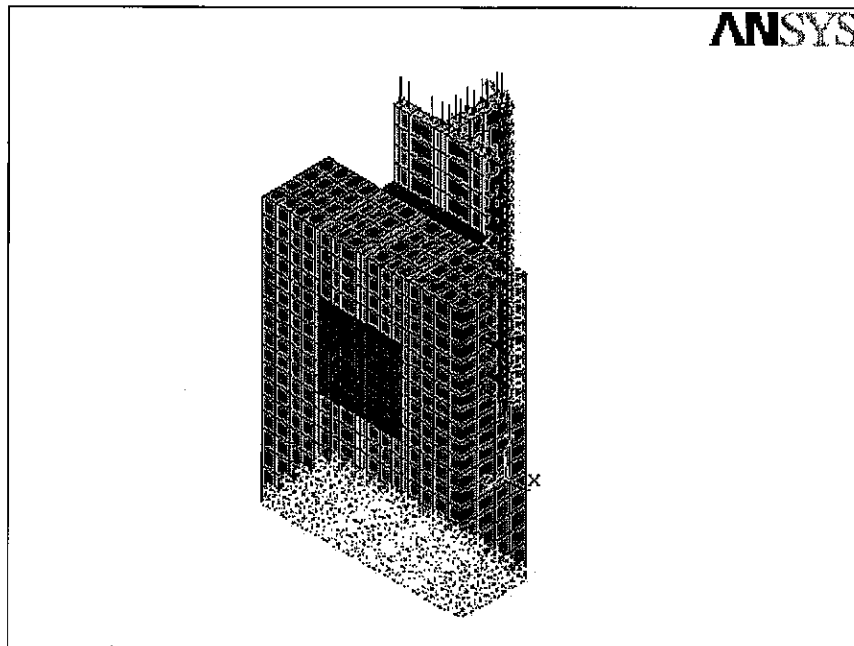


Fig. 3.3 Typical finite element mesh for pushout test model with one pocket

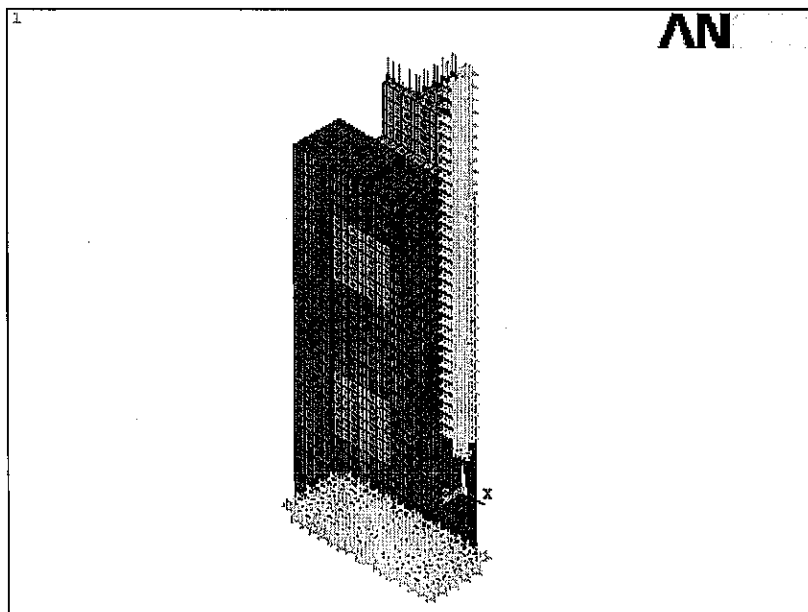


Fig. 3.4 Typical finite element mesh for pushout test model with two pockets

### 3.2 Direct Shear Test

Non-linear finite element analysis was performed for the direct shear test specimen using ANSYS. The main objectives of this analysis was to determine stress distributions and modes of failure for the joint using each of the four types of grouting material, namely, set 45, set 45 hot weather, set grout, and polymer concrete. The exact geometric configuration of the specimen was meshed using SOLID65 elements which are brick elements capable of depicting the nonlinear behavior of concrete and its failure in cracking or crushing. A maximum element size of 1 in. was adopted for the discretization of the model, and a full Newton-Raphson algorithm was employed to trace the solution path. The bottom flange of the specimen was restrained against translational motion and load was applied on the top flange of the specimen as shown in Fig. 3.5. Lateral movement of the two slabs was also restrained to prevent bending.

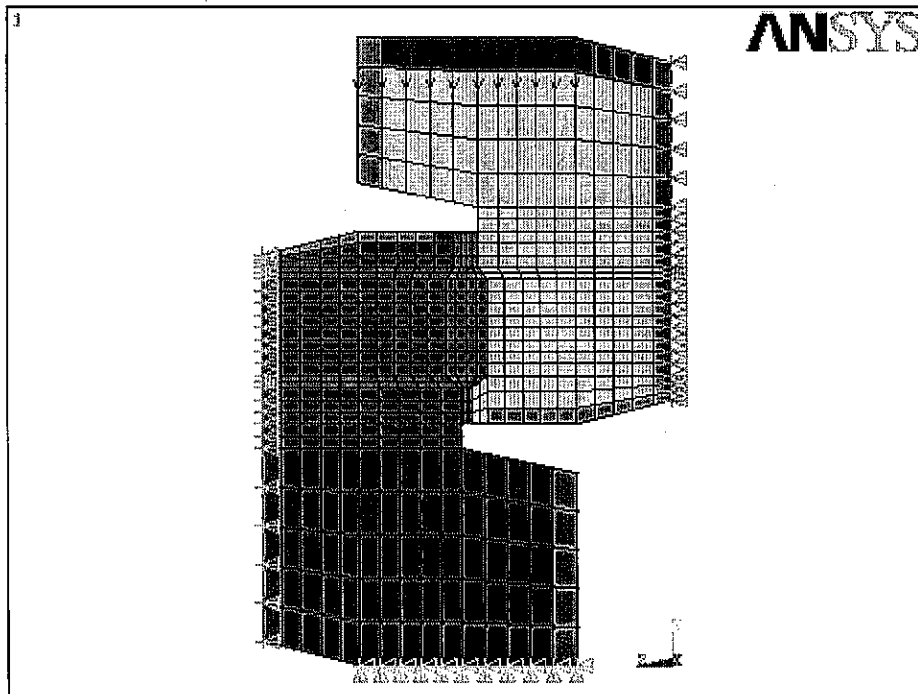


Fig. 3.5 Finite element mesh and boundary conditions

### **3.3 Finite Element Analyses of Full-Depth Bridge Deck System**

The prototype bridge deck was modeled using a three-dimensional finite element procedure in order to predict the response of the system under applied loads. The prototype deck system consists of concrete panels, grouted shear pockets and transverse joints, shear studs, post-tensioning steel, and mild reinforcing steel. The materials comprising each of these components display non-linear behavior, and in order to achieve good prediction of the expected performance, material properties had to be accurately modeled. The non-linear solution procedure is an iterative process in which several iterations are performed within each time step until a converged solution can be attained. The stiffness of the whole system is continuously updated to reflect the changing status of the model.

The prototype deck system was modeled using ANSYS structural analysis software. Four types of elements were used for the finite element discretization of the model. Concrete components and grouted joints were meshed using a special solid element type that is capable of depicting the failure of concrete in cracking or crushing. Post-tensioned tendons were modeled using cable type elements, which are axial elements with tension-only capability. Reinforcing bars were modeled using truss type elements capable of taking tension and compression.

A preliminary analysis was performed using a step-wise procedure in which prestressing effects were evaluated as an initial step prior to the application of superimposed loads. Vertical and lateral displacements, stresses, strains, and reactions were obtained for each load case. The following sections give a detailed description of the analysis.

#### **3.3.1 Geometry of the Prototype Model**

The geometry of the prototype was modeled, to the extent possible, to match the actual configuration. It was crucial to have a mesh that is fine enough for the smooth computation of stresses and strains since their variation is highly mesh dependent. SOLID65 and SOLID45,

BEAM188, LINK8, and LINK10 elements were used to represent concrete decks and grouted joints, steel beams, shear studs, post-tensioning bars, and post-tensioned tendons, respectively.

### Precast Panels

Solid elements were used to mesh the concrete components of the deck and transverse joint. To depict the non-linear material behavior of concrete, SOLID65 elements were employed for the purpose of meshing the precast panels, shear pockets, and transverse joints between the panels. SOLID65 is a three-dimensional reinforced concrete solid element with the capability of depicting concrete failure in crushing and cracking. Eight nodes, with three translational degrees of freedom at each node, define the element as shown in Figure 3.6. Reinforcement behavior can also be modeled via the rebar capability of the element. These rebars are capable of carrying tension and compression as well as plastic deformation and creep. The material model for this element predicts elastic behavior, cracking behavior, and crushing behavior beside plasticity and creep. Cracking can occur in three orthogonal directions and is represented by introducing a plane of weakness in a direction normal to the crack face. Shear transfer coefficients representing shear strength reduction are required for controlling shear sliding across the face of the crack. Crushing is assumed to occur if the material fails in compression at any point. Crushing is considered as a complete loss of structural integrity of the material due to strength degradation.

Basic input parameters for the concrete material include uniaxial compressive strength, uniaxial tensile strength, and shear transfer coefficients for open and closed cracks. Elastic modulus and Poisson's ratio are also required for the material description.

For the deck panels model, the following material properties are used:

Concrete compressive strength:	7,100 psi
Concrete tensile strength:	700 psi
Concrete modulus of elasticity:	$5.4 \times 10^6$ psi
Shear transfer coefficient, closed crack:	0.90
Shear transfer coefficient, open crack:	0.75

The grouting material for the shear pockets and transverse joints was modeled using the following properties:

Grout compressive strength:	6,200 psi
Grout tensile strength:	600 psi
Grout modulus of elasticity:	$4.8 \times 10^6$ psi
Shear transfer coefficient, closed crack:	0.90
Shear transfer coefficient, open crack:	0.75

Output for these elements include stress and strain distributions, nodal forces and deflections, and cracking and crushing of concrete.

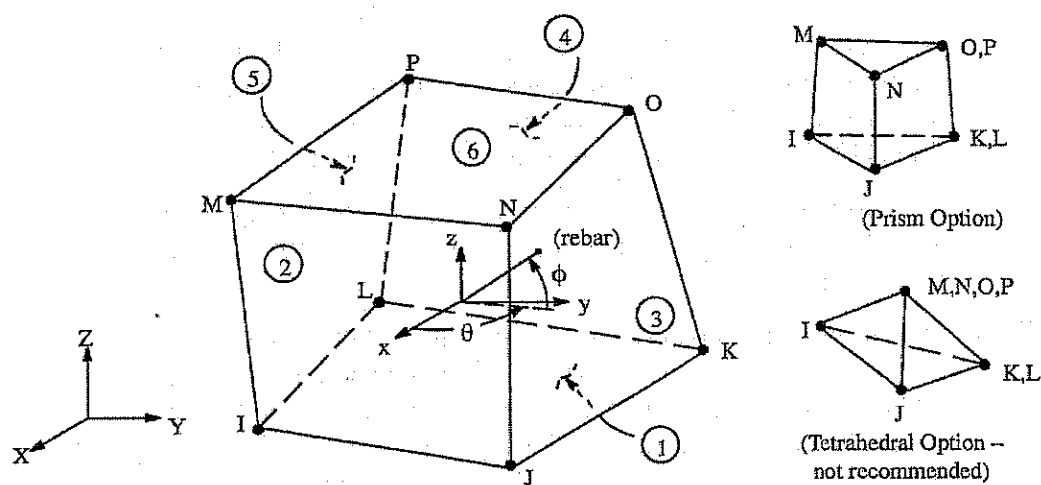


Fig. 3.6 SOLID65 (3-D reinforced concrete solid)

## Steel Beams

The steel beams were modeled using SOLID45 elements, which are solid elements defined by eight nodes in the three-dimensional space. This element is capable of depicting plastic behavior. Output includes displacements, and stress and strain distributions. Figure 3.7 shows the general description of the element.

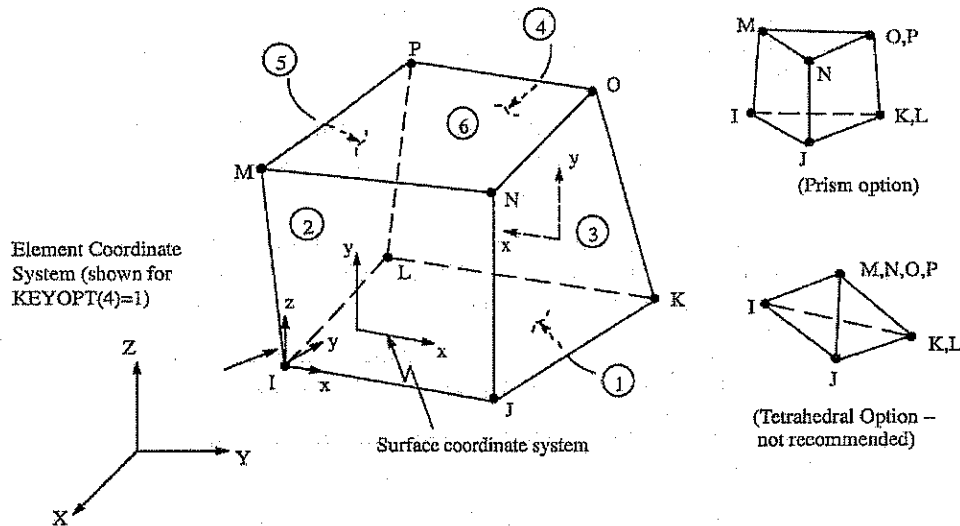


Fig. 3.7 SOLID45 (3-D solid)

## Shear Studs

The shear studs were modeled using BEAM188 elements. These are nonlinear beam elements defined in the three-dimensional space by two nodes and a line connecting the two nodes as shown in Figure 3.8. The elements are capable of undergoing large deformations, bending, and can have nonlinear material properties. Output for these elements includes stresses, strains, displacements, rotations, nodal forces, and nodal moments.

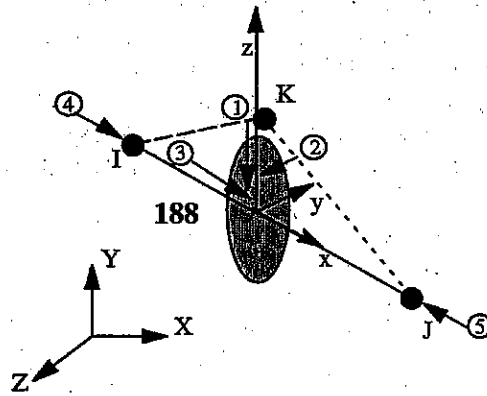


Fig. 3.8 BEAM188 (3-D line element)

### Post-Tensioning Tendons

Post-tensioning tendons were represented, in the finite element mesh, using LINK10 elements. These are three-dimensional cable elements with either tension-only or compression-only capability. The cable element is defined in the 3-dimensional space by two nodes with three translational degrees of freedom per node as illustrated in Figure 3.9. Prestress is defined by inducing an initial strain in the element. The changing status of the element across the solution is taken into account at each load step. Required input data include cross-sectional area, initial strain, and isotropic material properties. Tendon groups were represented using one line for each location with an equivalent diameter. The same initial strain equivalent to the actual prestressing forces applied in the tendons was input as a real constant for this element.

Output for this type of element includes nodal displacements, axial force, stress, strain, and status, slack or tension, at the end of each solution step.

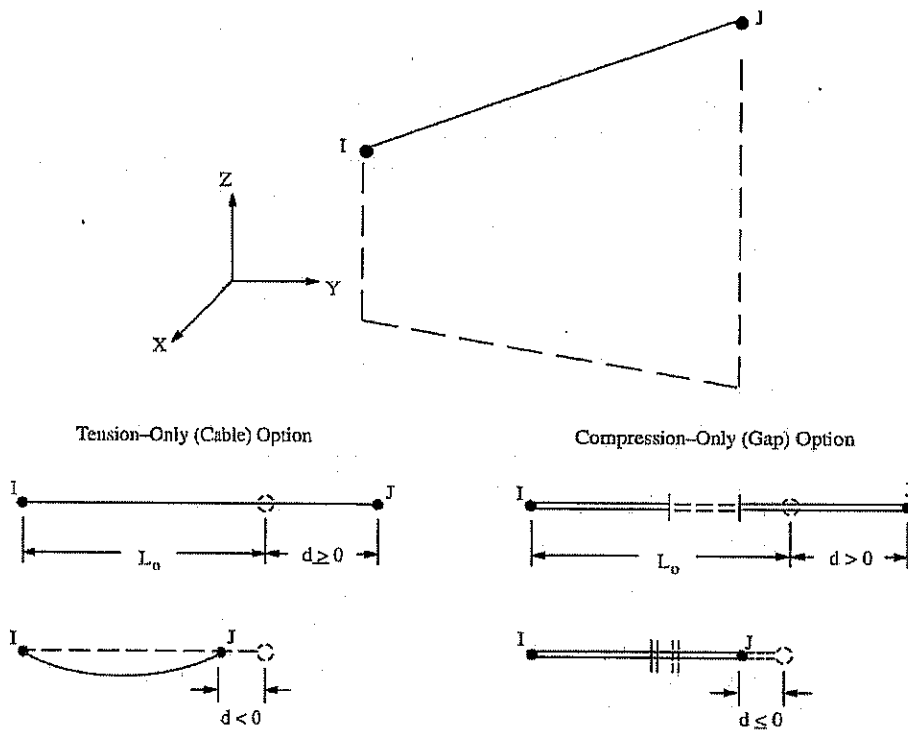


Fig. 3.9 LINK10 (Tension-only or compression-only spar)

### Post-Tensioning Bars

LINK8 elements were used for the post-tensioning bars. These are two-node truss elements with tension and compression capability. Three degrees of freedom are allowed at each node, as well as plasticity, creep, swelling, stress stiffening, and large deflections. Figure 3.10 shows the geometry, node locations, and coordinate system for this element. Input data include cross-sectional area, initial strain equivalent to the actual post-tensioning force, and material properties. Output data include nodal displacement, axial force, stress, and strain.

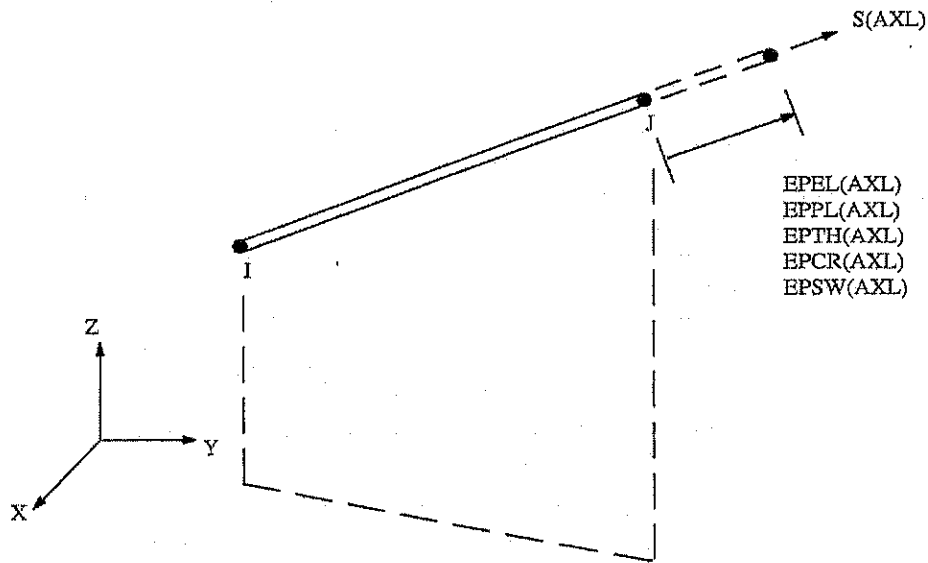


Fig. 3.10 LINK8 (3-D Spar)

### 3.3.2 Static Analysis Procedure

Analysis of this model involved nonlinear material properties as well as changing status elements. Due to these factors, a Full Newton-Raphson Method was used for the solution process. In this method, the model stiffness is updated at the beginning of the load step as well as at the beginning of the iteration within the load step, to reflect element status according to the previous converged solution. Load was applied in a step-wise process to smoothly depict the structural response of the deck system under self-weight, prestress, and imposed live load.

Loads were applied at the locations corresponding to the truck locations for cases simulating maximum negative bending moments and maximum positive bending moments. The analyses were carried out for six cases such as service positive, service negative, overload positive, overload negative, ultimate positive and ultimate negative loading. For service load application, a total load of 93.6 kips, simulating AASHTO HS-20 truck was applied at four locations. An impact factor of 1.3 was used. For over load cases, load corresponding to 1.5

times the service load was applied. At each load location, the total load was distributed over a number of nodes to avoid stress concentrations under point loads. Figure 3.11 shows the finite element discretization of the full-depth precast deck system. Figures 3.12 and 3.13 show the meshing of the steel beams, and transverse joints. This finite element analysis was necessary to implement a detailed instrumentation plan for the full-scale bridge testing. Results obtained from the finite element analysis are shown in Figs. 3.14-3.19.

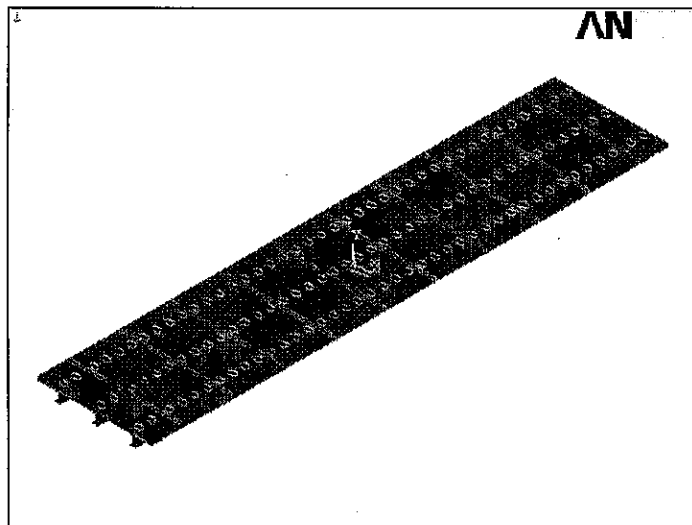


Fig. 3.11 Finite element meshing of the full-depth deck system

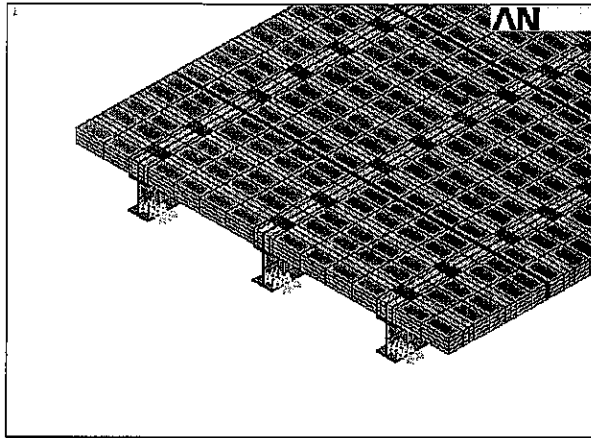


Fig. 3.12 Steel beams and precast deck meshing

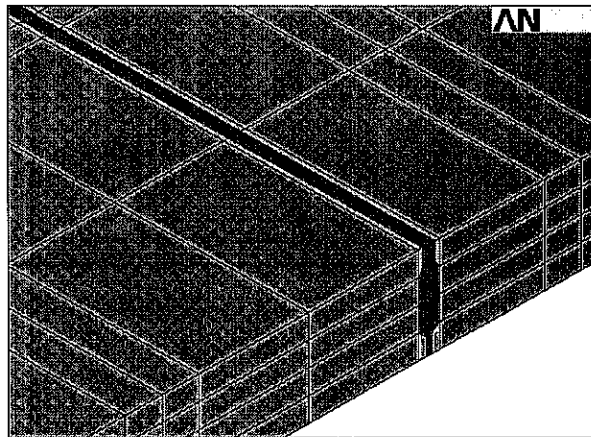


Fig. 3.13 Grouted shear key meshing

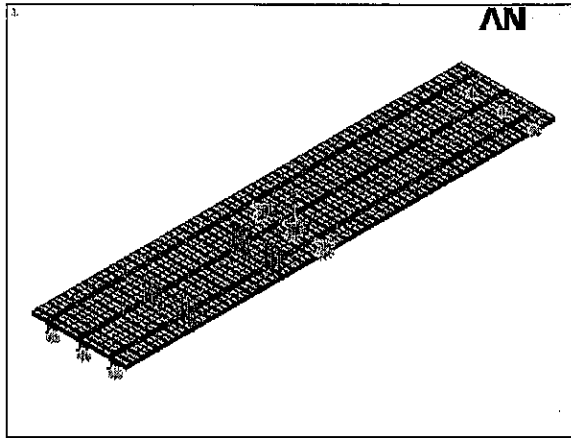


Fig. 3.14 Loading arrangement for positive service loading

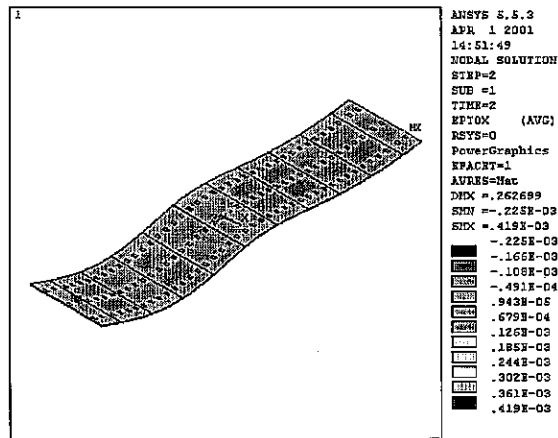


Fig. 3.15 Top strain distribution due to positive service loading

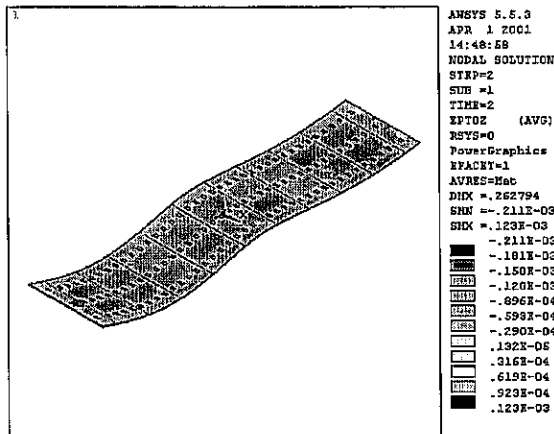


Fig. 3.16 Bottom strain distribution due to positive service loading

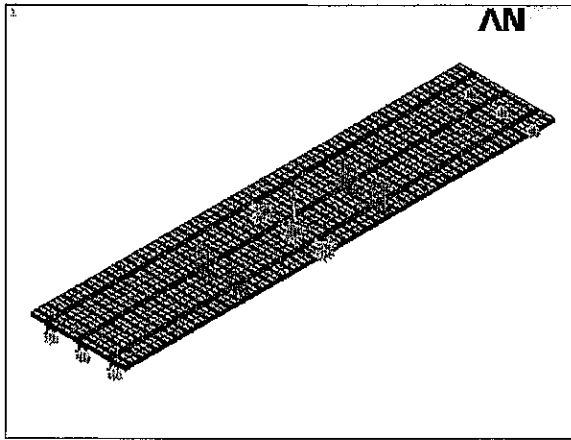


Fig. 3.17 Loading arrangement for negative service loading

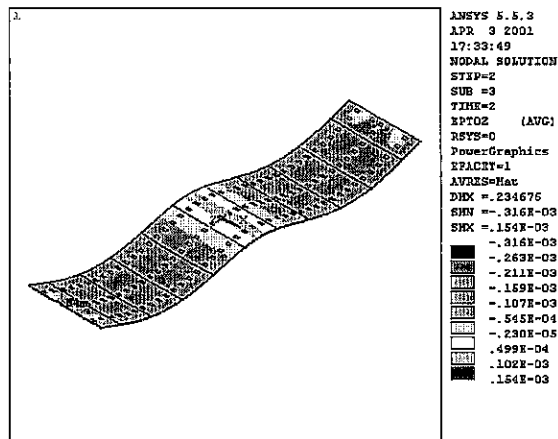


Fig. 3.18 Top strain distribution due to negative service loading

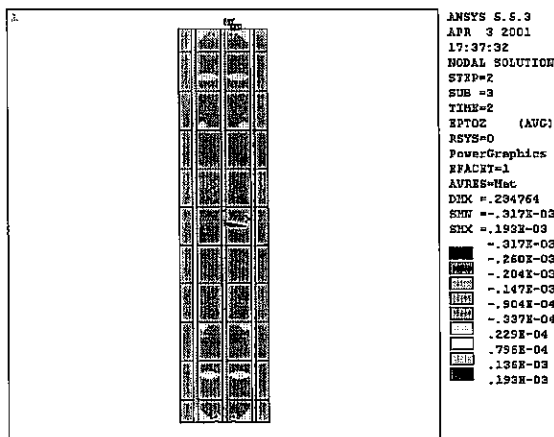


Fig. 3.19 Bottom strain distribution due to negative service loading



#### 4. EXPERIMENTAL PROGRAM

The experimental program consisted of testing a full-scale prototype bridge in the field as well as testing components of the bridge deck precast system in the laboratory. The testing of bridge components is reported in this chapter, while the testing of full-scale prototype is presented in Chapter 6. The component testing consisted of full-scale and quarter-scale shear connection systems and full-scale transverse joint testing. The shear connection tests entailed push-out tests, while the transverse joint tests consisted of direct shear, direct tensile, and flexural beam tests. The proposed full-scale bridge is a two-span continuous structure. Figures 4.1-4.3 show a typical bridge deck system supported on steel stringers with the connections between the elements depicted by the blockouts observed in the precast slab. Figure 4.1 shows the elevation of a two-span continuous bridge. Figure 4.2 presents a typical layout of the precast panels on steel girders. A typical cross section of the proposed prototype bridge is shown in Fig. 4.3.

The proposed plans show the configurations of the structural elements that are necessary to execute the experimental phase of the project (Figs. 4.4-4.6). The dimensions and details of all the structural elements are based on the results obtained from the previous study (identification and selection of related bridge systems nationwide). Transverse diaphragms will be provided at the maximum moment locations, i.e.,  $0.4L$  for the continuous bridge. In addition, diaphragms will be provided at the ends and central support. The experimental results will be used to understand the performance of the system and ultimately validate the theoretical model.

The shear connection affects the performance of the deck systems and as such the effectiveness of the proposed shear connection. The experimental program consisted of testing shear connectors in the arrangement shown in Fig. 4.7. The quarter scale and full scale shear connection tests, i.e., determination of full composite action, were performed using the dimensions and specifications shown in Tables 4.1 and 4.2, respectively. A total of twenty-eight full-scale and quarter-scale push-out specimens were fabricated and subjected to static loading. Each quarter-scale specimen was composed of a steel beam of S4 x 9.5 with 6.4 x 51 mm ( $\frac{1}{4}$  x 2 in.) long welded studs and two quarter-scale panels. The full-scale specimens included a steel

beam, W18 x 86 with 22 x 102 mm ( $\frac{7}{8}$  x 4 in.) long welded studs and two full-scale precast panels attached to both flanges of the steel beam. The width of the quarter-scale and full scale slabs were 152 mm (6 in.) and 600 mm (2 ft), respectively. The variables among the tests were the number of shear studs and the number of pockets. The most effective number of studs was determined through these tests. The original design calls for three studs in each pocket; however, additional tests were conducted to determine the optimum number of studs. Distribution of the studs is an important issue in achieving full composite action between the bridge deck and its supporting system. Figure 4.8 presents the forming for the precast panels for quarter scale. A 9.5 mm ( $\frac{3}{8}$  in.) and 25 mm (1 in.) thick haunches were cast between the steel beam flange and the precast panel for the contact length for quarter scale and full scale specimens, respectively. Slip deflections and strains were recorded. Detailed descriptions of the specimens and testing procedure are described in the next section.

Full scale tests were also conducted on the transverse joint shear key in terms of vertical shear, direct tensile strength and flexural behavior (Fig. 4.9). The forming for the panels pertaining to these tests are shown in Fig. 4.10. The materials within the joint such as set 45, set 45 hot weather, set grout and polymer concrete were also investigated. Table 4.3 lists the specimen configuration for transverse joint tests.

Table 4.1 Quarter scale shear connection test configuration

No. of pockets per side	No. of studs per pocket	Length of steel beam mm (in.)
1	1	203 (8)
1	2	203 (8)
1	3	203 (8)
1	4	203 (8)
2	1	356 (14)
2	2	356 (14)
2	3	356 (14)
2	4	356 (14)
3	1	508 (20)
3	2	508 (20)
4	1	508 (26)
4	2	508 (26)

Table 4.2 Full scale shear connection test configuration

No. of tests	No. of pockets per side	No. of studs per pocket	Length of steel beam mm (in.)
1	1	0	686 (27)
2	1	2	686 (27)
2	1	3	686 (27)
2	1	4	686 (27)
1	2	0	1295 (51)
2	2	2	1295 (51)
2	2	3	1295 (51)
2	2	4	1295 (51)

Table 4.3 Transverse joint test specimen configuration

Type of Test	Type of material	Specimen dimensions, mm (in.) width x length x height
Vertical shear	Set-45	127 x 432 x 660 (5 x 17 x 26)
	Set-45 HW (hot weather)	
	Set grout	
	Polymer concrete	
Tensile	Set-45	127 x 533 x 203 (5 x 21 x 8)
	Set-45 HW (hot weather)	
	Set grout	
	Polymer concrete	
Flexural	Set-45	152 x 533 x 152 (6 x 21 x 6)
	Set-45 HW (hot weather)	
	Set grout	
	Polymer concrete	

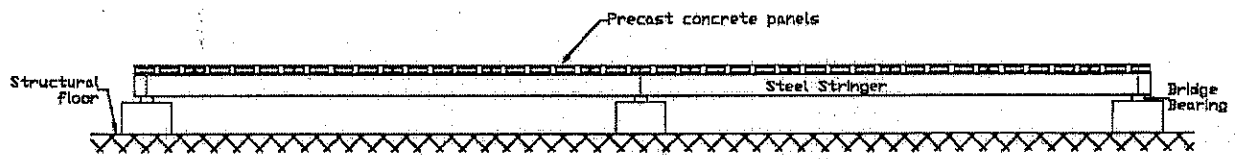


Fig. 4.1 Typical two-span continuous prototype bridge on steel girders

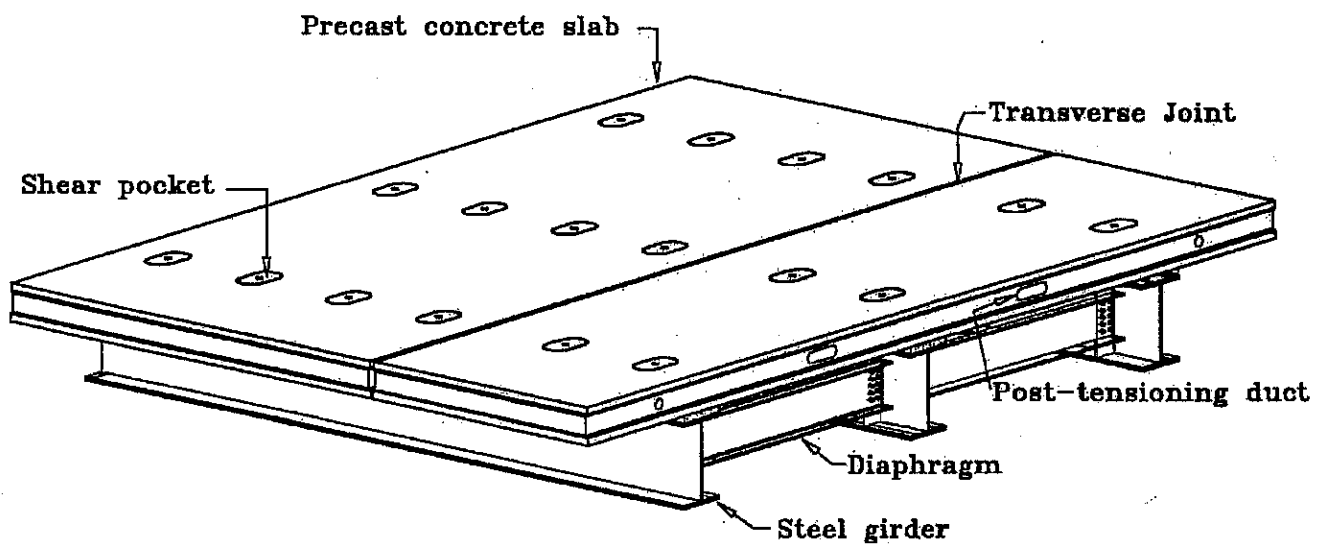


Fig. 4.2 Typical layout of precast slab on steel girders

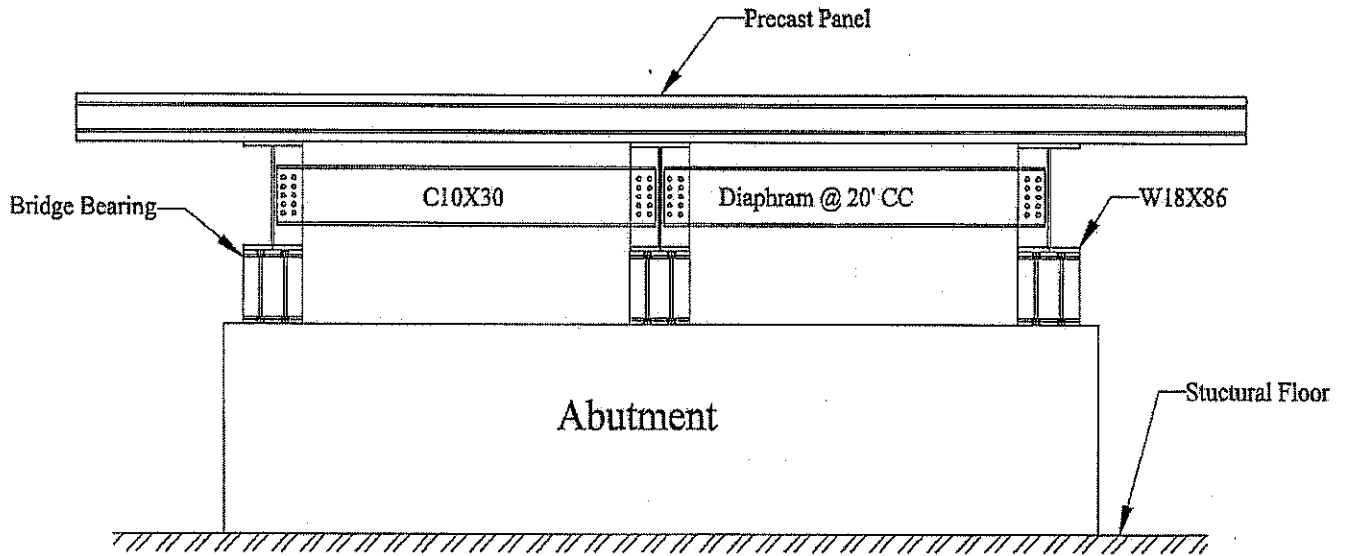


Fig. 4.3 Typical cross section for slab on steel stringers

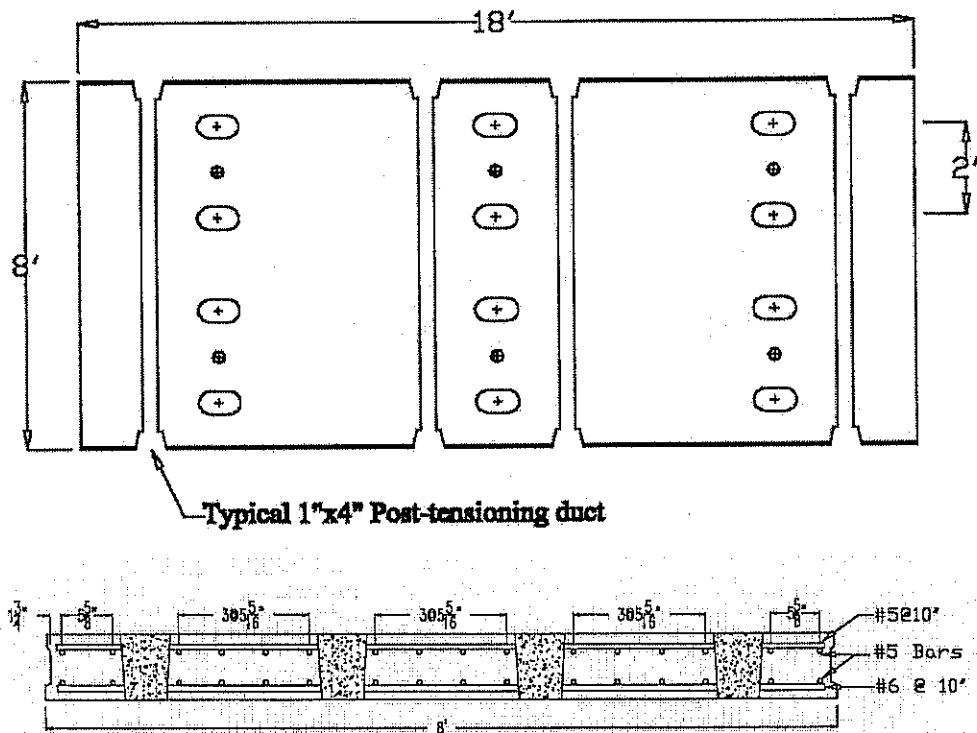


Fig. 4.4 Plan and section views of a typical precast panel

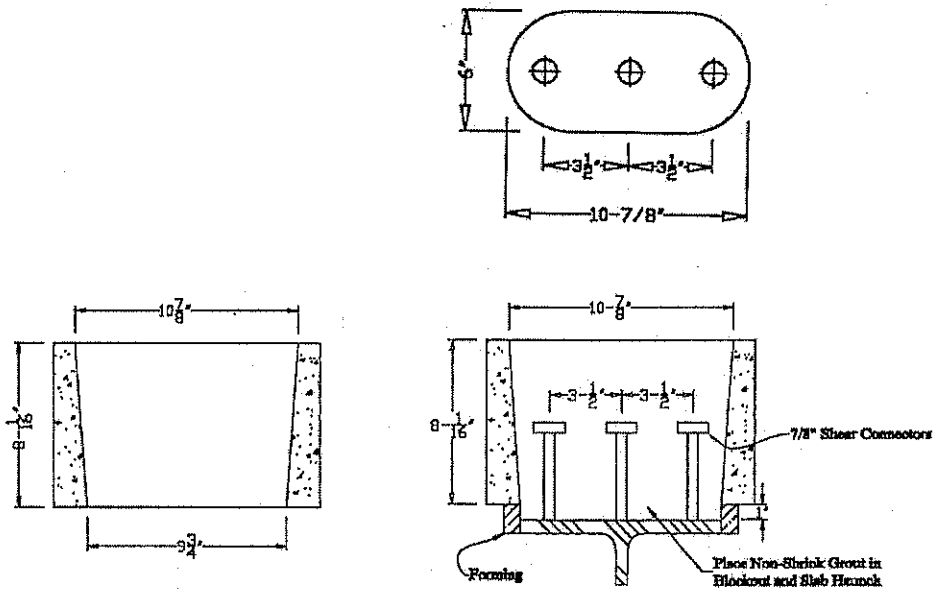


Fig. 4.5 Shear stud pocket connector details

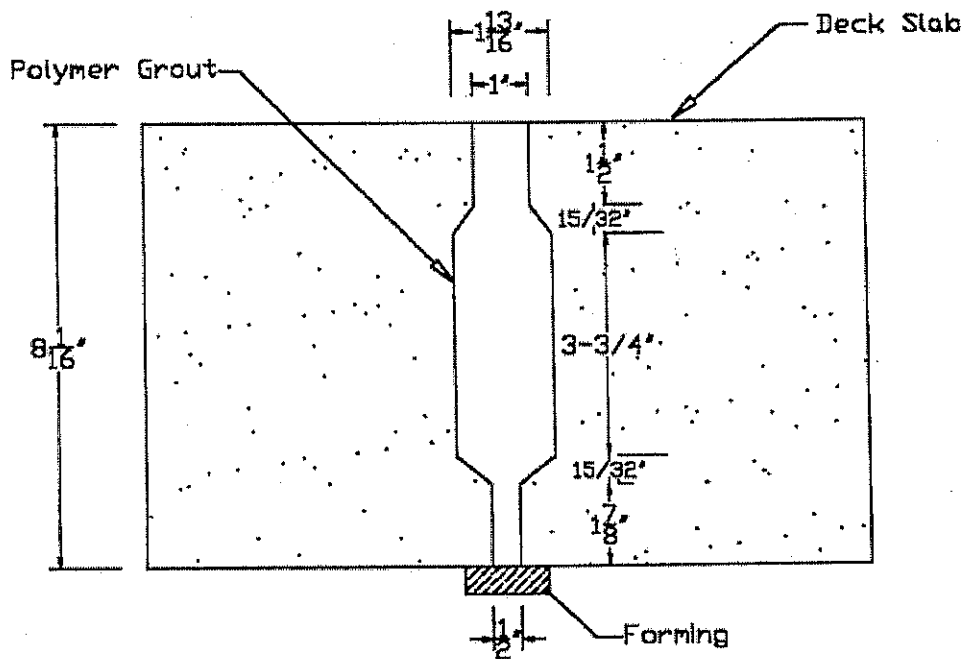


Fig. 4.6 Typical female to female type joint between precast panels

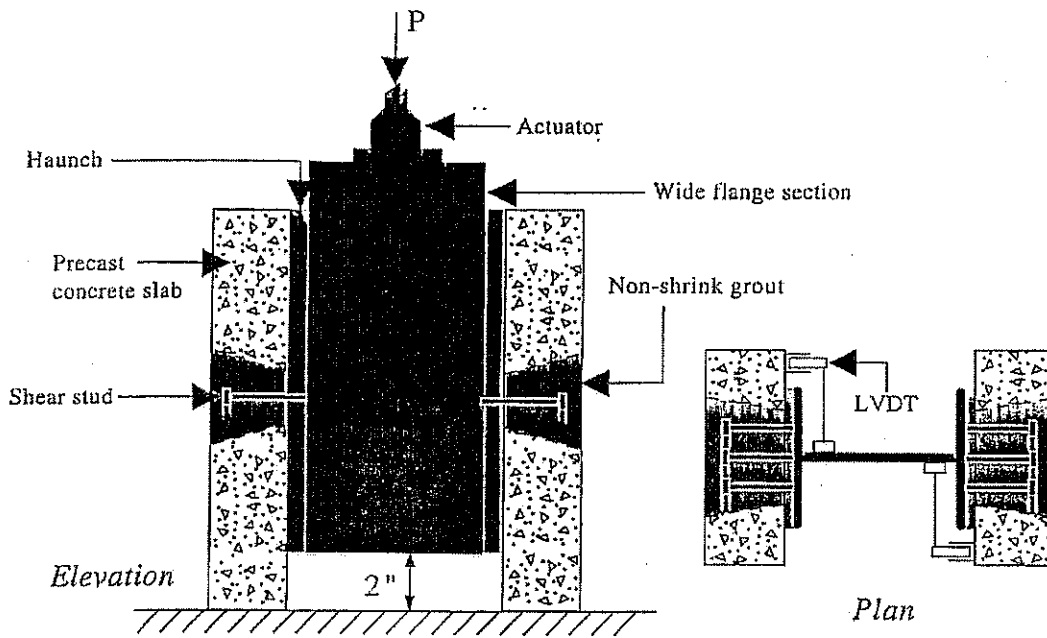


Fig. 4.7 Test setup for shear connection

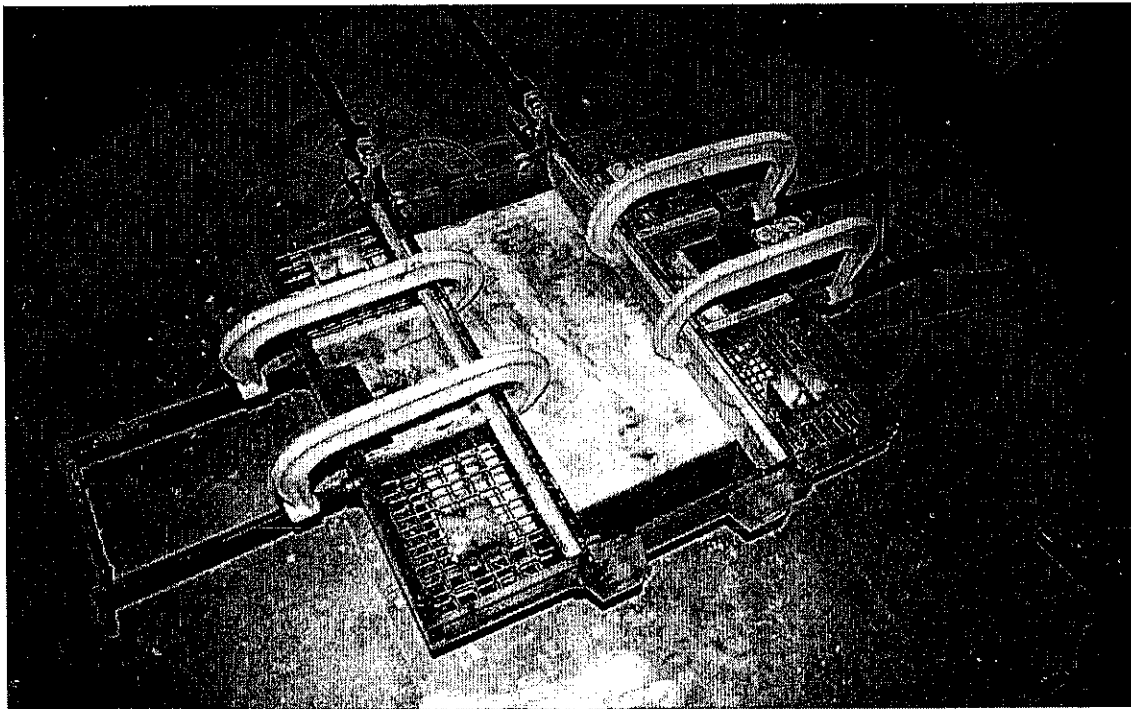
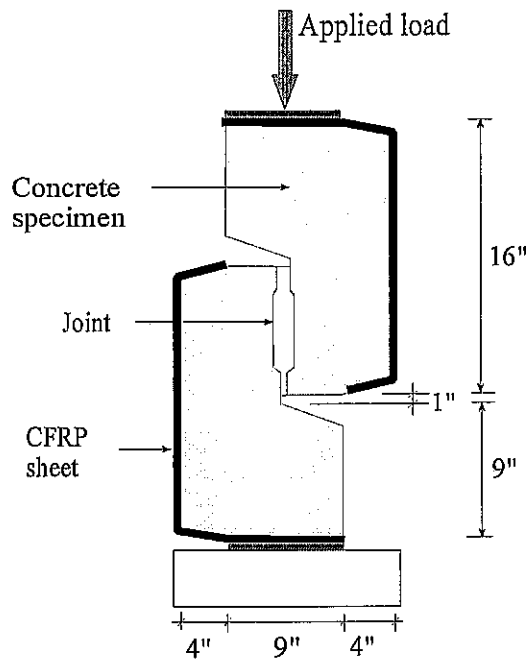
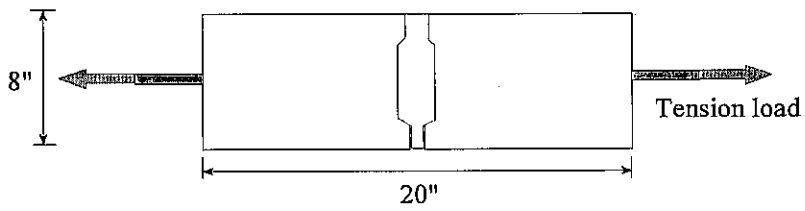


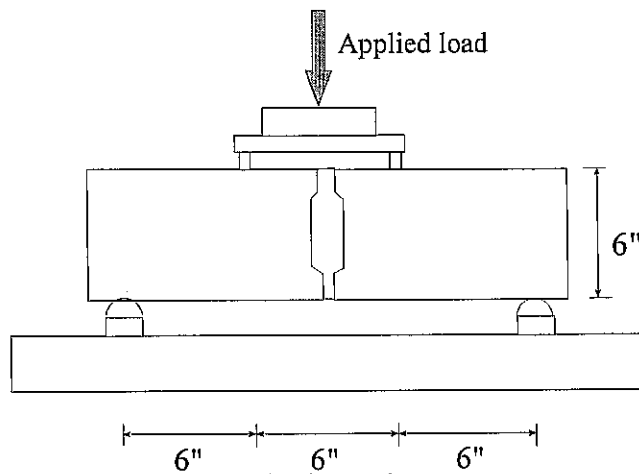
Fig. 4.8 Precast panel forming for shear connection test



(a) Vertical shear test



(b) Direct tensile test



(c) Flexural test

Fig. 4.9 Tests setup for transverse joints

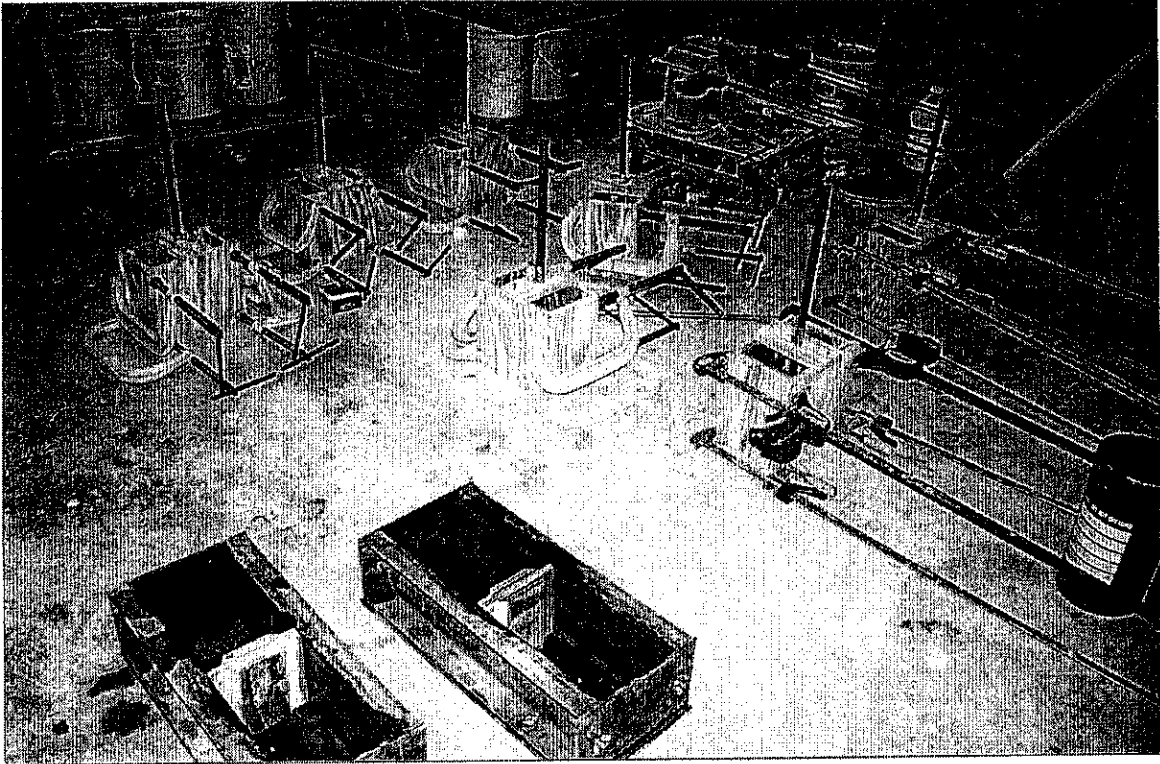


Fig. 4.10 Precast panel forming for transverse joint tests

## 4.1 Shear Connection Tests

The main purpose of this test is to assure effectiveness of the slab-to-beam connections. The slip between the steel beam and concrete slabs as well as the ultimate strength for the various stud configurations was investigated. Twelve quarter-scale and fourteen full-scale specimens with various pockets and studs were fabricated and tested at the University of Illinois at Chicago.

### 4.1.1 Quarter-Scale Shear Connection Tests

A quarter-scale experimental program was carried out to study the effect of number and configuration of studs on composite action. Twelve specimens were fabricated with a different number of pockets and stud configurations as shown in Fig. 4.11. The main purpose of this study was to measure the slip between the steel beam and concrete slabs as well as to determine the ultimate strength for the various stud configurations. As a result, the specimens were divided into four distinct groups of 1, 2, 3 and 4 pockets, respectively. The groups with 1 and 2 pockets had four different stud-configurations: 1, 2, 3 and 4 shear studs in each pocket as shown in Fig. 4.12. The group with 3 and 4 pockets had only two types of stud configurations: 1 and 2 studs connectors in each pocket. The groups of beams with the respective number of studs are shown in Fig. 4.13.

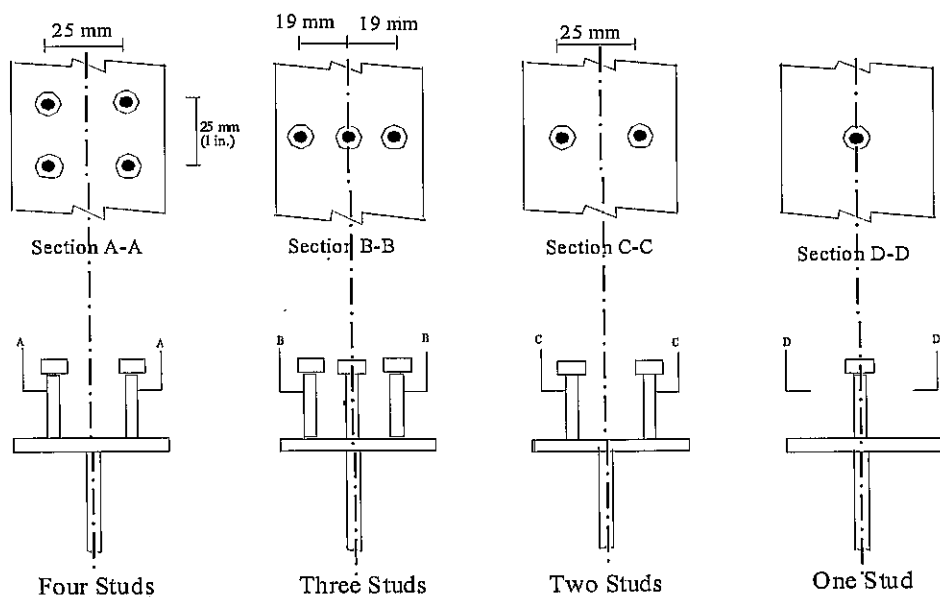


Fig. 4.11 Stud configurations

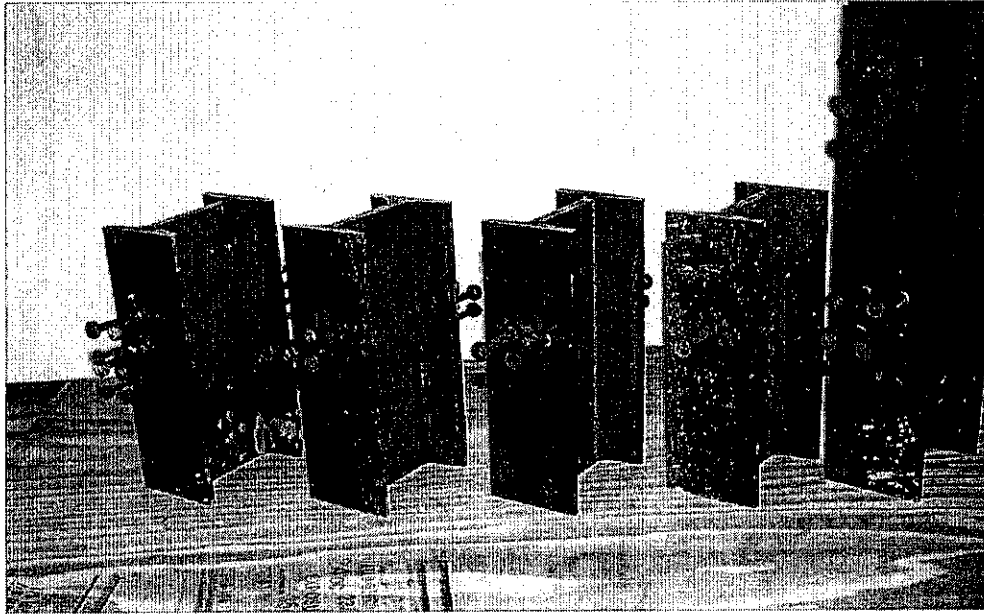


Fig. 4.12 Beam specimens with different stud configurations

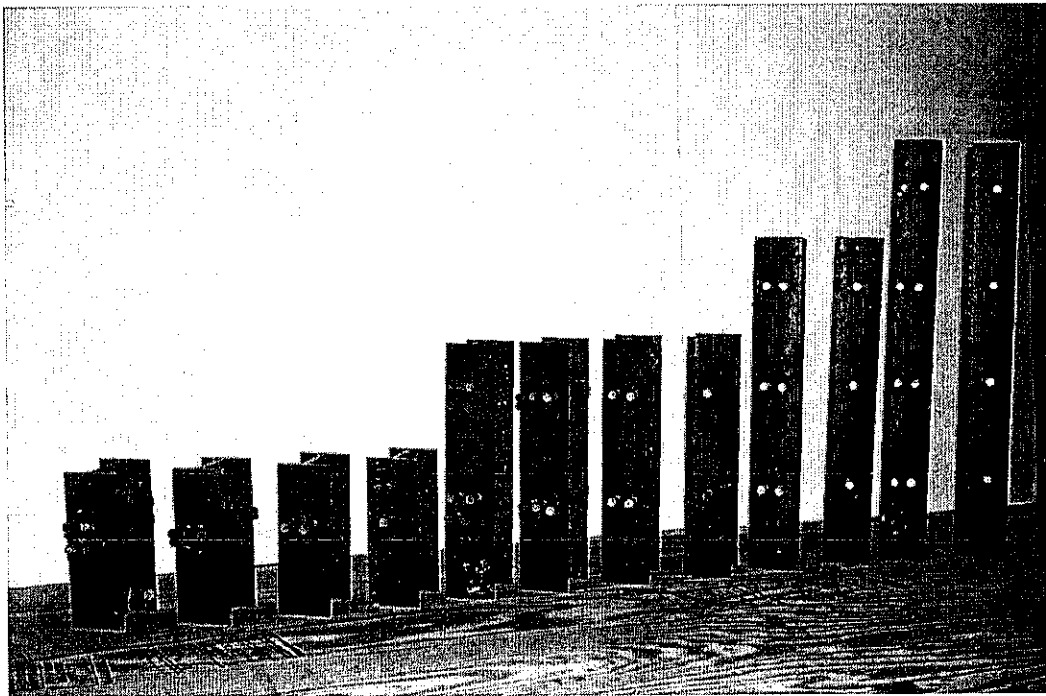


Fig. 4.13 Beam specimens used in push-out testing program

#### 4.1.1.1 Specimen Description and Material Properties

The ¼-scale specimens consisted of two concrete panels attached to a steel beam in the vertical position as shown in Fig. 4.14. The dimensions of the reinforced concrete slabs were 51 mm (2 in.) thick, 152 mm (6 in.) wide and 203, 356, 508, and 660 mm (8, 14, 20 and 26 in.) high, for the specimens with 1, 2, 3 and 4 pockets, respectively. The pocket dimensions were 64 x 64 mm (2½ x 2½ in.) on the top face of the slab and at the bottom 51 x 51 mm (2 x 2 in.). The steel beam was S4 x 9.5, A36, with 6.4 x 51 mm (¼ x 2 in.) long welded studs.

The precast panels were reinforced with two layers of welded wire mesh with the wires running parallel and perpendicular to the direction of traffic. A 25 x 25 mm (1 x 1 in.) wire mesh size was used with 3 mm (0.105 in.) diameter wires in both directions as shown in Fig. 4.15. The cover provided for the steel reinforcement was in accordance with the quarter-scale criteria, i.e., 12.7 mm (½ in.) on top and 6 mm (¼ in.) on bottom.

The concrete was a combination of cement, sand and fine aggregate with water cement ratio of (w/c) 0.65. Type I normal Portland cement was used as a binding material. U.S. No. 4 sieve (0.187 in or 4.7 mm) maximum aggregate size was used. This size was determined based on the model geometric scale, thickness of the specimens, reinforcement spacing, and concrete cover. The fine aggregate used was a mixture of river sand and gravel. The apparent specific gravity and unit weight of the river sand used were 2.70 and 1795 kg/m<sup>3</sup> (112 pcf), respectively. The river sand aggregate gradation used is presented in Table 4.4. The apparent specific gravity and unit weight of the gravel used were 2.79 and 1530 kg/m<sup>3</sup> (95.5 pcf), respectively. The mix proportions and slump of concrete are reported in Table 4.5. Control cylinders were prepared along with the panels to determine the compressive strength of the concrete.

Table 4.4 Aggregate gradation for model concrete

Sieve size	% of individual fraction retained by weight	Cumulative % passing, by weight	Cumulative % retained, by weight
No. 4	0	100	0
No. 8	12.47	87.53	12.47
No. 16	15.33	72.20	27.80
No. 30	21.60	50.60	49.40
No. 50	32.00	18.60	81.40
No. 100	15.20	3.40	96.60
Pan	3.40	0	-----
Total	100		268
			Finesses modulus = 268 /100 = 2.68

Table 4.5 Mix proportions of concrete for quarter-scale specimens

Ingredients	Mix proportions	
Cement	410 kg/m <sup>3</sup>	690 lb/yd <sup>3</sup>
Coarse aggregates	328 kg/m <sup>3</sup>	552 lb/yd <sup>3</sup>
Sand	1311 kg/m <sup>3</sup>	2209 lb/yd <sup>3</sup>
Total water content	266 kg/m <sup>3</sup>	449 lb/yd <sup>3</sup>
Water-cement ratio	0.65	
Slump	112 mm	4.4 in.
Compressive strength @ 28 days	42.8 MPa	6200 psi

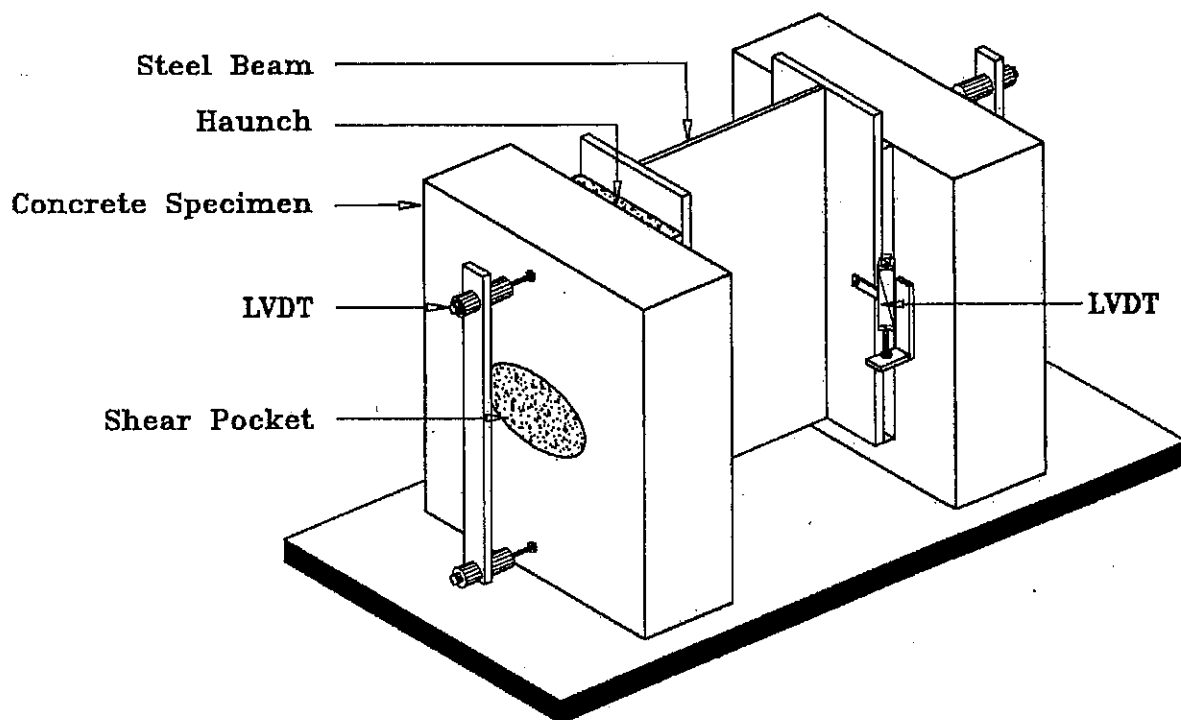


Fig. 4.14 Specimen configuration for push-out test

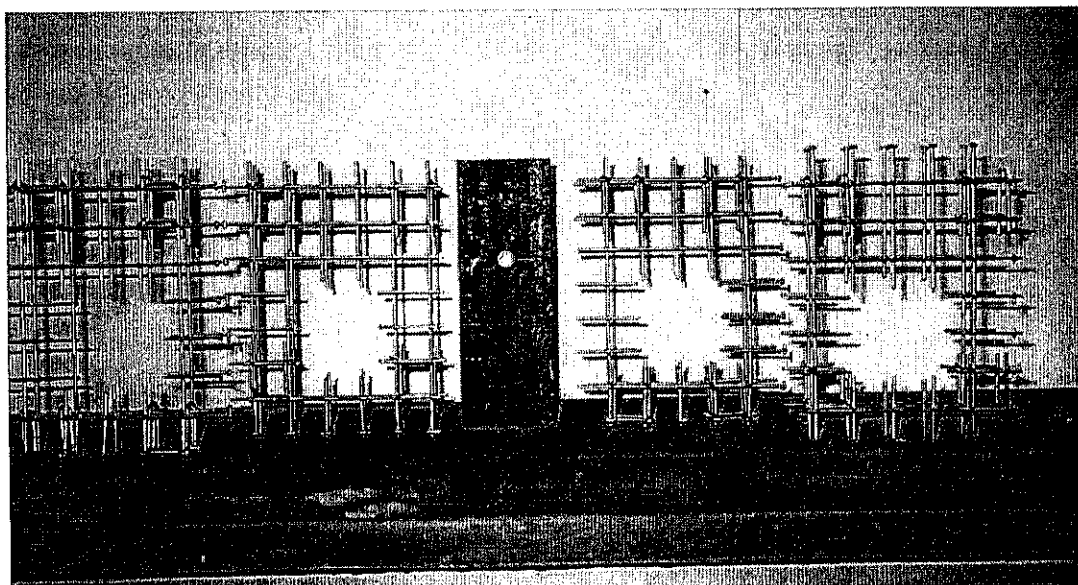


Fig. 4.15 Steel wire mesh, 25 x 25 mm

The panels were cast and cured accordingly in a controlled humidity and moisture room for at least a period of 28 days. The specimens were cast so that the pockets were over the studs and the haunch was filled with set grout as shown in Fig. 4.16. The set grout employed was mixed using a flowable proportion of 3.8 liters per 22.7 kg (50 lbs) of cement grout. In the curing process, the burlap was used for a period of 7 days as shown in Fig. 4.17. An important observation was that the slabs were not in direct contact with the steel beams, they were separated by 9.5 mm ( in.) haunch. This procedure is used intentionally to level the slabs during the construction of the bridge and to allow for any misalignment. The specimen designations adopted in this experimental program are presented in Table 4.6. The specimens with their respective pocket configuration are shown in Fig. 4.18.

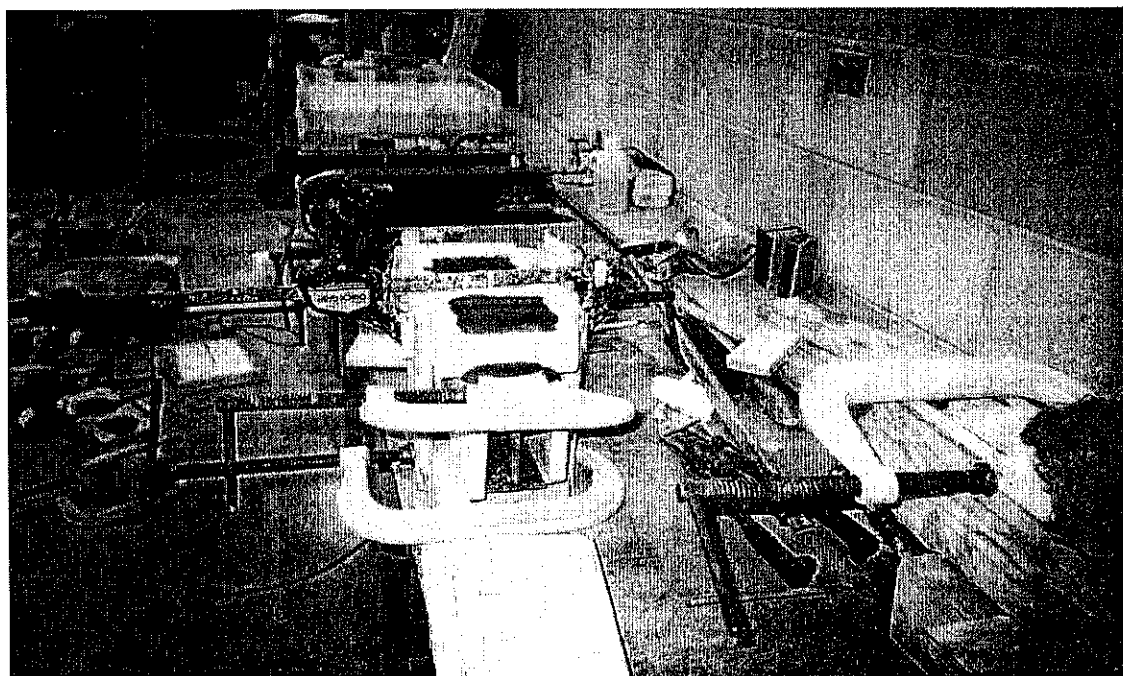


Fig. 4.16 Pocket pouring

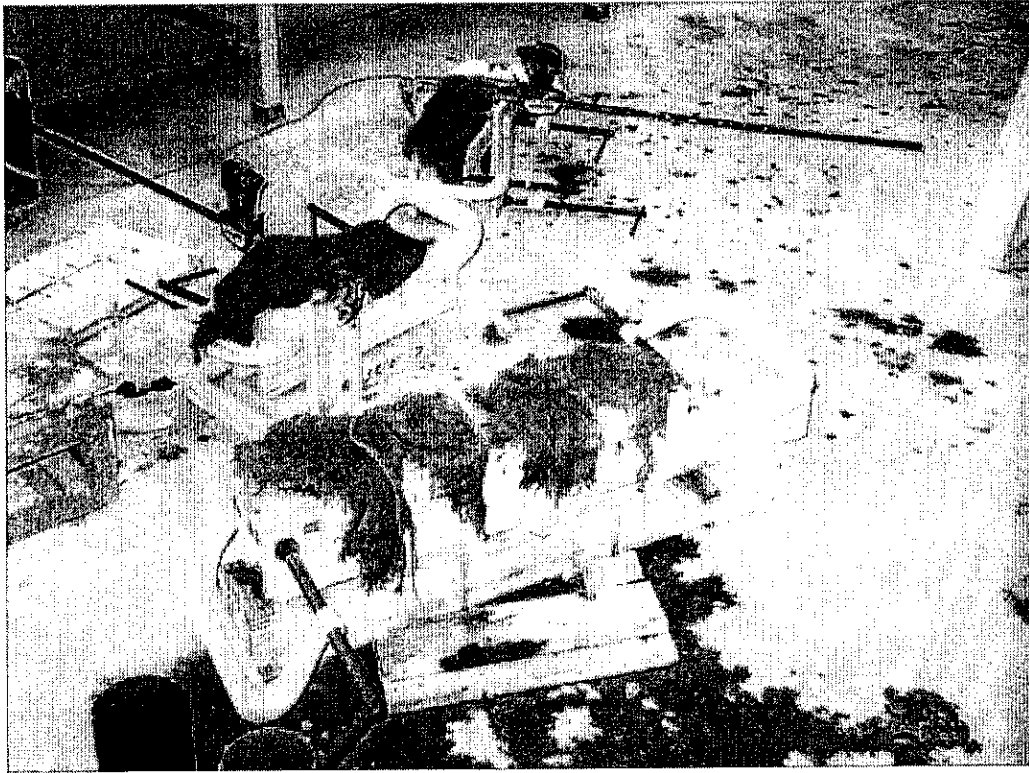


Fig. 4.17 Pocket curing

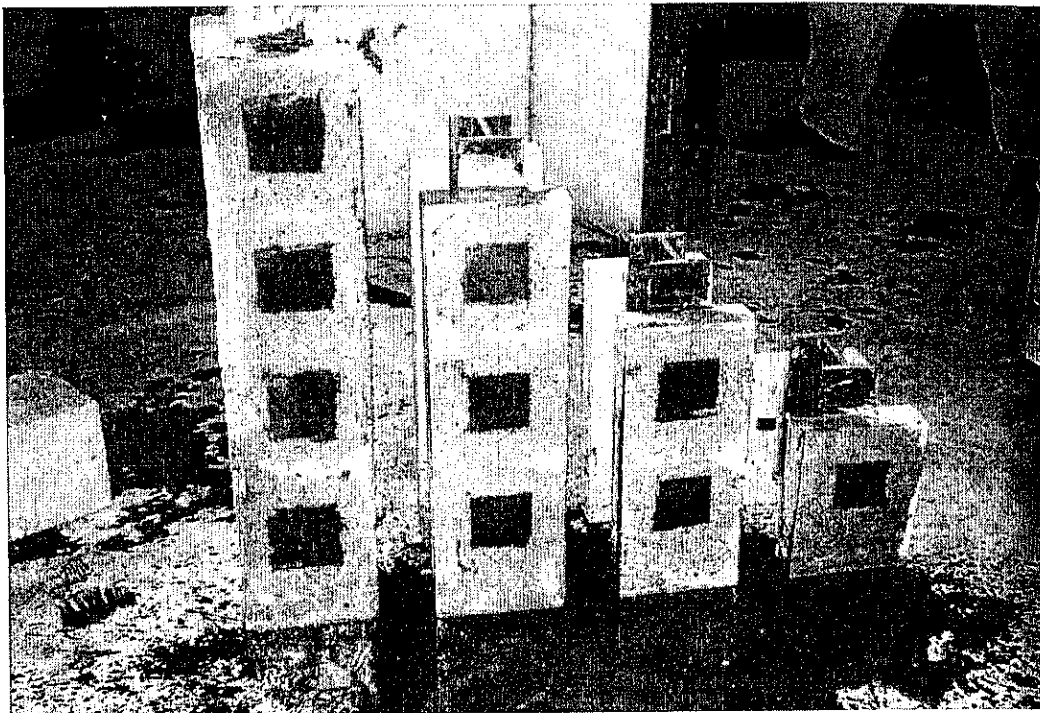


Fig. 4.18 Push-out specimens with different number of pockets

Table 4.6 Specimen designation

Designation	Description
QS1P1S	Quarter-scale, 1 pocket and 1 shear stud connector
QS1P2S	Quarter-scale, 1 pocket and 2 shear stud connectors
QS1P3S	Quarter-scale, 1 pocket and 3 shear stud connectors
QS1P4S	Quarter-scale, 1 pocket and 4 shear stud connectors
QS2P1S	Quarter-scale, 2 pockets and 1 shear stud connector
QS2P2S	Quarter-scale, 2 pockets and 2 shear stud connectors
QS2P3S	Quarter-scale, 2 pockets and 3 shear stud connectors
QS2P4S	Quarter-scale, 2 pockets and 4 shear stud connectors
QS3P1S	Quarter-scale, 3 pockets and 1 shear stud connector
QS3P2S	Quarter-scale, 3 pockets and 2 shear stud connectors
QS4P1S	Quarter-scale, 4 pockets and 1 shear stud connector
QS4P2S	Quarter-scale, 4 pockets and 2 shear stud connectors

#### 4.1.1.2 Test Setup

The experimental instrumentation consisted of several LVDTs for slip and uplift measurements. Specimens with one and two pockets had all pockets monitored from both sides, front and back as shown in Figs. 4.19 and 4.20, respectively. The three and four pocket specimens had a different setup, where at least one LVDT was used for each pocket. In the case of uplift, the measurements were taken perpendicular to the slabs. In the specimens with one pocket, the LVDTs were located 51 mm (2 in.) from the bottom of the slab and the center of the pocket as shown in Fig. 4.21. However, for the specimens with more than one pocket, the LVDTs were positioned at the center of the lowest and highest pocket.

The bottom of the specimens was fixed with a steel belt so that stud failure was initiated by shear. Lead and steel plates were placed at the top of the steel beam to uniformly distribute the load. Gypsum was also placed at the base of the specimen for leveling the concrete slabs.

#### 4.1.1.3 Push-out Test Procedure

The principal objective of the push-out test was to measure the load at which the bond between the steel beam and the concrete slab yielded. The slippage at bond failure, i.e., concrete-steel separation were recorded by means LVDTs. Before starting the real test a pre-load of approximately of 2.2 kN (0.5 kips) was applied through a lead plate that was placed between top of steel bar and load plate. The application of a pre-load force insured that the force was distributed uniformly across the beam flanges.

After the pre-load force was released, equilibrium was established in the system. After achieving equilibrium, the specimen was loaded at a rate of 0.025 mm/min. (0.001 in./min). During loading, load and slippage were measured and recorded via the data acquisition system. The crack initiation and propagation were also monitored throughout the test. When failure occurred, the ultimate load was recorded and photographs were taken to record the final modes of failure. The effects of the loading on the slabs and shear connectors were determined by observing the broken and disassembled specimens.

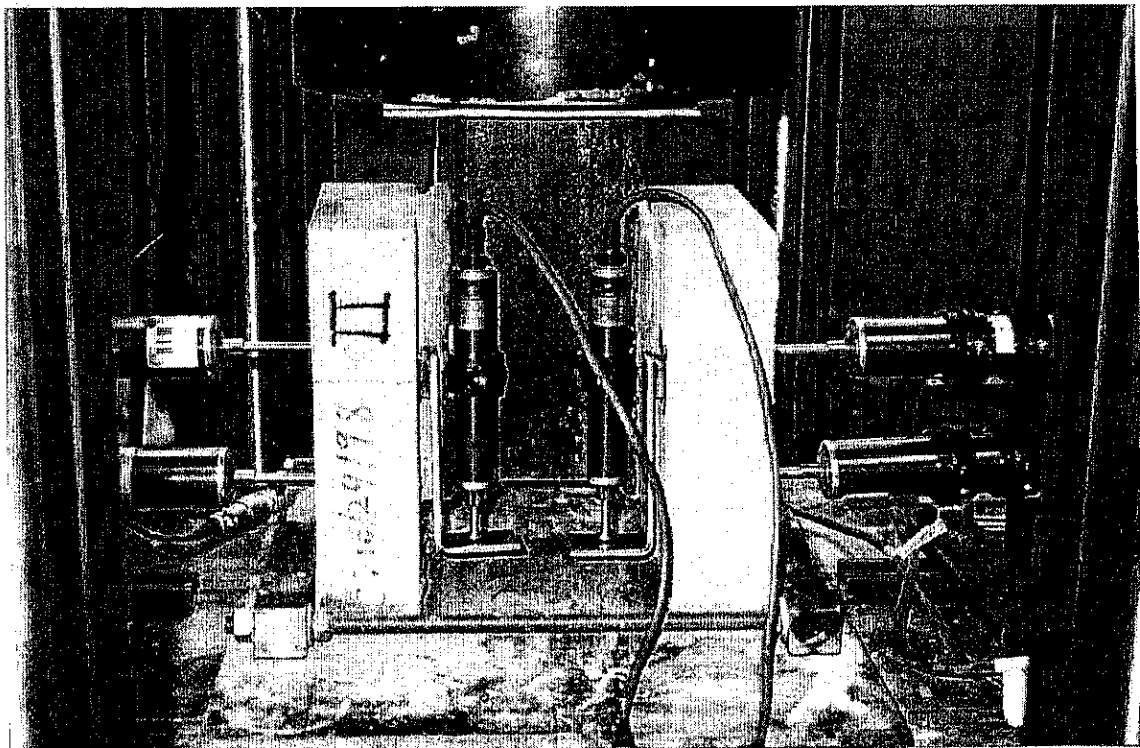


Fig. 4.19 Slip instrumentation for one-pocket specimen

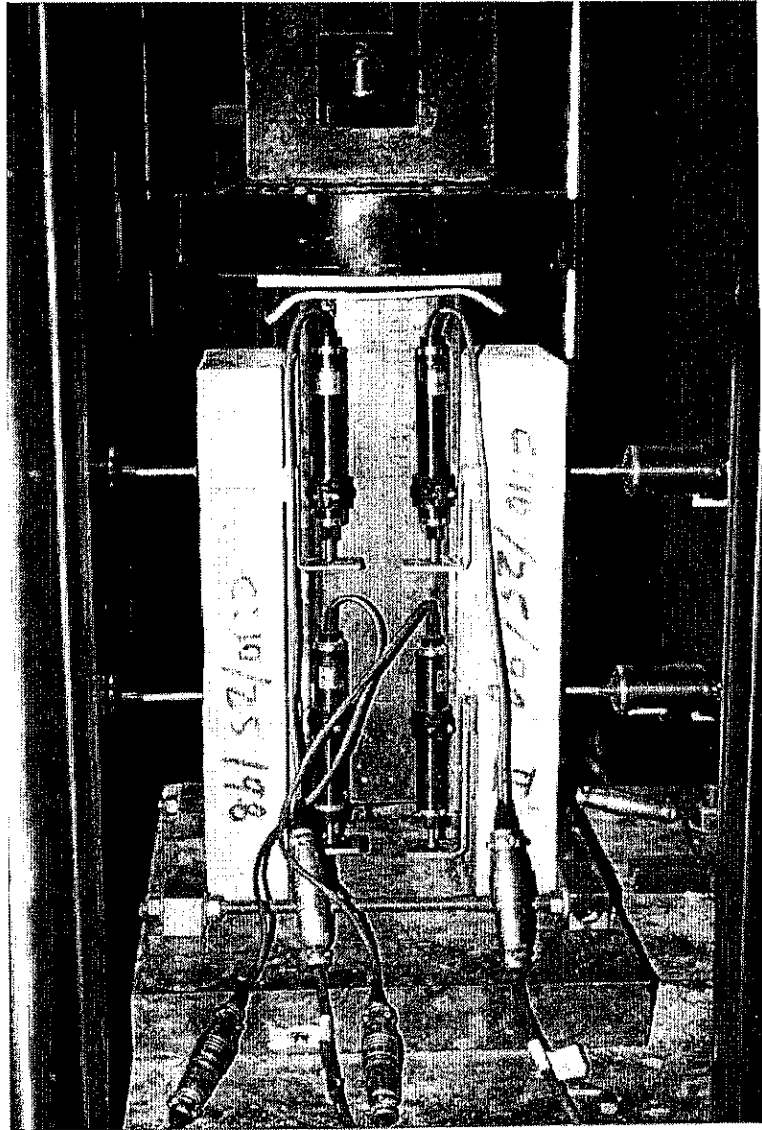


Fig. 4.20 Slip instrumentation for two-pocket specimen

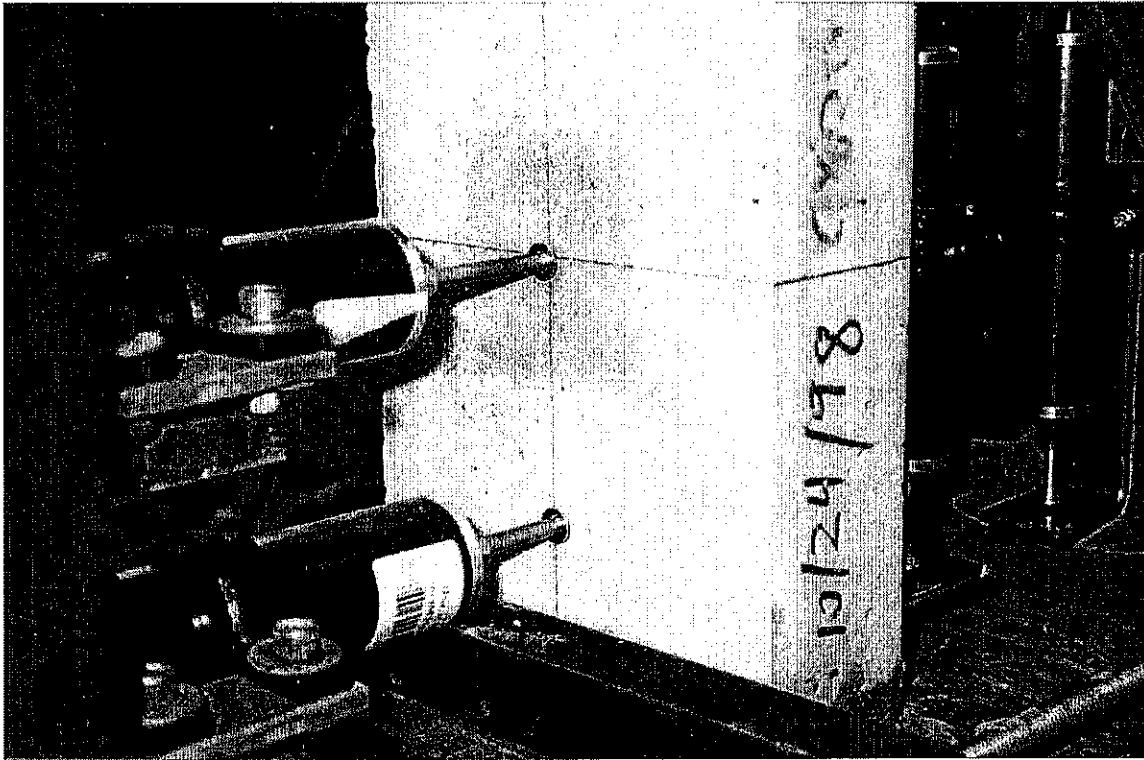


Fig. 4.21 Uplift measurements in specimen with one pocket

#### 4.1.2 Full-Scale Shear Connection Tests

Fourteen specimens were fabricated with different number of pockets and stud configurations. Two sets of specimens were fabricated for each pocket-stud configuration except for the zero-stud configurations where only one specimen was fabricated for the one and two pocket configurations. The main purpose of this study was to measure the slip between the steel beam and concrete slabs as well as to determine the ultimate strength for the various stud configurations. As a result, the specimens were divided into two distinct groups of 1 and 2 pockets, respectively. These groups had four different stud-configurations: 0, 2, 3 and 4 shear studs in each pocket.

##### 4.1.2.1 Specimen Description and Material Properties

The full-scale specimens consisted of two concrete panels attached to a steel beam in the vertical position. The dimensions of the reinforced concrete slabs were 203 mm (8 in.) thick, 610 mm (24 in.) wide and 813 and 1422 mm (32 and 56 in.) high, for the specimens containing 1 and

2 pockets, respectively. The dimensions for the beveled pockets were 279 x 152 mm (11 x 6 in.) on the top face of the slab and 254 x 127 mm (10 x 5 in.) at the bottom. The steel beam was W18 x 86, A36, with 22 x 102 mm ( $\frac{7}{8}$  x 4 in.) long welded studs.

The precast panels were reinforced with two layers of top and bottom steel in accordance with ILDOT slab design standards. The cover provided for the steel reinforcement was 51 mm (2 in.) on top and 25 mm (1 in.) on bottom. Figures 4.22 and 4.23 present the forming of the one- and two-pocket precast panels.

The concrete was a combination of cement, sand and aggregate with water cement ratio of (w/c) 0.45 as reported in Table 4.7 (mix 2). Type I normal Portland cement was used as a binding material. A 19 mm ( $\frac{3}{4}$  in.) maximum aggregate size was used. Superplasticizer of 8fl oz per 100 lb of cement was added to the mix to attain required workability. Control cylinders were prepared along with the panels to determine the compressive strength of the concrete. The mix proportion, slump, air content and compressive strength are reported in Table 4.7. Figure 4.24 shows the casting of precast panels for full-scale shear connection test. The finished panels for the one and two pocket specimens are shown in Figs. 4.25 and 4.26, respectively.

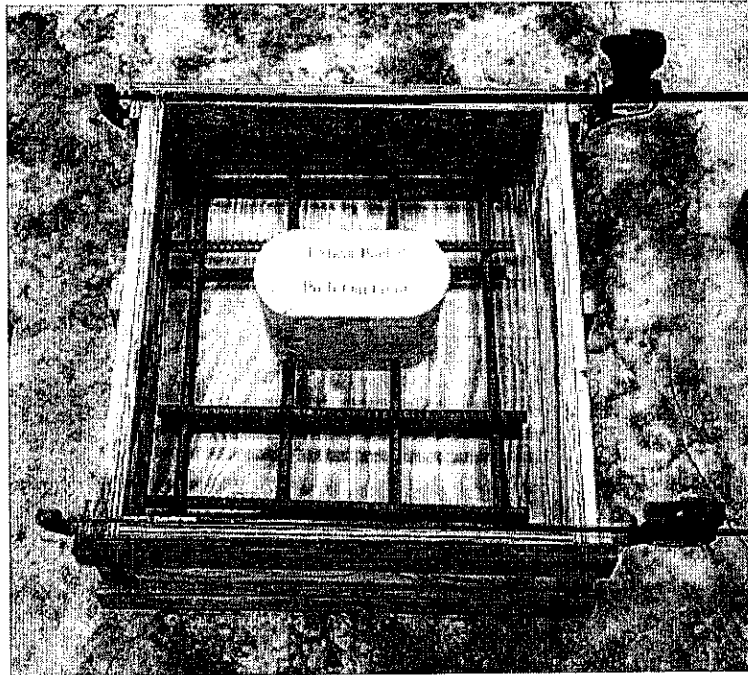


Fig. 4.22 Forming of the one-pocket precast panel

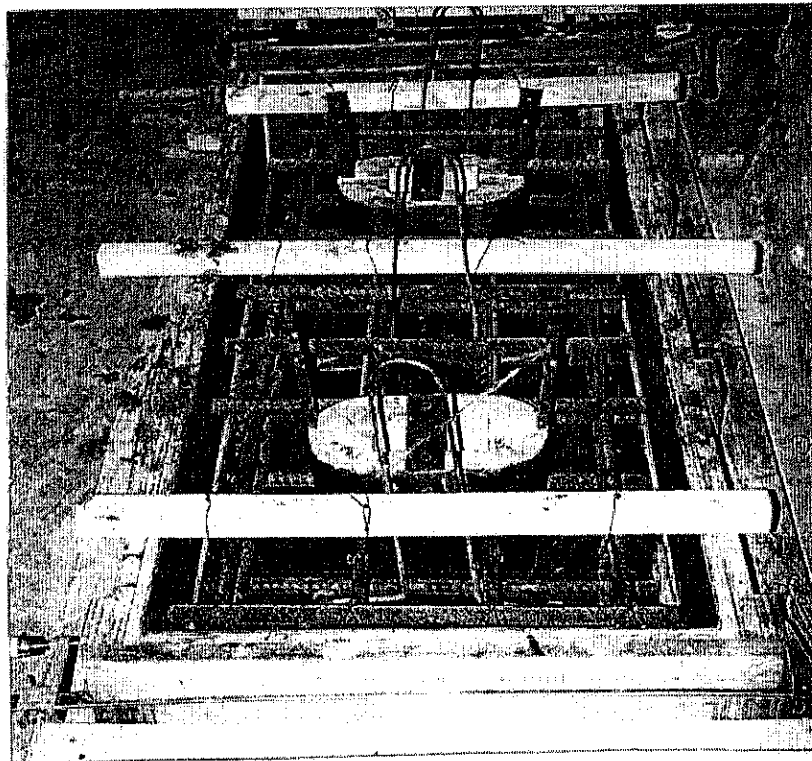


Fig. 4.23 Forming of the two-pocket precast panel

Table 4.7 Mix proportions

Mix Design	Mix 1		Mix 2	
Cement	354 kg/m <sup>3</sup>	597 lb/yd <sup>3</sup>	368 kg/m <sup>3</sup>	621 lb/yd <sup>3</sup>
Coarse aggregates	990 kg/m <sup>3</sup>	1668 lb/yd <sup>3</sup>	1161 kg/m <sup>3</sup>	1958 lb/yd <sup>3</sup>
Sand	866 kg/m <sup>3</sup>	1460 lb/yd <sup>3</sup>	675 kg/m <sup>3</sup>	1138 lb/yd <sup>3</sup>
Total water content	191 kg/m <sup>3</sup>	322 lb/yd <sup>3</sup>	165 kg/m <sup>3</sup>	279 lb/yd <sup>3</sup>
Superplasticizer, RB-1000	None		8 fl oz per 100 lb cement	
Water-cement ratio	0.54		0.45	
Slump	88 mm	3.5 in.	114 mm	4.5 in.
Air content	1.7 %		1.5 %	
Compressive strength	43.1 MPa	6250 psi	44.8 MPa	6500 psi

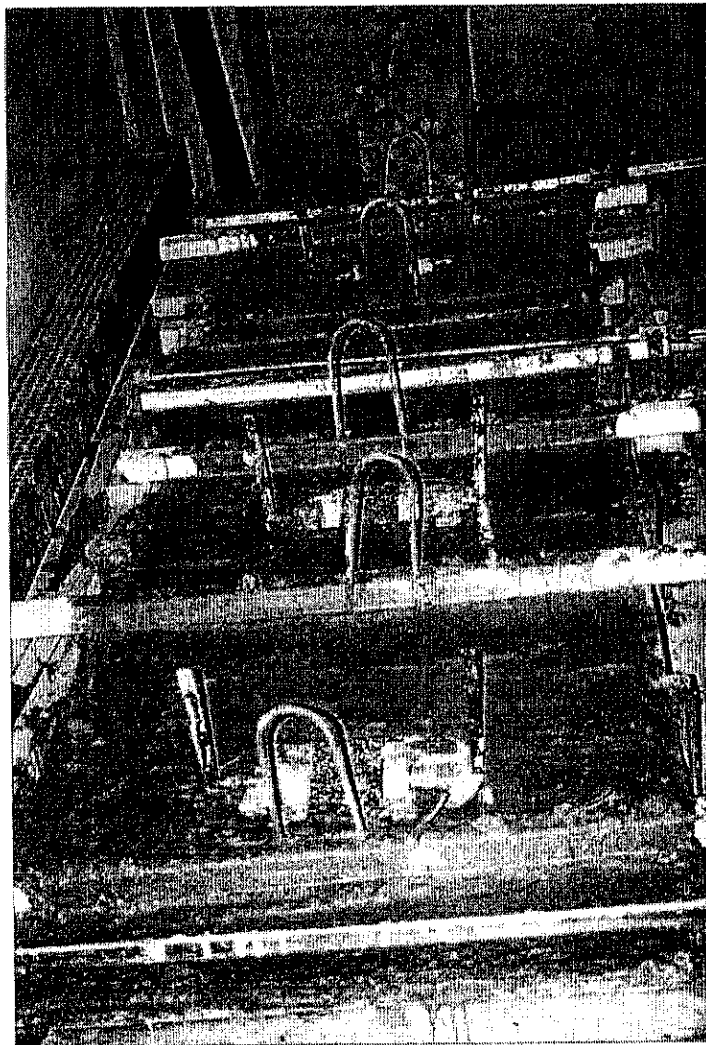


Fig. 4.24 Casting of precast panels for full-scale shear connection test

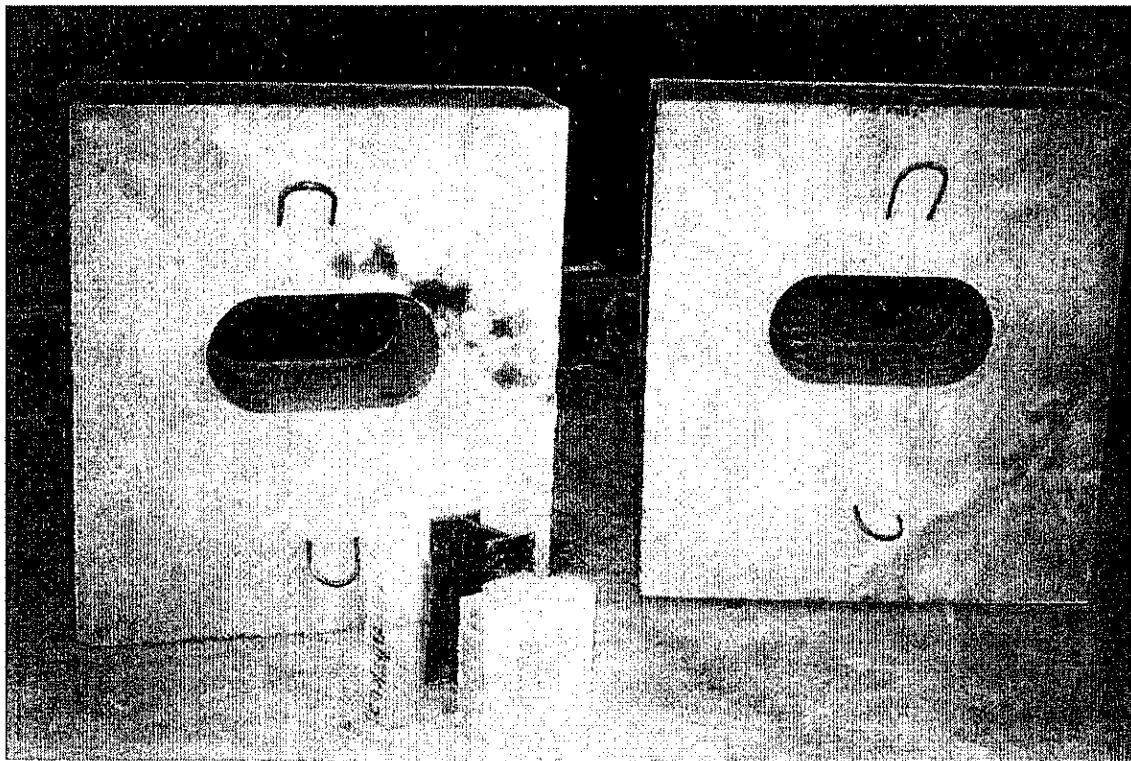


Fig. 4.25 Full-scale panel configuration for one-pocket specimen



Fig. 4.26 Full-scale panel configuration for two-pocket specimen

The panels were cast and cured accordingly using wet burlap for a period of 7 days. Then the panels were cured under the laboratory temperature and humidity for a period of 21 days. Afterwards, the pockets of the panels were sandblasted and washed with high water pressure. The panel was placed over the steel beam in such a way that the studs were exactly at the desired locations inside the pockets. An important observation was that the slabs were not in direct contact with the steel beams, they were separated by 25 mm (1 in.) haunch as shown in Fig. 4.27. This procedure is used intentionally to level the slabs during the construction of the bridge and to allow for any misalignment. Alignment was carefully checked with leveling equipment. Then the shear pockets and the haunch were filled with set grout. The set grout employed was mixed using a flowable proportion of 3.8 liters per 22.7 kg (50 lbs) of cement grout. After 6 hours from casting time, the pockets were coated with impermeable coating material as shown in Fig. 4.28. The specimen designations adopted in this experimental program are presented in Table 4.8.

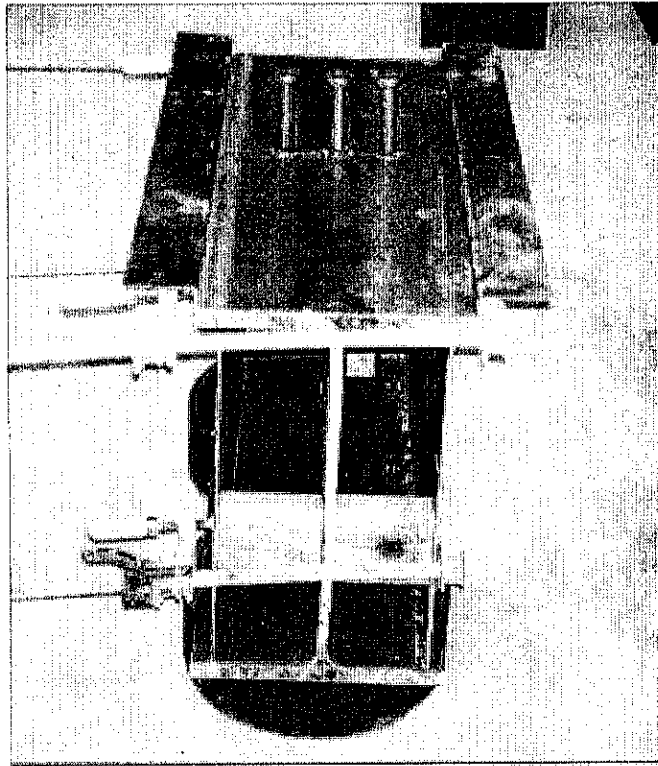


Fig. 4.27 Steel forming used to create haunch

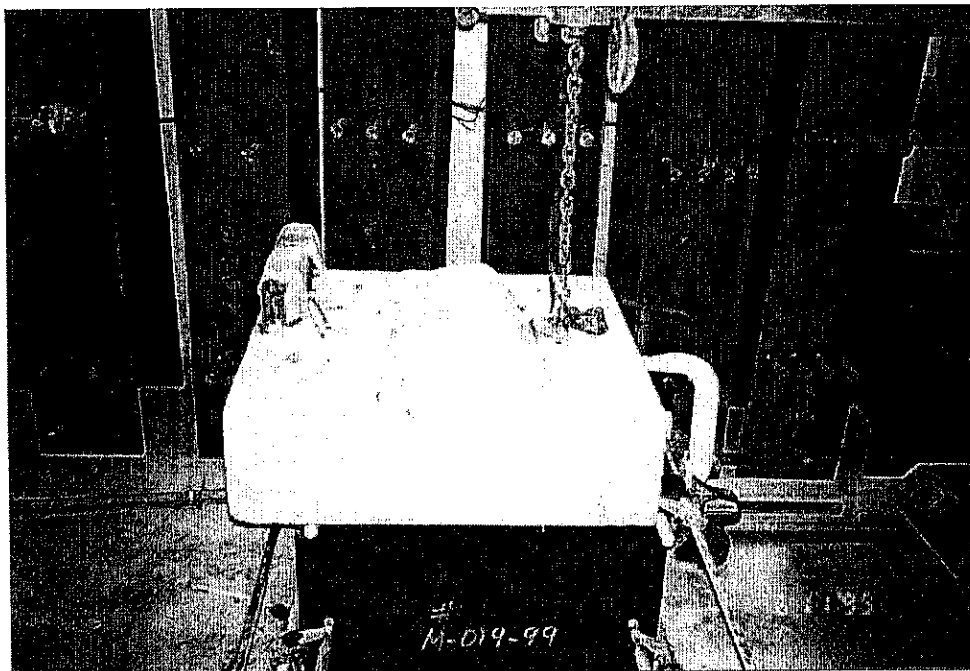


Fig. 4.28 Curing of shear pocket after set grout casting

Table 4.8 - Full-scale specimen designation

Designation	Description
FS1P0S	Full-scale, 1 pocket and 0 shear stud connectors
FS1P2S	Full-scale, 1 pocket and 2 shear stud connectors
FS1P3S	Full-scale, 1 pocket and 3 shear stud connectors
FS1P4S	Full-scale, 1 pocket and 4 shear stud connectors
FS2P0S	Full-scale, 2 pockets and 0 shear stud connectors
FS2P2S	Full-scale, 2 pockets and 2 shear stud connectors
FS2P3S	Full-scale, 2 pockets and 3 shear stud connectors
FS2P4S	Full-scale, 2 pockets and 4 shear stud connectors

#### 4.1.2.2 Full-Scale Push-out (Shear Connection) Test Setup and Procedure

The same procedure described for the quarter-scale push-out tests was adhered in carrying out the full scale tests. An overview of the test setup for two-pocket specimen is presented in Fig. 4.29.

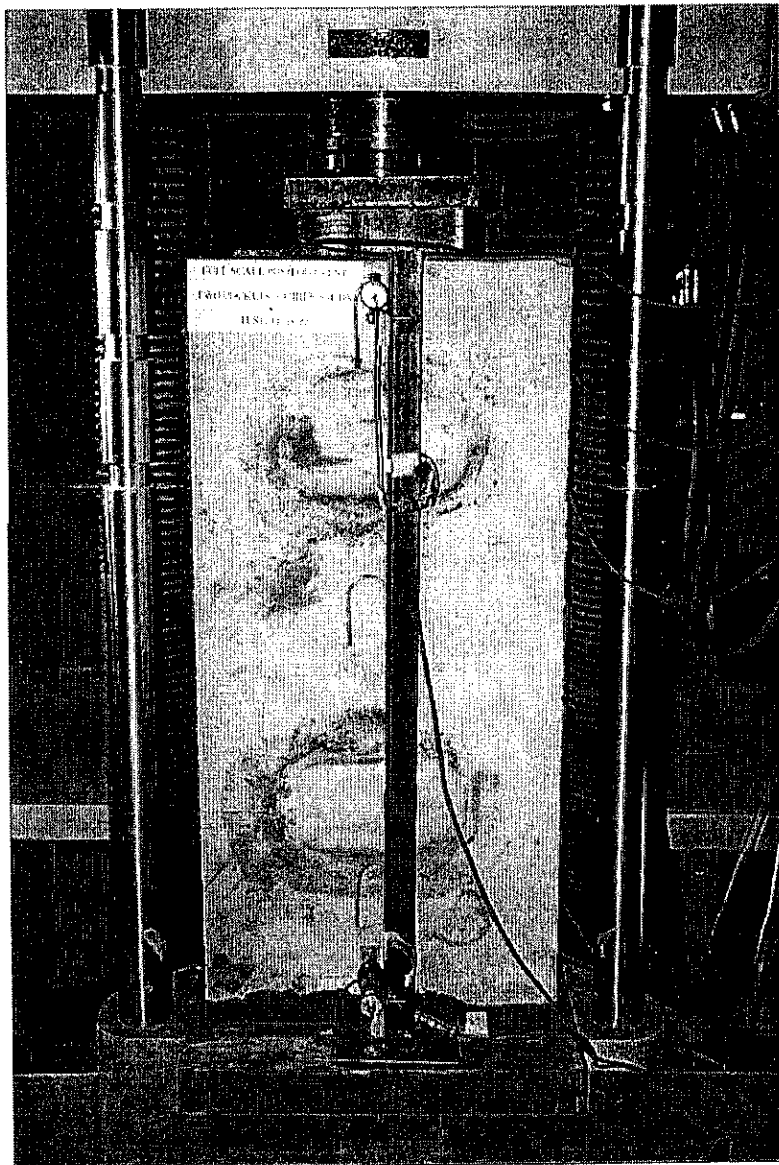


Fig. 4.29 Test setup for full-scale shear connection specimen (two pockets)

## 4.2 Transverse Joint Tests

The study focused on the development of bond between the grouting material and the concrete. Testing program was divided into three different varieties of tests; vertical shear, direct tension, and flexure. The joint configuration and dimensions for the tested specimens are presented in Fig. 4.30. The vertical shear specimens consisted of two panels connected via grouting materials and load was transmitted to the joint causing shear. The tensile specimens were proportioned for direct tension by a steel bar in each panel. The flexural specimen consisted of two panels connected via grouting materials and was subjected to three point loading.

Four different materials were used in the joint; set grout, set 45 at normal temperatures, set 45 in hot weather conditions, and polymer concrete. The concrete material properties for the slab units are shown in Table 4.7. Two different mixes were used for the slab units.

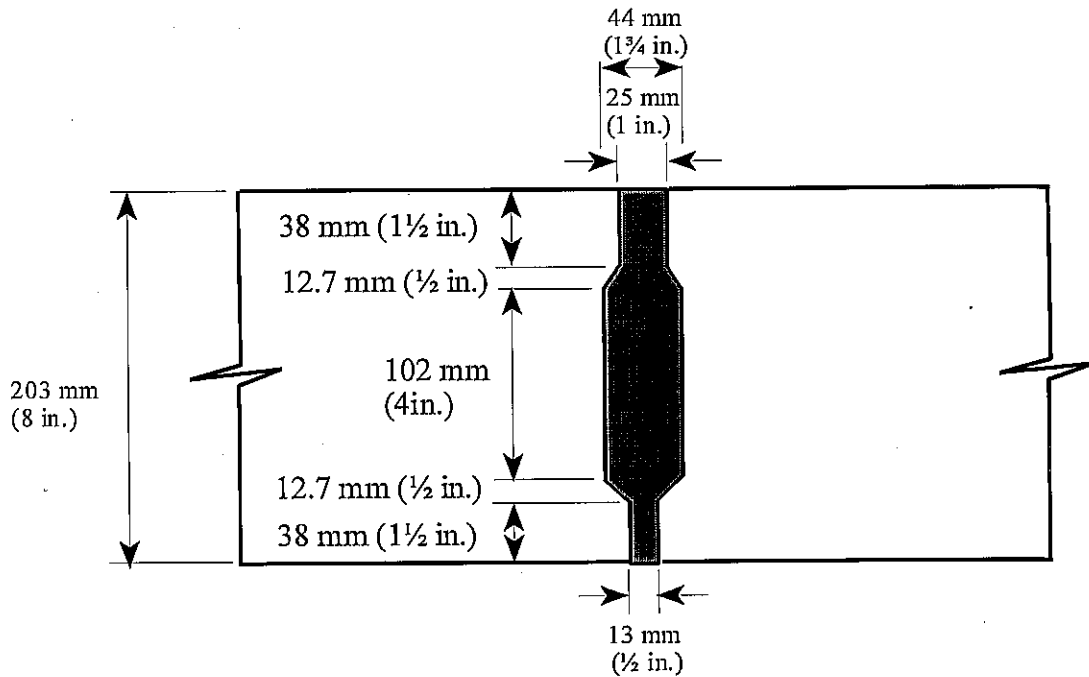


Fig. 4.30 Typical female to female type joint between precast panels

#### **4.2.1 Set 45 and Set 45 Hot Weather**

The set 45 grout material has a prescribed proportion of water ranging between 1.5 and 1.9 liters per 22.7 kg (50 lbs) of cement. In this study, the 1.9 liters per 22.7 kg (50 lbs) of cement was used initially, however, since set 45 is very sensitive to the amount of water, better results were obtained once the joint surface was dry and the water was reduced to 1.8 liters per 22.7 kg (50 lbs) of cement. The curing procedure involved the use of plastic sheets over the joints for a period of 24 hours. In casting the joint, a duration of 10 minutes was found to be optimal and recommended not to exceed. In the case of set 45 hot weather, casting duration was extended to 35 minutes.

After sandblasting the joint surface, it was washed with high pressure water and let it dry for at least 4 hours before application of the mortar. The identification of a carbonated surface is critical for the development of bond, where a substance with 10 % HCl was used to identify the carbonation. The set 45 is a heterogeneous material and it is composed of various elements, which consist of different properties. Hence, the mixes were carried out in 22.7 kg (50 lbs) concrete batches, since the set 45 bags are 22.7 kg (50 lbs) each.

##### **4.2.1.1 Mixing and Placing Procedure**

The following procedure was adhered to in mixing and placing the set 45 material:

Add to the mixer 1.8 liters of water per 22.7 kg (50 lbs) of set 45.

Start the mixer.

Add set 45 in the mixer.

Mix for 1 minute and 30 seconds.

Check if the mix is uniform.

Place and distribute the cement paste into the joint using a thin steel bar before it sets.

#### **4.2.2 Set Grout**

The mixes were prepared in 13.6 kg (30 lbs) concrete batches for the set grout material. The non-shrink grout was cast with a water proportion of 3.2 liter per 22.7 kg (50 lbs) of cement.

The strength results for the cubes revealed that the mix is classified as flowable. The joint surface was sandblasted properly and was cured for 24 hours inside the humidity room. Casting of the joint took place before the surface dried. The humidity on the surface improves the bond and prevents any exchange of water between the surface and the cement paste. After casting the joint specimens were cured for 6 hours using wet burlap and after set time, a curing compound was used.

#### **4.2.2.1 Mixing and Placing Procedure**

The following procedure was adhered to in mixing and placing the set grout material:

Add set grout into the mixer.

Start the mixer.

Add the water (3.2 liters per 22.7 kg of set grout).

Mix for three minutes.

Place and distribute the cement paste into the joint using a thin steel bar before it sets.

#### **4.2.3 Polymer Concrete**

The polymer concrete (EMACO 2020 Regular) is composed of three materials, denominated A, B and C, binder, aggregate and initiator, respectively. The mix proportions were 1:10.9:0.1. The mix is very liquid, making it very easy for pouring. At first the joint surface of the specimen was sandblasted and was cleaned with water at high pressure to remove any dust or loose particles. Then the surface was dried and a primer was placed 3 hours before mixing.

##### **4.2.3.1 Mixing and Placing Procedure**

The following procedure was adhered to in mixing and placing the polymer concrete:

Apply on the surface of the joint the primer (EMACO 2041).

Add the liquid component first (part A).

Add the aggregate component (part B).

Start the mixer.

Mix for 1 minute.

Add part C, however, inspect the material first and brake any lumps that exist in the material.

Mix for 30 seconds.

Place the polymer in the joint and vibrate for a short period of time.

### **4.3 Direct Shear Test**

The specimen surface was sandblasted for better bond between the materials as shown in Fig. 4.31. The first direct shear test was initiated by testing the configuration shown in Fig. 4.32. However, the area provided in the upper stub rendered the concrete to fail prematurely at that juncture. A consequent design was implemented by increasing the area of this stub and wrapping the specimens with Carbon Fiber Reinforced Polymer (CFRP) sheets. This application rendered the ultimate implementation of the specimen configuration shown in Fig. 4.33.

The specimens were designed in order to transfer the load to the joint in such a manner so that the joint experienced only shear forces. The final specimen configuration and test setup is shown on Fig. 4.9(a). The load was applied on a spread area of  $290 \text{ cm}^2$  ( $45 \text{ in.}^2$ ) and the resultant of the load acted exactly at the center. As a result, the load transferred into the joint, forcing the joint to fail in shear. In the shear test, a lead plate was placed on the top and bottom to secure a uniform distribution of the load. The load rate used was  $0.25 \text{ mm/min}$  ( $0.01 \text{ in./min}$ ).

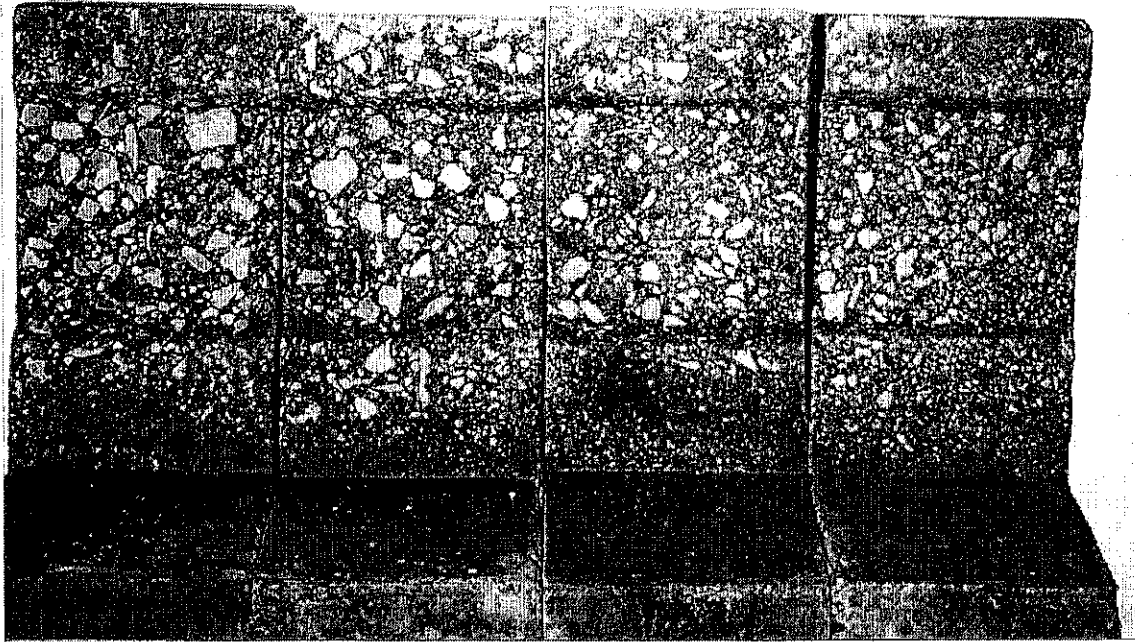


Fig. 4.31 Direct shear test specimen with sandblasted surface

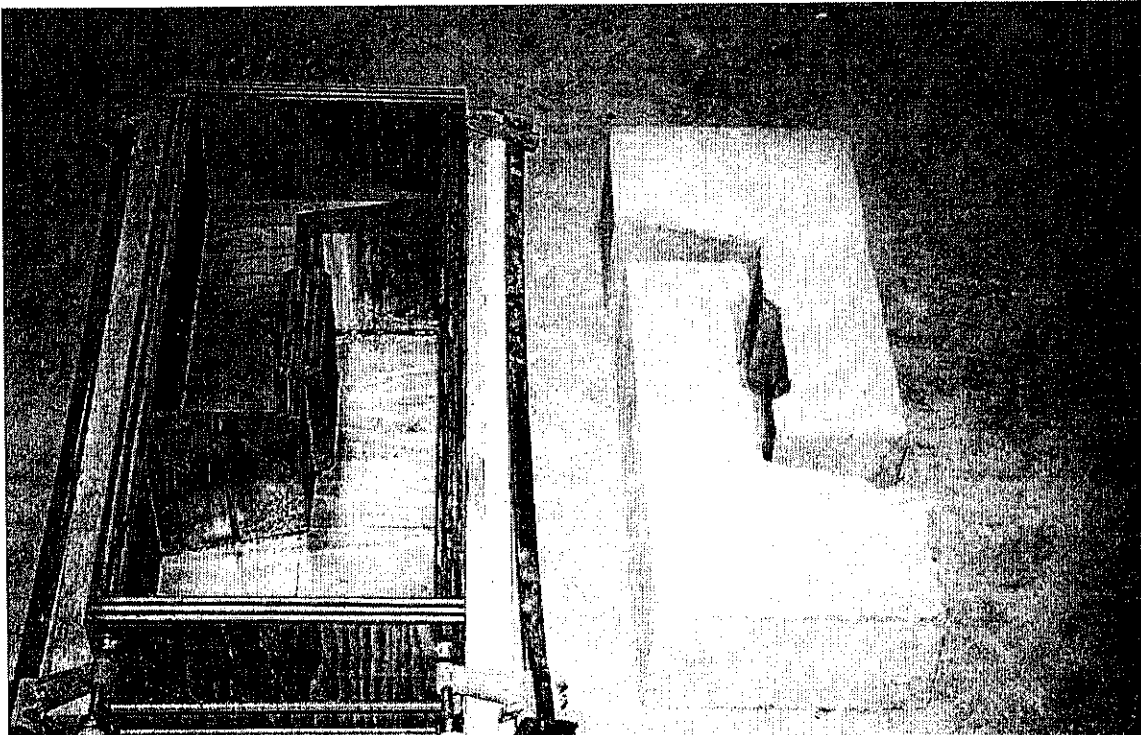


Fig. 4.32 First direct shear test model

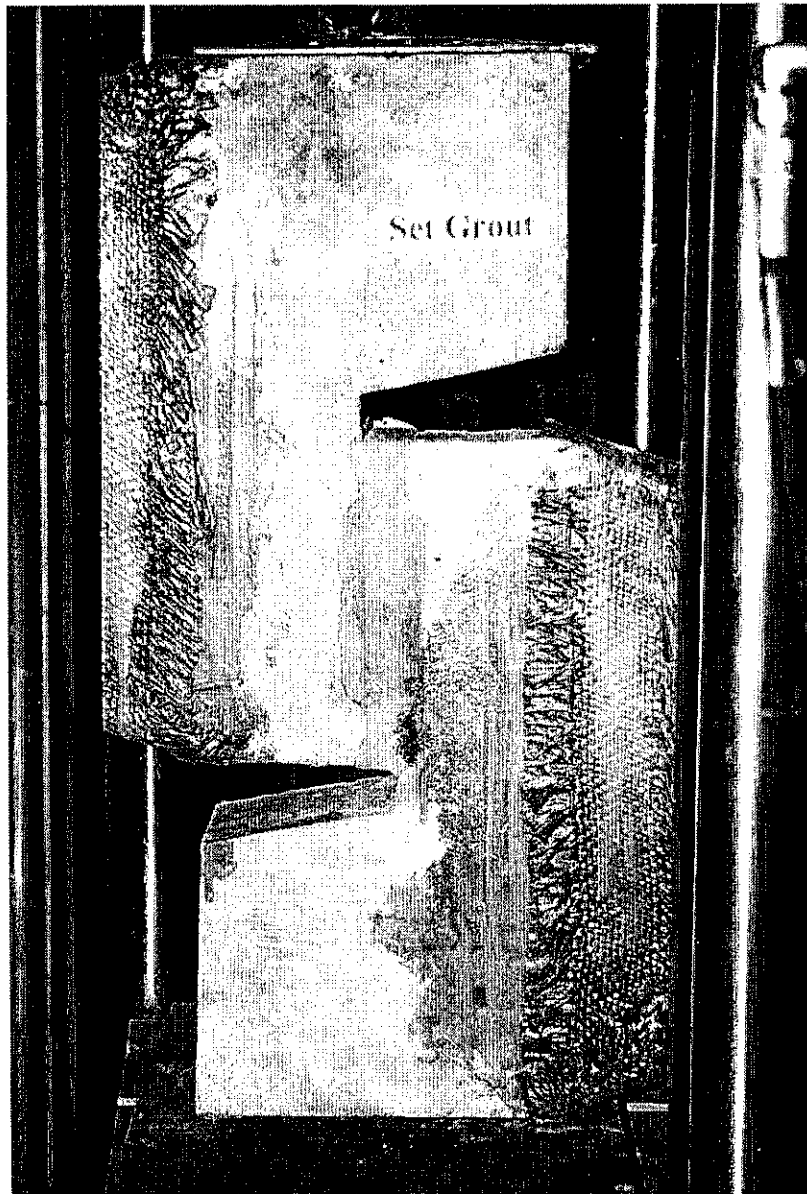


Fig. 4.33 New specimen wrapped with carbon fiber for direct shear test

#### 4.4 Direct Tension Test

The tests were performed on three specimens for each type of material. All specimens were moist cured for a period of 28 days and sandblasted prior to jointing as shown in Fig. 4.34. The transverse section of the tensile specimen was  $258 \text{ cm}^2$  (40 in.<sup>2</sup>). A No. 5 steel rebar was cast inside of a block of concrete 203 mm (8 in.) high, providing sufficient area to anchor the load. A cross shape was added, 51 mm (2 in.) from the end (steel rebar No. 5 (102 mm (4 in.) long)). A second specimen was fabricated using No. 4 steel rebar without the cross shape. In the second specimen, a length of 203 mm (8 in.) anchor into a concrete specimen 229 mm (9 in.) high, was satisfactory. The load was transferred to the specimen using the same fixture used in the rebar tensile tests, which consisted of gripping the ends of the rebars to the cross head and applying tension forces as shown in Fig. 4.35. The specimen was tested in a load control mode.

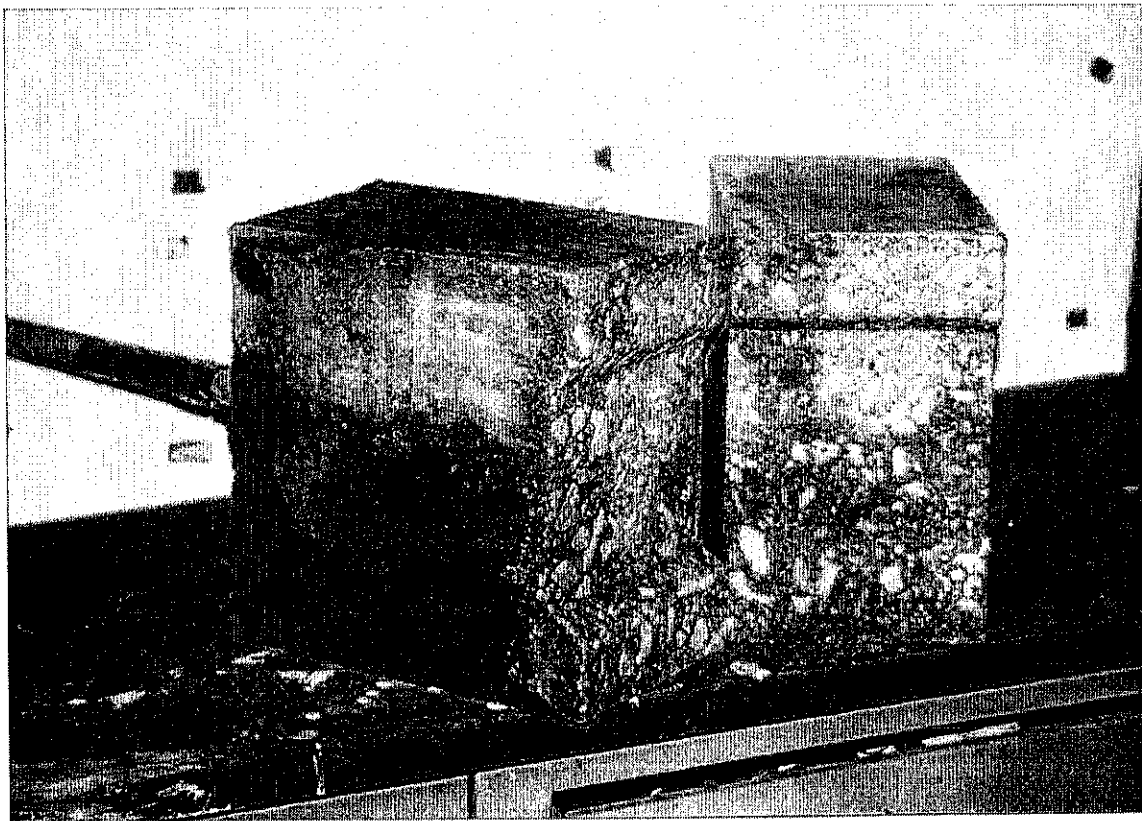


Fig. 4.34 Direct tensile test specimen with sandblasted surface

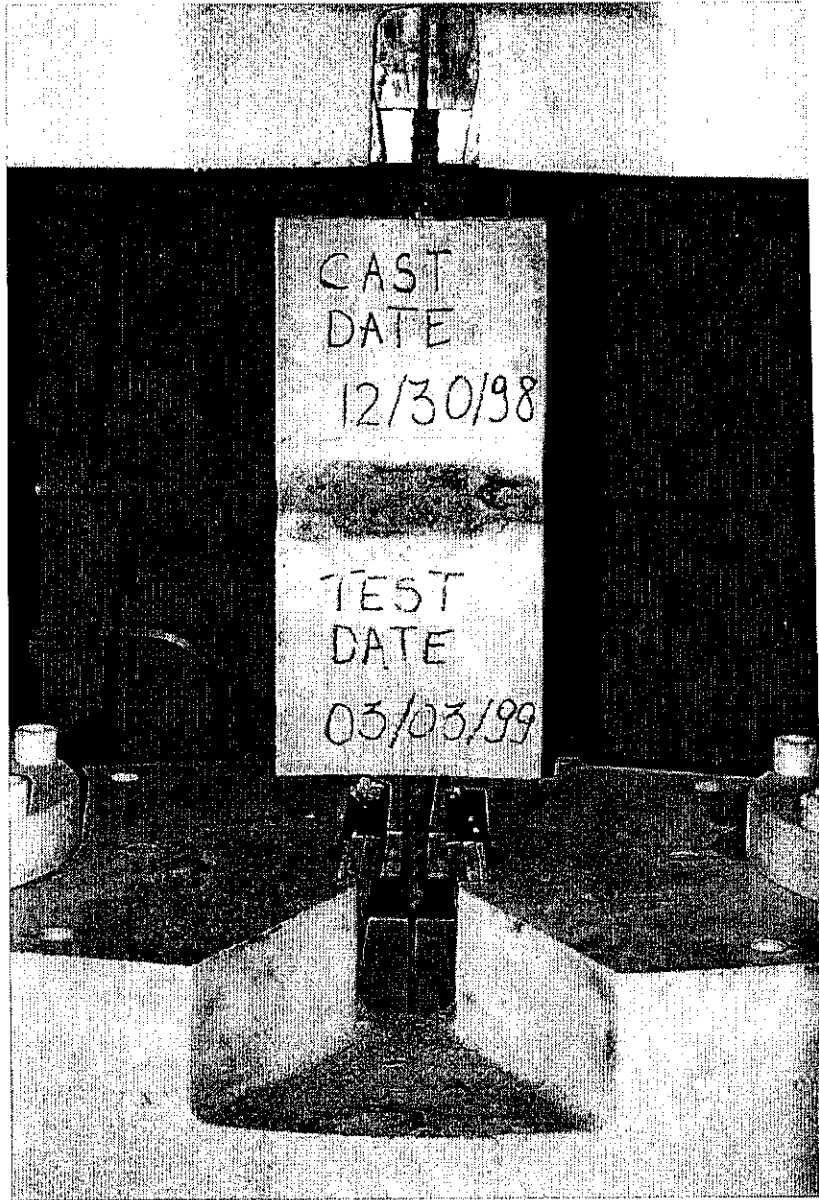


Fig. 4.35 Direct tension test setup

#### 4.5 Flexural Testing

The flexure test was conducted using the same fixture used in ordinary flexure tests of three-point bending concrete beams. The concrete specimens were submitted to moisture curing for a period of 28 days prior to jointing. The specimens were sandblasted to provide better bond surface. Specimen configuration is presented in Fig. 4.36, while the test setup is shown in Fig. 4.9 (c).

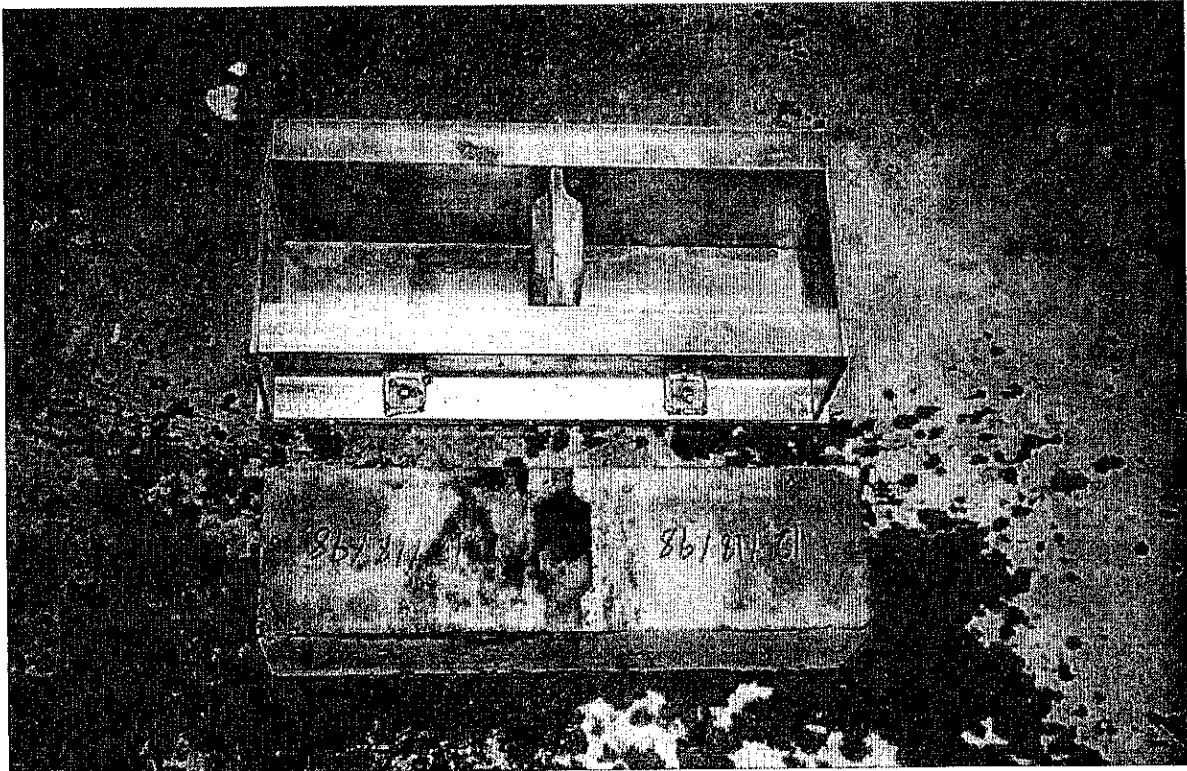


Fig. 4.36 Specimen configuration for flexural testing

## 5. TEST RESULTS

Full-scale and quarter-scale shear connection specimens with various number of pockets and shear studs were fabricated and tested. A total of 12 quarter-scale and 14 full-scale shear connection specimens were tested. Slip between the steel and concrete, ultimate load and mode of failures of these specimens were monitored and recorded. The data was analyzed and the observed results were compared. The influence of number of shear pockets and studs on the composite action of the bridge deck system is reported in this section. A total of 36 transverse joint specimens were fabricated and tested. The tests included vertical shear, direct tension and flexural tests. These joints were prepared with four different types of grouting materials such as set 45, set 45 hot weather, set grout and polymer concrete.

### 5.1 Test Results for Quarter-Scale Shear Connection

In the majority of the specimens, the cracks initiated at the level of the stud, where in principle, the cracks propagated at a 45-degree angle. Stud failures were easy to identify during the test, and overall stud failure occurred after the ultimate load. The mode of failure in all cases occurred at the base of the stud, while all studs failed in shear. The ultimate load was divided by 2 since specimen configuration was symmetric. The test results are shown in Table 5.1. The typical shape of the push-out specimens after failure is shown in Figs. 5.1 and 5.2.

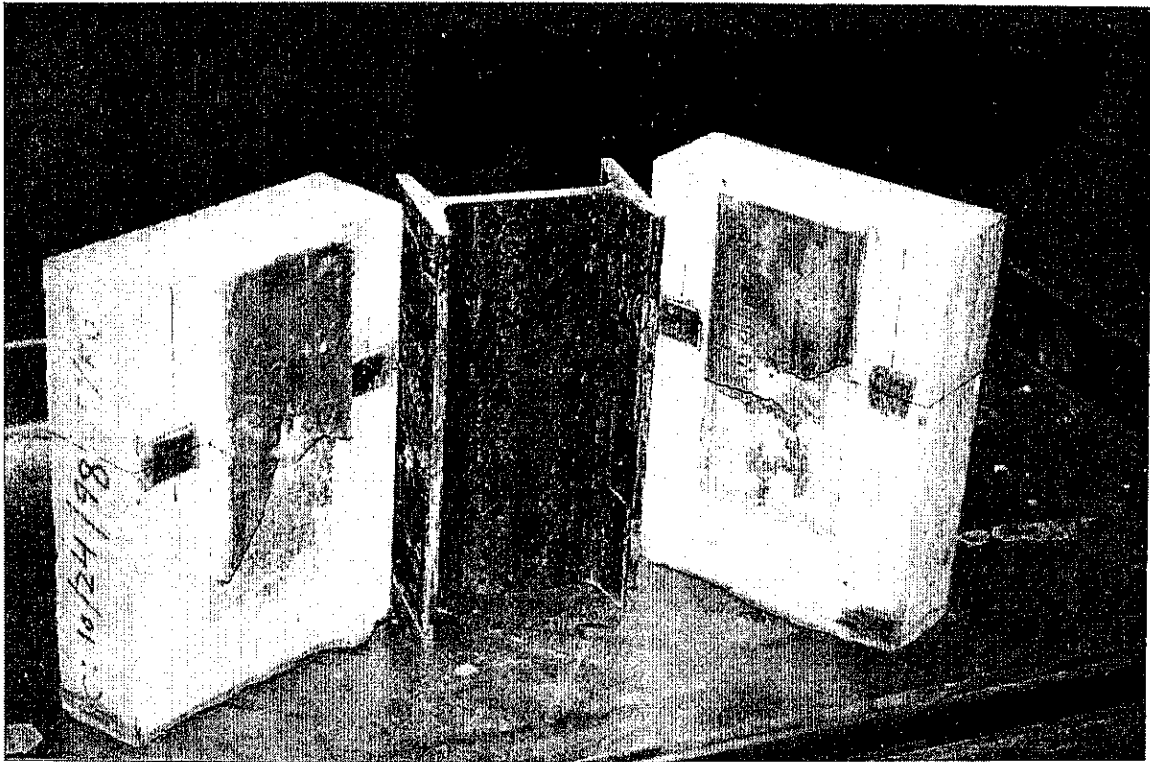


Fig. 5.1 Mode of failure for QS1P1S

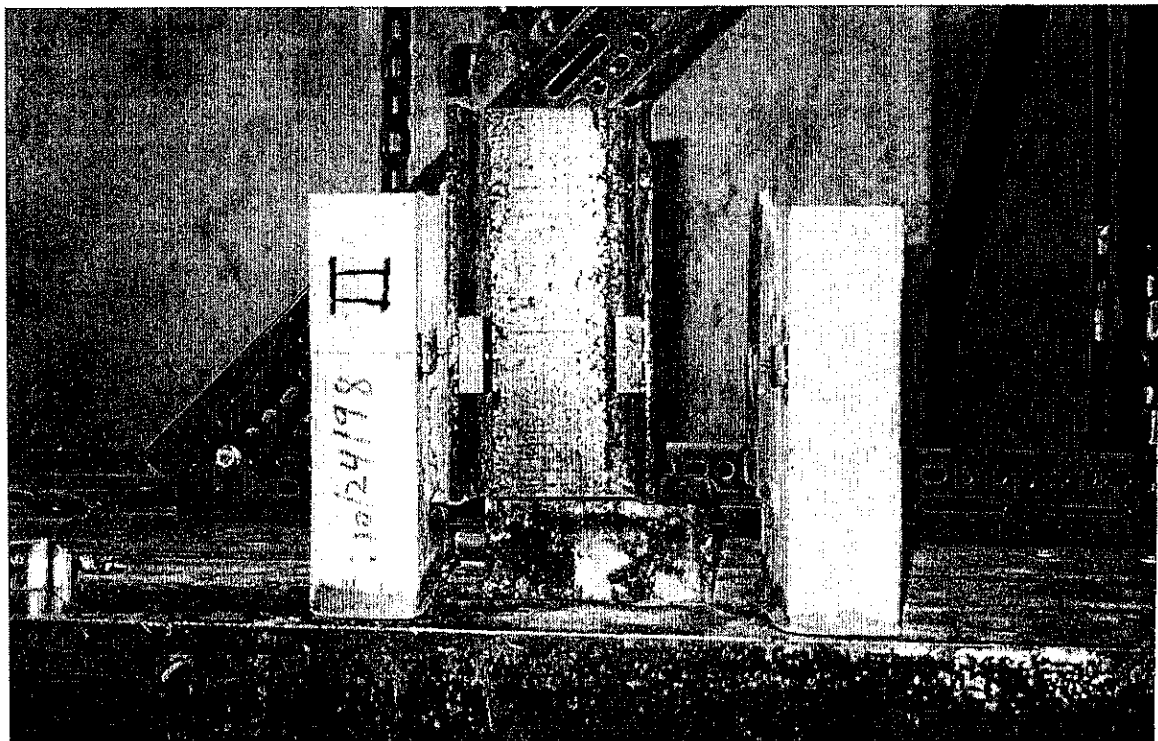


Fig. 5.2 Mode of failure for QS1P2S

Table 5.1 Tests results for quarter-scale specimens

Specimen designation	Ultimate load, kN (kips)	Predicted ultimate load, kN (kips)	First stud failure, kN (kips)	Slip load, kN (kips)	Concrete compressive strength, MPa (psi)	Set grout Compressive strength, MPa (psi)
QS1P1S	17.96 (4.01)	19.57 (4.40)	11.73 (2.63)	4.18 (0.94)	42.40 (6145)	46.19 (6694)
QS1P2S	30.32 (6.77)	29.36 (6.60)	26.88 (6.04)	6.84 (1.54)	42.40 (6145)	46.19 (6694)
QS1P3S	32.12 (7.17)	32.34 (7.27)	31.80 (7.15)	6.40 (1.44)	42.40 (6145)	46.19 (6694)
QS1P4S	43.27 (9.66)	---	24.32 (5.46)	11.20 (2.52)	42.40 (6145)	46.19 (6694)
QS2P1S	32.12 (7.24)	---	29.61 (6.65)	10.00 (2.25)	42.40 (6145)	49.23 (7135)
QS2P2S	54.83 (12.24)	---	52.26 (11.74)	13.78 (3.10)	42.54 (6165)	49.23 (7135)
QS2P3S	62.54 (13.96)	---	51.65 (11.61)	13.43 (3.02)	42.54 (6165)	49.23 (7135)
QS2P4S	96.76 (21.60)	---	77.14 (17.34)	27.97 (6.29)	42.54 (6165)	49.23 (7135)
QS3P1S	43.05 (9.61)	---	32.48 (7.30)	10.80 (2.43)	41.50 (6014)	48.12 (6974)
QS3P2S	72.12 (16.1)	---	51.83 (11.65)	17.83 (4.01)	41.50 (6014)	48.12 (6974)
QS4P1S	58.86 (13.14)	---	53.22 (11.96)	20.14 (4.53)	44.12 (6394)	48.33 (7004)
QS4P2S	121.94 (27.41)	---	95.96 (21.57)	16.01 (3.60)	44.12 (6394)	48.33 (7004)

Note: all specimens experienced shearing of stud mode of failure.

The load-slip curves with the initial slip, ultimate load, and first indication of stud failure of all the quarter scale push-out specimens are shown in Figs 5.3 to 5.14. After ultimate, the studs carried the load and slippage occurred until complete shearing of the studs. For instance, the ultimate load for the specimens with one shear pocket on each side and one stud per pocket occurred at 17.8 kN (4.0 kips). After ultimate, the studs carried the load up to a slip of 4 mm (0.17 in.). The corresponding load on the descending region of the curve was 11.6 kN (2.6 kips). The load-slip behavior of specimen QS1P1S is shown in Fig. 5.3. The initial slip between the steel and concrete took place at 4.2 kN (0.94 kips). During the test, a linear relationship was noticed between the slip and load increment.

Cracking in the set grout haunch was an important parameter in determining the propagation of the load in the specimen. The cracks initiated at the stud level until the end of the set grout haunch, i.e., 51 mm (2 in.) before the end of the specimen, while the respective load was 15.6 kN (3.5 kips). Ultimate load occurred once the slip reached 1.2 mm (0.046 in.) and the first stud collapse occurred at a slippage of 1.5 mm (0.06 in.) and at a load of 11.1 kN (2.5 kips). Separation occurred initially on one side of the specimen as shown in the relative difference between the two lines in Fig. 5.3.

The behavior of specimen QS1P2S is shown in Fig. 5.4. The slip initiated at 6.8 kN (1.54 kips), while visual cracks occurred at 28.9 kN (6.5 kips). The slip increased up to 1.2 mm (0.048 in.), where the maximum load occurred, indicating that there is a good agreement between the slip and ultimate load. It is possible to see graphically that the load decreased systematically until stud failure, which is easy to identify once the collapse provokes a constant slippage for a significant load range. First stud failure occurred at 26.9 kN (6.04 kips) and was identified by a characteristic sound and load drop. Separation occurred on one side only.

Specimen QS1P3S developed an ultimate load close to that of QS1P2S as shown in Fig. 5.5. Specimen configuration of the studs played an important role in the ultimate load. The studs were spaced 19 mm (0.75 in.) center to center. As QS1P2S, QS1P3S had all the studs in the same row. The ultimate load was 31.9 kN (7.2 kips) and the initial slip occurred at 6.4 kN (1.44 kips),

while the initial cracks occurred at 22.24 kN (5.0 kips). The load-slip behavior was similar to the previous specimens in that the slip at ultimate load was 1.1 mm (0.044 in.). Stud failure occurred at nearly the ultimate load of 31.8 kN (7.07 kips), indicating that specimen QS1P3S was more rigid than QS1P2S specimen.

Specimen QS1P4S had studs configured in pairs with two staggered rows spaced 32 mm (1.25 in.) apart and 25 mm (1.0 in.) between the studs. Fig. 5.6 shows that specimen QS1P4S performed better based on the ultimate load. However, the ultimate load was not four times that of specimen QS1P1S. Slip initiated at 11.2 kN (2.52 kips) indicating good agreement between slip and stud configuration, while the first visible cracks occurred at 26.7 kN (6.0 kips) at the stud level. The ultimate load occurred at 0.8 mm (0.031 in.) slippage and at a load of 43.0 kN (9.7 kips). The slip indicated that the system was more rigid according to the number of studs and configuration. The first stud failure started at 24.3 kN (5.46 kips) and ultimate failure occurred with a gradual separation of both sides.

Specimen QS2P1S had twice the number of pockets of specimen QS1P1S, however, the ultimate load did not double. As a result, there was no direct relationship between the number of studs in the pocket and the corresponding ultimate load, i.e., the load associated with 2, or 3 studs in a respective pocket did not necessarily correlate in doubling or tripling the ultimate load. Specimen developed a load up to 10.0 kN (2.25 kips) where the slip started and kept increasing until it reached an ultimate load of 32.2 kN (7.24 kips) and a slip of 1.4 mm (0.057 in.) as shown in Fig. 5.7. The initial slip was double that of the one pocket specimen and the initial cracks appeared at 27.8 kN (6.25 kips). First stud failure occurred at 29.6 kN (6.65 kips), which was characterized by constant slip. Failure of the studs occurred at approximately the ultimate load, indicating that the specimen with two pockets was more rigid than the specimen with one pocket.

The results for specimen QS2P2S are presented in Fig. 5.8. This specimen was quite similar to QS1P2S in its response to loading. In the specimen with one pocket, stud failure occurred at 52.3 kN (11.75 kips). The maximum load was 54.8 kN (12.2 kips) that corresponds to a slippage of 1.0 mm (0.038 in.). The first sign of slippage was recorded at 13.8 kN (3.1 kips),

while the initial visual crack occurred at 23.8 kN (5.4 kips). The load that was necessary to initiate slippage was approximately double that of the one pocket specimen.

Figure 5.9 shows the results for the two pocket specimen with three studs QS2P3S. The ultimate load was practically double that of the specimen with one pocket. The ultimate load was 62.1 kN (14.0 kips) at a slippage of 1.2 mm (0.047 in.). After it reached ultimate load, the first stud failure occurred at 51.6 kN (11.6 kips) and visual cracks were observed at 25.6 kN (5.8 kips). Separation initiated on one side and consequently ended with both sides separating.

The results for specimen QS2P4S are shown in Fig. 5.10. The load and slip were proportional to the specimen with one pocket. The specimen was loaded up to 28.0 kN (6.3 kips), where consequently the first sign of slippage occurred. The ultimate load was recorded at 96.0 kN (21.6 kips), and consequently decreased to 77.1 kN (17.3 kips), where the first stud failure occurred. The slip due to the ultimate load was 1.0 mm (0.040 in) and the separation initiated on one side ending with both slabs separating.

The results for specimen QS3P1S are shown in Fig. 5.11. The ultimate load was 42.8 kN (9.6 kips) at a slippage of 0.8 mm (0.033 in.). The slip initiated at 10.8 kN (2.4 kips) and first cracking appeared on one side at 34.7 kN (7.8 kips). The separation occurred in both slabs at the same time. The load-slip behavior of specimen QS3P2S is represented by Fig. 5.12. The specimen confirmed the non-linear relationship between the specimens with the same number of studs and different number of pockets. The ultimate load was 71.2 kN (16.1 kips), 2.4 times the ultimate load of the specimen with one pocket. The first slip occurred at 17.8 kN (4.0 kips), which was 2.6 times that for specimen QS1P2S and cracks were identified at 38.0 kN (8.6 kips).

The performance of specimen QS4P1S is shown in Fig. 5.13. The strength of the specimen was below expected, where the maximum load was 58.4 kN (13.1 kips) and the respective slippage was 0.9 mm (0.037 in.). The specimen initial slip occurred at 20.1 kN (4.5 kips), which represented approximately four times the load-slip of specimen QS1P1S. Cracks were noted at 40.7 kN (9.2 kips) on one side of the specimen. First stud failure occurred at 53.2

kN (12.0 kips) with a final separation of one side at 37.4 kN (8.4 kips). The results for specimen QS4P2S are presented in Fig. 5.14. The ultimate load was 121.0 kN (27.22 kips), which was 4 times the ultimate load of specimen QS1P2S. The slippage at that point was 0.4 mm (0.016 in.). The initial slip occurred at 16.0 kN (3.6 kips), while the first stud failure at 96.0 kN (21.6 kips).

The plots shown in Fig. 5.15 represent the average load-slip behavior for the specimens with one pocket. The ultimate load was approximated at the same slip for all four plots. However, first stud failure occurred at different slippage for each specimen. The ultimate loads for 2, 3 and 4 stud specimens were as much 1.7, 1.8 and 2.4 as of 1 stud specimen, respectively. It is observed that the ultimate loads for two and three stud specimens were almost the same. This may be due to the stud configuration.

Figure 5.16 shows the slip average of the two pocket specimens. The behavior is quite similar for all specimens and the ultimate load was observed at the same slippage point. The ultimate loads for 2, 3 and 4 stud specimens were as much 1.7, 1.9 and 3 as of 1 stud specimen, respectively. Similar trend was obtained among the specimens with 2 and 3 studs as noticed for one pocket specimens. These results confirm that the stud configuration is very important in load carrying capacity of shear connection. The addition of two studs in a second line improves the composite performance more than the addition of one stud in the same line. Fig. 5.17 summarizes the behavior of the specimens with three pockets. The slippage during the ultimate load is almost coincident. The behavior of the specimens under the loading is basically the same, however, stud failure occurred at different slippage. The ultimate load for 2 stud specimen was 1.7 times that of 1 stud specimen following the similar trend with 1 and 2 pockets. Fig. 5.18 shows the average of the slip readings at the critical slab side for the specimens with four pockets. The loading behavior was significantly different and the ultimate load occurred at different slippage points. However, the results were satisfactory since specimen QS4P2S carried 2 times the load of QS4P1S.

Comparison between the different number of studs and ultimate load is illustrated in Fig. 5.19. This figure shows that there is no direct relationship between the number of studs and

ultimate load. The ultimate strength increased significantly when the number of studs was increased. However, the rate of increment of load with 3 studs slowed down which is attributed to the stud configuration. It is also observed that the rate of increment of ultimate load increases as the number of pocket increases.

Comparison between the number of pockets and the ultimate load is presented in Fig. 5.20. This figure shows a good conformity among specimens with different number of pockets. For the specimens with a fixed number of studs, as the number of pocket increased, total contact area of concrete increased, hence the load was larger. The figure also shows a steeper slope for the specimens with higher studs. The specimens with three studs showed a very little improvement in terms of ultimate load when compared to the two stud specimens.

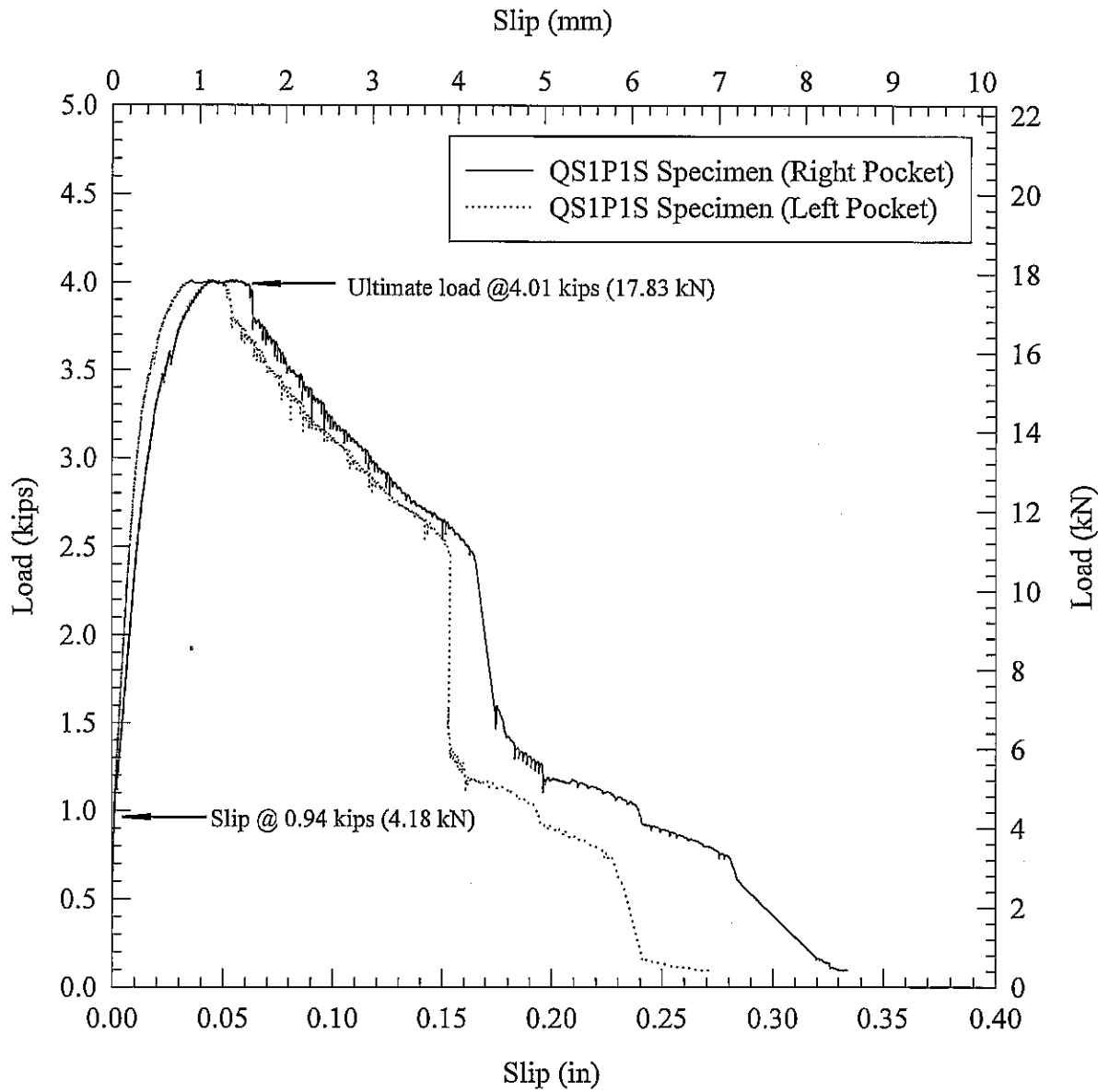


Fig. 5.3 Load-Slip curves for specimen with 1 shear pocket and 1 stud per pocket

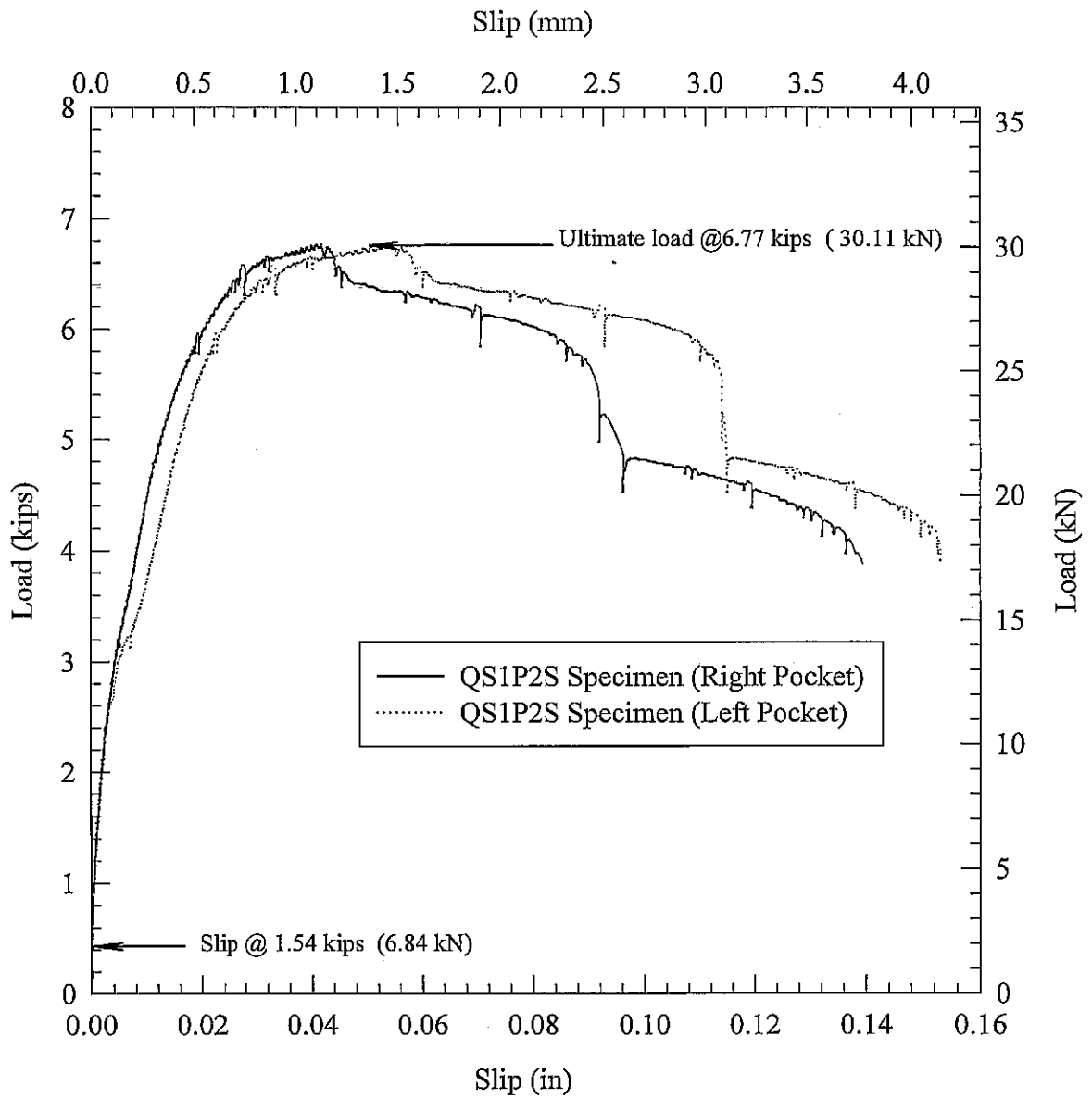


Fig. 5.4 Load-Slip curves for specimen with 1 shear pocket and 2 studs per pocket

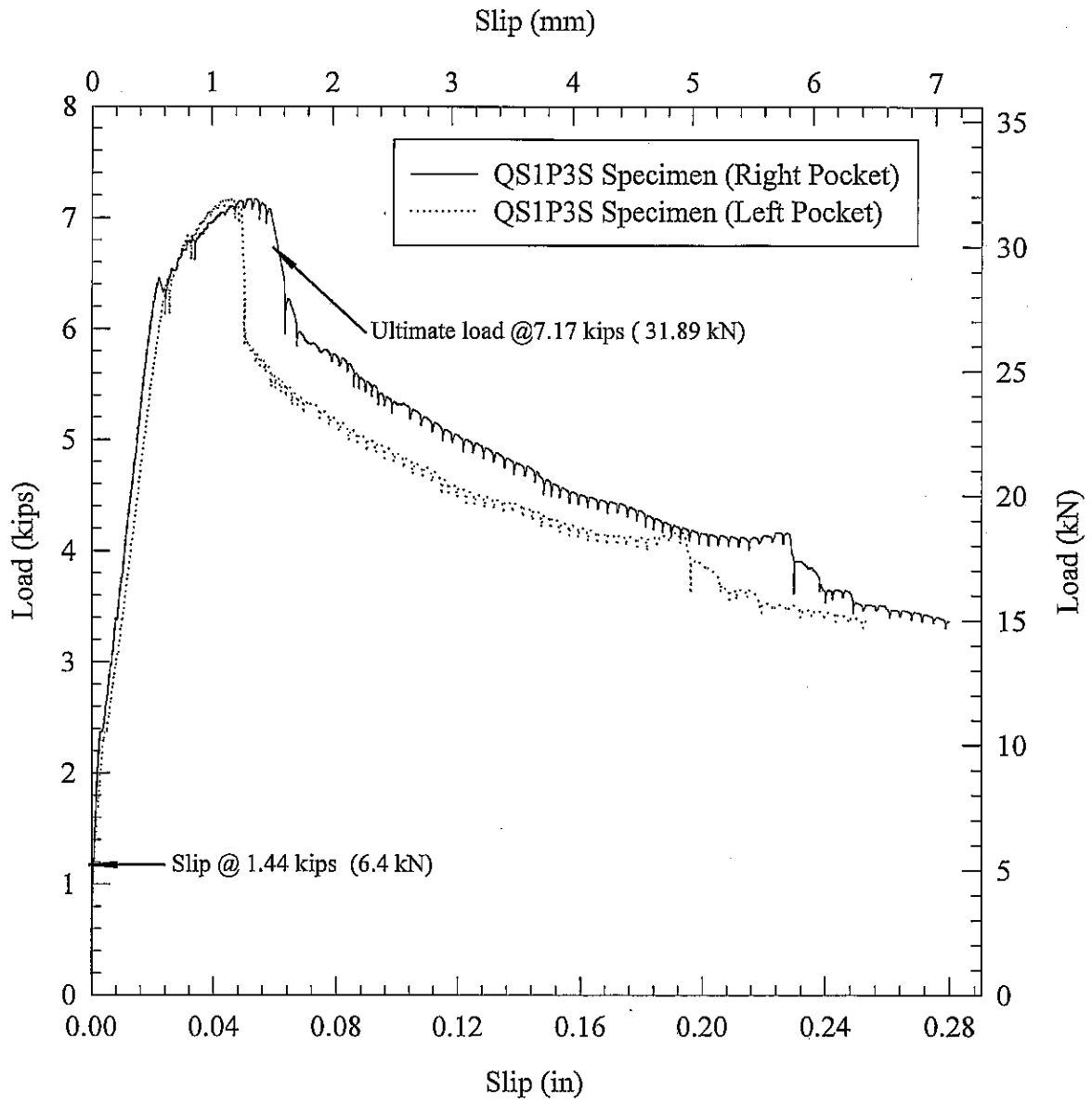


Fig. 5.5 Load-Slip curves for specimen with 1 shear pocket and 3 studs per pocket

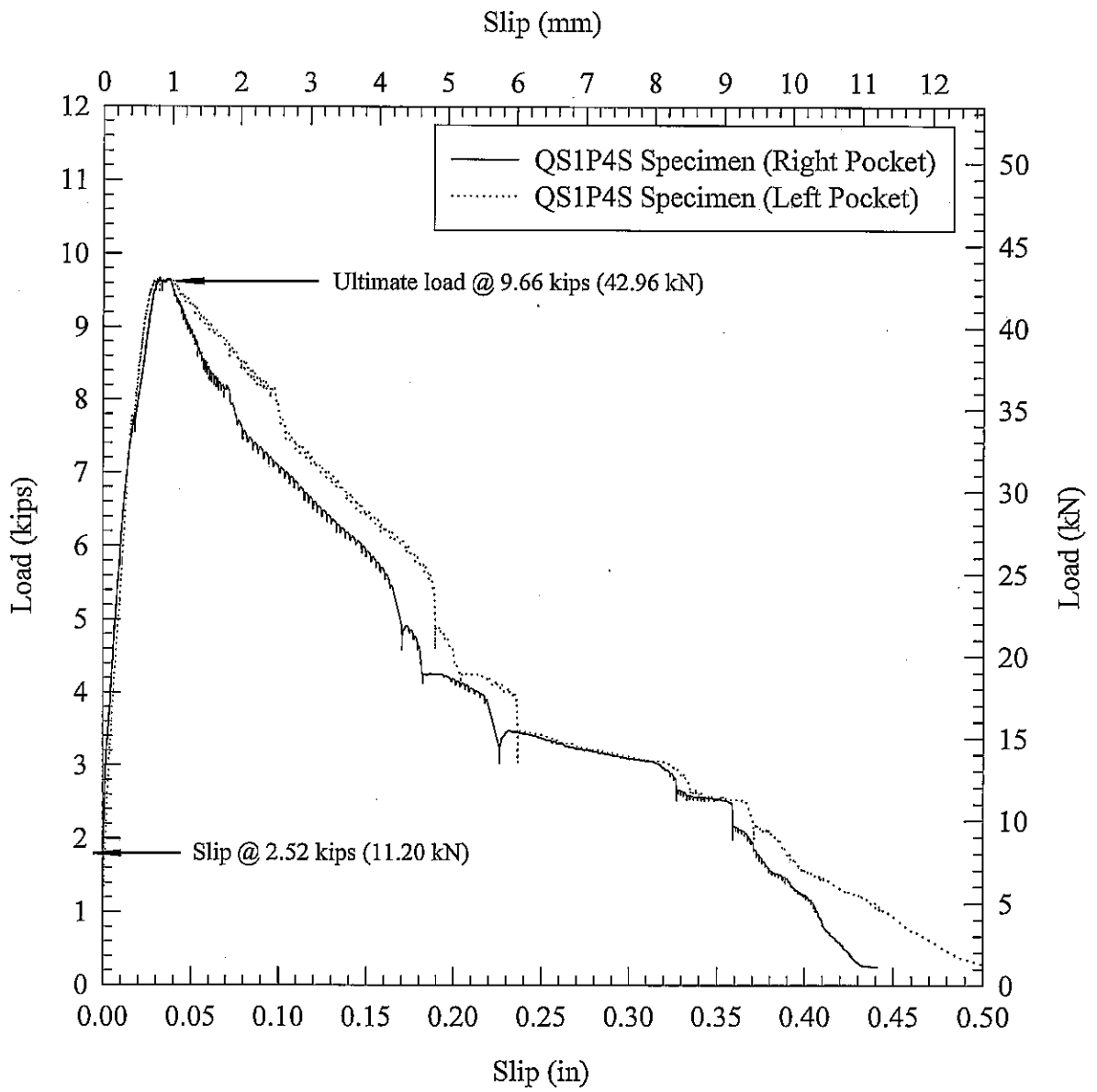


Fig. 5.6 Load-Slip curves for specimen with 1 shear pocket and 4 studs per pocket

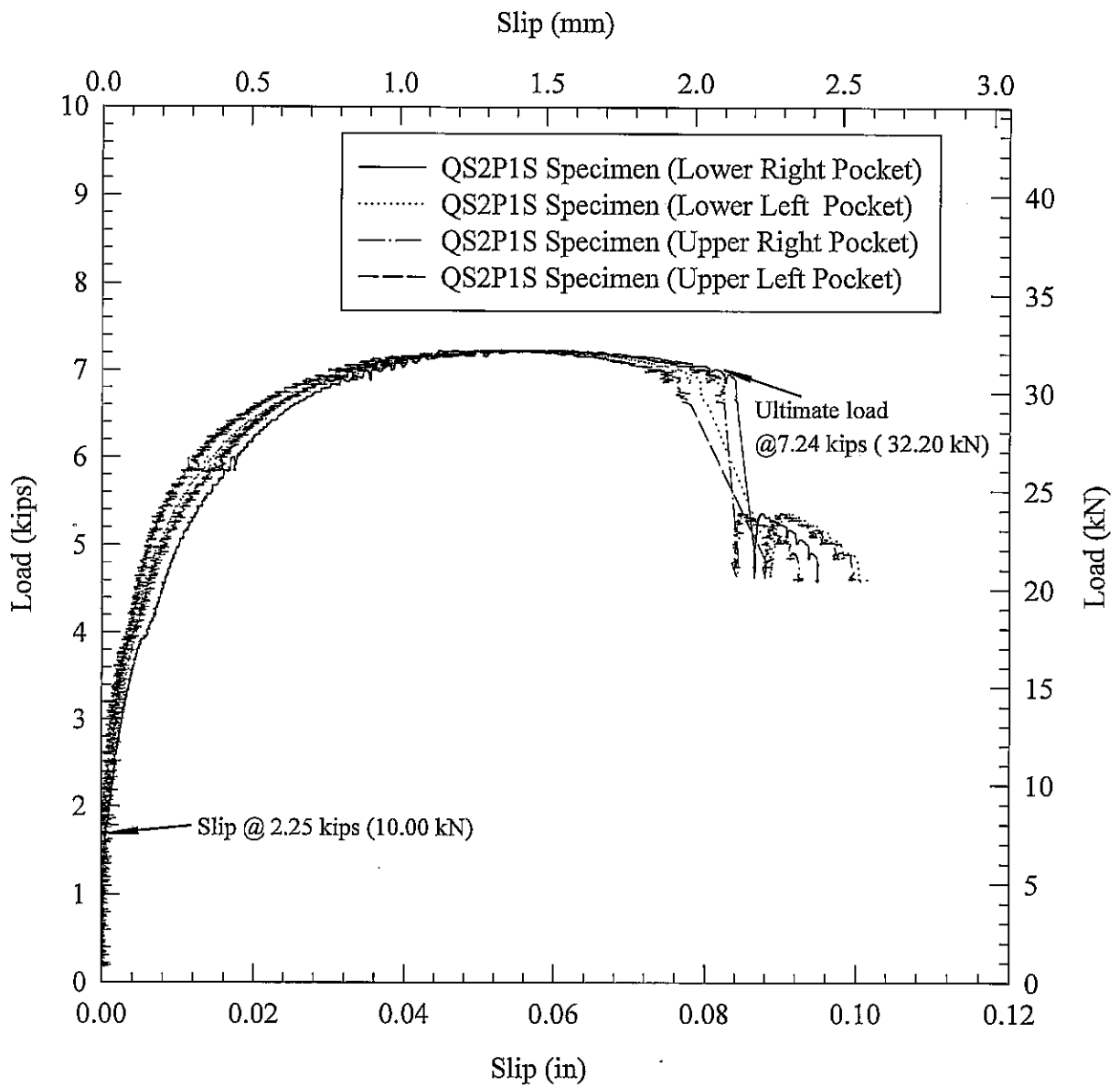


Fig. 5.7 Load-Slip curves for specimen with 2 shear pockets and 1 stud per pocket

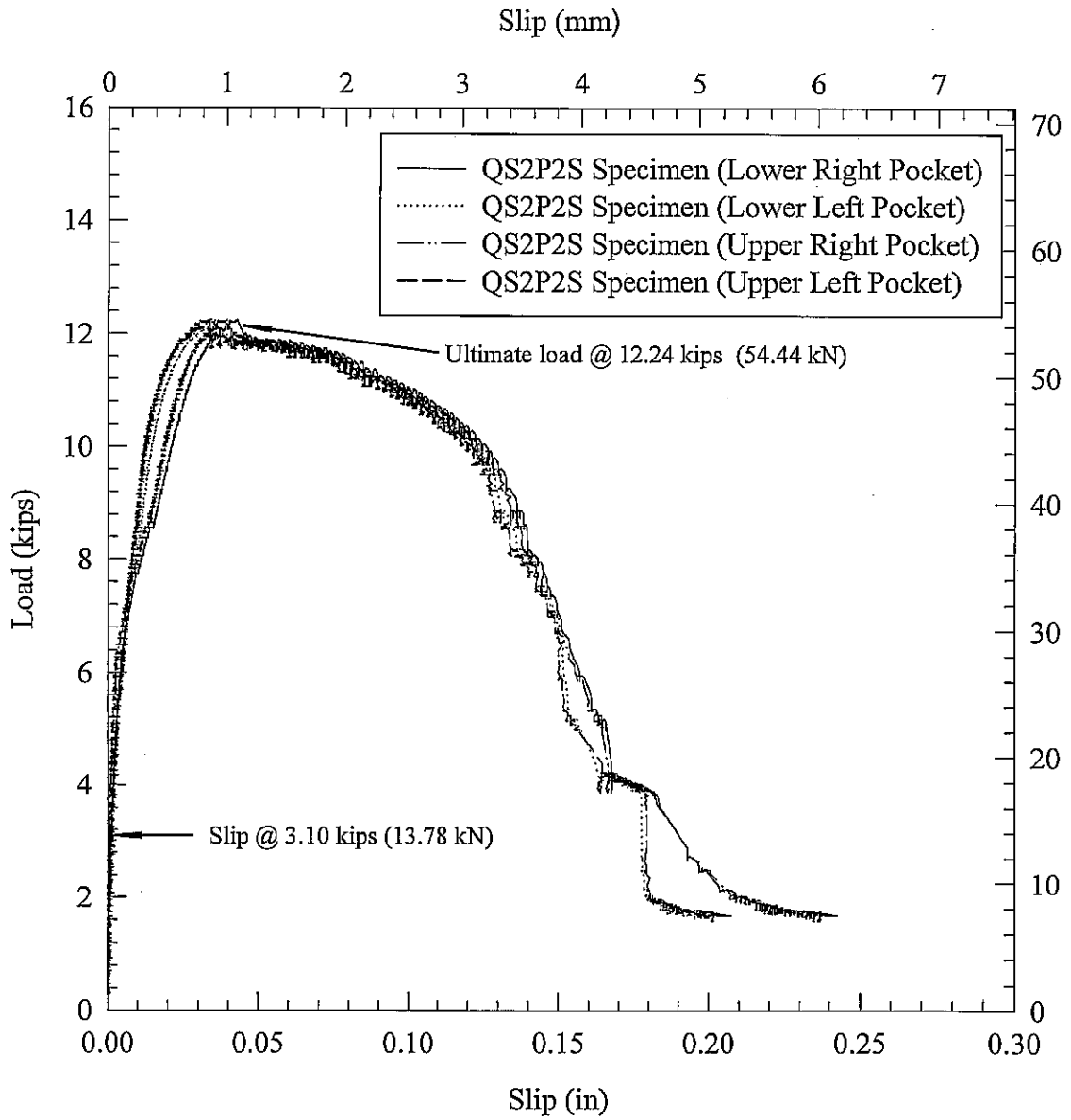


Fig. 5.8 Load-Slip curves for specimen with 2 shear pockets and 2 studs per pocket

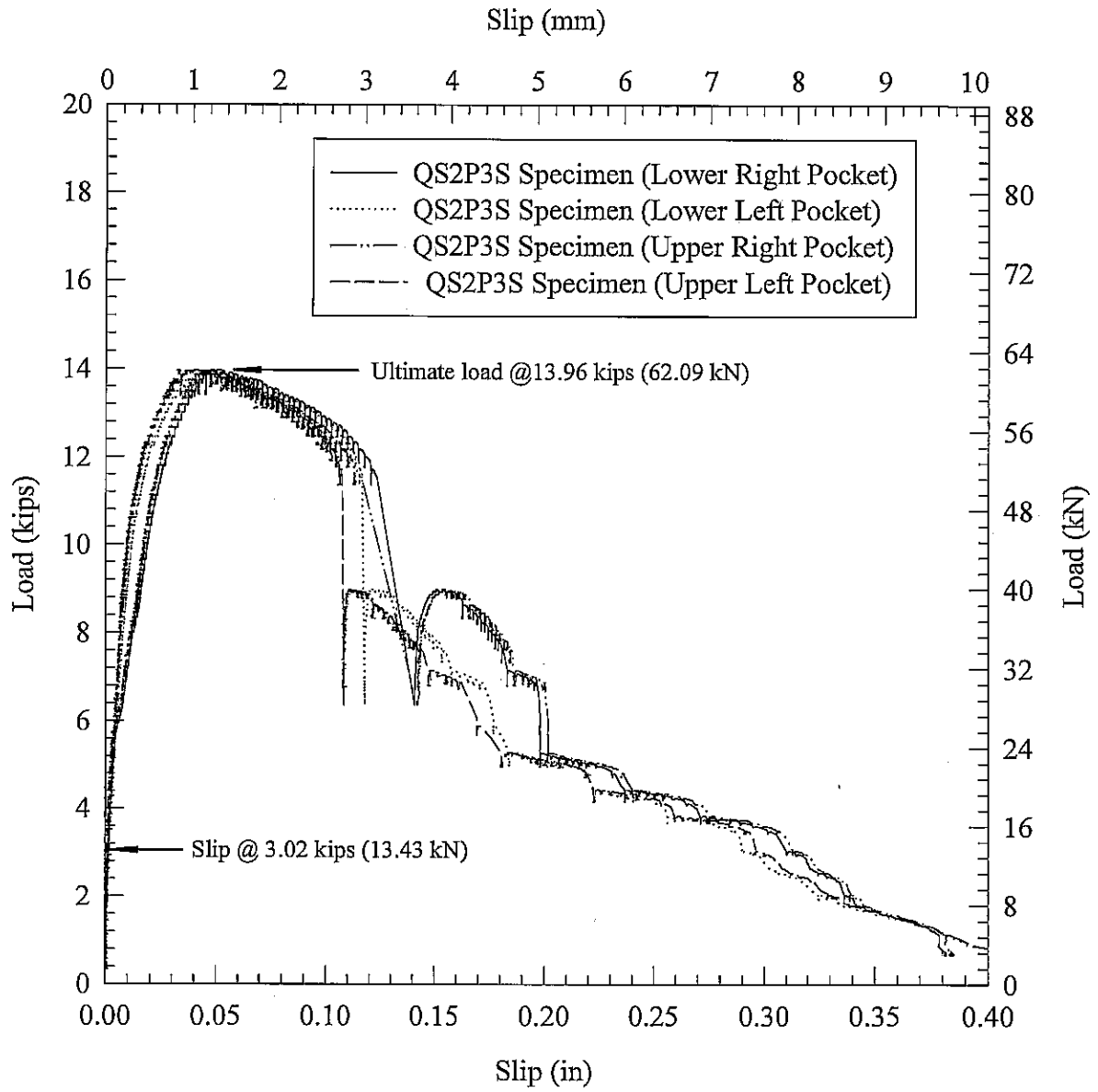


Fig.5.9 Load-Slip curves for specimen with 2 shear pockets and 3 studs per pocket

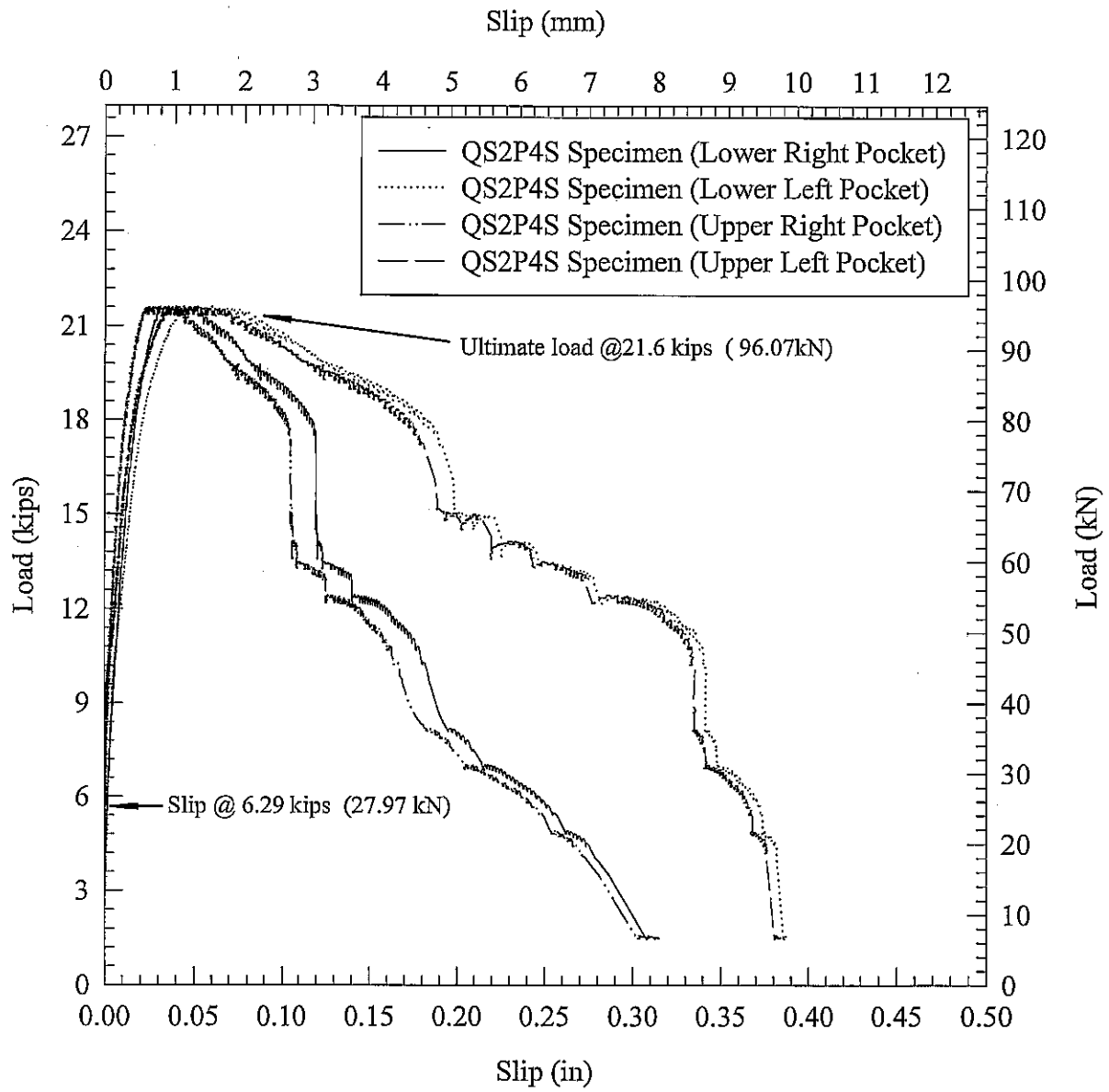


Fig. 5.10 Load-Slip curves for specimen with 2 shear pockets and 4 studs per pocket

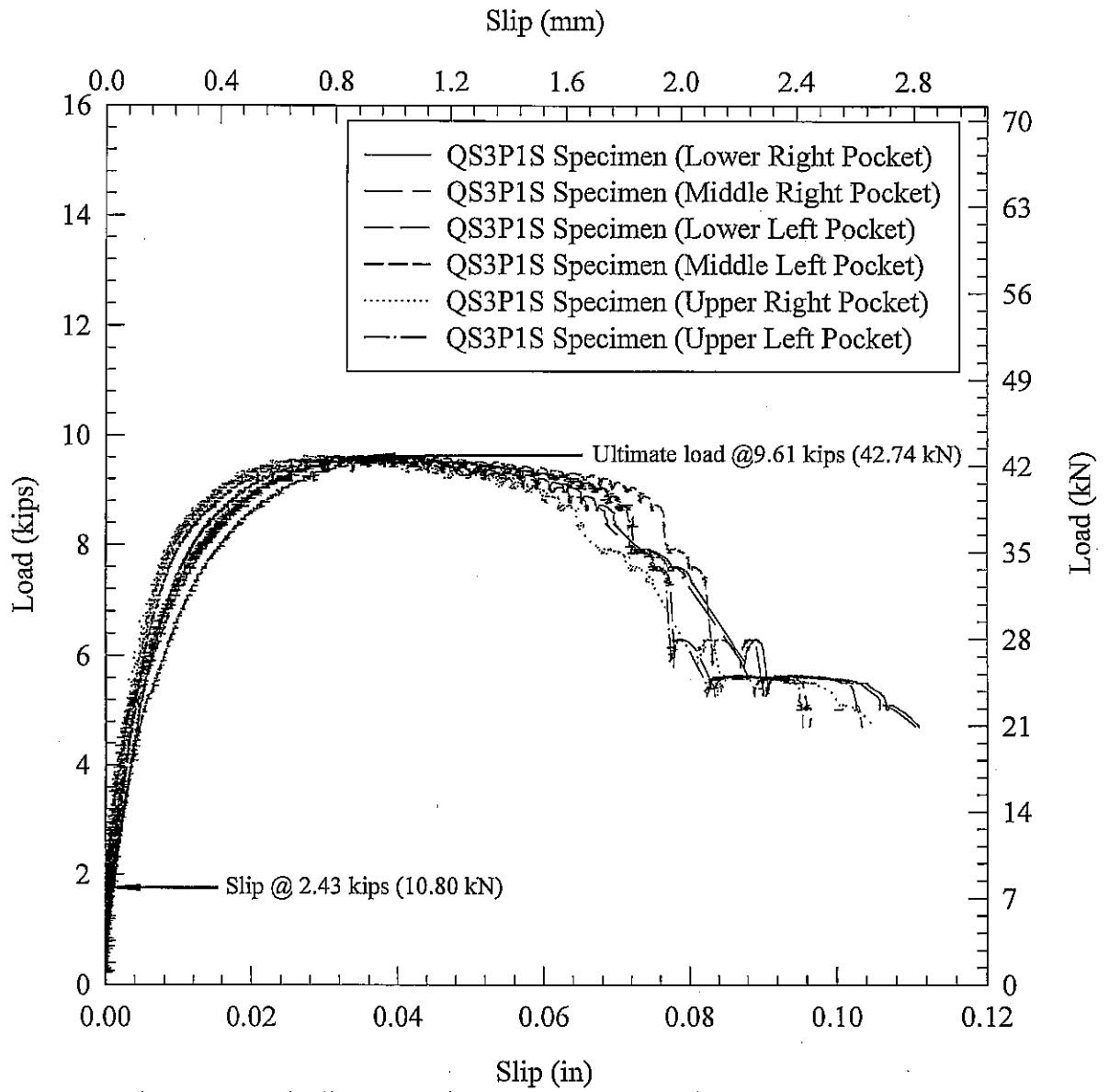


Fig. 5.11 Load-Slip curves for specimen with 3 shear pockets and 1 stud per pocket

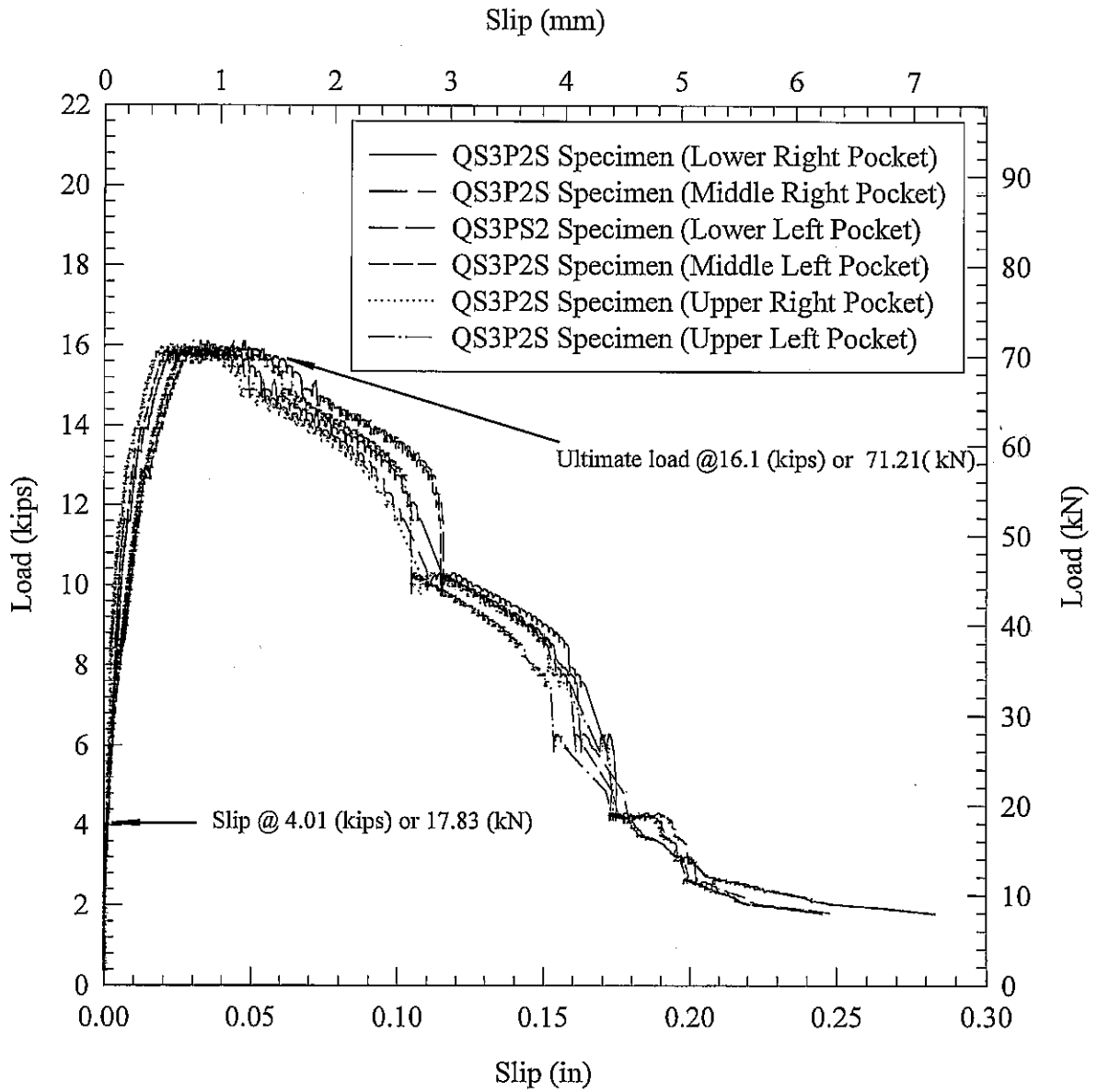


Fig. 5.12 Load-Slip curves for specimen with 3 shear pockets and 2 studs per pocket

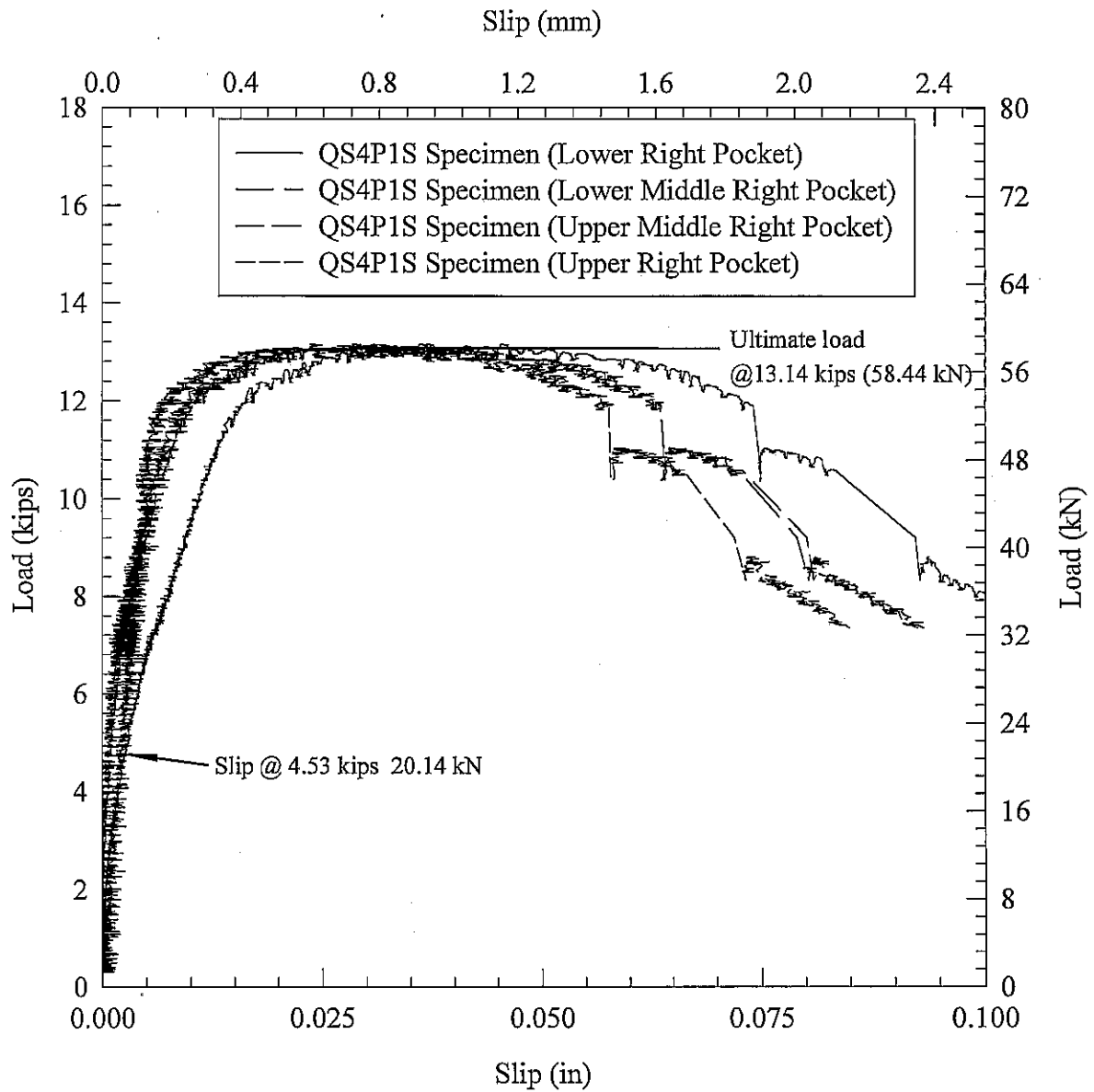


Fig. 5.13 Load-Slip curves for specimen with 4 shear pockets and 1 stud per pocket per pocket.

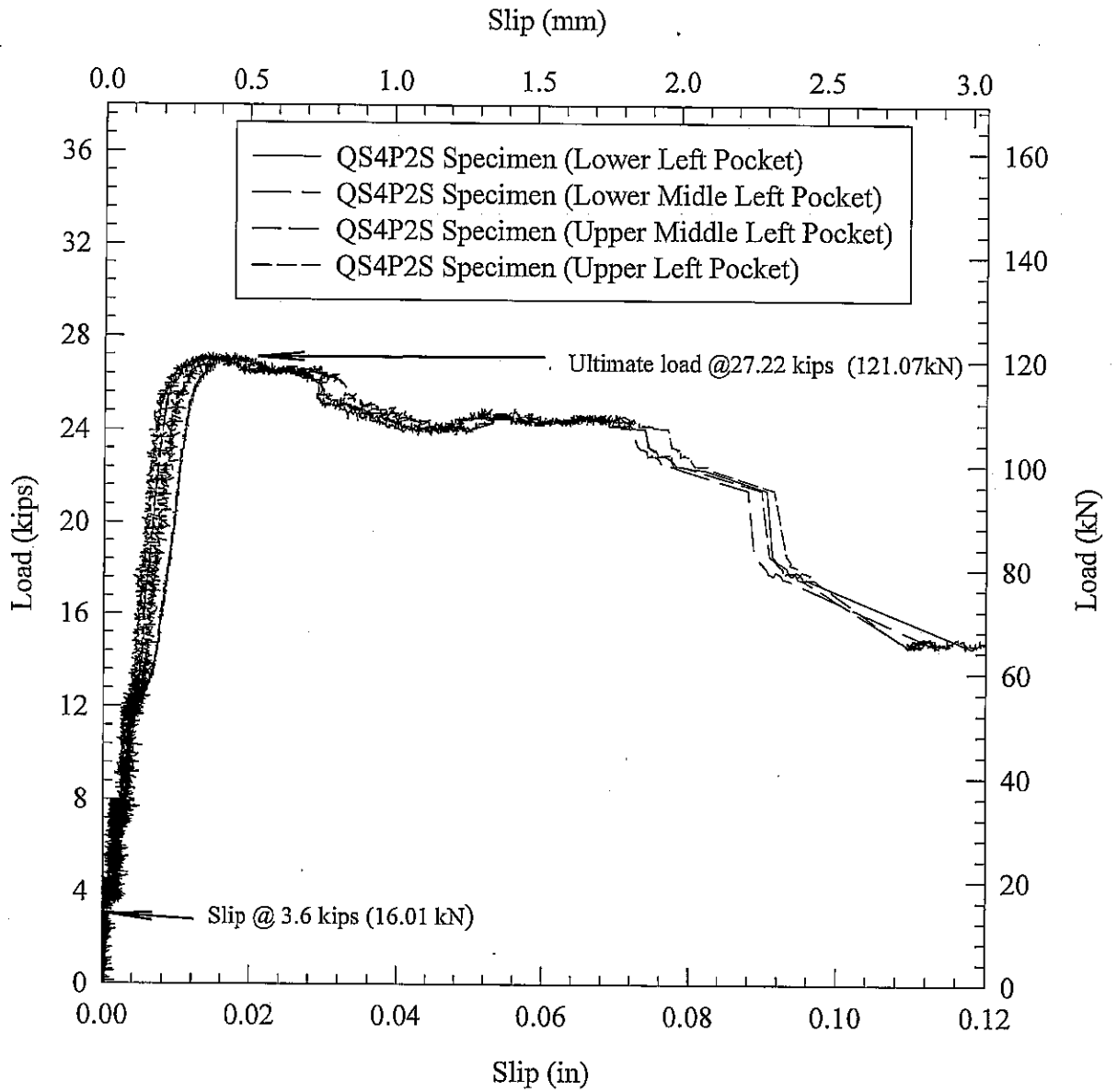


Fig. 5.14 Load Slip curves for specimen with 4 shear pockets and 2 studs per pocket

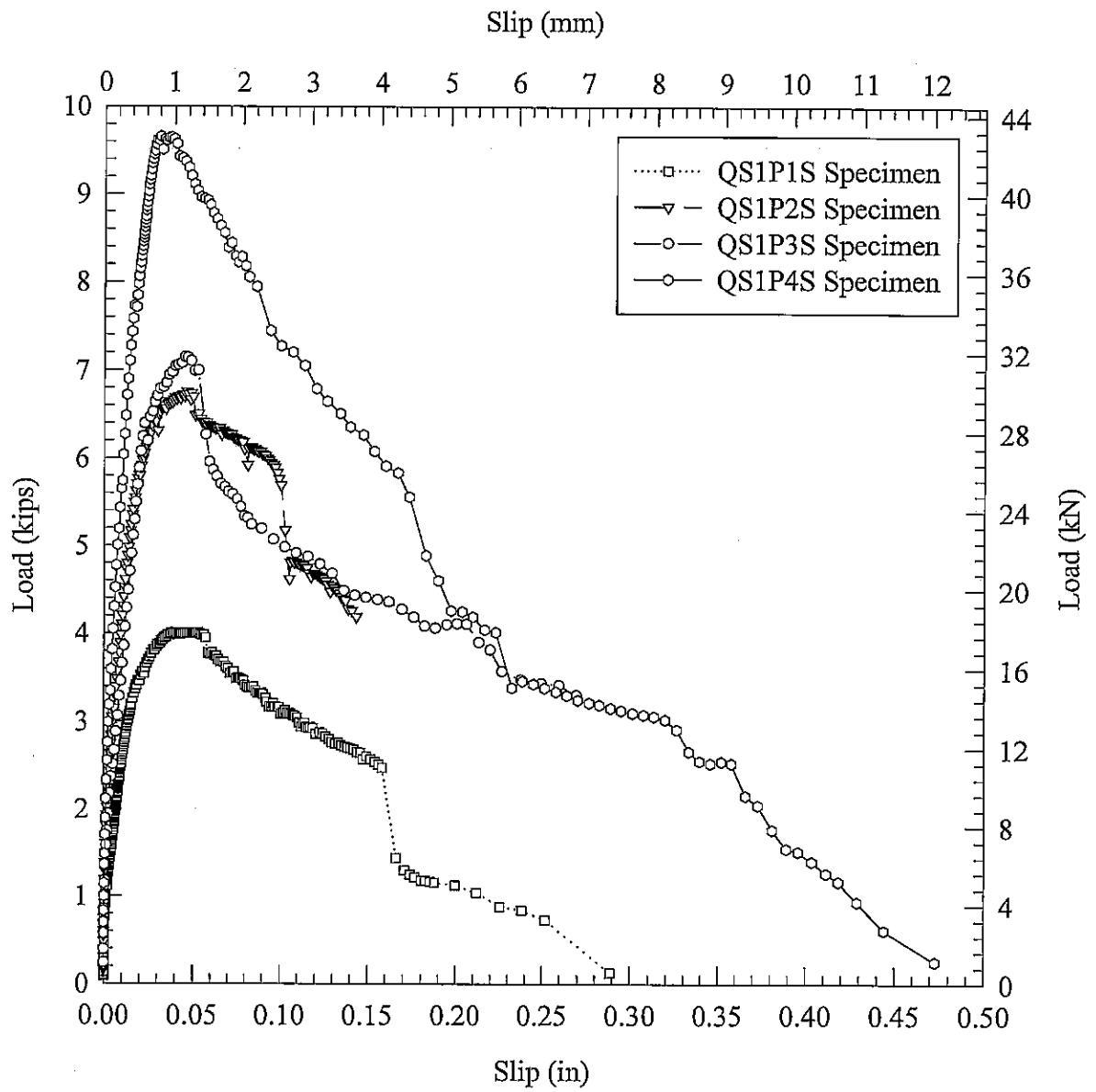


Fig.5.15 Load-Slip curves for specimens with one pocket

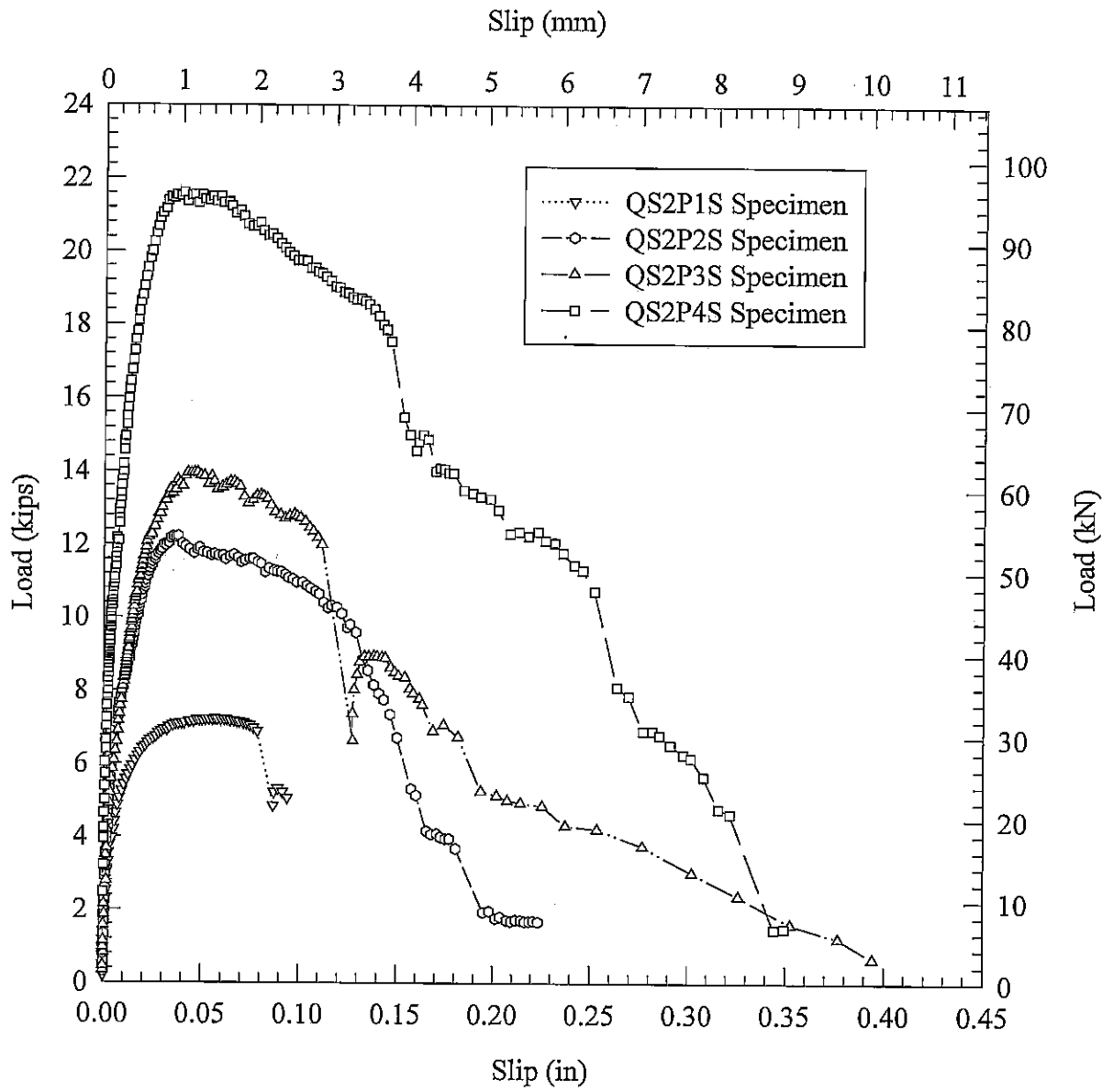


Fig. 5.16 Load-Slip curves for specimens with two pockets

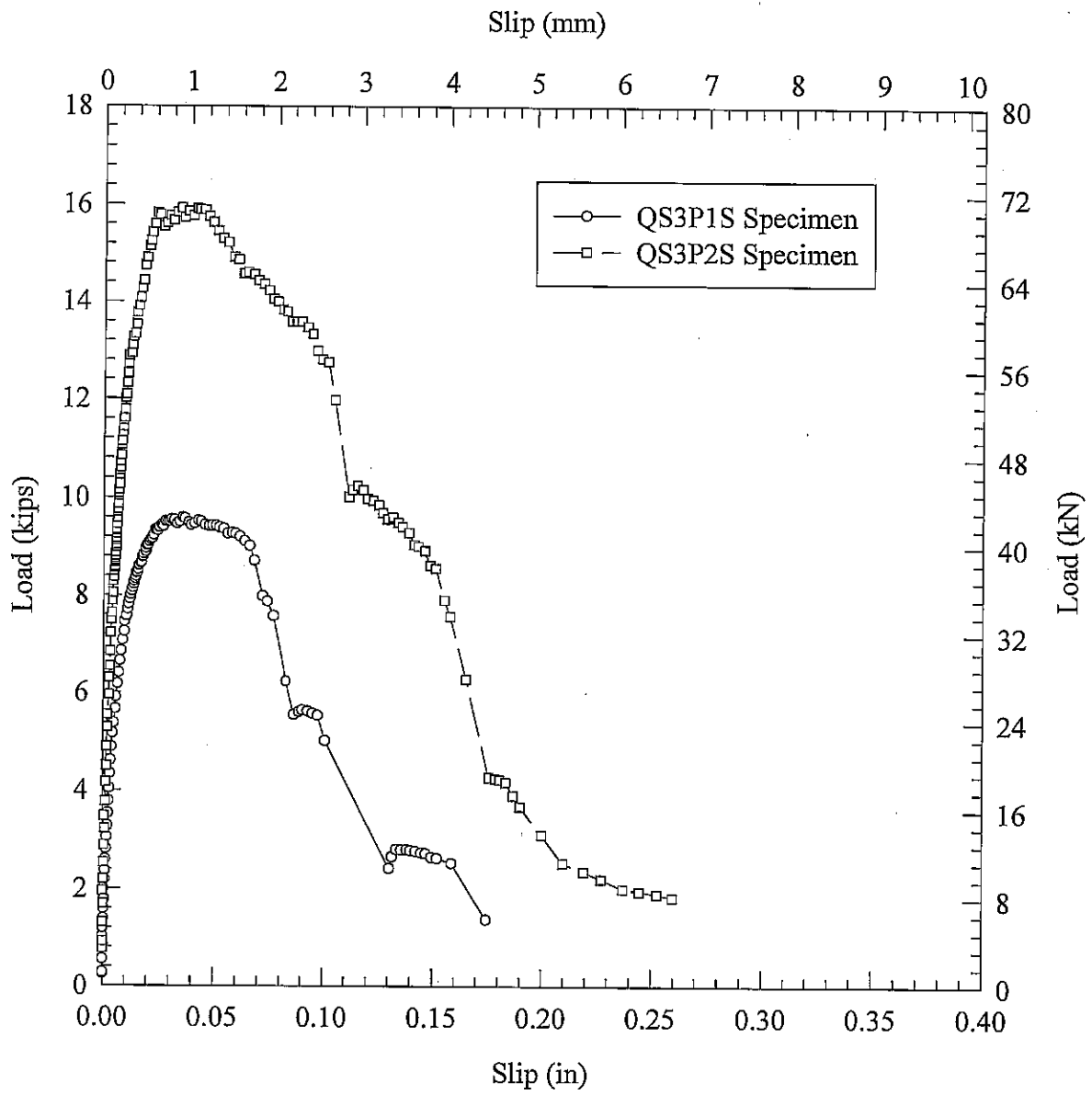


Fig 5.17 Load-Slip curves for specimens with three pockets

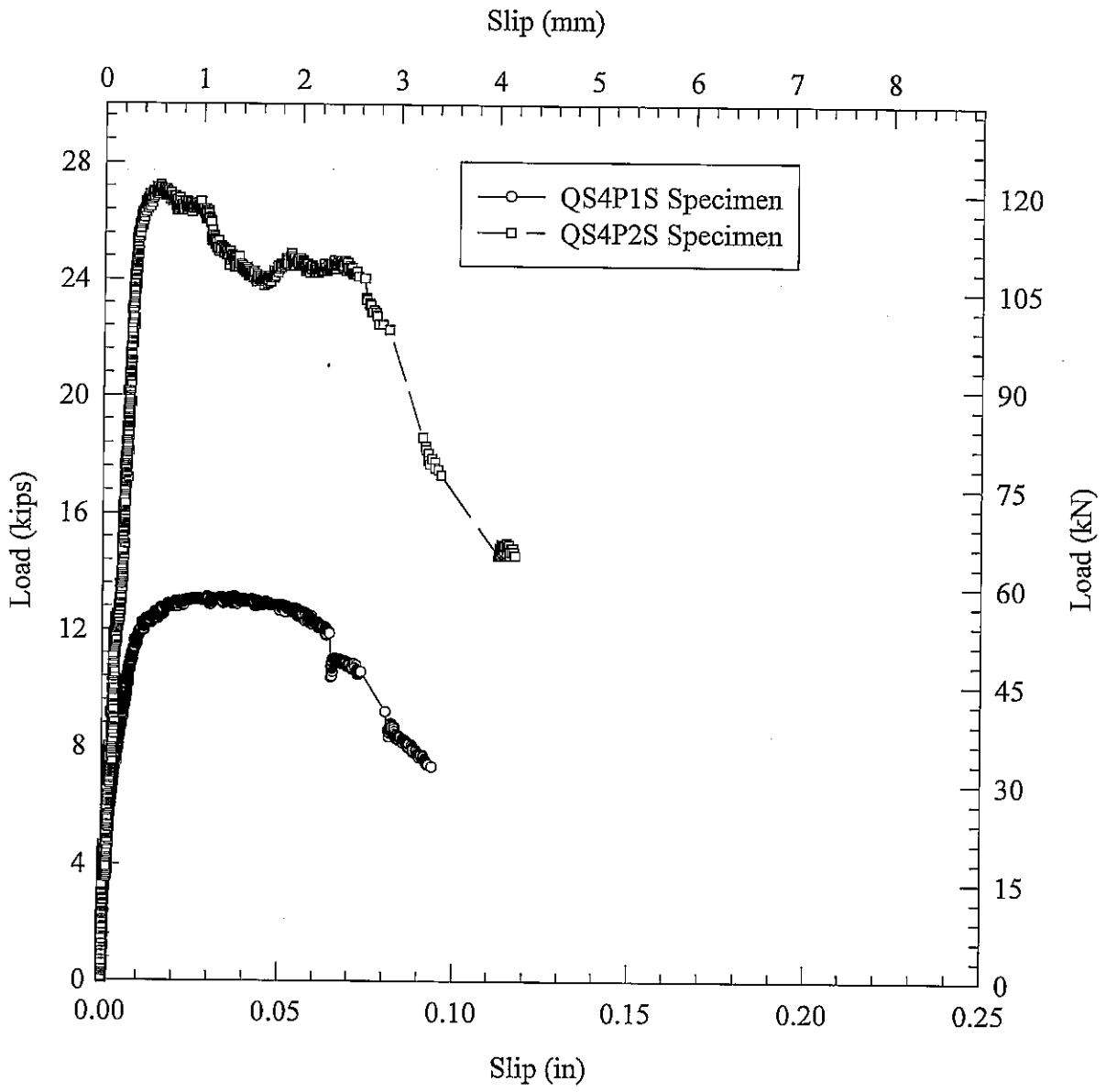


Fig 5.18 Load-Slip curves for specimens with four shear pockets

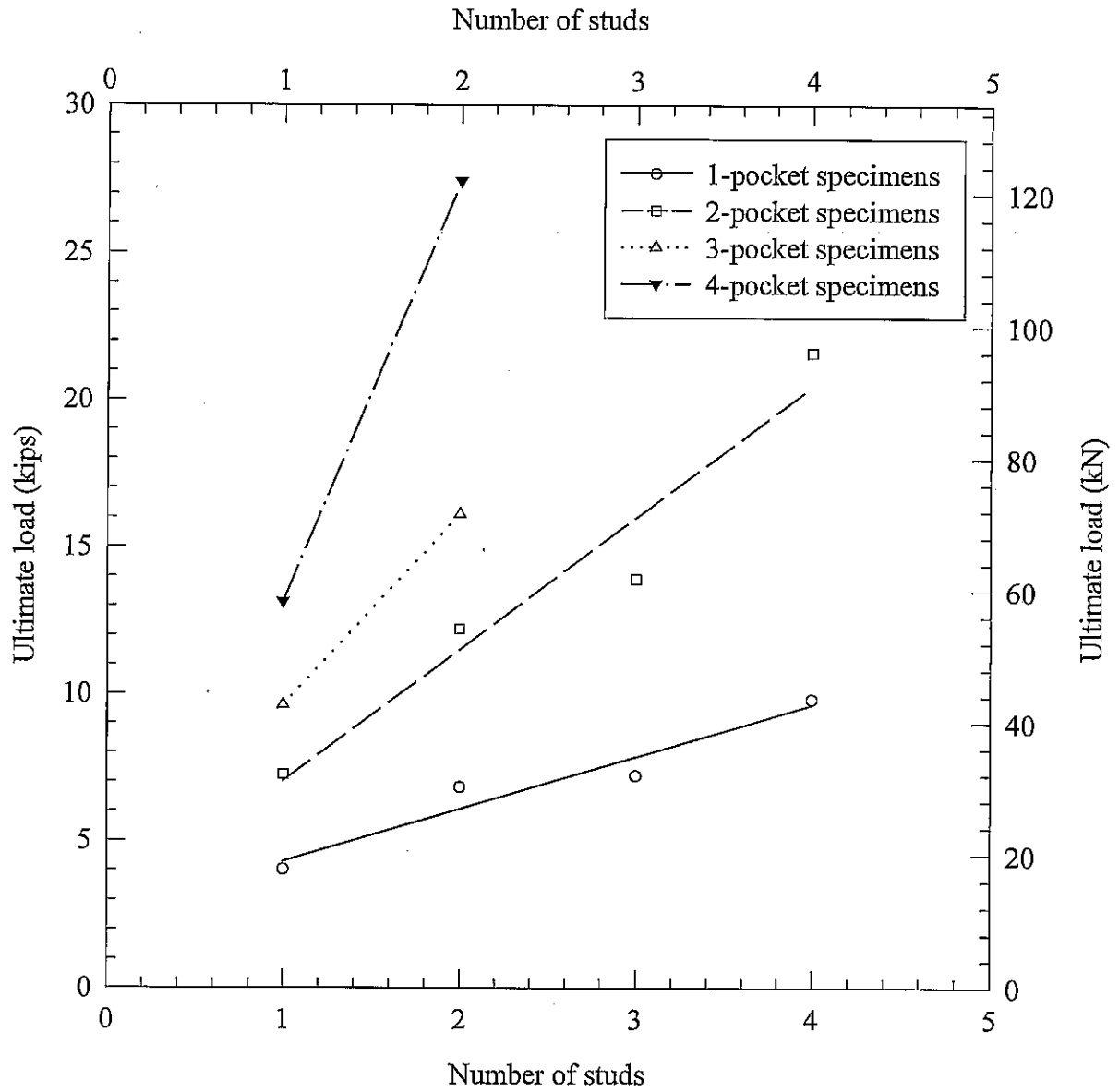


Fig. 5.19 Ultimate load versus number of studs for quarter-scale specimens

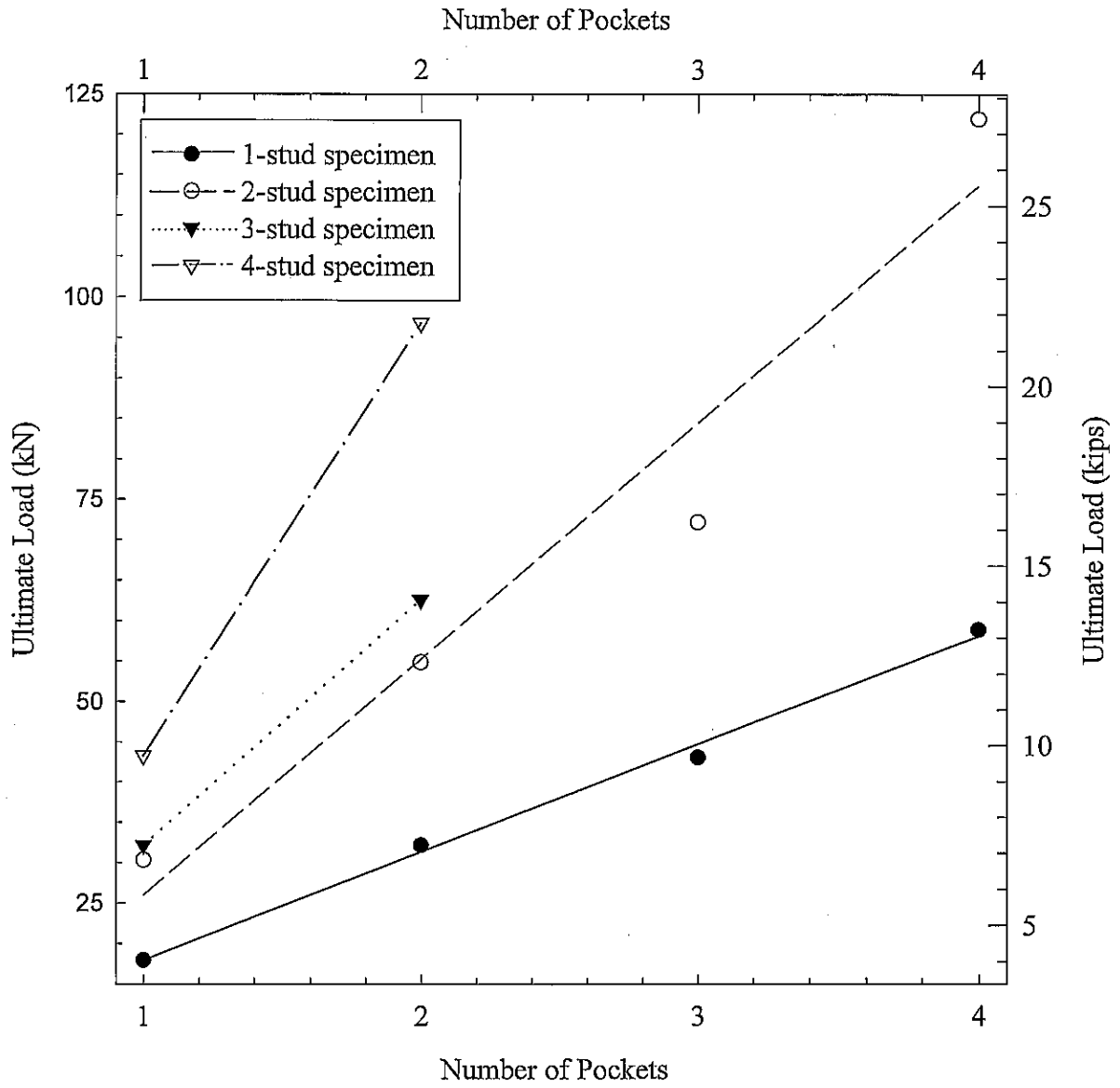


Fig. 5.20 Ultimate load versus number of pockets

## 5.2 Test Results for Full-Scale Shear Connection

During tests it was observed that in most of the specimens, the cracks initiated at the level of the stud. The first stud failure was easy to identify during the test since it occurred after the ultimate load with a sudden drop of load. The modes of failure in all cases occurred at the base of the stud, while all studs failed in shear. In some cases, the studs were subjected to bending, however, the dominant mode of failure was shear. The test results are shown in Table 5.2. The typical shape of the push-out specimens after failure is shown in Fig. 5.21. The shearing of studs and the grouting material for one-pocket four-stud specimen is shown in Fig. 5.22.

The load-slip curves are presented in Figs. 5.23-5.31. After ultimate load, only the studs carried the load and slippage occurred until complete shearing of the studs. The ultimate load for the specimens with one shear pocket on each side and two studs per pocket occurred at 604 and 627 kN (141 and 136 kips) for specimens 1 and 2, respectively. The load-slip behavior of specimen FS1P2S is shown in Fig. 5.23. During the test, a linear relationship was noticed between the slip and load increment.

Cracking in the set grout haunch was an important parameter in determining the propagation of the load in the specimen. The cracks initiated at the stud level until the end of the set grout haunch, i.e., 203 mm (8 in.) before the end of the specimen. Separation occurred initially on one side of the specimen as shown in the relative difference between the two lines of Fig. 5.23.

The behavior of specimen FS1P3S is shown in Fig. 5.24. It is observed that the load decreased systematically until stud failure, which is easy to identify once the collapse provokes a constant slippage for a significant load range. Separation occurred on one side only. Specimen FS1P4S developed an ultimate load of 1065 and 1094 kN (239 and 246 kips) as shown in Fig. 5.25. All the one pocket specimens FS1P2S, FS1P3S and FS1P4S had all the studs in the same row. The ultimate loads carried by the 3 and 4 stud specimens were 1.3 and 1.8 times the ultimate load carried by 2 stud specimen, respectively. It can also be seen from Table 5.2 that

addition of 2 studs in one pocket specimens increases the shear capacity as much as 11 times the specimen with no stud.

The load-slip behavior of FS2P2S specimens is shown in Fig. 5.26. The ultimate loads for both specimens were 553 and 504.5 kN (124.5 and 113.5 kips). Although FS2P2S specimens had twice the number of pockets of specimen FS1P2S, the observed ultimate load was not double. As a result, there was no direct relationship between the number of pockets and the corresponding ultimate load.

The results for specimen FS2P3S are presented in Fig. 5.27. The ultimate load carried by the specimens were 1579 and 1566 kN (355 and 352 kips). The load necessary to initiate slip was approximately double that of the one pocket specimen. Both slabs separated at the end of the test. The ultimate load carried by the 3 stud specimens was 1.5 times that of 2 stud specimen. It can also be observed from Table 5.2 that addition of 2 studs in two pocket specimens increases the shear capacity as much as 8 times that of the specimen with no stud.

Comparison between the different number of studs and load-slip behavior are illustrated in Figs. 5.28 and 5.29 for one and two pockets, respectively. These figures show that there is no direct relationship between the number of studs and load-slip behavior. The ultimate strength increased significantly when the number of studs was increased. Comparison between the number of pockets and load-slip behavior is presented in Figs. 5.30 and 5.31 for 2 and 3 studs, respectively. These figures show a good conformity among specimens with different number of pockets.

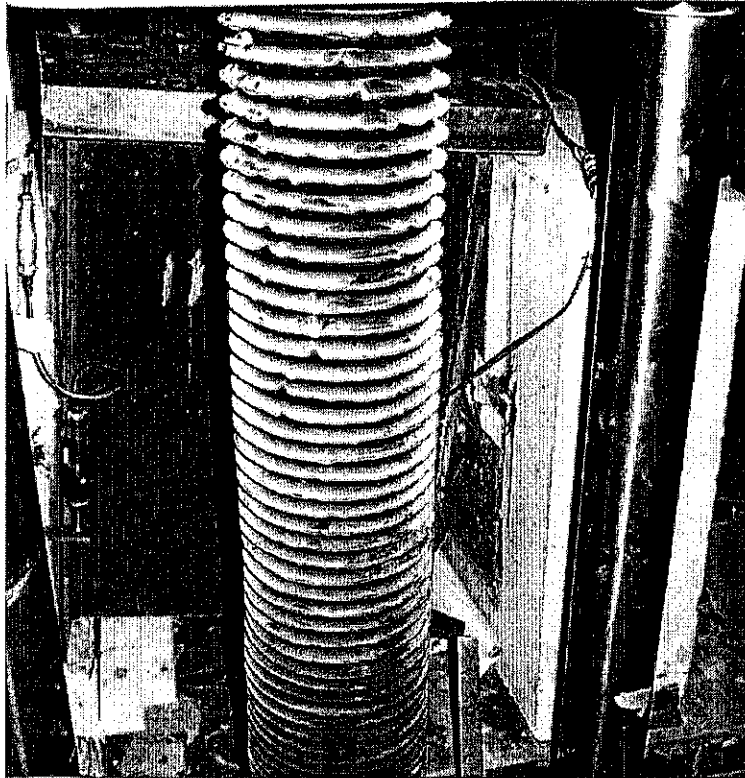


Fig. 5.21 Mode of failure for typical full-scale shear connection specimen

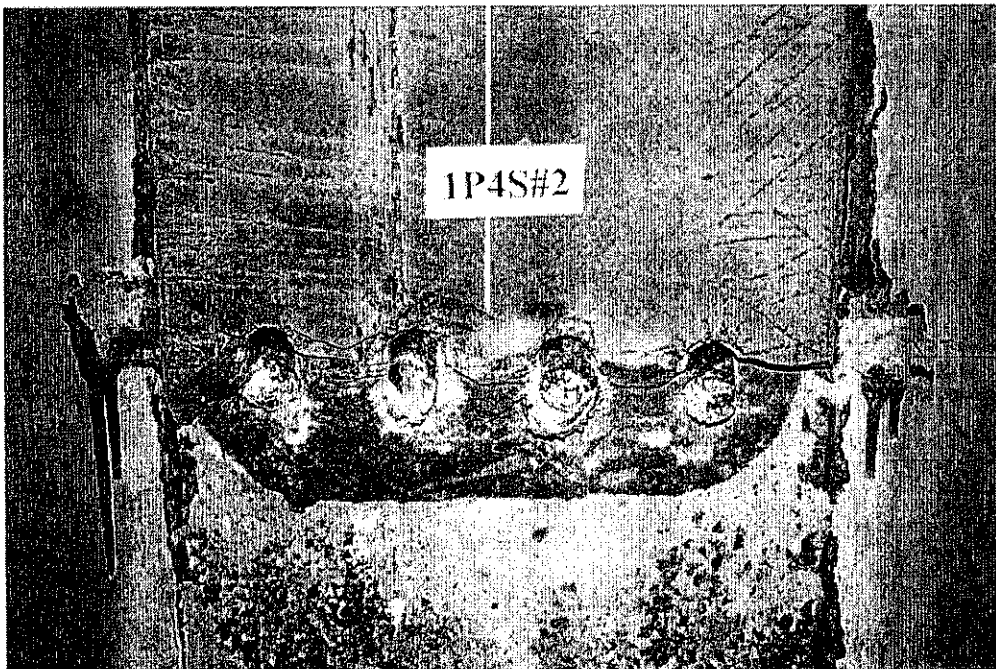


Fig. 5.22 Shearing of studs and the grouting material in typical full-scale specimen

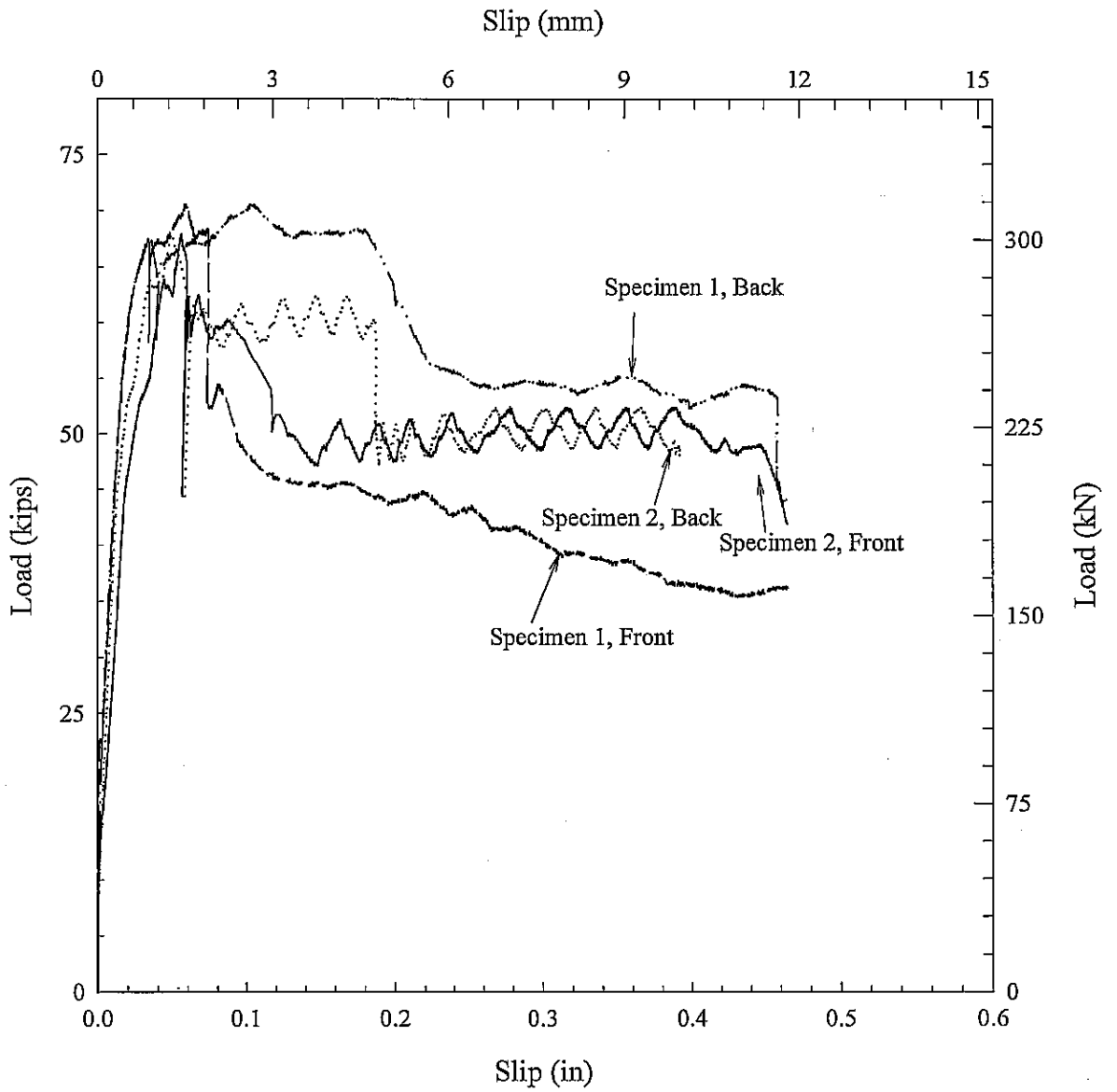


Fig. 5.23 Load-slip behavior for one pocket specimen and two studs per pocket

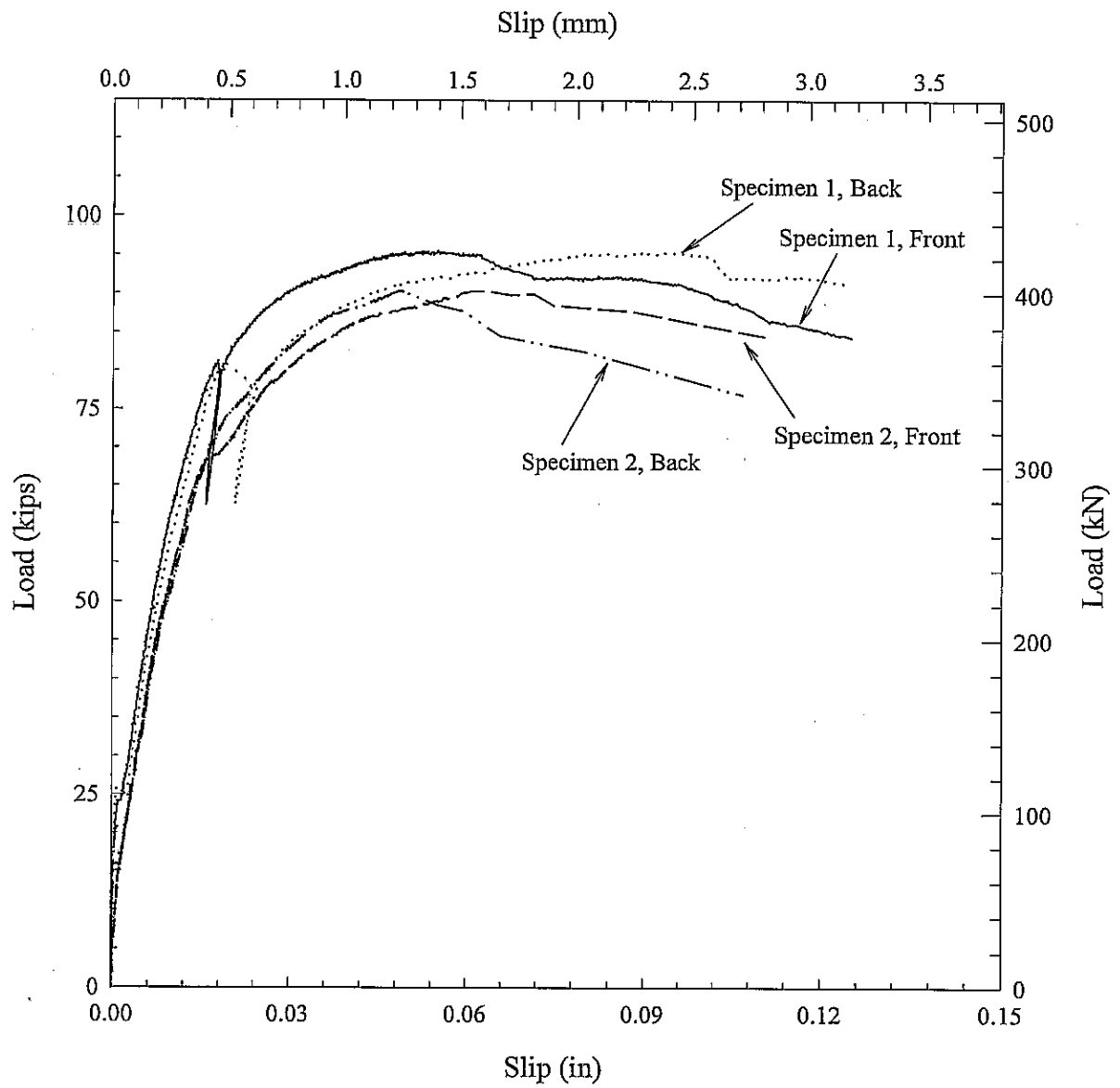


Fig. 5.24 Load-slip behavior for one pocket specimen and three studs per pocket

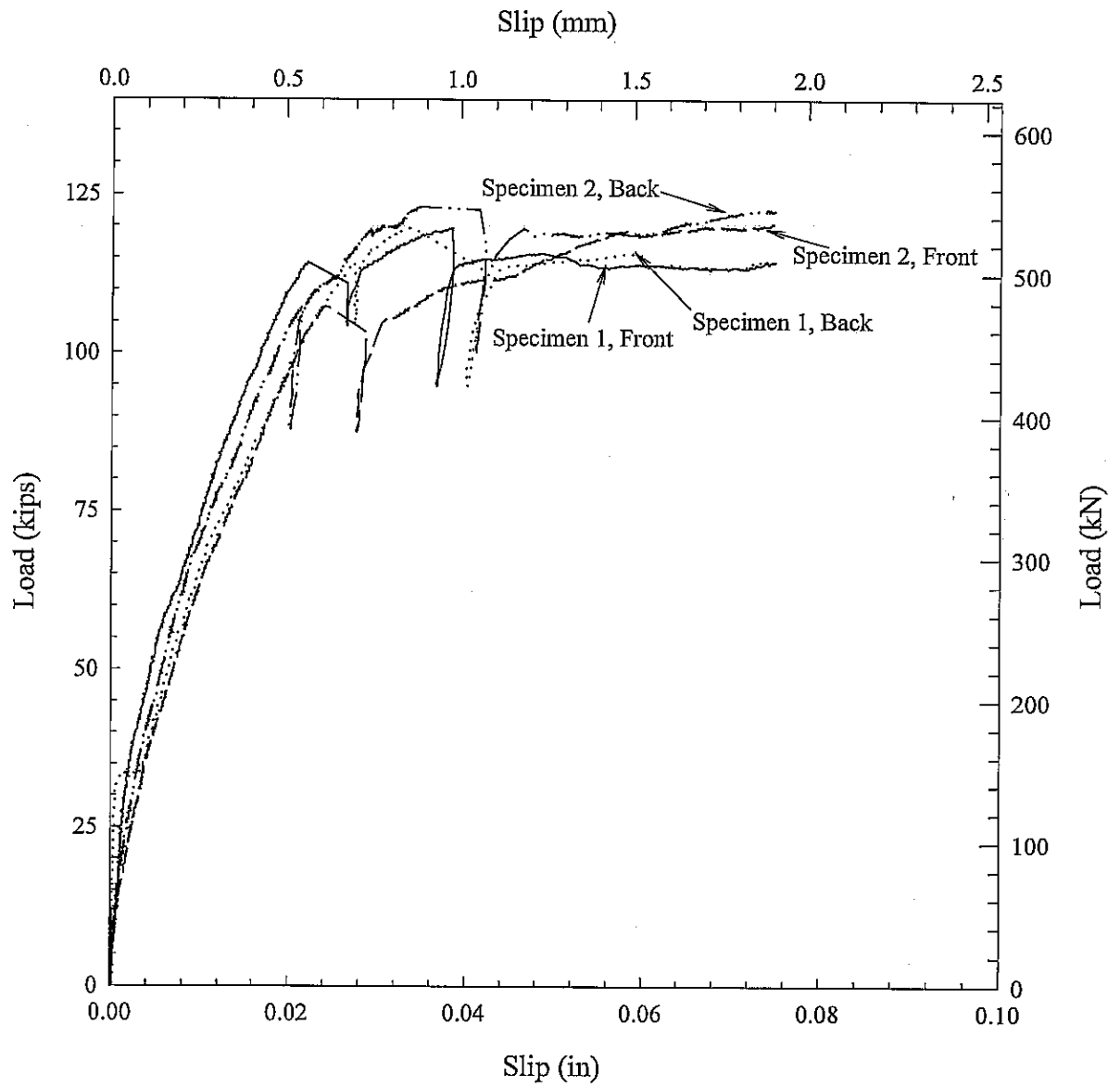


Fig. 5.25 Load-slip behavior for one pocket specimen and four studs per pocket

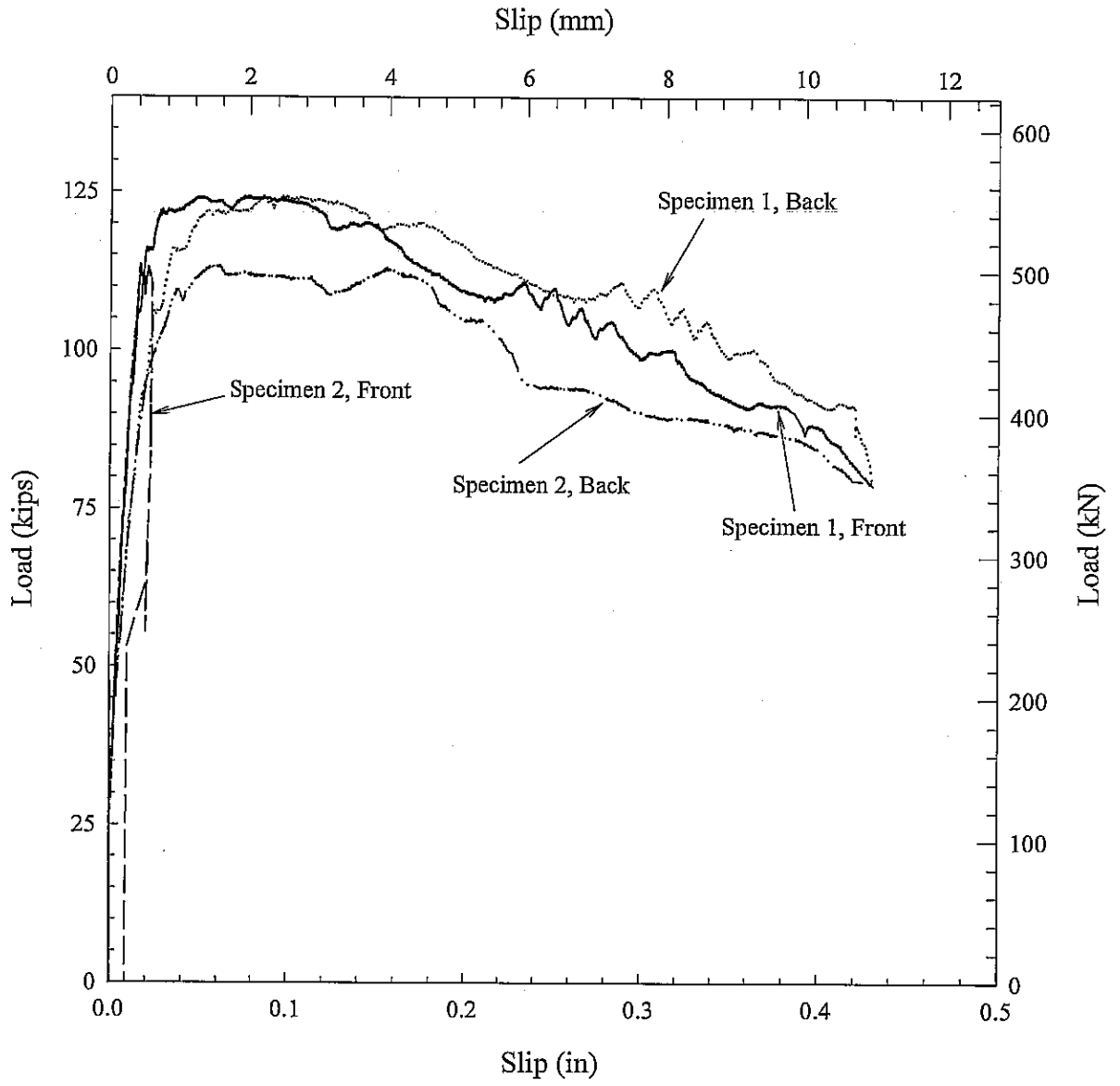


Fig. 5.26 Load-slip behavior for two pocket specimen and two studs per pocket

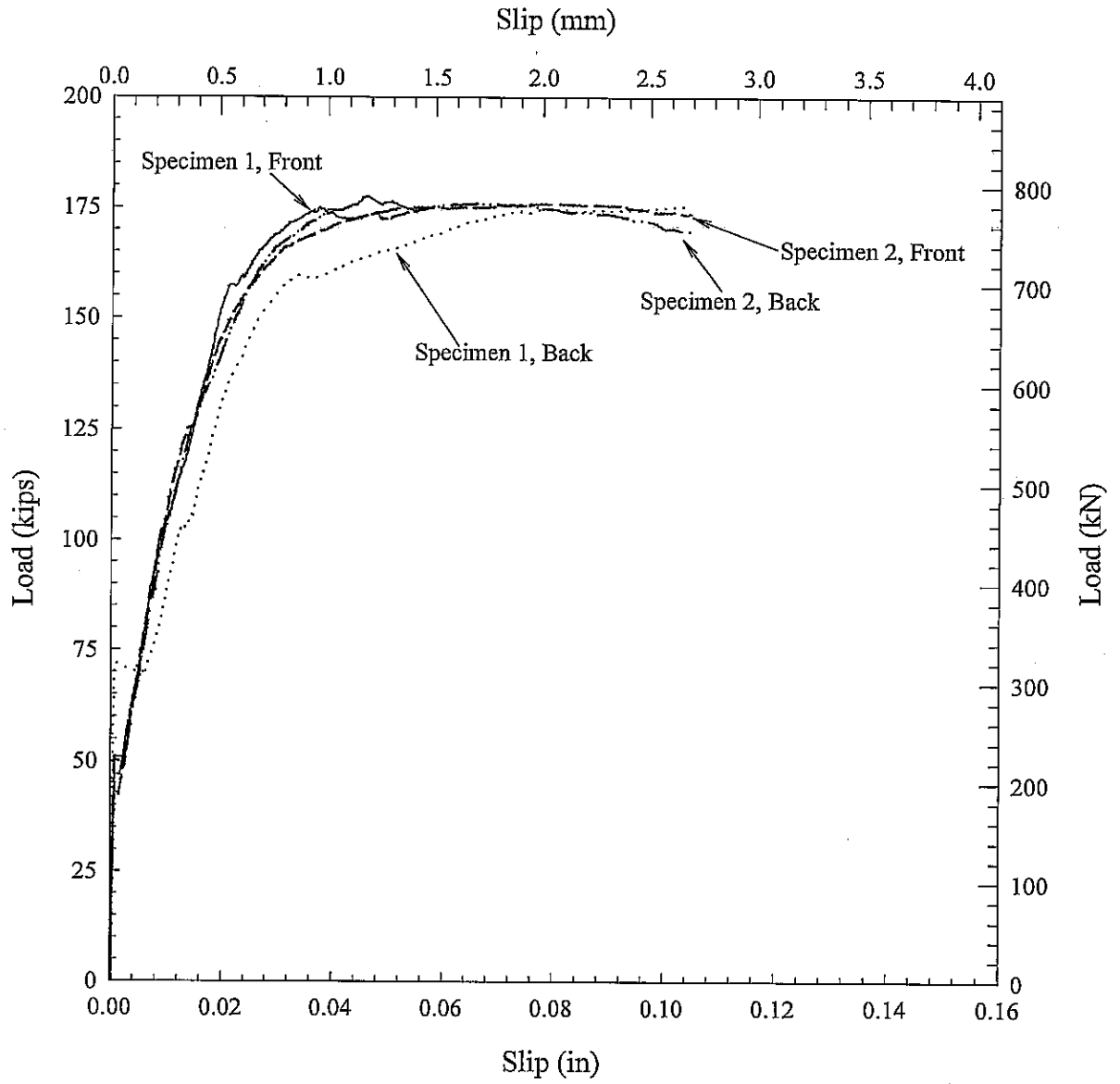


Fig. 5.27 Load-slip behavior for two pocket specimen and three studs per pocket

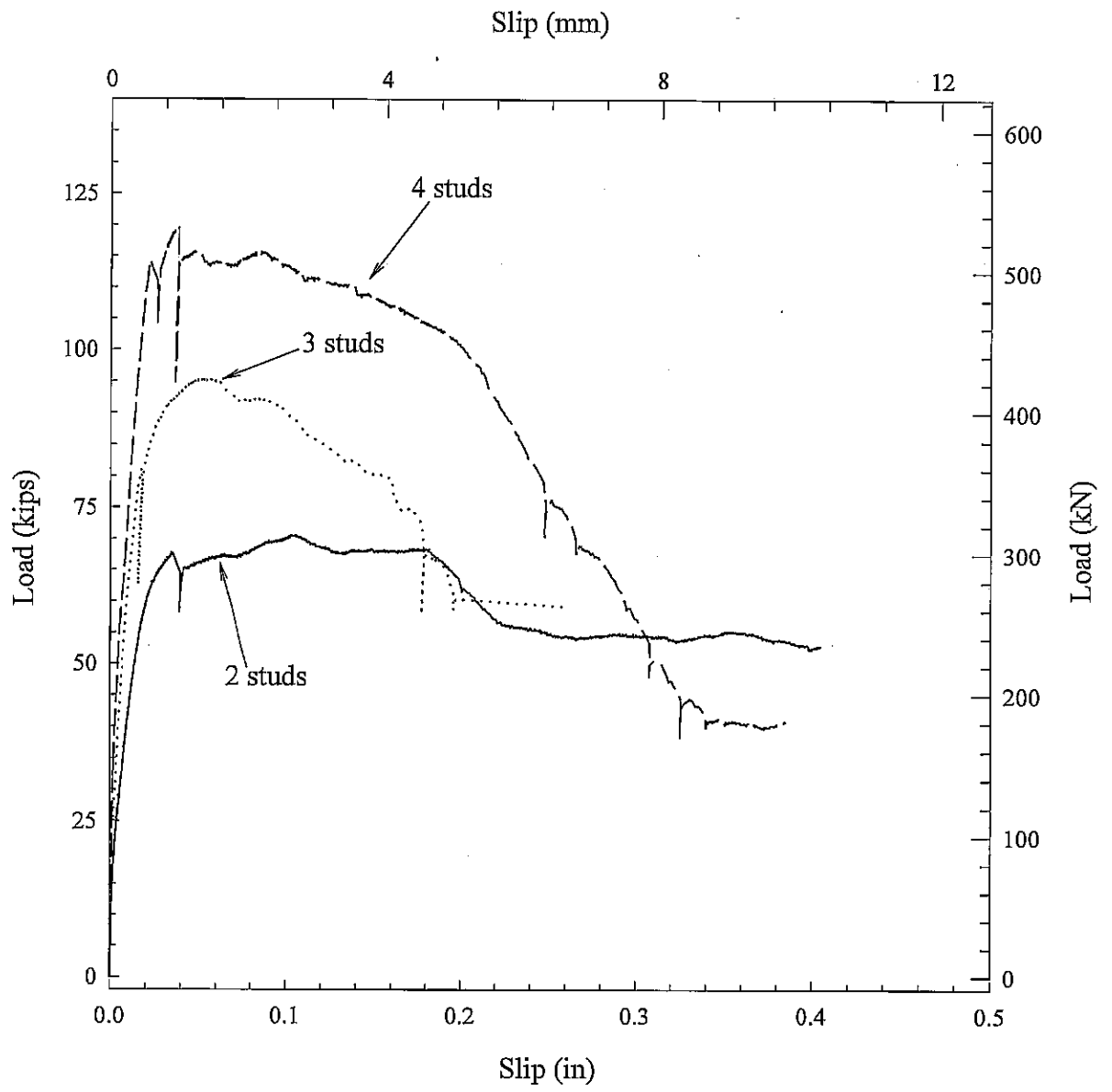


Fig. 5.28 Load-slip behavior for one pocket, various number of studs

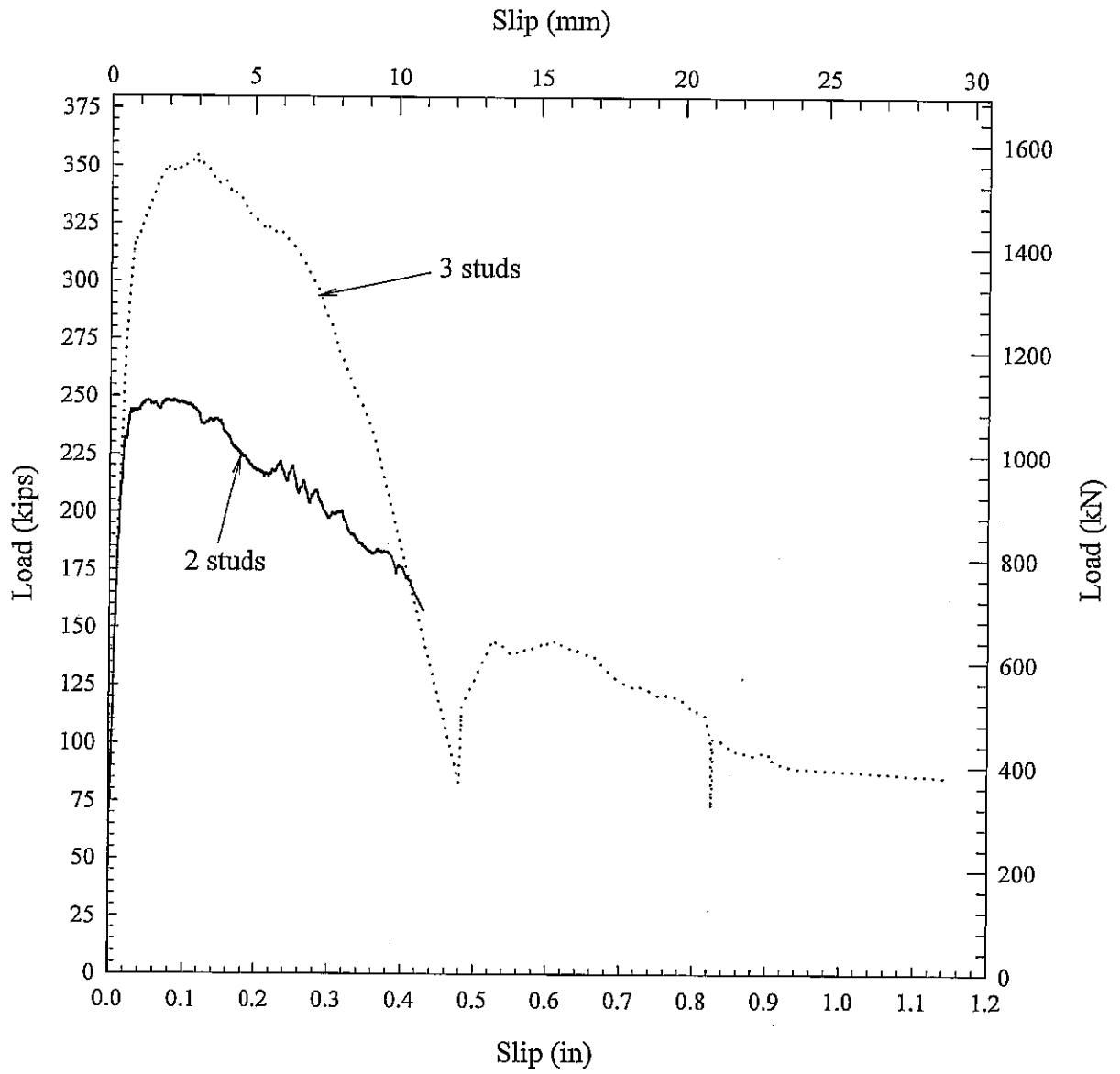


Fig. 5.29 Load-slip behavior for two pockets, various number of studs

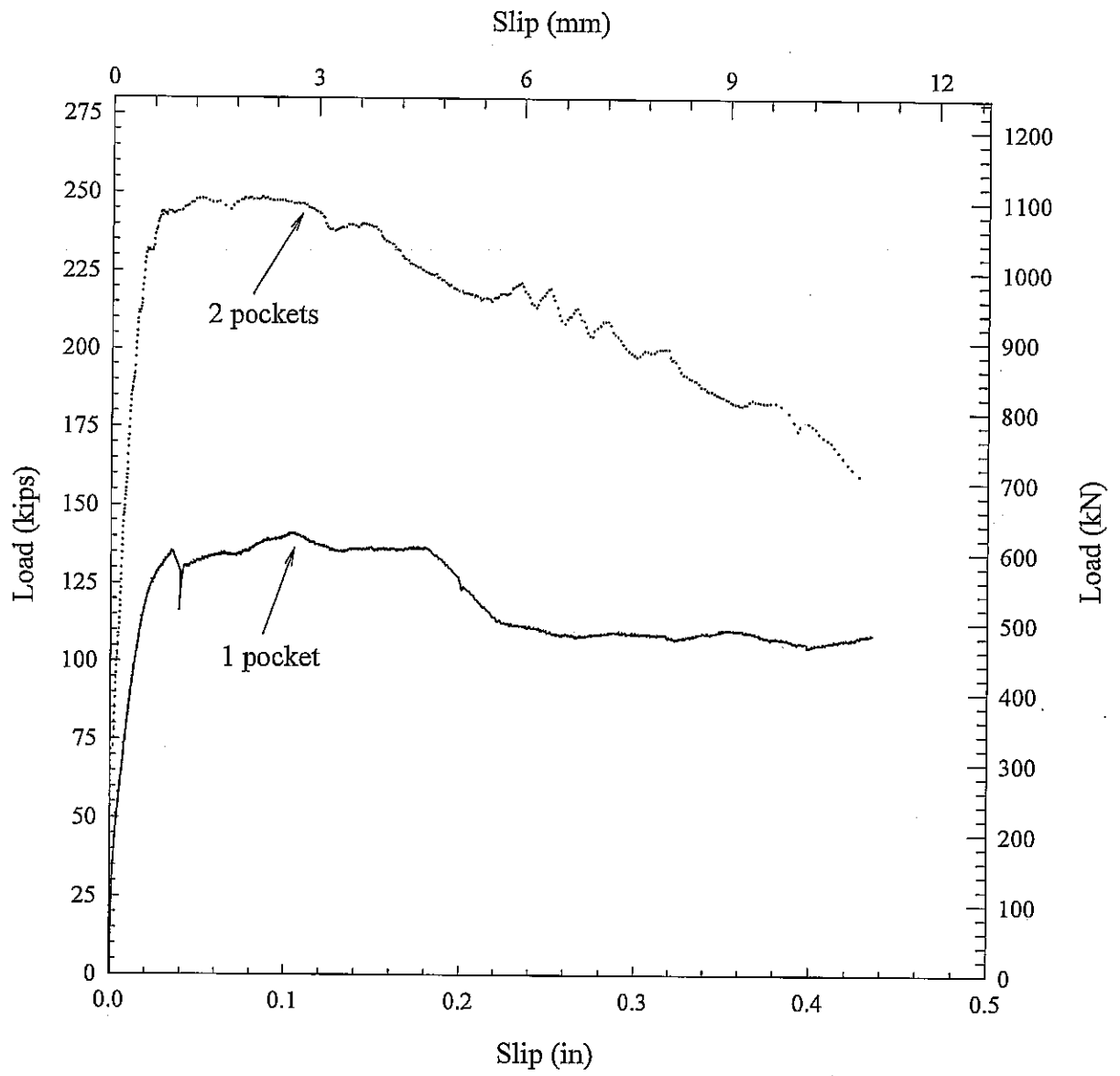


Fig. 5.30 Load-slip behavior for two studs, various number of pockets

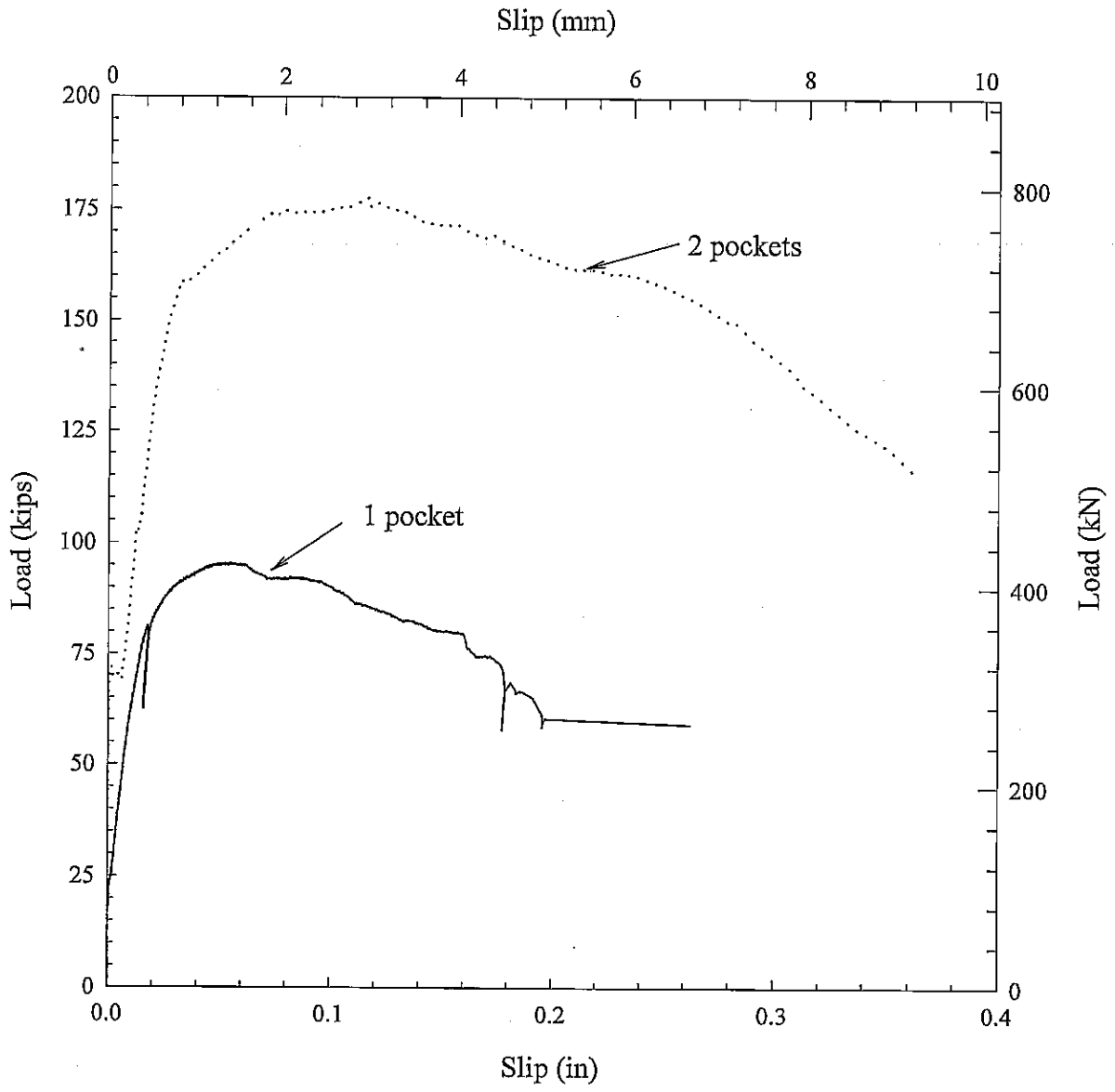


Fig. 5.31 Load-slip behavior for three studs, various number of pockets

Table 5.2 Full-scale test results

Specimen designation	Specimen no.	Ultimate load, kN (kips)	Concrete compressive strength, MPa (psi)	Set grout compressive strength, MPa (psi)
FS1P0S	1	28.2 (6.3)	52.74 (7650)	46.67 (6770)
FS1P2S	1	313.6 (70.5)	50.81 (7370)	46.31 (6716)
	2	301.8 (67.9)		
FS1P3S	1	424.6 (95.5)	51.50 (7470)	63.45 (9203)
	2	401.4 (90.3)		
FS1P4S	1	532.4 (119.7)	49.99 (7250)	43.33 (6285)
	2	547.2 (123.0)		
FS2P0S	1	66.9 (15.1)	51.23 (7430)	---
FS2P2S	1	552.8 (124.3)	52.74 (7650)	---
	2	504.7 (113.5)		
FS2P3S	1	789.5 (177.5)	49.99 (7250)	---
	2	783.1 (176.1)		
FS2P4S	1	---	51.50 (7470)	---

Note: all specimens experienced shearing of stud mode of failure

### **5.3 Correlation between Quarter-Scale and Full-Scale Shear Connection Testing**

Results from the full-scale push-out specimens were compared with those of quarter-scale specimens. The load-slip behavior of both types of specimens was found to be similar. The contact area between the steel and grout interface for the full-scale specimens was 15.8 times the contact area of the quarter-scale specimens. However, the area of studs in the full-scale specimens was 12.25 times the area of the studs in the quarter-scale specimens. An extrapolation factor of 12.25 was used to predict the ultimate load for the full-scale specimens based on the results of the quarter-scale specimens. It was observed that the predicted values were higher than the experimental results. This indicates that a size effect exists and it must be taken into consideration. Observed and theoretical values of the ultimate load for quarter- and full-scale specimens are presented in Table 5.3.

Table 5.3 Test results (¼ scale vs full scale)

Specimen designation	Specimen no.	Ultimate load, kN (kips)	Concrete compressive strength, MPa (psi)	Set grout compressive strength, MPa (psi)
FS1P0S	1	28.2 (6.3)	52.74 (7650)	46.67 (6770)
FS1P2S	1	313.6 (70.5)	50.81 (7370)	46.31 (6716)
	2	301.8 (67.9)		
QS1P2S	1	30.3 (6.8)	42.40 (6145)	46.19 (6694)
FS1P3S	1	424.6 (95.5)	51.50 (7470)	63.45 (9203)
	2	401.4 (90.3)		
QS1P3S	1	32.1 (7.2)	42.40 (6145)	46.19 (6694)
FS1P4S	1	532.4 (119.7)	49.99 (7250)	43.33 (6285)
	2	547.2 (123.0)		
QS1P4S	1	43.4 (9.8)	42.40 (6145)	46.19 (6694)
FS2P0S	1	66.9 (15.1)	51.23 (7430)	---
FS2P2S	1	552.8 (124.3)	52.74 (7650)	---
	2	504.7 (113.5)		
QS2P2S	1	54.8 (12.2)	42.54 (6165)	49.23 (7135)
FS2P3S	1	789.5 (177.5)	49.99 (7250)	---
	2	783.1 (176.1)		
QS2P3S	1	62.5 (13.9)	42.54 (6165)	49.23 (7135)
FS2P4S	1	---	51.50 (7470)	---
	2	---		
QS2P4S	1	96.8 (21.6)	42.54 (6165)	49.23 (7135)

Note: all specimens experienced shearing of stud mode of failure.

Table 5.4 Full-scale test results and predictions

Specimen	Average observed ultimate load, kN (kips)	Predicted ultimate load based on ¼-scale, kN (kips)
FS1P0S	28.2 (6.3)	---
FS1P2S	307.7 (69.2)	371.2 (83.4)
FS1P3S	413.0 (92.9)	393.2 (88.4)
FS1P4S	539.8 (121.4)	531.6 (119.5)
FS2P0S	66.9 (15.1)	---
FS2P2S	528.8 (118.9)	671.3 (150.9)
FS2P3S	786.3 (176.8)	765.6 (172.1)
FS2P4S	---	1185.8 (266.6)

#### 5.4 Comparison of Experimental and Finite Element Analysis Results for Push-Out Test

The observed results from the nonlinear finite element analyses were compared with the experimental results. The stress intensity distribution of beam-stud joint, concrete slab and haunch were found very reasonable. Stress intensity distribution on the face of a typical haunch is shown in Fig. 5.32. It is clearly evident that maximum stresses occurred in regions surrounding the shear studs. Typical experimental and analytical load-slip curves for a quarter-scale one-pocket four-stud specimen are presented in Fig. 5.33, which shows a good correlation between the experimental and finite element analysis results. The ultimate loads for one-pocket specimens with various studs for both quarter- and full-scale specimens are shown in Table 5.5. It is clearly shown that the observed ultimate loads were in good agreement with finite element analysis results.

Table 5.5 Comparison of experimental and finite element analysis results

Specimen designation	Quarter-scale specimen ultimate load, kips (kN)		Full-scale specimen Ultimate load, kips (kN)	
	Experimental	FEM analysis	Experimental	FEM analysis
1-pocket, 2-stud	6.8 (30.3)	6.79 (30.2)	69.2 (307.7)	67.3 (299.4)
1-pocket, 3-stud	7.2 (32.1)	7.25 (32.3)	92.9 (413.0)	93.2 (414.7)
1 pocket, 4-stud	9.8 (43.4)	9.87 (43.9)	121.4 (539.9)	127.7 (568.0)

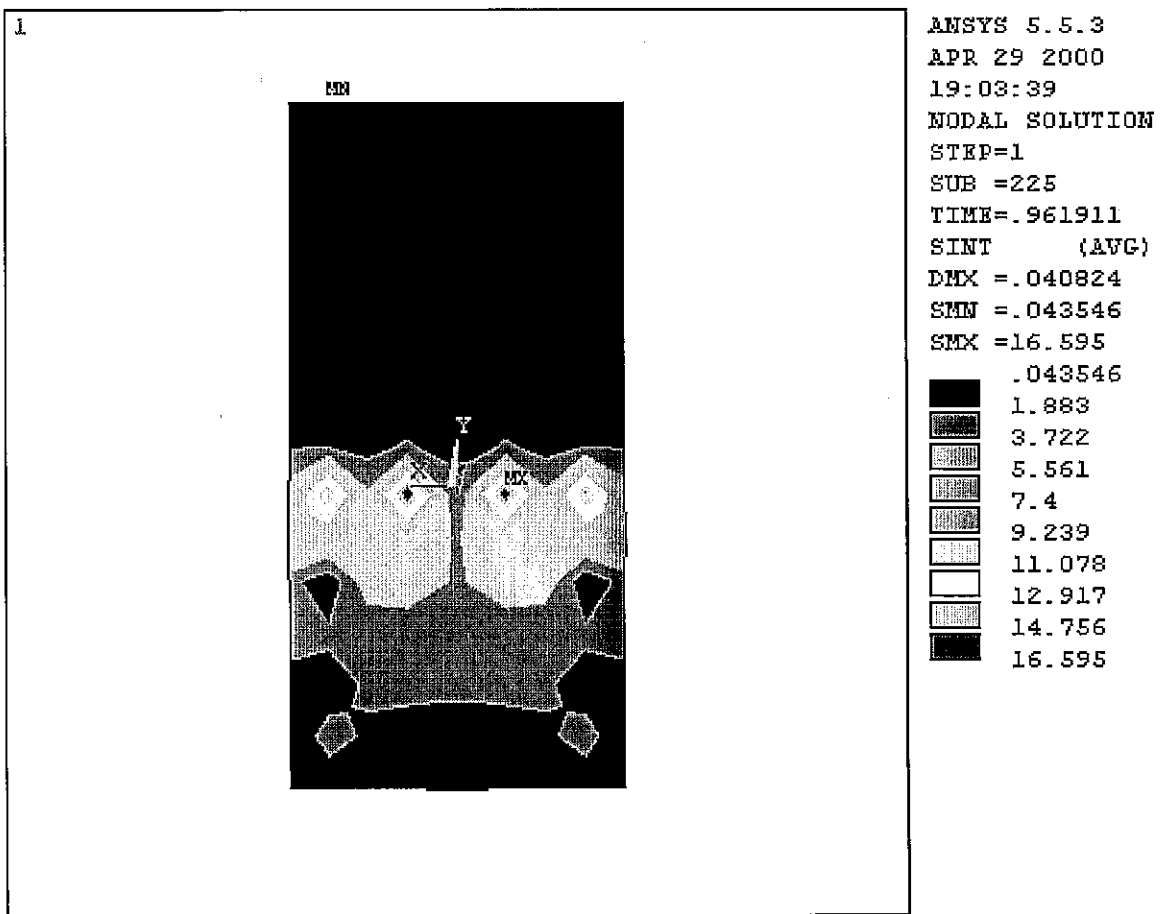


Fig. 5.32 Stress intensity distribution in a typical haunch of quarter-scale specimen

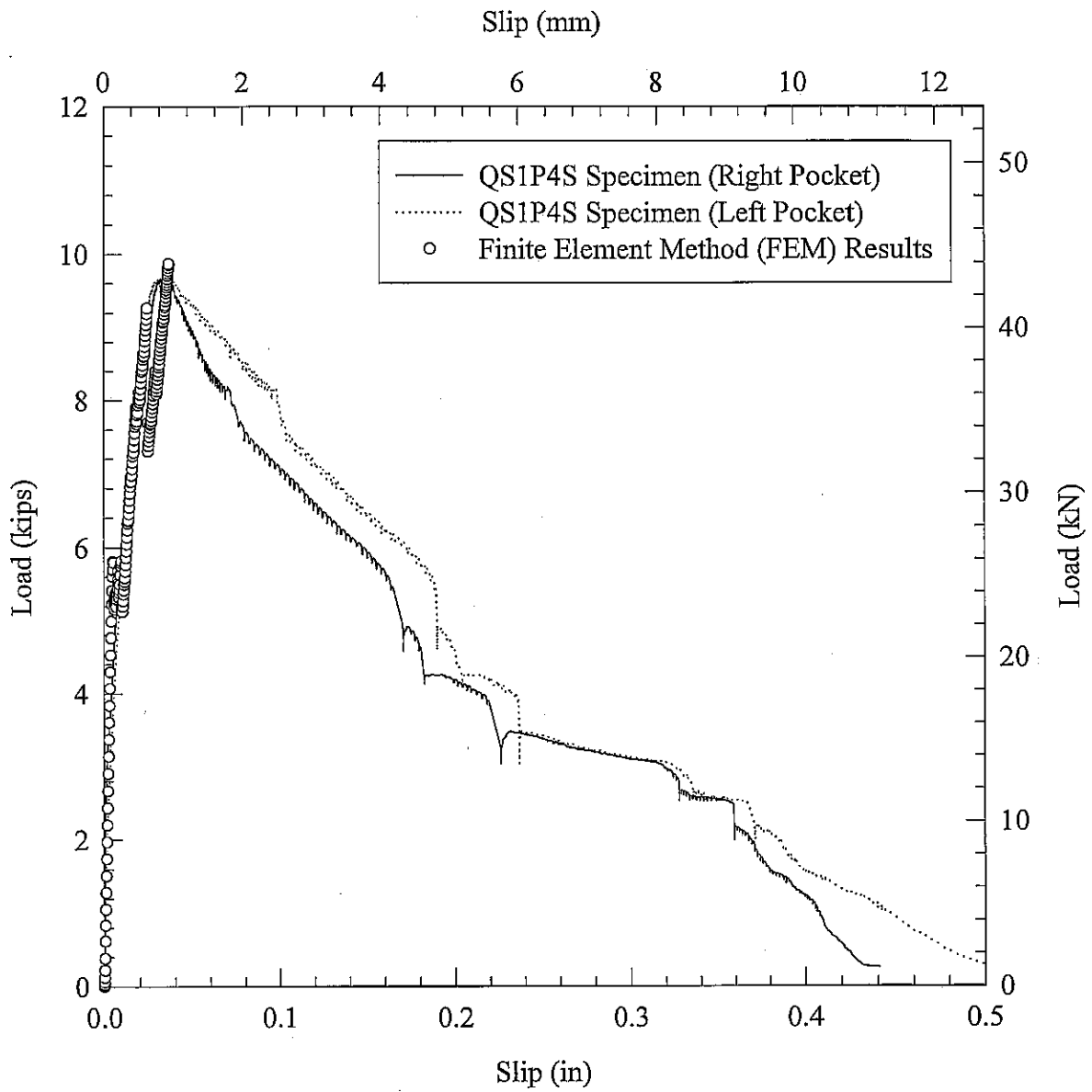


Fig. 5.33 Comparison of experimental and FEM results for a typical quarter-scale specimen

## **5.5 Test Results for Transverse Joint**

A total of 36 specimens were tested for vertical shear, direct tension, and flexure. The joints were cast using four different materials; set grout, set 45 at normal temperatures, set 45 HW, and polymer concrete. The observed strengths and modes of failure were compared.

### **5.5.1 Direct Shear Results**

At the inception of testing, the joint surfaces were not sandblasted, hence bond failure was prominent. As a result, all the specimens were sandblasted thereafter. Once that procedure was adhered to, the test results proved to be satisfactory. Moisture condition of the joint surface was also a very important parameter in the testing.

In the initial stage, a significant number of specimens with set 45 were rejected because the failure was predominately at the joint interface, i.e., bond failure. This was attributed to the moisture at the joint surface and the quality of the set 45 mix. The shear load carried by the specimens with dry joint surface was nearly twice that with moisture surface. Failure was initiated by fracture through the joint. Shear stresses for the specimens made with set 45 and set 45 HW are reported in Table 5.6. The average shear stresses in set 45 specimens were a little higher than those of set 45 HW specimens. This is because of the lower compressive strength of set 45 HW grouting material as reported in Table 5.6. From the observed results, it can be concluded that great care should be taken in the application of set 45 in terms of joint surface preparation and mixing of the set 45 grouting material.

The joint surface was saturated at the time of casting of the set grout. This condition was prevalent since preliminary tests indicated that this procedure improves the bond. Shear stresses carried by the set grout specimens are presented in Table 5.6. The failure was through both the joint material and the surrounding concrete.

Joints cast with polymer concrete proved to be the best in terms of shear strength, fracture and bond as shown in Table 5.6. The shear strength of polymer concrete joint was twice the shear strength of the joints cast with set 45, set 45 HW, and set grout. Bond was excellent and no

apparent cracks were observed at these joint interfaces. Fracture was always encountered away from the joint, i.e., in the concrete (Fig. 5.34). However, the ideal procedure for casting polymer concrete must be adhered to. This proved to be vital in the preliminary casting of the material.



Fig. 5.34 Failure in polymer concrete specimen

Table 5.6 Direct shear test results

Material type	Specimen Number	Shear stress (psi)	Concrete comp. $f_c$ (psi)	Grouting Material comp. strength $f_c$ (psi)	Mode of failure
Set 45	S1	301.1	6500	5820	Fracture through joint
	S2	320.4			
	S3	354.1			
Set 45 HW	S1	285.3	6250	5658	Fracture through joint
	S2	305.9			Fracture through joint
	S3	305.0			Fracture through joint and concrete
Set grout	S1	401.5	6500	7700	Fracture through joint and concrete
	S2	343.3			
	S3	330.1			
Polymer concrete	S1	748.4	6500	10810	Fracture of concrete away from joint
	S2	667.1			
	S3	697.4			

### 5.5.2 Direct Tension Results

The same conditions were prevalent in the specimens with set 45 and set 45 HW as in the direct shear test. Once the specimens were sandblasted and a dry surface was provided in casting the joint, better bond was apparent and the shear strength dramatically increased. In all specimens cast with set 45 and set 45 HW grouting material, failure was through the joint, except that one specimen made with set 45 HW failed in the bond interface. The observed tensile stress values are reported in Table 5.7. It can be seen that the tensile stresses of specimens with set 45 and set 45 HW are almost the same.

The observed tensile stresses and the failure mode of the specimens made with set grout are presented in Table 5.7. Failure in the set grout specimens was always in the form of fracture in both the joint and the surrounding concrete. Hence, better bond was attributed to this type of material.

The polymer concrete once again proved to be superior to the other materials as shown in Table 5.7. The tensile strengths were higher than those for set 45 and set grout materials. Failure was away from the joint, i.e., in the concrete slab units. The mode of failure for set grout, set 45, and polymer concrete specimens are shown in Figs. 5.35-5.37, respectively.

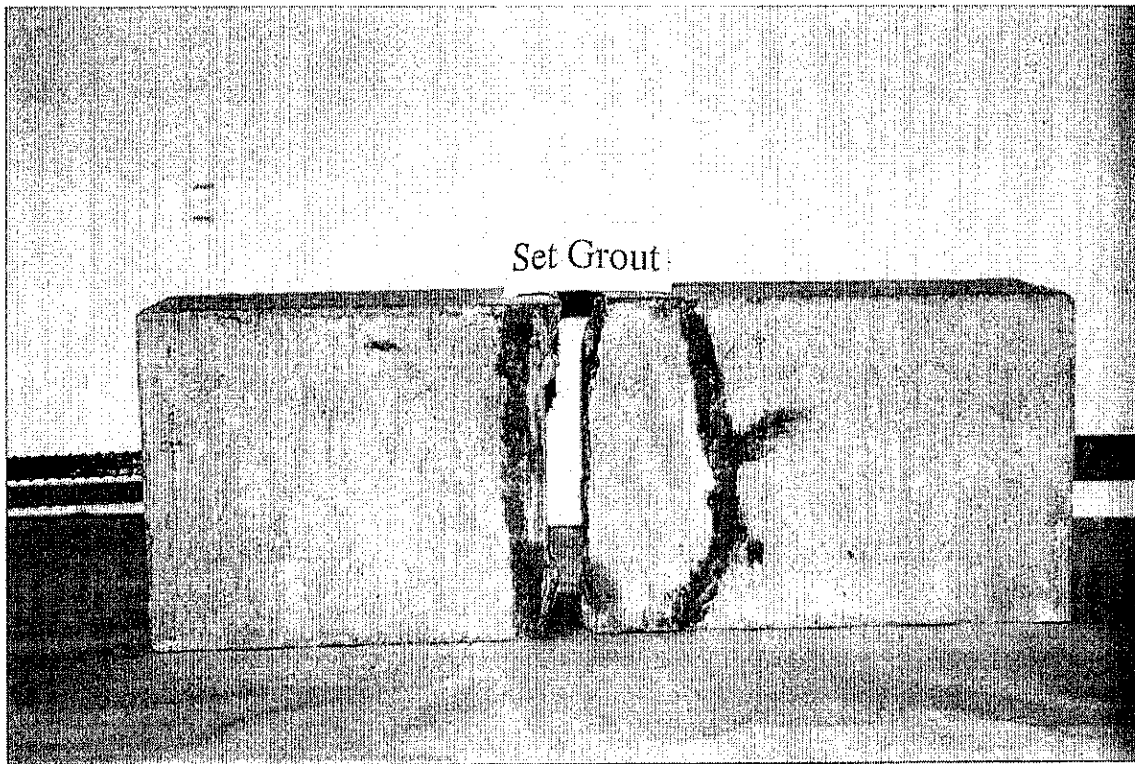


Fig. 5.35 Failure mode in set grout direct tension specimen

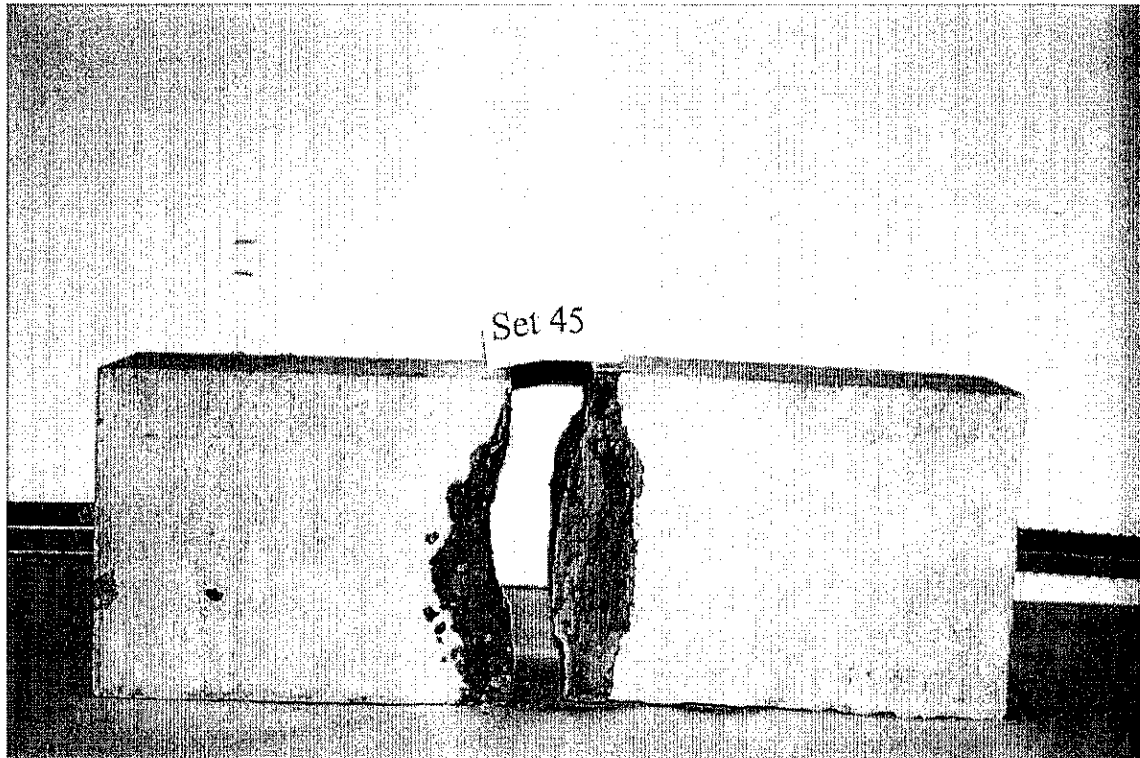


Fig. 5.36 Failure mode in set 45 direct tension specimen

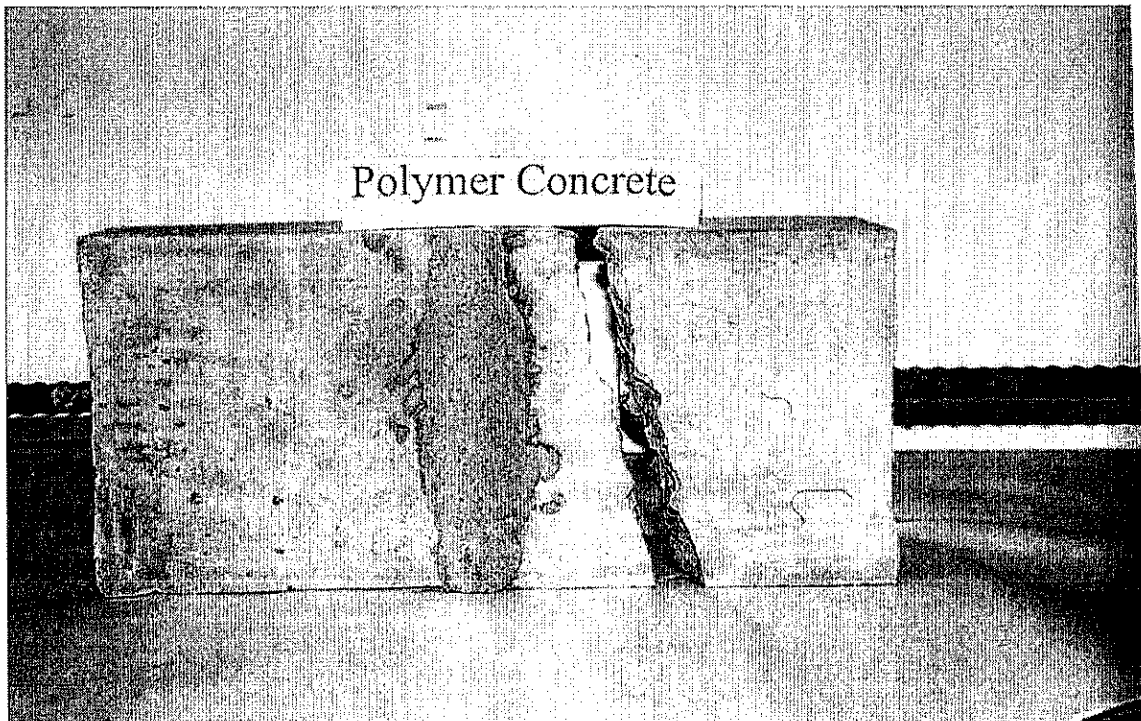


Fig. 5.37 Failure mode in polymer concrete direct tension specimen

Table 5.7 Direct tensile test results

Material type	Specimen number	Tensile stress (psi)	Concrete comp. $f_c$ (psi)	Grouting material $f_c$ (psi)	Mode of failure
Set 45	T1	207.8	6250	5820	Fracture through joint
	T2	175.9			
	T3	219.0			
Set 45 HW	T1	198.4	6250	5658	Bond (interface)
	T2	214.6			Fracture through joint
	T3	203.8			Fracture through joint
Set grout	T1	197.0	6250	7700	Fracture through joint and concrete
	T2	246.3			
	T3	227.9			
Polymer Concrete	T1	330.1	6250	10810	Fracture of concrete away from joint
	T2	288.8			
	T3	256.0			

### 5.5.3 Flexural Results

The same trend was observed for the three materials tested under flexural testing. A dryer surface was more appropriate for specimens cast with set 45. Set grout specimens performed better when the joint surface was saturated. Observed flexural strength results are reported in Table 5.8. It can be seen that the flexural strength of polymer concrete joints was 2.8, 1.5 and 1.2 times the shear strength of joints with set 45, set 45 HW and set grout, respectively. Bond was superior in the polymer concrete specimens, followed by the set grout specimens, and finally the set 45 specimens. The modes of failure for the three materials followed the same trend as previously encountered in the direct shear and direct tension tests. Failure occurred at the joint juncture with some apparent loss of concrete for the set 45 specimens. On the other hand, failure occurred at the joint interface for the set grout specimens, however, more concrete adhered to the grout material at fracture. Once again, failure for the polymer concrete specimens was away from the joint, i.e., in the concrete material. Figs. 5.38-5.40 show the modes of failure for the set grout, set 45, and polymer concrete specimens, respectively.

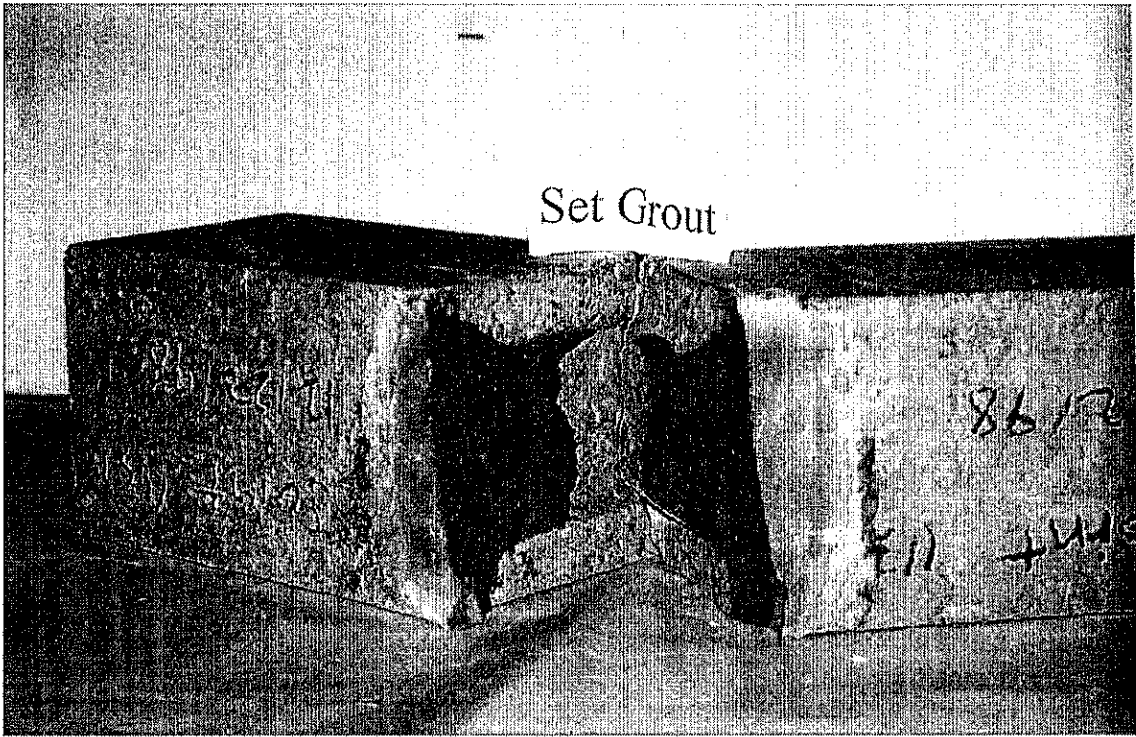


Fig. 5.38 Failure mode in set grout flexural specimen

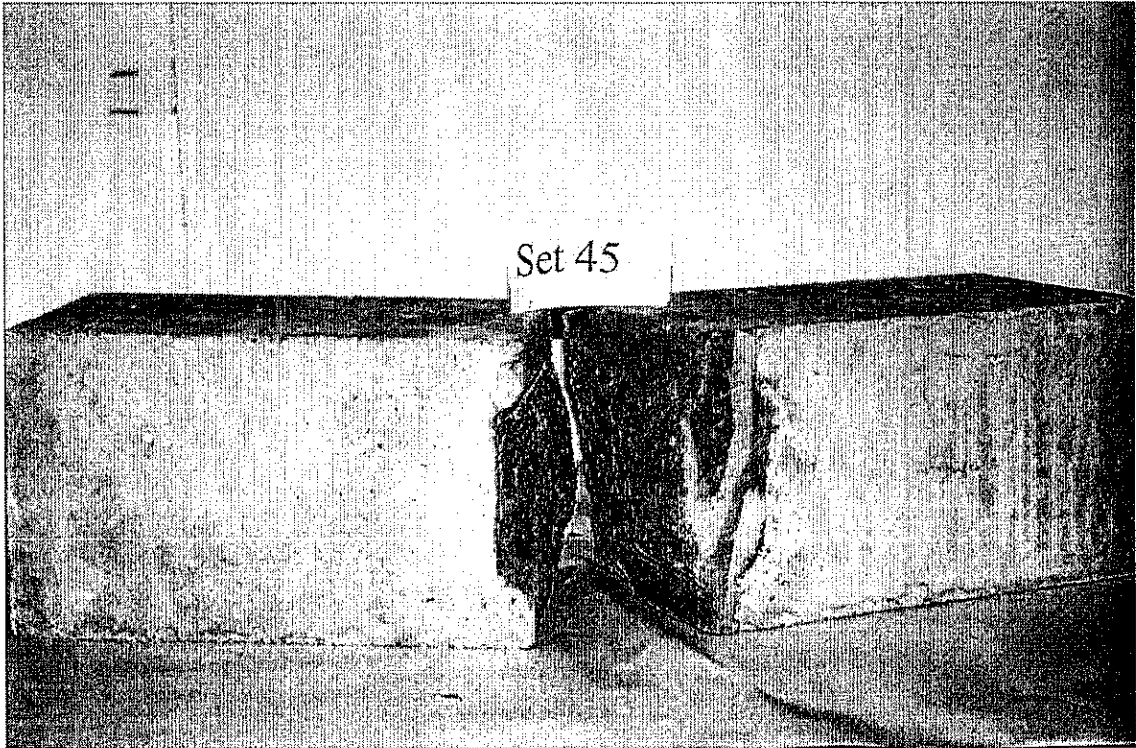


Fig. 5.39 Failure mode in set 45 flexural specimen

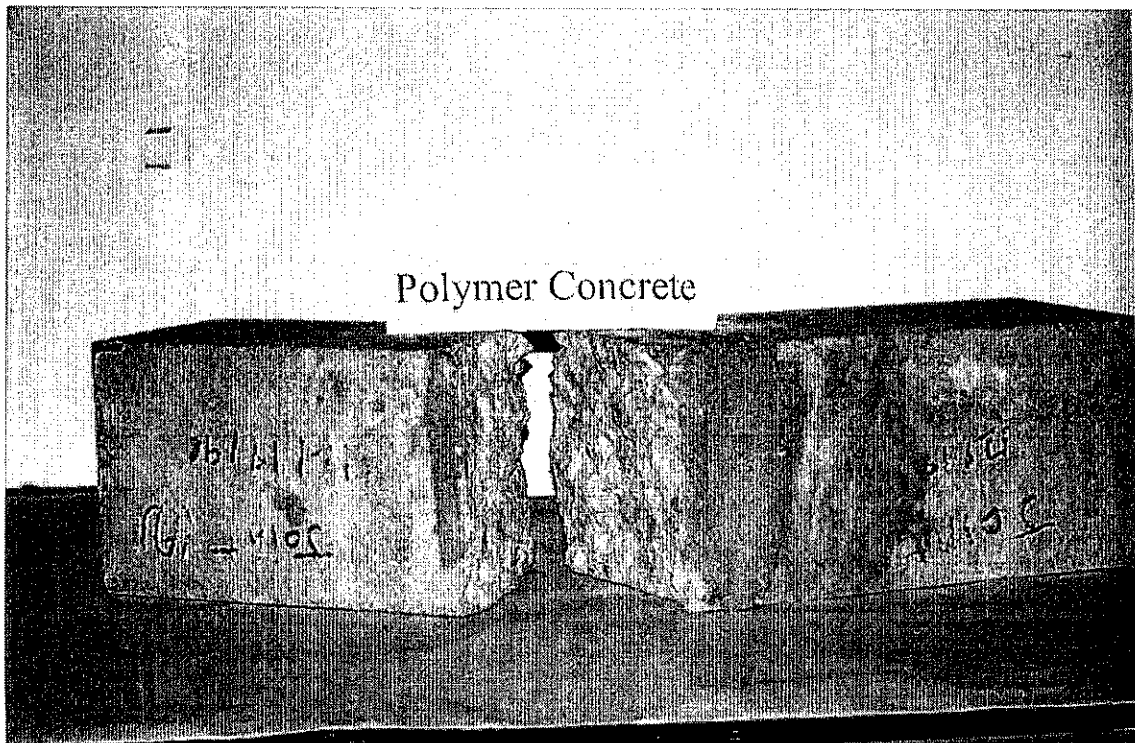


Fig. 5.40 Failure mode in polymer concrete flexural specimen

Table 5.8 Flexural test results

Material type	Specimen number	Flexural stress (psi)	Concrete $f_c$ (psi)	Grouting material $f_c$ (psi)	Mode of failure
Set 45	F1	266.6	6250	5820	Fracture through joint
	F2	284.3			
	F3	267.6			
Set 45 HW	F1	516.5	6500	5658	Bond (interface)
	F2	531.4			
	F3	446.5			
Set grout	F1	633.9	6250	7700	Fracture through joint and concrete
	F2	601.4			
	F3	625.6			
Polymer concrete	F1	783.9	6250	10810	Fracture of concrete away from joint
	F2	685.6			
	F3	849.7			

#### 5.5.4 Strength, Permeability and Shrinkage Measurement

To monitor the strength development of the grouting materials, cubes and briquettes were prepared from set 45, set grout and polymer concrete and tested at different ages. The compressive and tensile strengths of the grouting materials tested at different ages are shown in Table 5.9.

A permeability investigation was carried out in accordance with ASTM C1202-97, which entails the determination of the electrical conductance of concrete to provide a rapid indication of its resistance to the penetration of chloride ions. 100 x 200-mm cylinders were sliced to get disks 100 mm in diameter and 50 mm thick. In this method, electrical current passes through a concrete sample during a six-hour exposure period and the result is expressed in terms of a Coulomb number. The average results from three samples for each type of material are shown in Table 5.10. It is evident from that polymer concrete is the least permeable among all the materials studied. A considerably higher Coulomb value was observed for the set grout specimens. It maybe attributed to the higher amount of water used for the set grout mixes.

Shrinkage of mortars was determined according to ASTM C157. Three prism specimens of size 1 x 1 x 11¼ in. were cast from each joint material. After six hours from casting time, the specimens were demolded and immersed in lime saturated water for a period of 15 minutes. After taking comparator readings, all the prisms were kept under laboratory temperature and humidity conditions. Comparator readings for each specimen were taken every day for 7 days and once every week thereafter. The observed shrinkage values are plotted in Fig. 5.41. It was observed that polymer concrete is the best among all joint materials in terms of shrinkage. The very high value of shrinkage for the set grout specimens is due to the high water content used in the mix to make the mix flowable.

Table 5.9 Strength development of grouting material

Age at testing	Type of test	Strength of grouting material, psi		
		Set 45	Set grout	Polymer concrete
3-hour	Compressive	---	---	9752
6-hour	Compressive	3718	---	10169
1-day	Compressive	3775	2841	10357
3-day	Compressive	4294	5109	10460
	Tensile	574	548	988
7-day	Compressive	5516	6312	10550
	Tensile	587	598	1130
28-day	Compressive	6122	10031	10756
	Tensile	605	703	1153

Note: 1 psi = 0.00689 MPa

Table 5.10 Coulomb permeability test results

Material type	Average Coulomb value	Chloride Ion Permeability
Set-45	606	Very low
Set-grout	2544	Moderate
Polymer concrete	22	Negligible

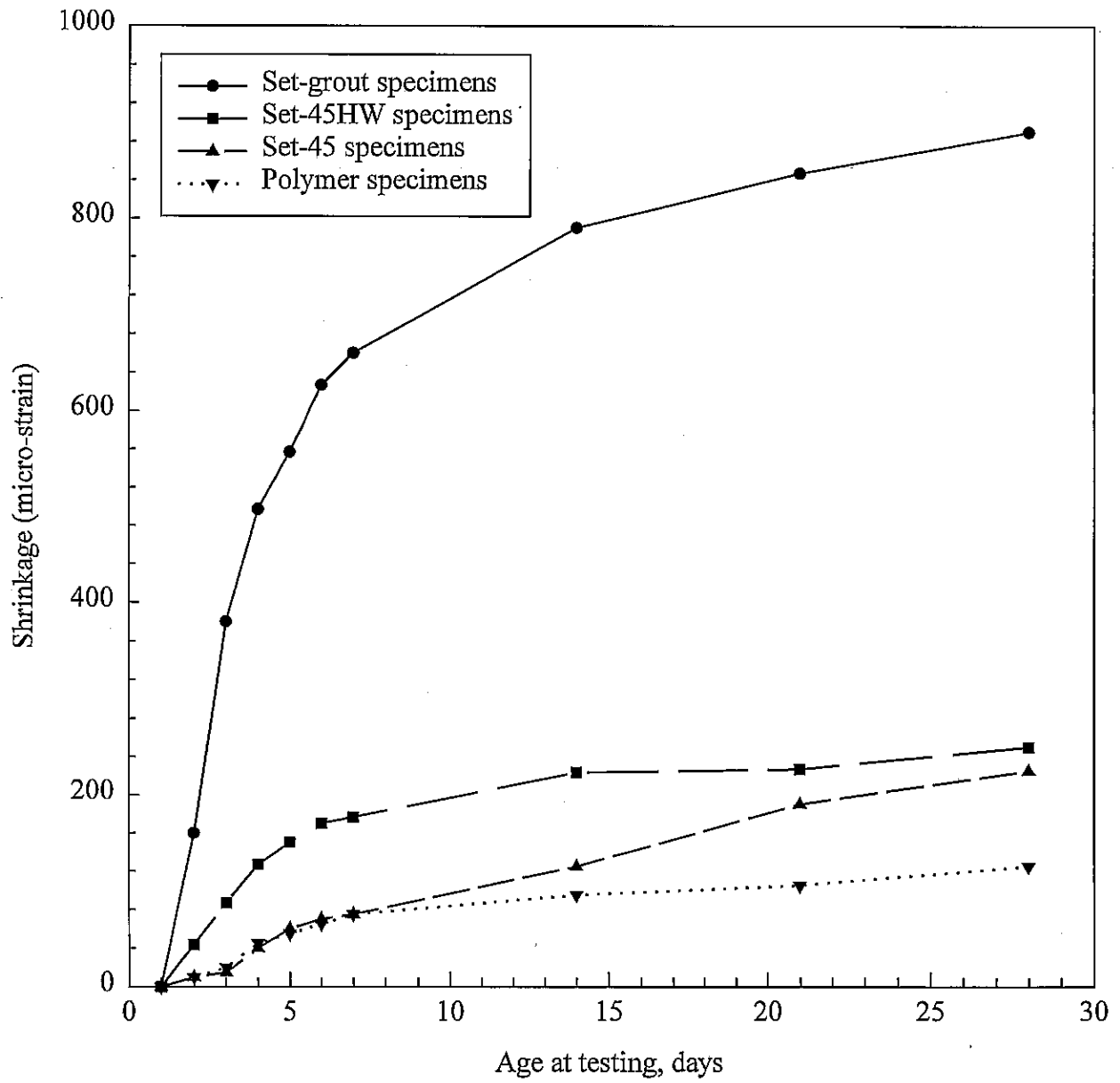


Fig. 5.41. Shrinkage test results of joint materials

## 5.6 Comparison of Material Behavior in Transverse Joints

A significant number of specimens were tested to evaluate the performance of the material subjected to vertical shear, direct tension, and flexure. The joints were cast with four different materials; set grout, set 45 at normal temperatures, set 45 HW, and polymer concrete. It was found that the shear, tensile and flexural strengths of polymer concrete specimens were the highest among all specimens cast with four grouting materials as mentioned above. Bond was superior in the polymer concrete specimens, followed by the set grout specimens, and the set 45 specimens. In the set 45 specimens, failure occurred through the joint, whereas in set grout specimens the failure occurred through the joint and concrete. In the case of polymer concrete specimens, the failure occurred away from the joint, i.e., in the concrete material.

Based on the experimental study it is advisable to use polymer concrete in critical joint locations and set grout for the rest of the joints. Since set 45 is very susceptible to the moisture condition of the joint surface, it is not advisable to use set 45 in the transverse joints of the deck system.

## 5.7 Comparison of Finite Element Analysis

Analysis showed failure mainly occurred by crushing and cracking of the grouting material along the joint. Polymer concrete experienced the least amount of cracking and crushing, and the specimen failed at an applied load of 25.15 kips. Minor cracks occurred in the lower neck of the joint but mostly in the concrete slab along the joint line as shown in Fig. 5.42. Shear stress for this specimen ranged between 477 and 757 psi across the face of the joint, while values in the order of 898 psi occurred at the upper and lower edges of the joint as shown in Fig. 5.43. The average shear stress from experimental results was 704 psi.

Set grout failed at a load of 17.1 kips with a more pronounced crushing pattern at the upper and lower necks of the joint as shown in Fig. 5.44. Shear stresses ranged between 288 and 458 psi across the joint as depicted in Fig. 5.45. It also showed shear stresses of 800 psi at the upper and lower necks of the joint. The average shear stress obtained experimentally was 358 psi.

Set 45 and set 45 hot weather had comparable compressive strengths, and hence experienced similar crushing patterns within the joint material at failure loads 16.5 kips and 15.5 kips, respectively. Shear stress distribution for set 45 model is shown in Fig. 5.46. The distribution ranged between 277 and 441 psi, while values as high as 750 psi occurred across the narrow portions of the joint. The experimental average shear stresses for set 45 and set 45 hot weather were 325 and 299 psi, respectively.

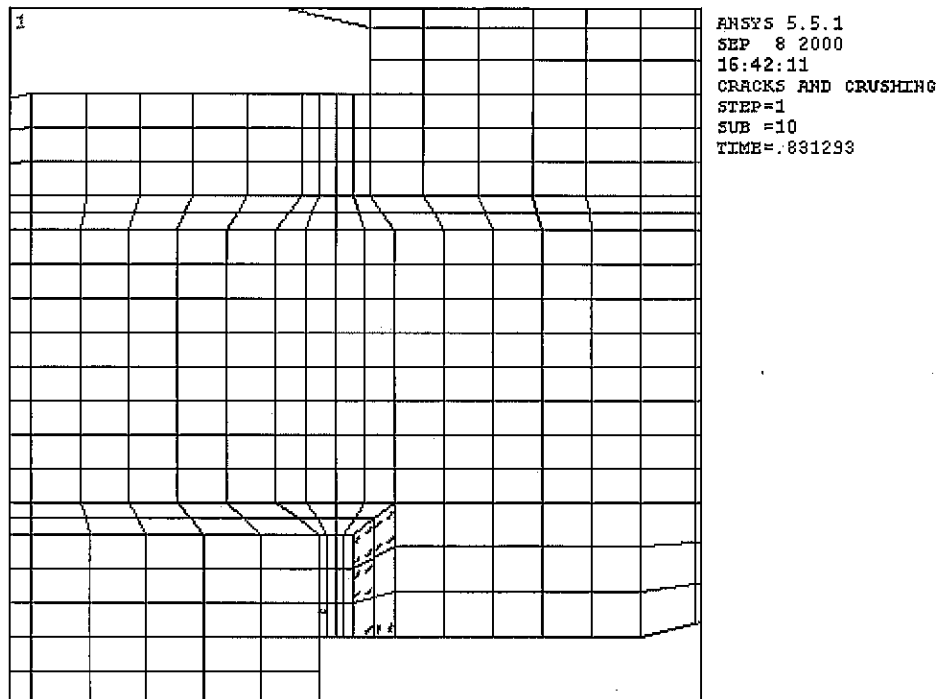


Fig. 5.42 Crack pattern in polymer concrete model

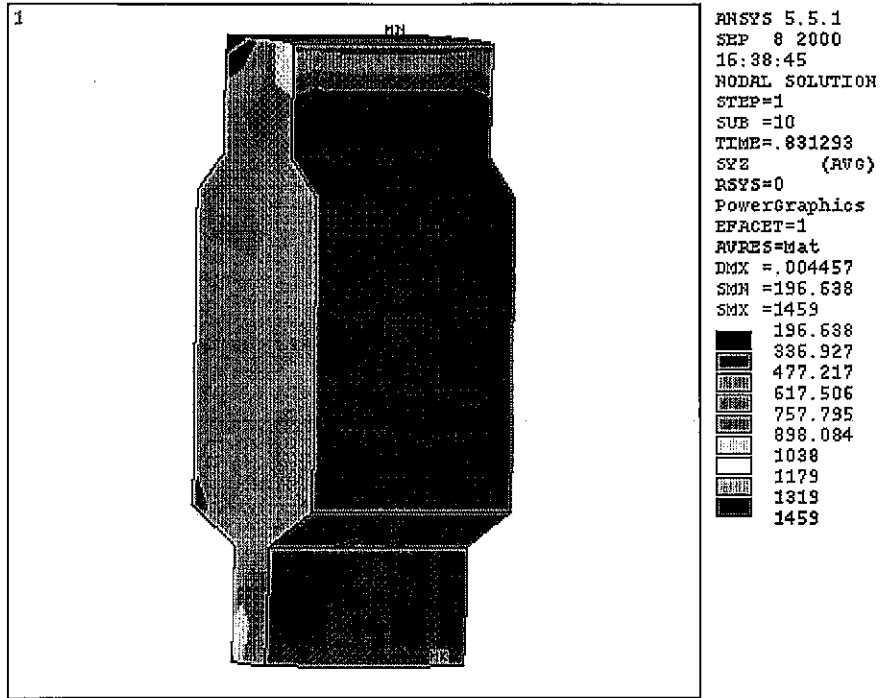


Fig. 5.43 Shear stress distribution in polymer concrete

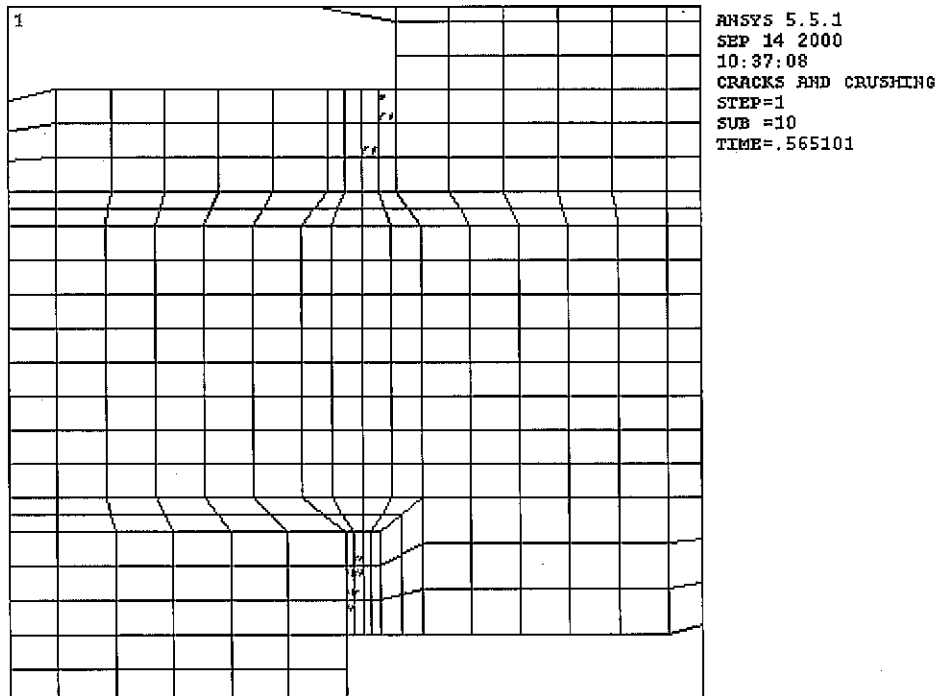


Fig. 5.44 Crack pattern in set grout model

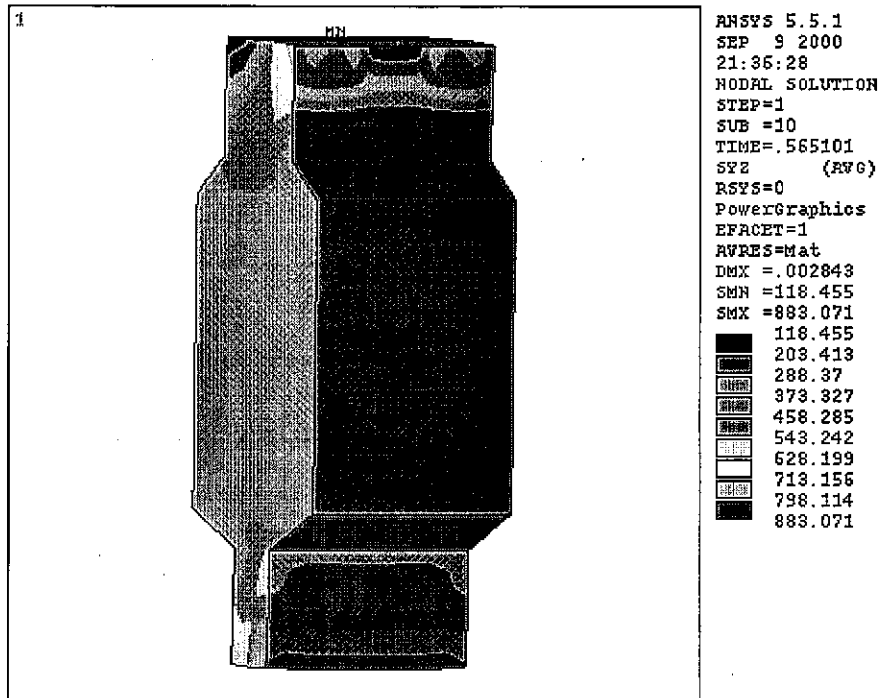


Fig. 5.45 Shear stress distribution in set grout

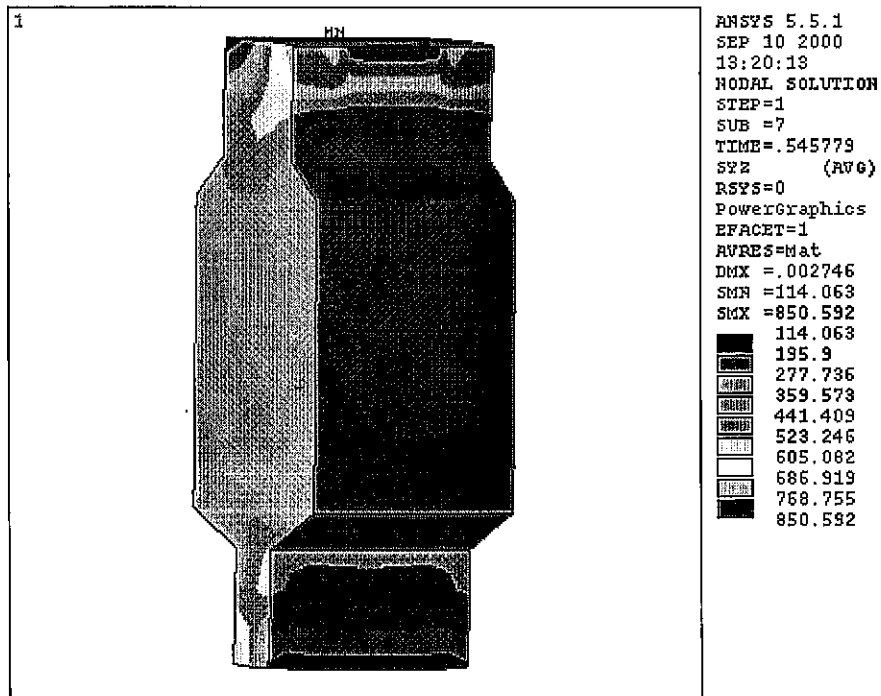


Fig. 5.46 Shear stress distribution in set 45



## 6. FULL-SCALE BRIDGE TESTING

### 6.1 Description of Full-Scale Bridge

Design of the full-scale bridge was for a two-span, two-lane, continuous prototype bridge. The bridge was designed and constructed using procedures that are very similar to those adopted in actual construction. The major parameters needed in designing the bridge are:

- Precast panel dimensions and configuration.
- Size of mild reinforcement.
- Shear pocket dimensions and spacing, number and size of shear connectors that are required to achieve full composite action between the precast panels and the supporting system.
- Configuration of the joint between the adjacent precast panels (type and material).
- Post-tensioning prestressing force that is needed longitudinally (i.e., strand sizes), to secure the tightness of the joints, and transversely, to account for handling and erection stresses.
- Spacing of the longitudinal supporting members.

The two-span full-scale bridge is 18 ft wide and 82 ft long with equal span lengths of 40 ft. It is composed of 11 precast deck slabs that are 8 in. thick and three W18 x 86 steel girders. The girders are supported on standard expansion bearings at both ends, and standard fixed bearings without cover plates at the interior support. The precast deck slabs are placed on the steel girders and made composite by means of shear pockets and studs. The plan and cross section of the bridge are shown in Fig. 6.1. Three different panel configurations were used due to placement requirements, i.e., interior or end panels, and post-tensioning requirements.

### 6.2 Construction Procedure

The adopted construction procedures were very effective in terms of scheduling, materials, and actual work techniques. The construction procedure is described in more detail as follows:

#### 6.2.1 Panel Fabrication

A total of eleven panels were needed for the full-scale bridge. All panels were 18 ft wide and 8 in. thick. Nine panels were 8 ft long, while two panels were 4 ft long to avoid placing the joint at the central pier location. Assembly of the bridge involved installation of these panels on three steel girders. As a result, there were three rows of beveled shear pockets,  $10\frac{7}{8}$  x 6 in. on the top, tapered to  $9\frac{3}{4}$  x 6 in. on the bottom, spaced 2 ft apart as shown in Figs. 4.4-4.5. The openings provided for the shear pockets and sheath ducts for the strands are shown in Fig. 6.2.

The panels were designed for transverse flexure with mild reinforcement (main reinforcement perpendicular to traffic) in accordance with IDOT specifications for slab design with the main reinforcement perpendicular to traffic. The panels were reinforced with two layers of reinforcement, #5 bars at 10 in. c/c on top and #6 bars at 10 in. c/c on the bottom. The cover provided for the steel reinforcement was 2 in. on top and 1 in. on the bottom. The panels were furnished with #5 bars distribution reinforcement comprising of mild steel. A typical layout of the steel reinforcement in the full-scale bridge panel is shown in Fig. 6.3. Bursting reinforcement was provided for each of the longitudinal ducts at the outer side of the end panels (P1) to prevent cracking of the section during prestressing. In addition, steel anchor plates were placed at both end panels for each of the longitudinal ducts.

Two types of post-tensioning ducts were used. One type of duct had a 2.87 in. outer diameter to accommodate the Dywidag bars, while the other type of duct had a rectangular shape, 1 x 4 in. to accommodate the strands. All eleven panels were designed to have two post-tensioning Dywidag bars on either side and two sets of strands in the middle. The middle five panels were designed to have two additional post-tensioning Dywidag bars as shown in Fig. 6.4. These ducts were placed at mid-height of the deck slab. Great care was taken during placement of the ducts since, misalignment of the post-tensioning duct at the transverse joint would result in a small angle break at each joint, thereby increasing wobble friction. Grouting vents were provided at the ends of each duct. A close-up view of the configuration for the post-tensioning ducts is shown in Fig. 6.5.

Leveling screws were used to adjust the precast slab units during placement. Location of the leveling screws on each panel was deliberately chosen in such a way to provide the same number of leveling screws over each girder. As a result, each girder was subjected to the same load. A close-up view of the configuration for the leveling screws is shown in Fig. 6.6

Once forming was finalized, and prior to casting, some panels were instrumented using embedded strain gages in addition to strain gages that were mounted on the reinforcing steel as shown in Figs. 6.7-6.8. Location of this instrumentation was determined through a theoretical analysis for the critical stress areas in the concrete and steel. Fig. 6.9 shows a typical panel after forming and instrumentation and prior to casting.

### **6.2.2 Casting and Curing of Panels**

The precast panels were fabricated in the precasting yard using concrete with the mix proportions shown in Table 6.1. The water cement ratio was 0.36. Type I Portland cement was used as a binding material. A  $\frac{3}{4}$  in. maximum aggregate size was used, while river sand was used as fine aggregate. Superplasticizer in the amount of 80 fl oz per cubic yard was added to the mix to obtain the required workability and a slump of 5 in. An air entraining agent was added in the amount of 4 fl oz per cubic yard for durability purposes. A retarder in the amount of 20 fl oz per cubic yard was used to retard the setting time so that placement and finishing could be carried out in an efficient manner. Fig. 6.10 shows a typical panel after concrete pouring. Control cylinders were prepared along with the panels to determine the compressive strength of the concrete at the time of testing. The panels and control cylinders were cured under blankets for a period of 3 days and then cured at outside temperature and humidity conditions. After fabricating the required panels and after proper curing for a period of 60 days, they were delivered to the field (IDOT Biesterfield yard, Elkgrove, IL) as shown in Figs. 6.11-6.12.

### **6.2.3 Abutment**

The full-scale bridge is supported on three abutments, two at the ends and one in the middle (two-span continuous bridge). The abutments were fabricated in the precast yard using the concrete with the mix proportions shown in Table 6.1. Each of the abutments is 2 x 2 ft and

16 ft long. Layout of the bridge abutments is shown in Fig. 6.13. A steel plate, 18.5 x 9 x 1 in. was placed at each bearing location, i.e., there were three steel plates for each abutment as shown in Fig. 6.13. A total of six 1½ in. diameter and 12 in. deep holes were made in each abutment to facilitate bolting of three bearings to the abutment. In addition, two 3 in. diameter holes were made in each abutment to bolt it to the testing bed as shown in Fig. 6.13. Reinforcement was provided in the abutment as shown in Fig. 6.14.

Table 6.1 Mix proportions of concrete for full-scale bridge deck panels

Ingredients	Mix proportions	
	Cement	390 kg/m <sup>3</sup>
Coarse aggregates	1037 kg/m <sup>3</sup>	1748 lb/yd <sup>3</sup>
Sand	730 kg/m <sup>3</sup>	1230 lb/yd <sup>3</sup>
Water	142 kg/m <sup>3</sup>	28 gal/yd <sup>3</sup>
AEA (Daravair 1400)	5.2 fl oz./m <sup>3</sup>	4 fl oz./yd <sup>3</sup>
Retarder (WRDA-17)	26.2 fl oz./m <sup>3</sup>	20 fl oz./yd <sup>3</sup>
Superplasticizer (WRDA-19)	104.6 fl oz./m <sup>3</sup>	80 fl oz./yd <sup>3</sup>
Slump	127 mm	5 in.

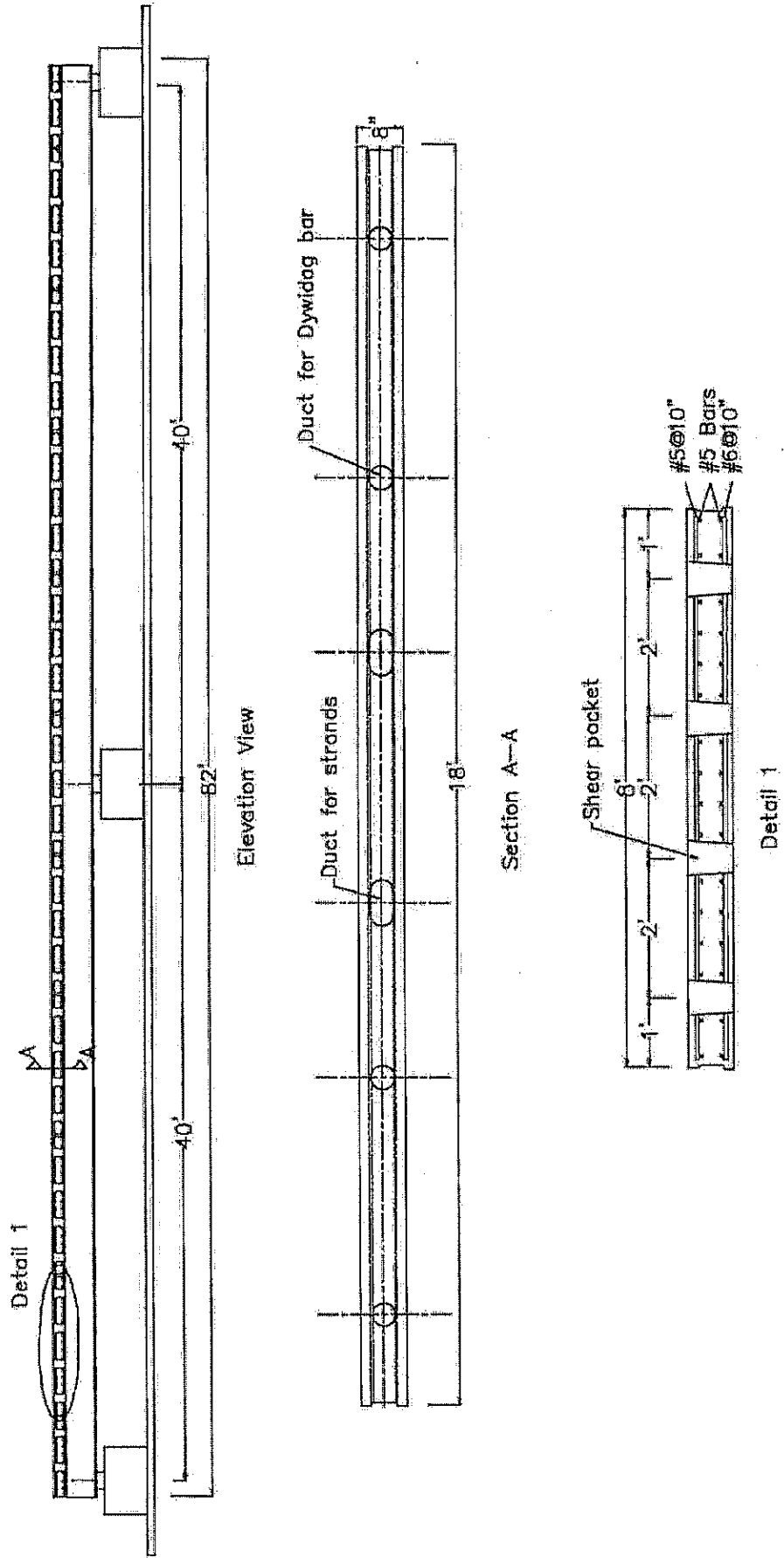


Fig. 6.1 Plan and cross section of the prototype bridge

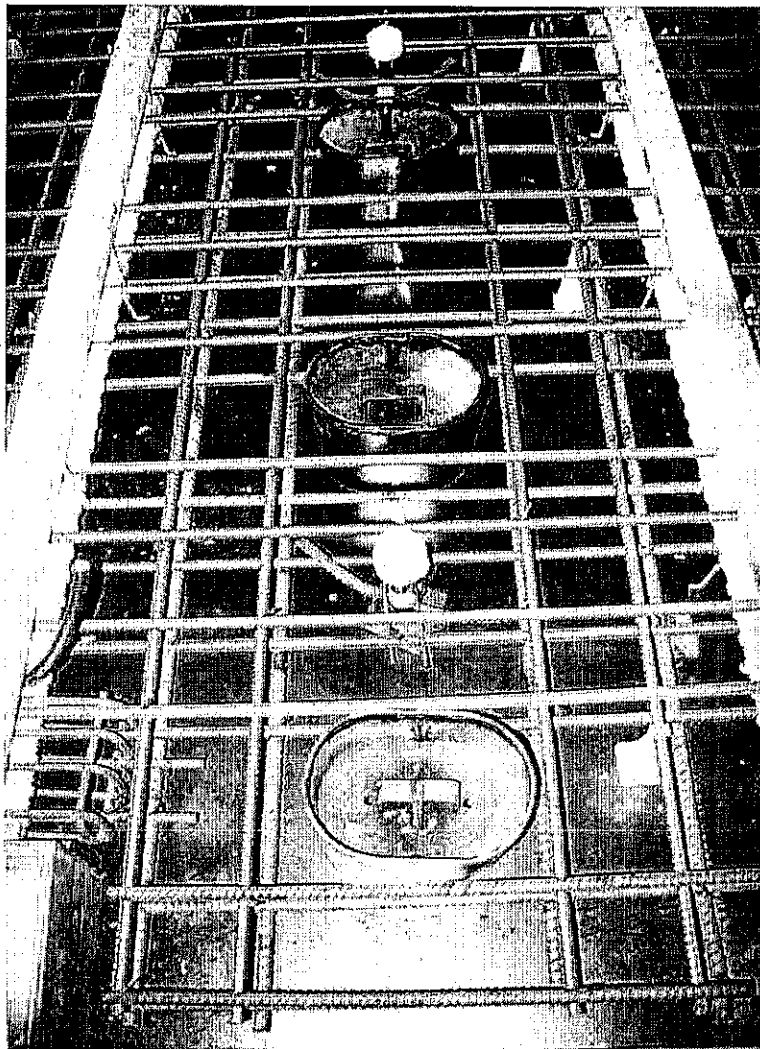


Fig. 6.2 Forming of typical precast panel

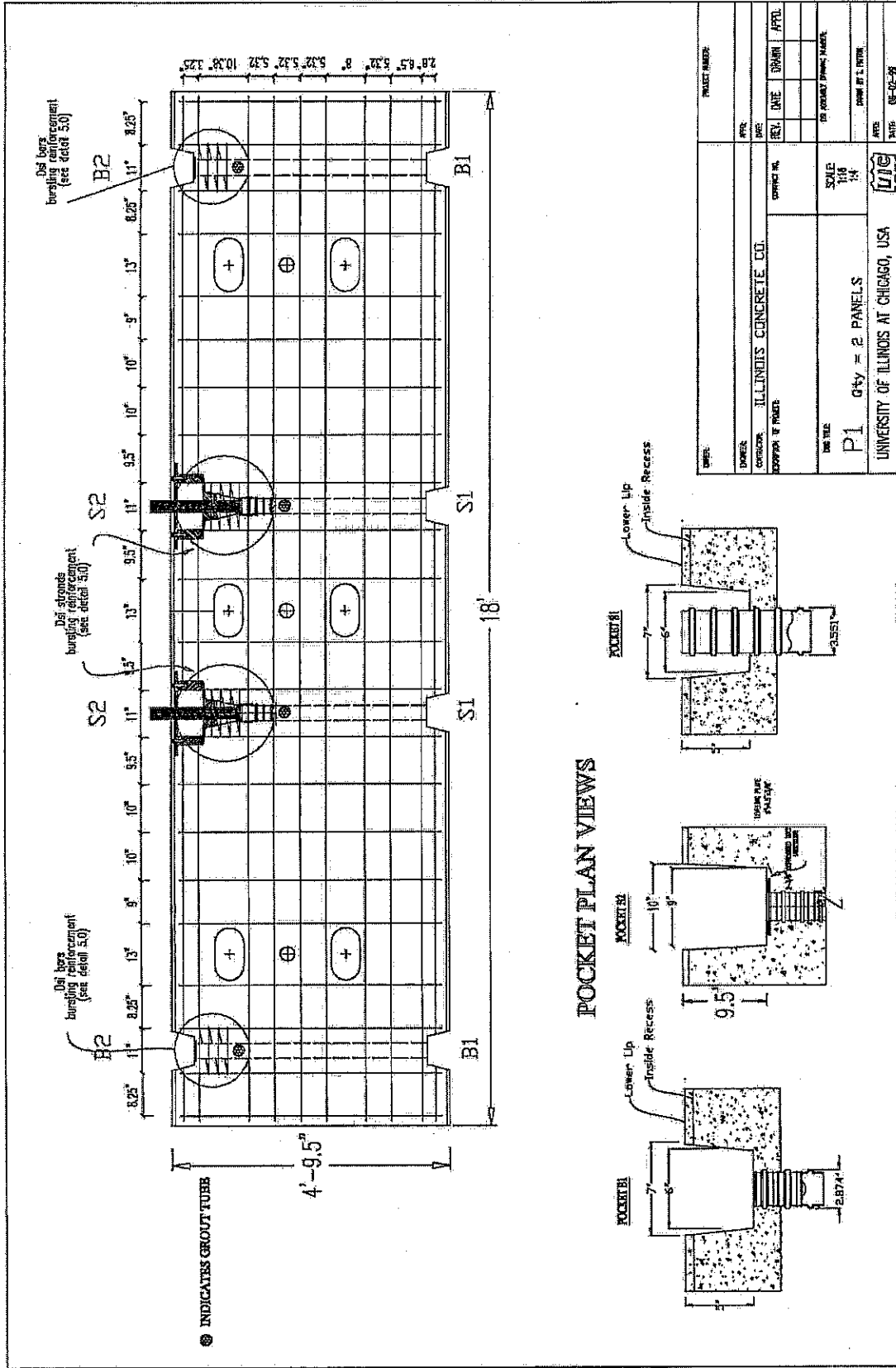


Fig. 6.3 Typical layout of steel reinforcement in full-scale panel

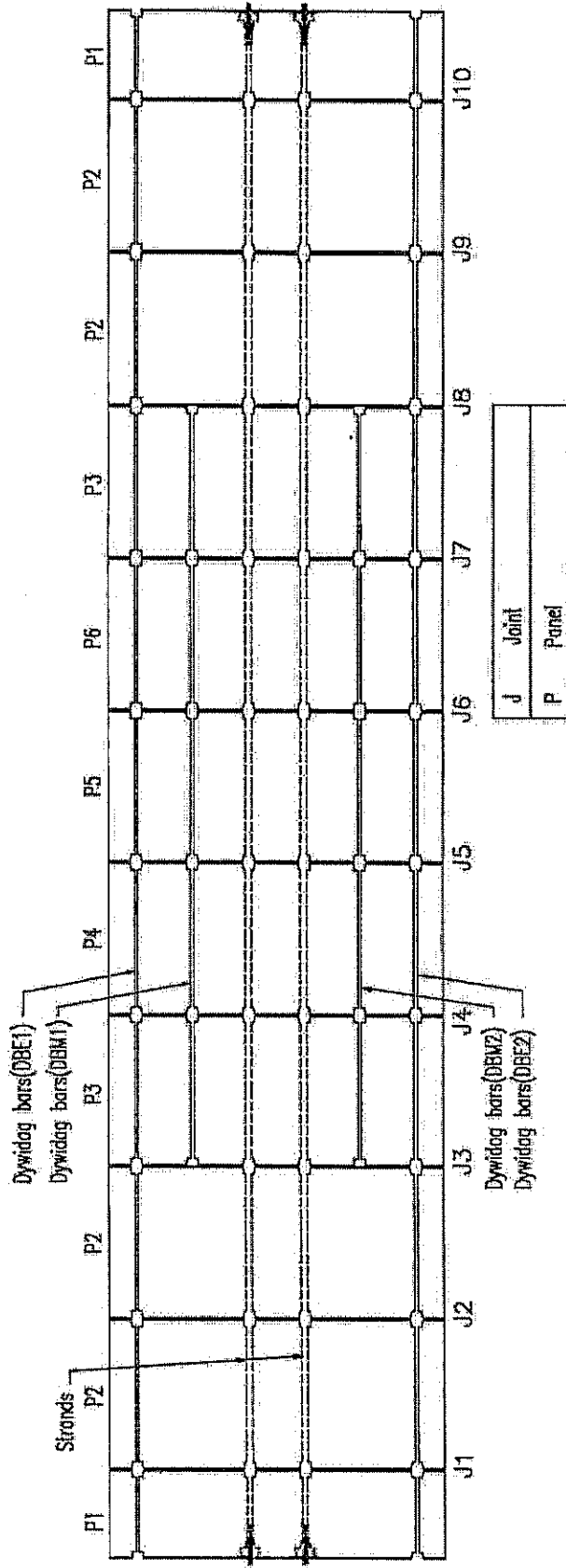


Fig. 6.4 Arrangements of Dywidag bars and strands in full-scale bridge

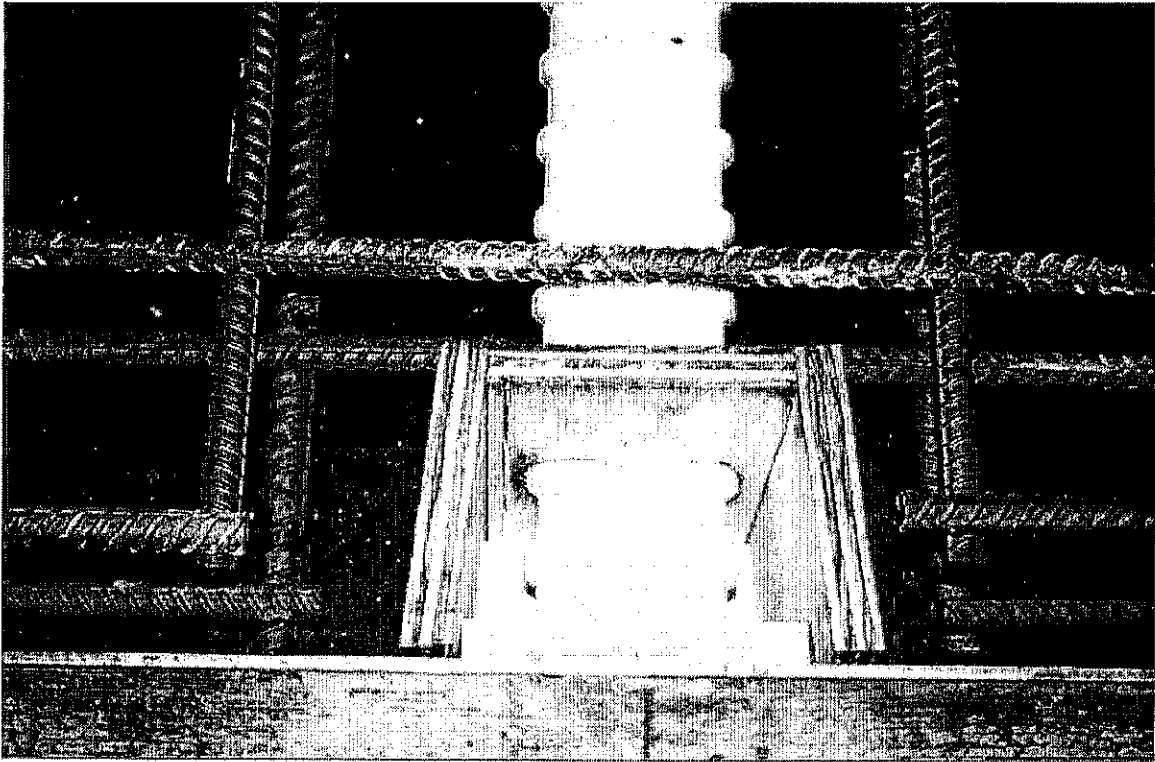


Fig. 6.5 Post-tensioning duct configuration

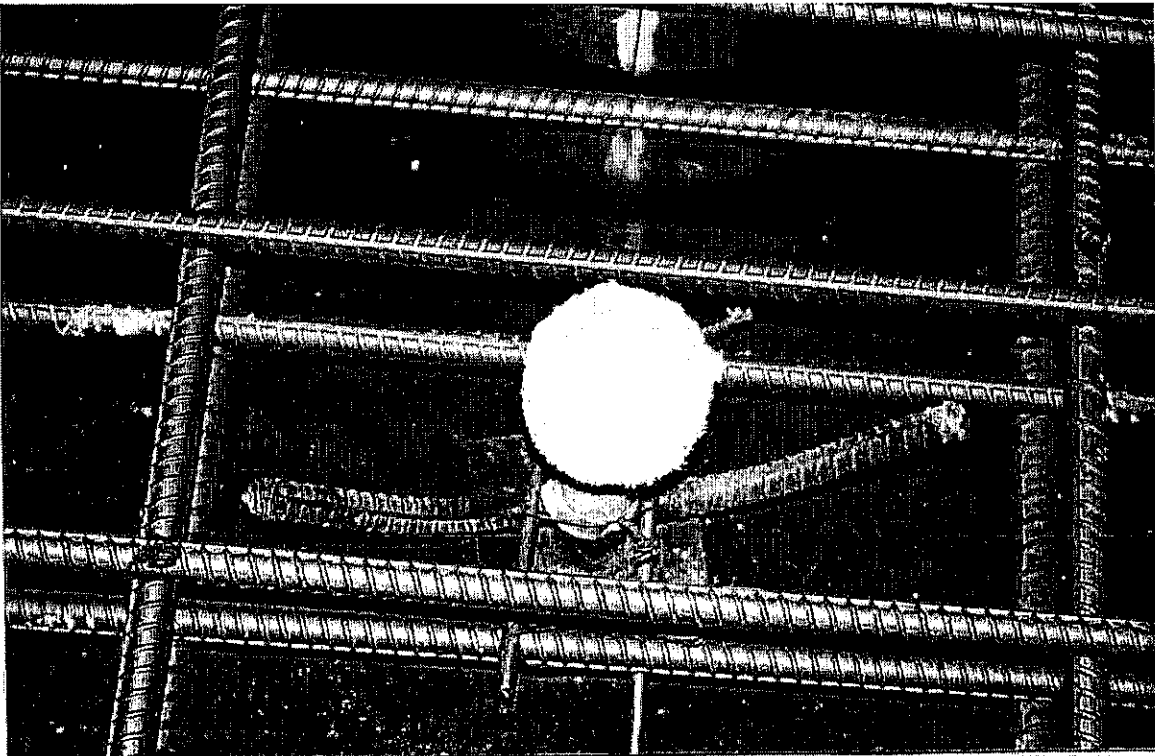


Fig. 6.6 Leveling screw configuration

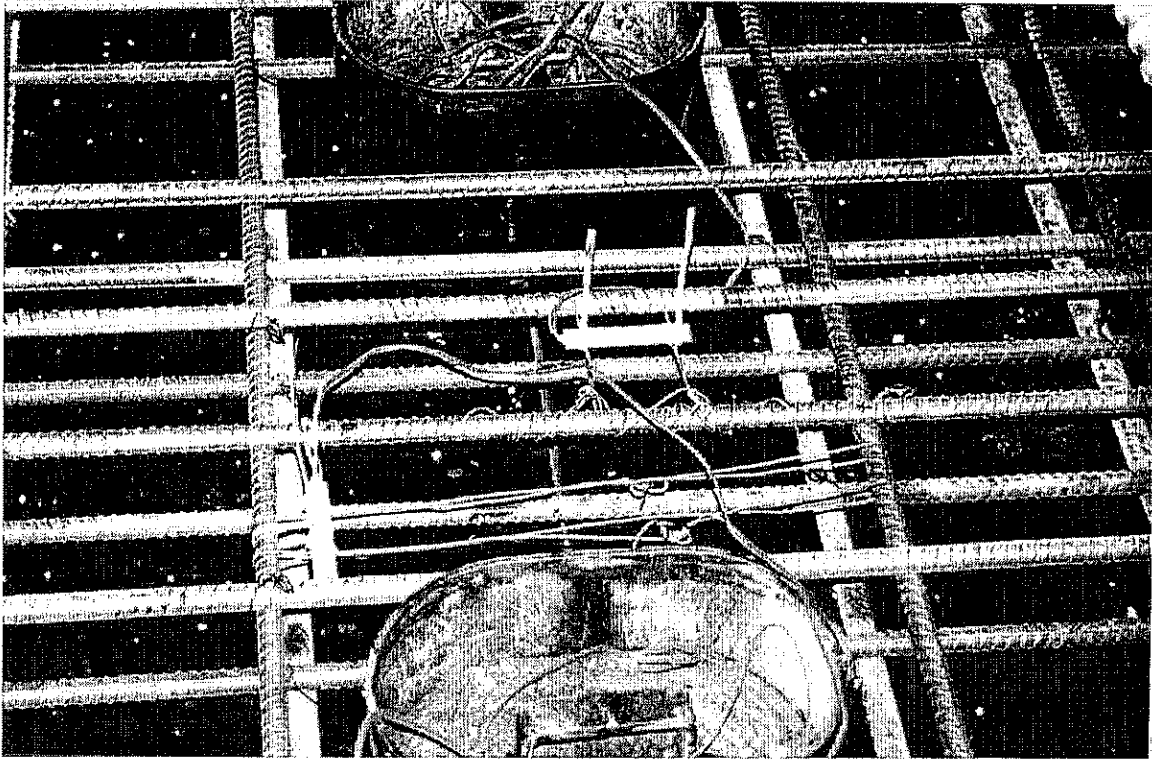


Fig. 6.7 Instrumentation for precast panel

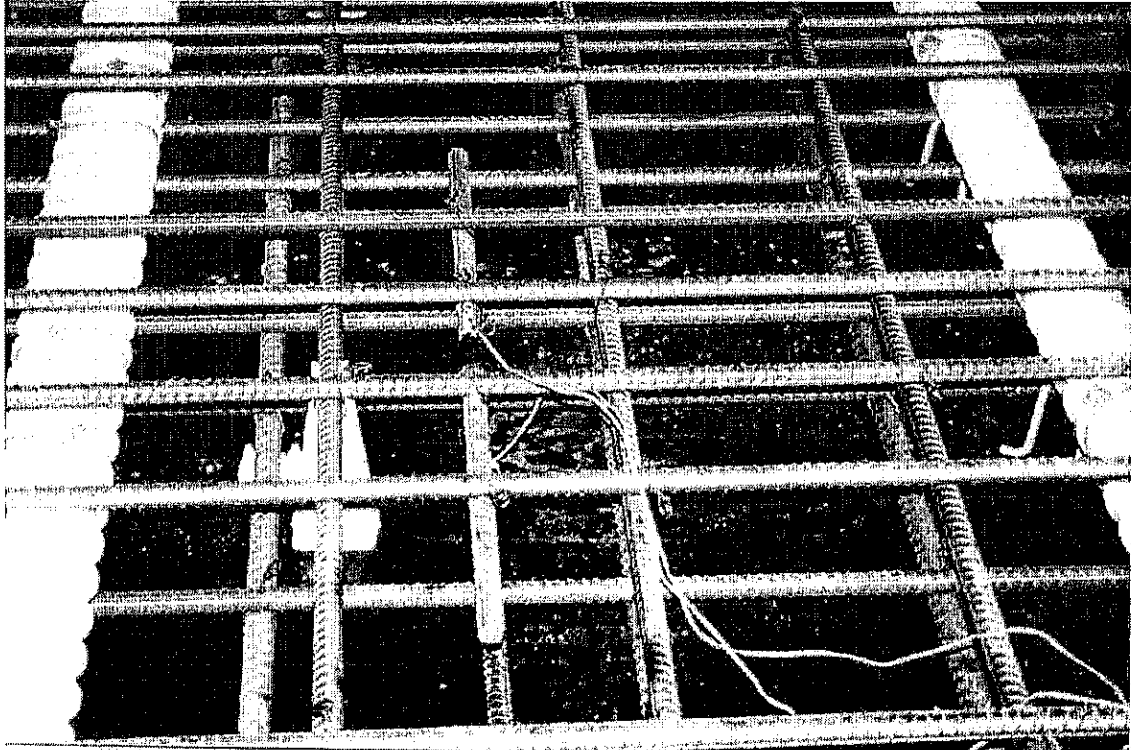


Fig. 6.8 Instrumentation for precast panel

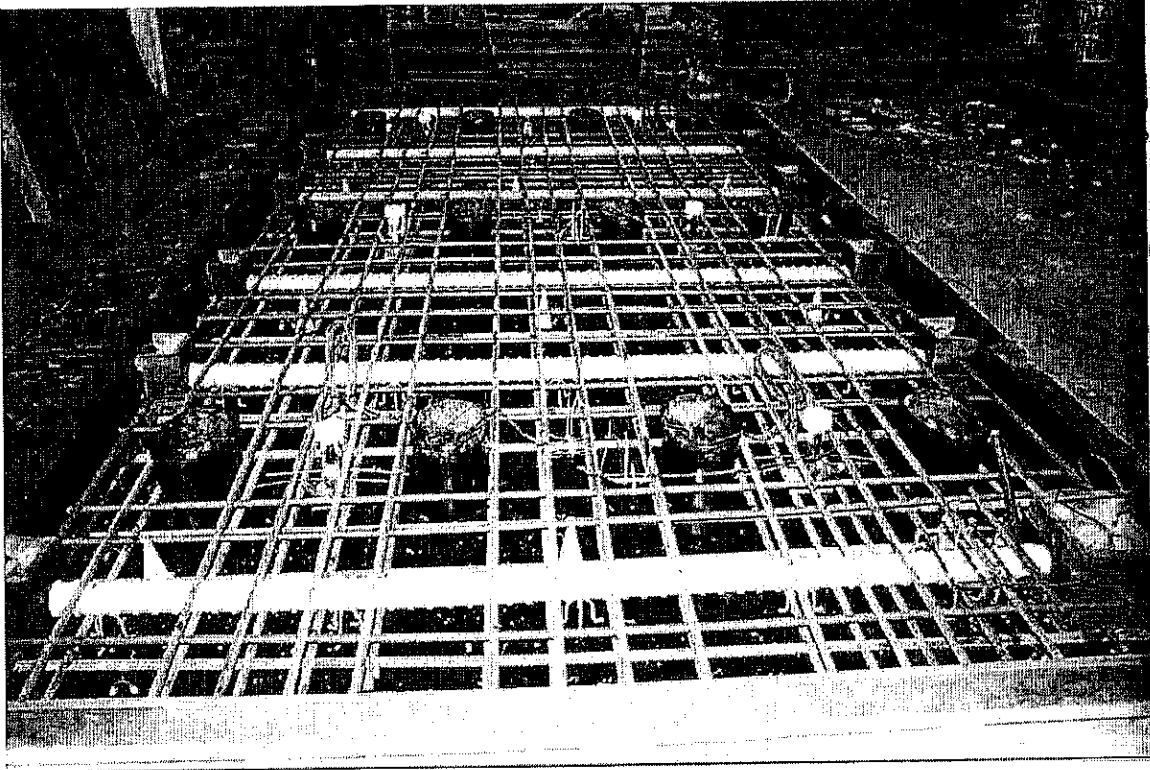


Fig. 6.9 Typical panel after forming and instrumentation

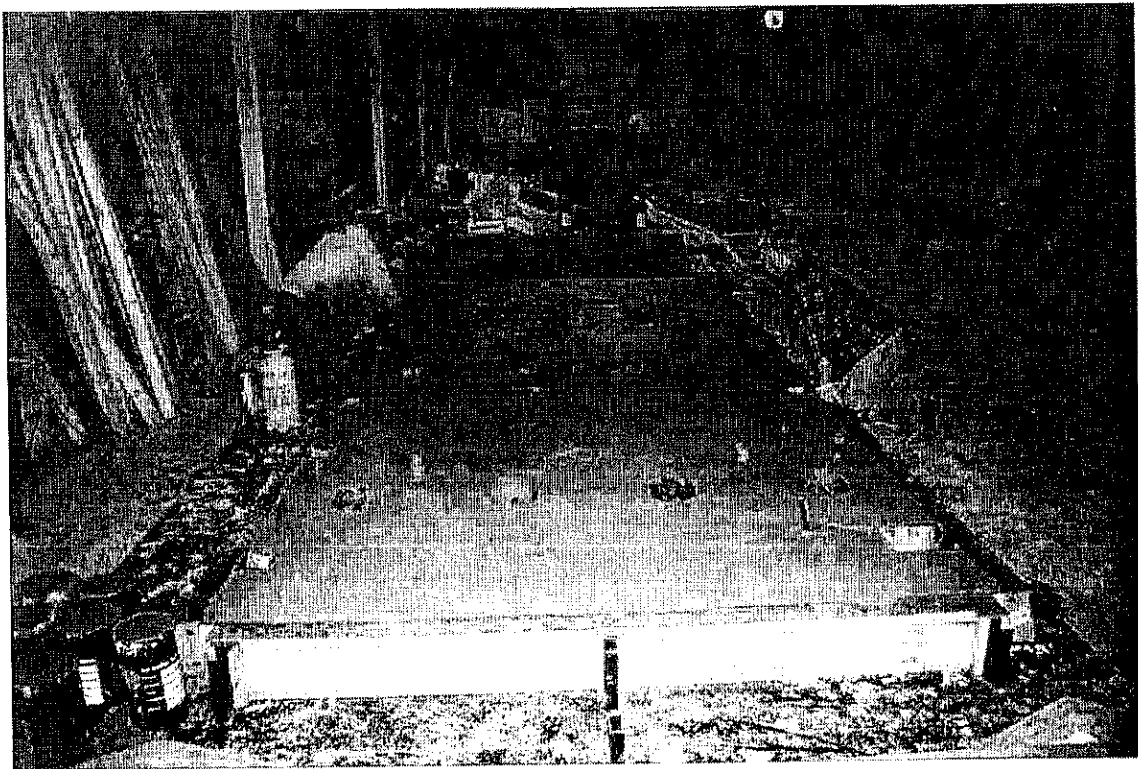


Fig. 6.10 Finished precast concrete panel

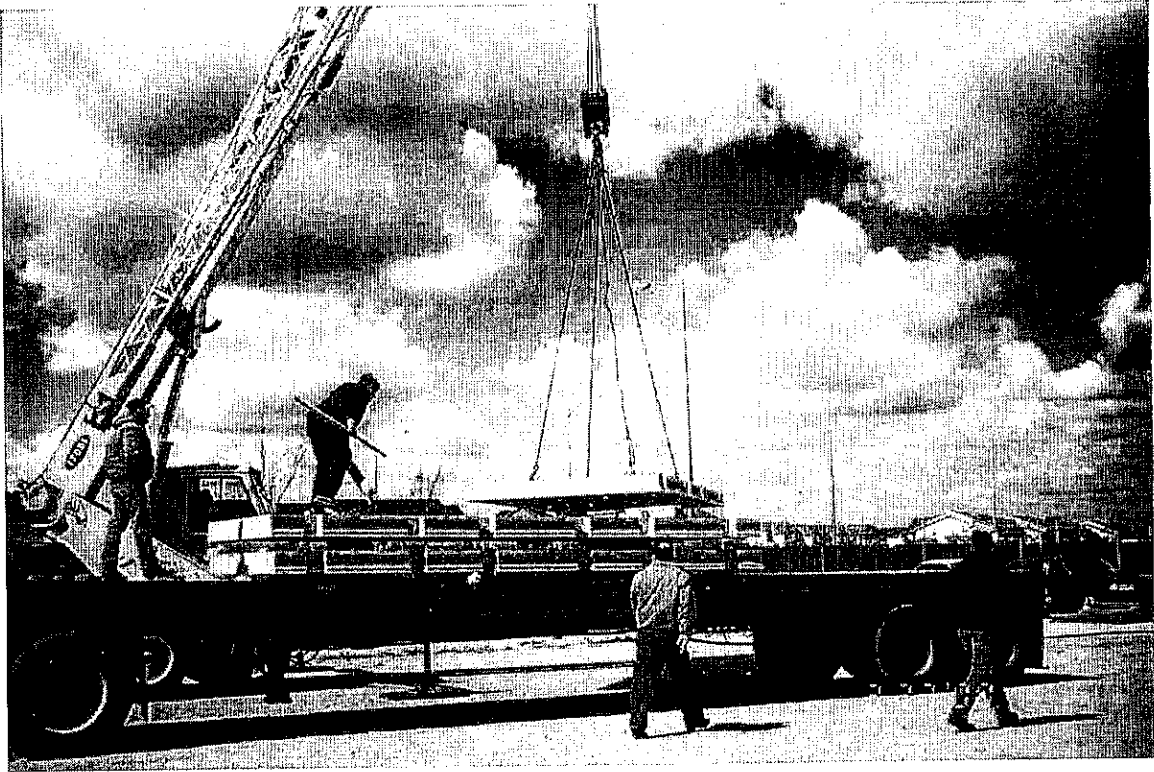


Fig. 6.11 Unloading of cured precast concrete panels in the field

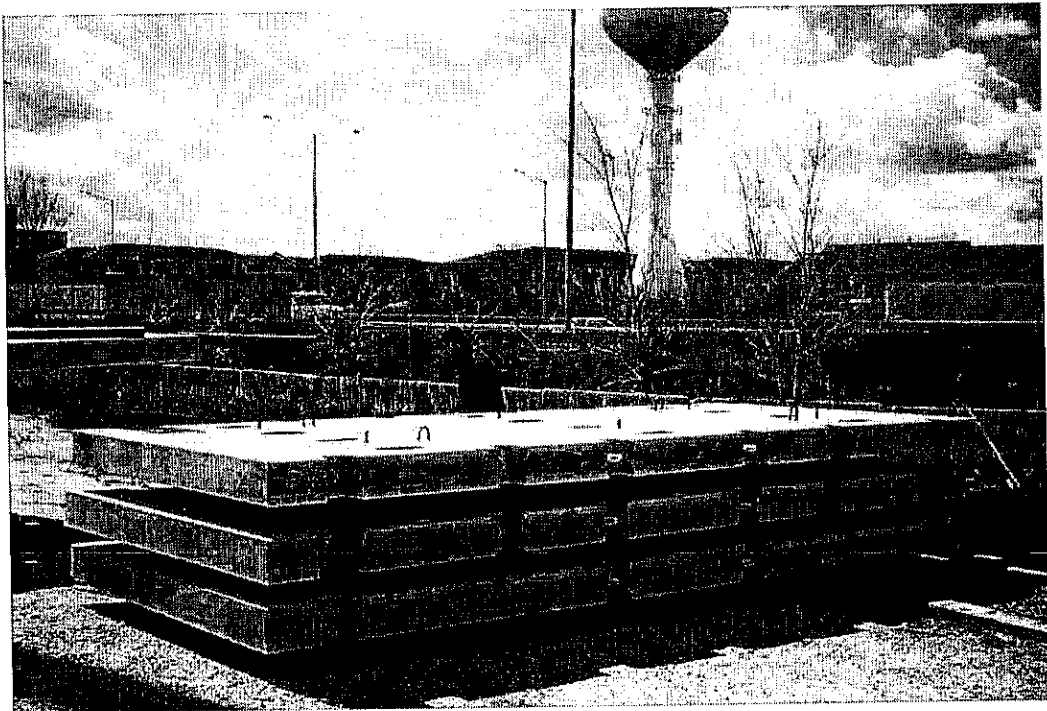
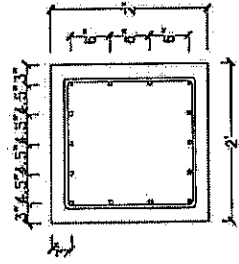
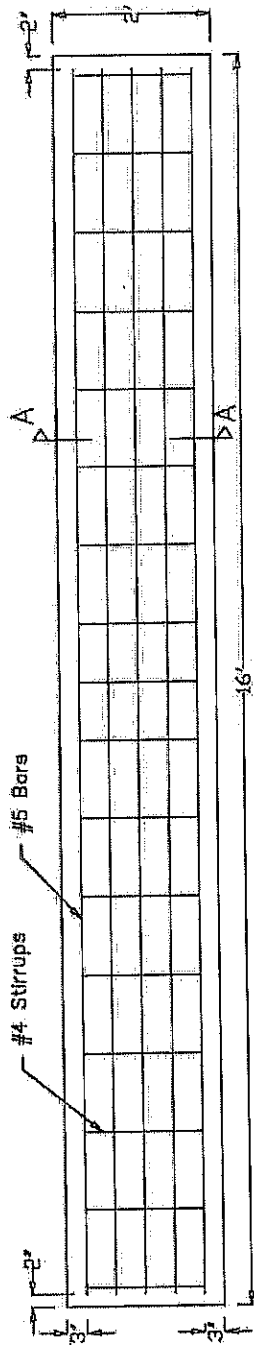


Fig. 6.12 Set of cured precast concrete panels

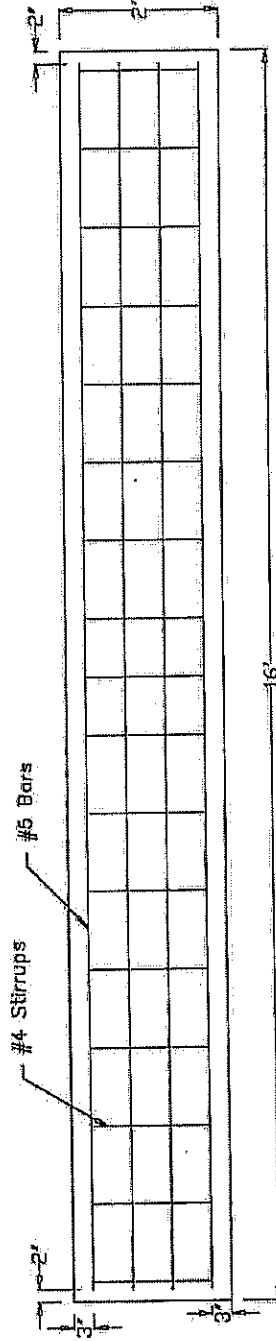




Section A-A



Elevation View (Reinforcement)



Plan View (Reinforcement)

Fig. 6.14 Reinforcement details of abutment

## **6.3 Bridge Assembly**

### **6.3.1 Preparation of Testing Bed**

Prior to initiating the bridge assembly process, the testing area was prepared in the field in terms of cleanup and surface leveling. The first step entailed assembly of the testing bed. A heavy duty crane was used to assemble 7 plate girders for the testing bed as shown in Fig. 6.15. This testing bed is 22 ft wide and 100 ft long to accommodate the 18 ft wide deck and 82 ft long bridge. Under each reinforced concrete support, a steel plate of 4 x 22 ft, 1 in. thick was placed to level the support as well as to provide the essential load distribution. These plates were bolted to the top flanges of the plate girders. A large number of high strength bolts were also required for all the connections. Following placement of the supports, three lines of steel girders were installed.

### **6.3.2 Panel Preparation**

Once the beams were placed over the supporting systems accordingly, the process of placing and leveling the precast panels was initiated. The joint surfaces between the precast slabs were thoroughly sandblasted and cleaned using high air pressure to remove all the dirt, oil, grease, etc. so that good bonding could be achieved. The ends of the ducts for strands and Dywidag bars were cleaned properly to facilitate easy installment.

### **6.3.3 Placement of Panels**

Prior to placement of the precast deck slabs on the steel girders, all the leveling screws were set to 1 in. clear below the bottom of the slab. Each panel was lifted, placed, and adjusted in its proper location as shown in Figs. 6.16-6.17. The proper leveling was adhered to in order to place the panels, while horizontal alignment was accomplished to allow for the required clearances between the panels, i.e., the transverse joints as shown in Fig. 6.18.

### **6.3.4 Forming for Transverse Joints**

Once proper placement and leveling of the panels was accomplished, the bottom and sides of the transverse joints were formed. Plywood of ¼ in. thickness was used as a base and 2

x 4 in. wood was used to support the base against the bed as shown in Figs. 6.19-6.20. The entire forming joints were caulked to guard against any leakage of the grouting material.

### **6.3.5 Placement of Longitudinal Post-Tensioning Strands and Bars**

Longitudinal post-tensioning is provided for continuity between the precast panels. An additional prestress force is also needed to overcome the tensile stress due to negative composite dead and live load moments in continuous spans. One post-tensioning Dywidag bar was run through each of the four sheath ducts and four strands were run through each of the two sheath ducts. At the transverse joints between adjacent precast panels (female to female type joint), the post-tensioning sheath ducts were made continuous between the precast slabs with watertight sleeves. Metal sheets were placed over the ducts and taped accordingly to secure them prior to grouting.

### **6.3.6 Grouting of Transverse Joints**

After tightly securing the ducts, the transverse joints were then grouted using set grout. The process of applying the set grout consisted of wetting the concrete surfaces, mixing, and placing set grout for closure of the transverse joints between precast deck panels. The set grout was prepared with a water proportion of 3.2 liters per 22.7 kg (50 lbs) of cement. The optimal time of mixing set grout with water for achieving the best consistency was found to be 3 minutes. As the mixture was poured in the joint, a finger vibrator was used to fill the joints more efficiently. Proper curing was carried out by covering the joint with wet burlap and plastic sheets as shown in Fig. 6.21. A close-up view of the grouted transverse joint is shown in Fig. 6.22.

### **6.3.7 Post-Tensioning of Strands and Dywidag Bars**

The longitudinal post-tensioning was accomplished after the transverse joints between precast panels were grouted and properly cured. After the set grout between the precast slabs had attained a compressive strength of approximately 5,000 psi at 7 days, the longitudinal post-tensioning was provided as proposed in terms of strands and Dywidag bars, and the post-tensioning tendons were tensioned. At this stage, the decks were not made fully composite with

the girders in order to avoid inducing unusual stresses in the girders. Post-tensioning details are shown in Fig. 6.23.

The Dywidag bars were placed in the ducts prior to post-tensioning as shown in Fig. 6.24. Initially, eight panels were placed on the steel girders and seven transverse joints were cast. This was performed deliberately so that post-tensioning could be applied to the Dywidag bars at joint 8. Post-tensioning of the end Dywidag bars (DBE1 and DBE2) was first completed at section A-A as shown in Fig. 6.25. Post-tensioning was then applied to the middle Dywidag bars (DBM1 and DBM2) at joint 8 to avoid tension cracks in joint 3. The post-tensioning system used for the Dywidag bar is shown in Fig. 6.26 and comprises of a self contained hydraulic power unit connected to a dial cylinder jacking ram by two hydraulic hoses. The required force was obtained by jacking the Dywidag bar against the embedded end plates and controlled by a load cell and calibrated pressure gage provided by Dywidag System International (DSI). Fig. 6.27 shows the end plates for the post-tensioned Dywidag bar. Strains were measured during the post-tensioning process in order to estimate losses as shown in Fig. 6.28. This type of instrumentation is very critical in terms of monitoring the actual strains in the joints during the post-tensioning process, service and ultimate loading. Load-strain calibration curves of the Dywidag bar are shown in Fig. 6.28. Block-out and coupling of the Dywidag bars are shown in Figs. 6.29 and 6.30, respectively. Coupling was formed for continuation of the Dywidag bars to the other end of the bridge.

All prestressing strands were instrumented at the joint between panels P3 and P2 to monitor the actual stresses in the strands and to make sure that the proposed prestressing level was provided as shown in Fig. 6.31. The strands were post-tensioned by adhering to the proper sequence as shown in Fig. 6.32. The required force was obtained by jacking the strands against the embedded end plates at section B-B as shown in Fig. 6.25 and controlled by a load cell and calibrated pressure gage provided by DSI. Figure 6.33 shows the strands in the post-tensioned end panel. Load-strain calibration curves for prestressing strands and strain readings recorded before and after release are shown in Fig. 6.34. The tensioning load as well as elongation of the tendon was measured at all times.

### **6.3.8 Installation of Shear Studs**

After post-tensioning, the shear studs were welded within each shear pocket (3-7/8-in. diameter and 5 in. long studs). The shear pockets were prepared as shown in Figs. 6.35-6.36 by cleaning the top surface of the beams and providing enough clearances between the studs. Once preparation of the pockets was completed, stud welding was performed by a certified technician as shown in Figs. 6.37-6.38. These studs were tested to withstand shearing by hammering them and rendering the stud at 45 degrees prior to breakage.

### **6.3.9 Grouting of Shear Pockets and Haunches**

Once all the shear studs were welded and proper forming was provided, the post-tensioning ducts, shear pockets, and haunches were grouted using set grout. Fig. 6.39 shows forming of haunches and shear pockets, while Fig. 6.40 grouted shear pockets. Fig. 6.41 shows finished pockets along with control cylinders for testing the strength properties of the grout, while Fig. 6.42 shows the haunch after grouting. All shear pockets and haunches were completely filled with set grout. Haunches between the top of the girders and the bottom of deck panels were grouted through the shear pockets in sequence so that the set grout was observed entering the next shear pocket. Figs. 6.43-6.44 present an overview of the bridge after completion of all the described processes.

### **6.3.10 Grouting of Longitudinal Ducts**

The longitudinal ducts for the Dywidag bars and strands were grouted by high performance grout for highly stressed steel. Water in the range of 1.3-1.5 gallons per bag of grout was added and mixed thoroughly until a flowable mix was obtained. Grout was then pumped into one end of the sheath duct and stopped when it came out of the vent at the other end.



Fig. 6.15 Assembly of testing bed

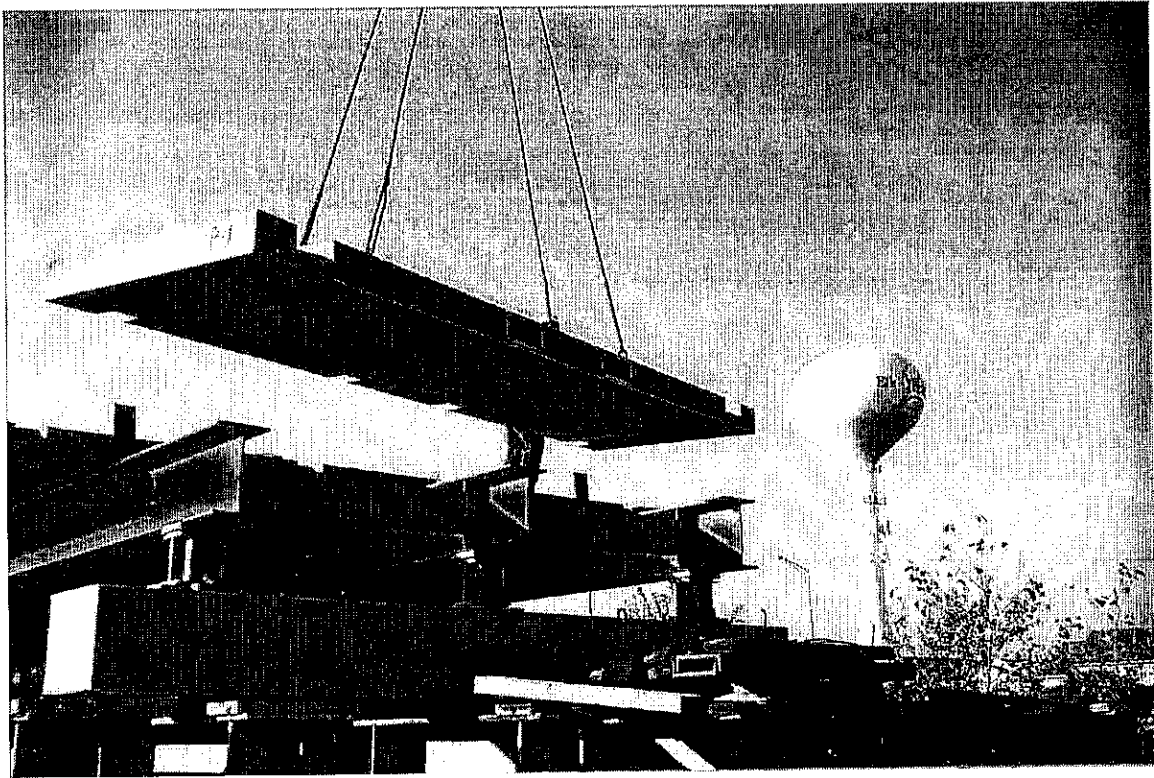


Fig. 6.16 Placement of precast panels

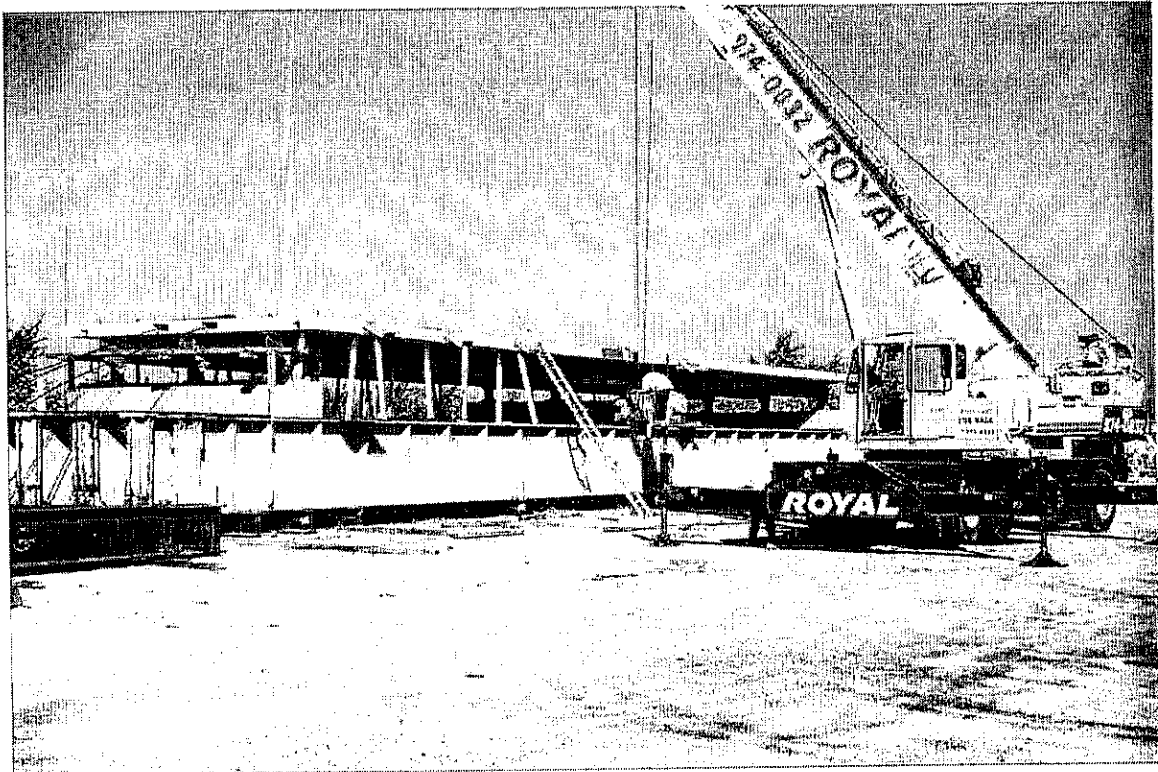


Fig. 6.17 Placement of precast panels

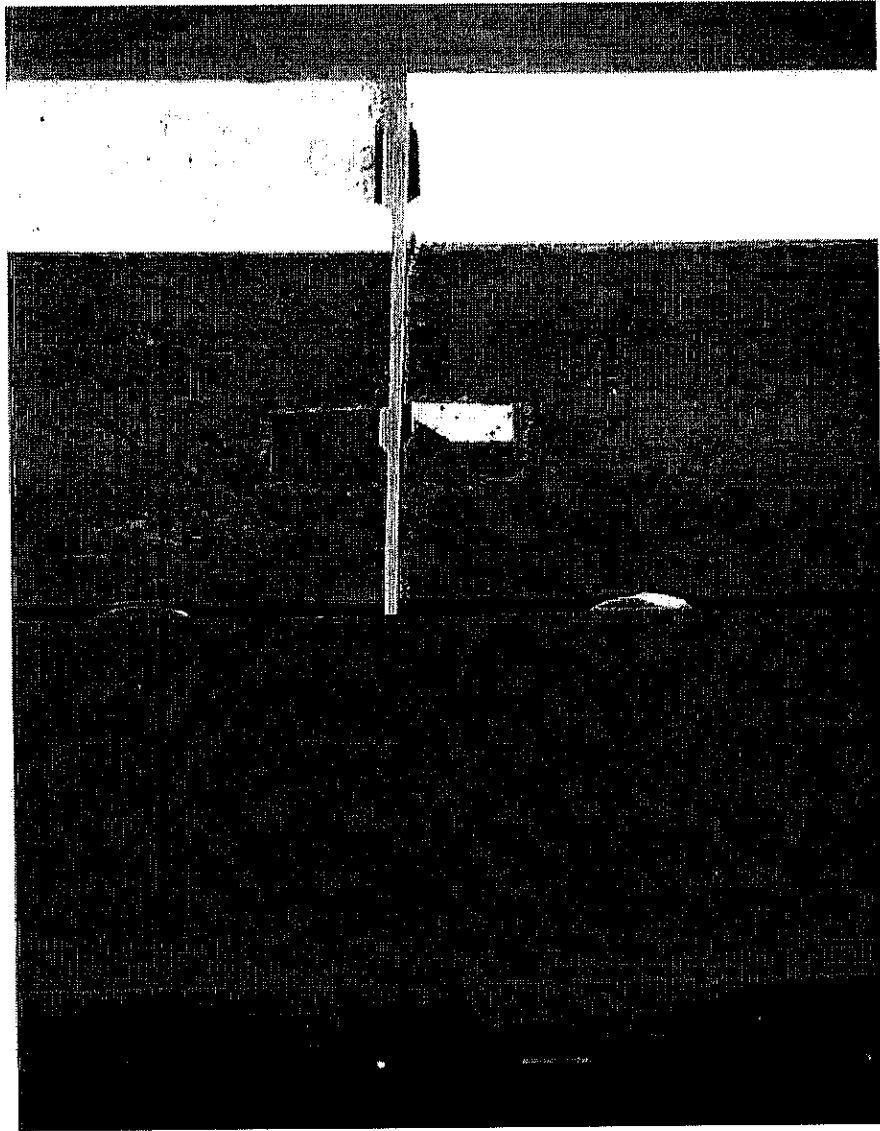


Fig. 6.18 Transverse joint configuration

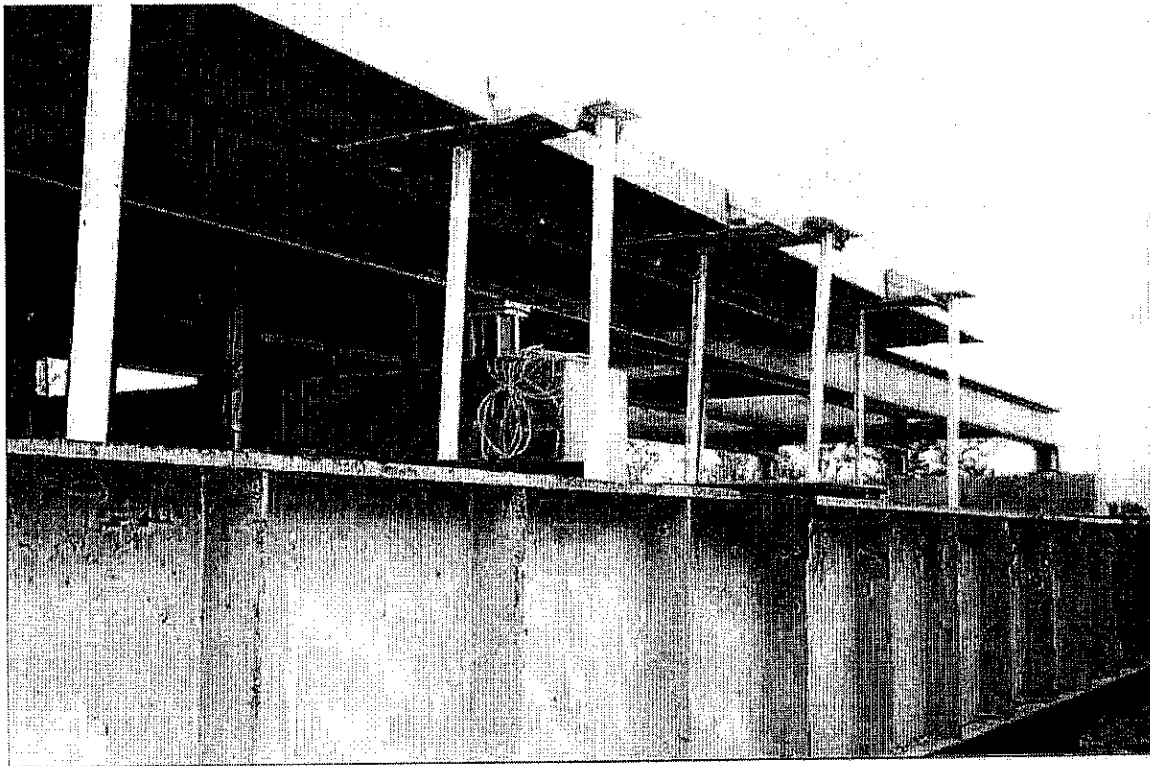


Fig. 6.19 Forming of transverse joints

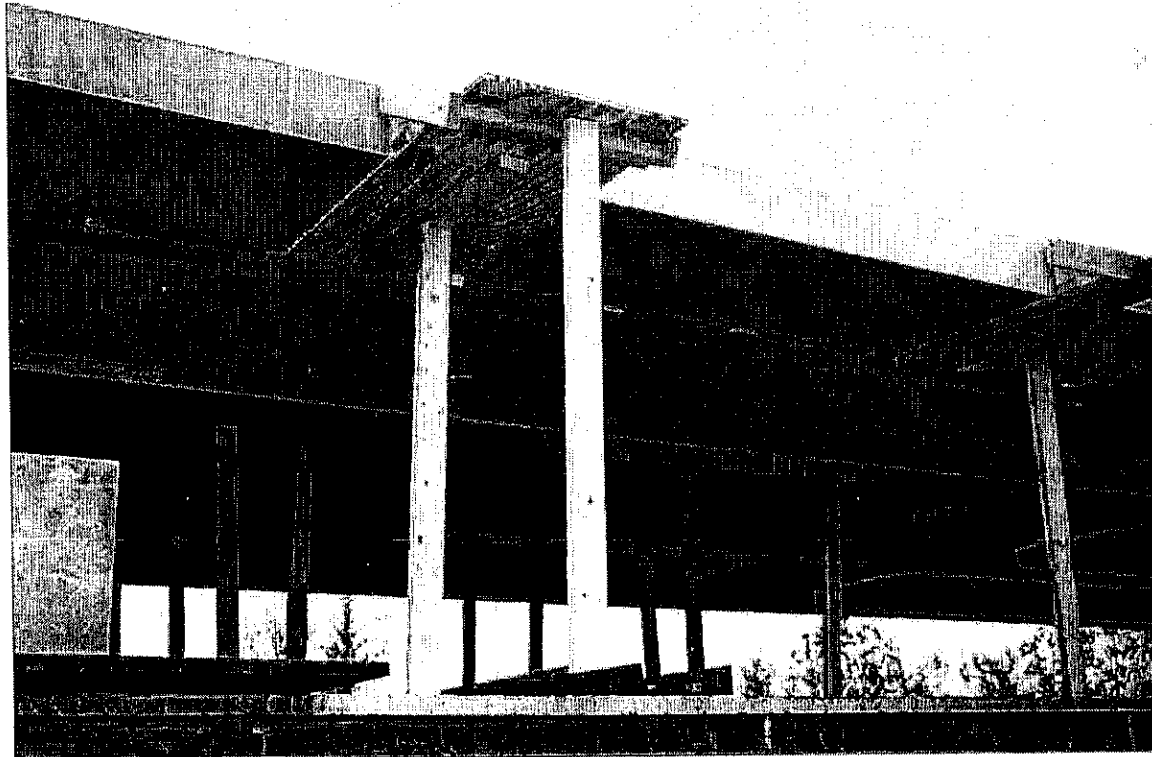


Fig. 6.20 Forming of transverse joints



Fig. 6.21 Curing of transverse joints

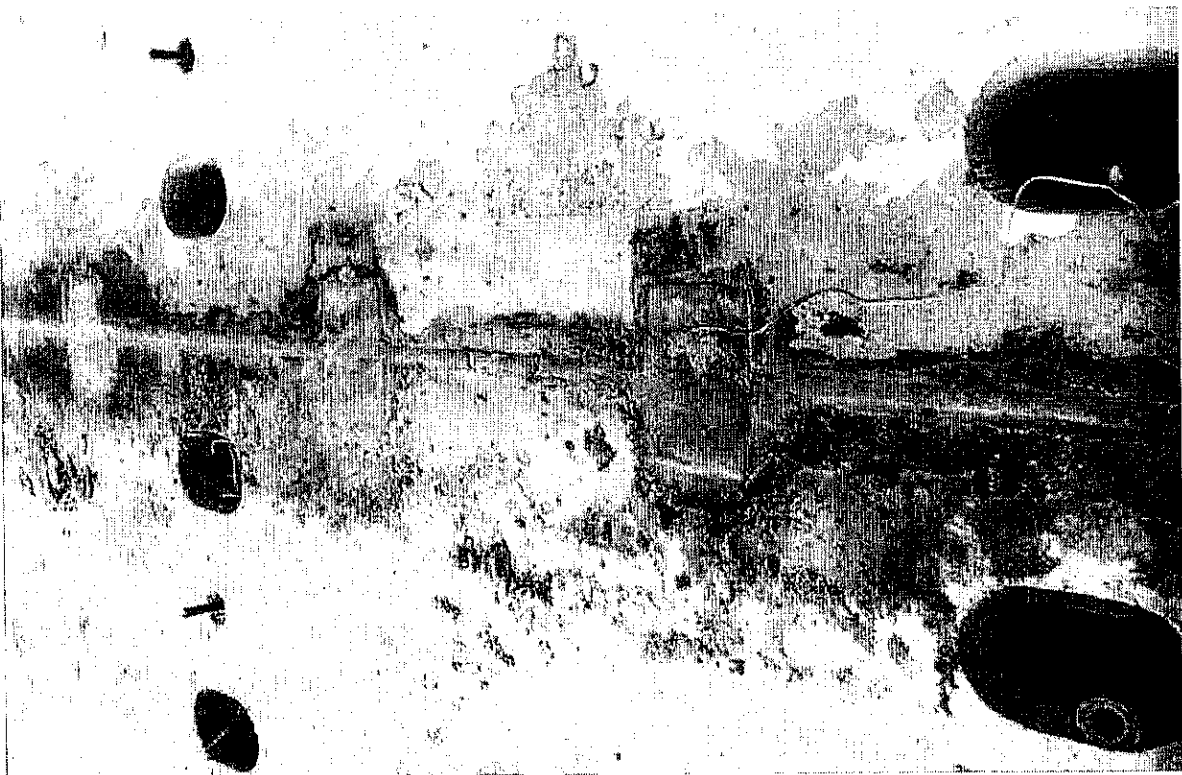
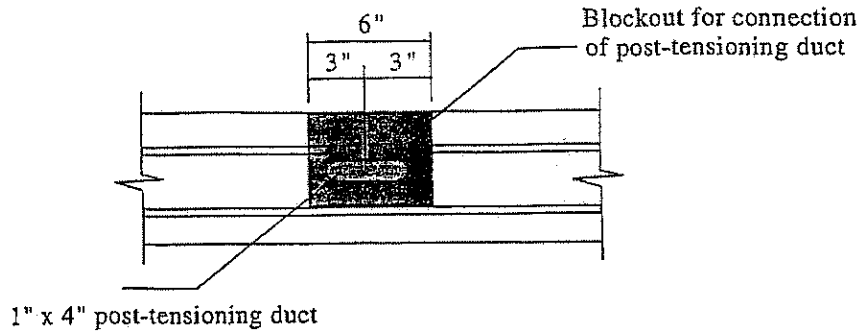
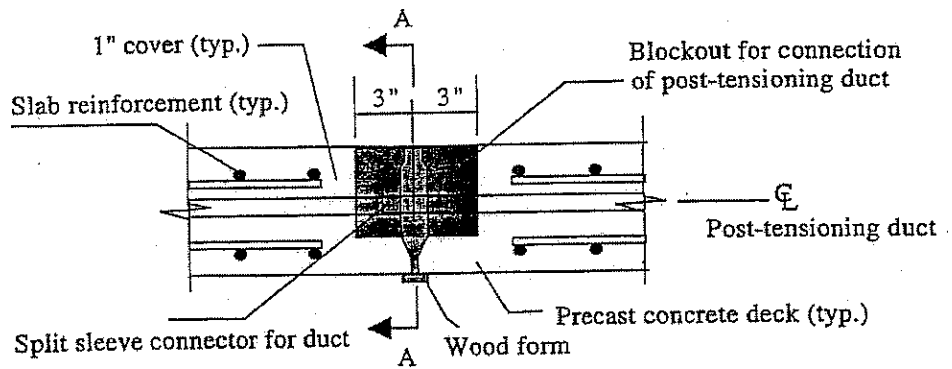


Fig. 6.22 Grouted transverse joints

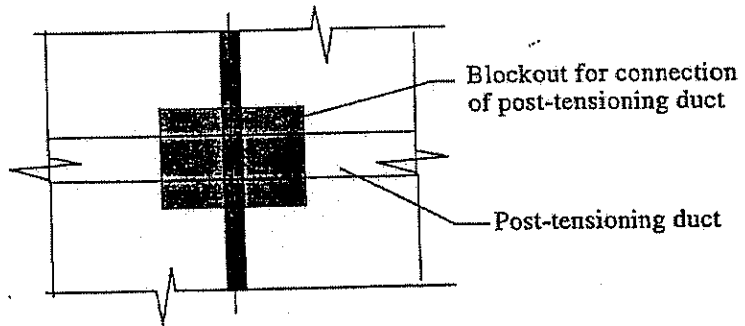


SECTION A-A



TYPICAL SECTION

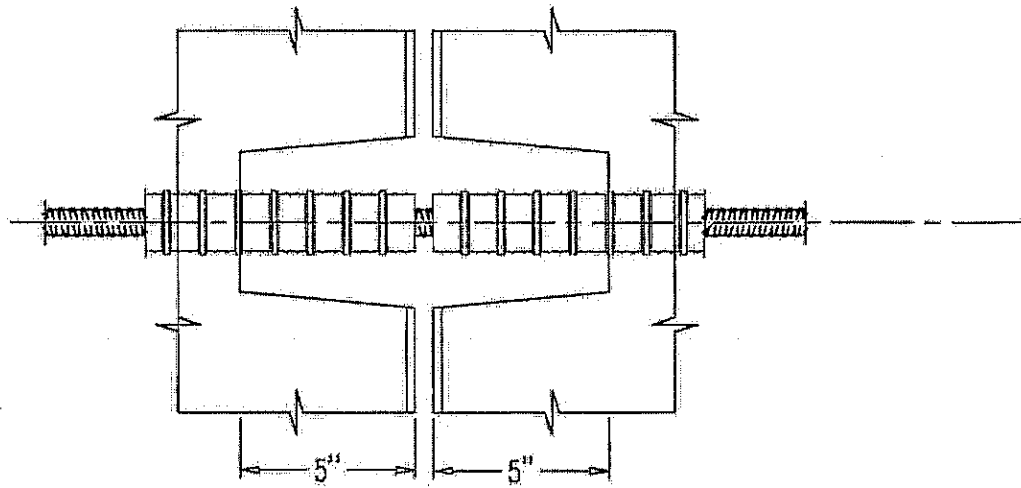
TRANSVERSE DECK JOINT AT POST-TENSIONING DUCT



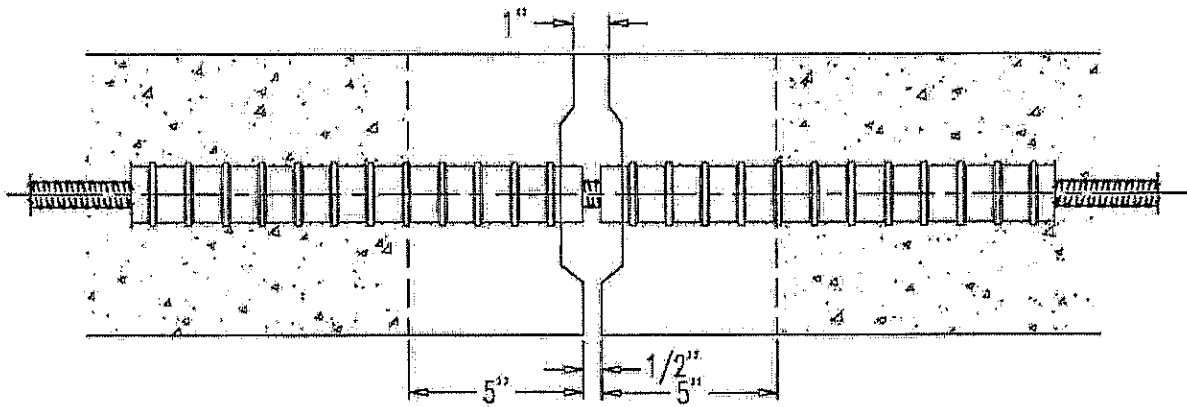
PLAN

BLOCKOUT FOR POST-TENSIONING DUCT

Fig. 6.23 Post-tensioning details



Plan View



Section View

Fig. 6.24 Arrangement of Dywidag bars prior to post-tensioning

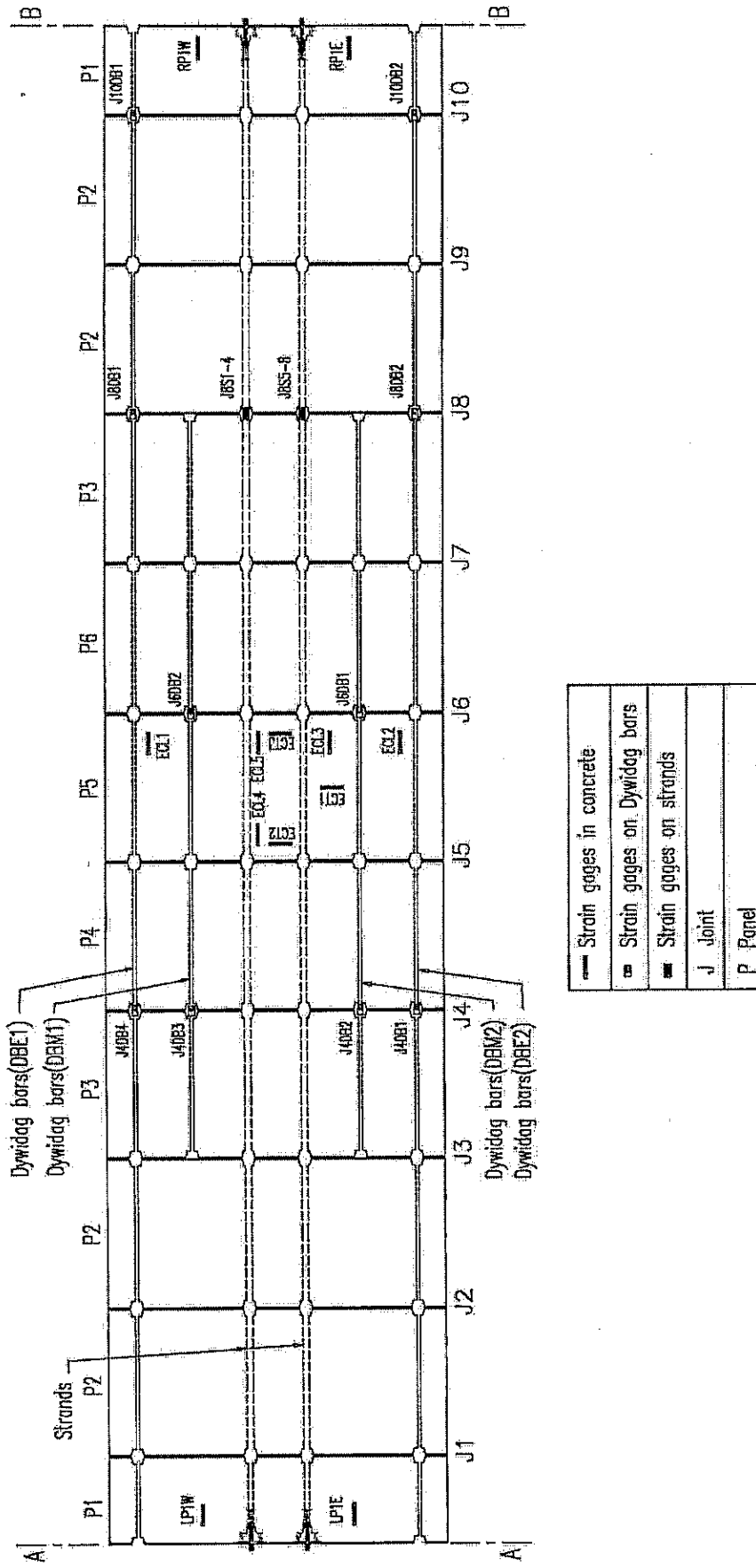


Fig. 6.25 Strain gages mounted on prestressing steel and placed inside concrete deck

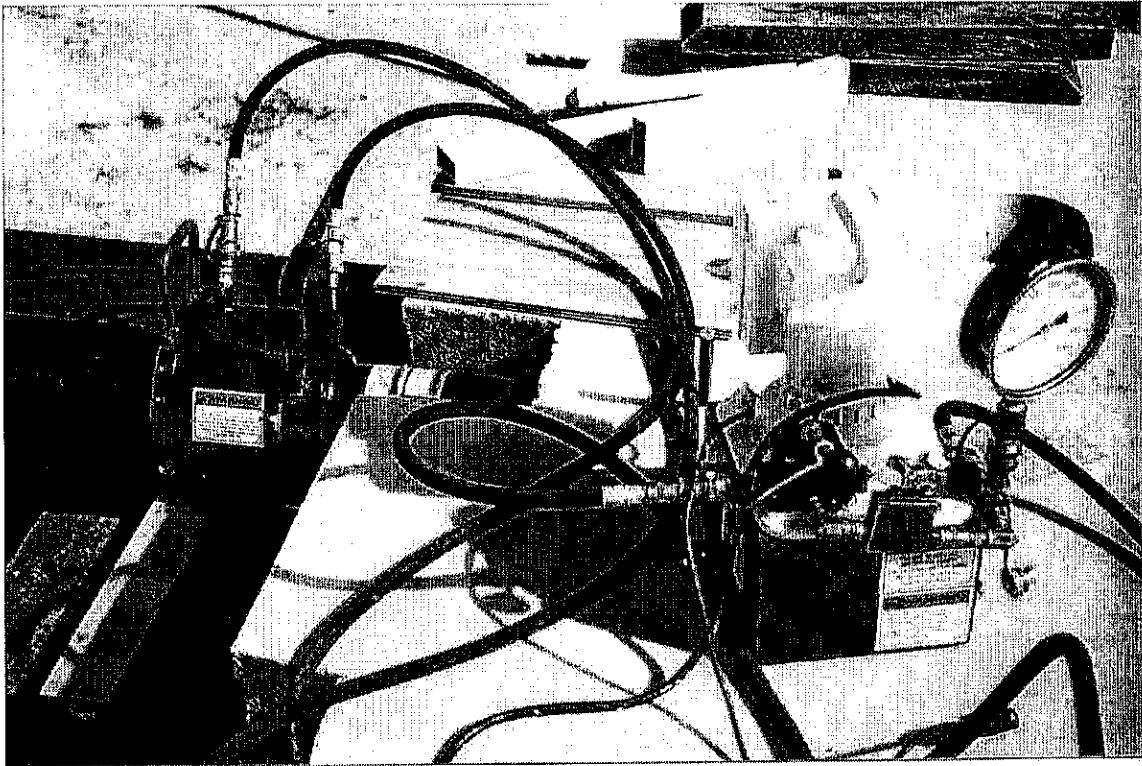


Fig. 6.26 Post-tensioning of Dywidag bars

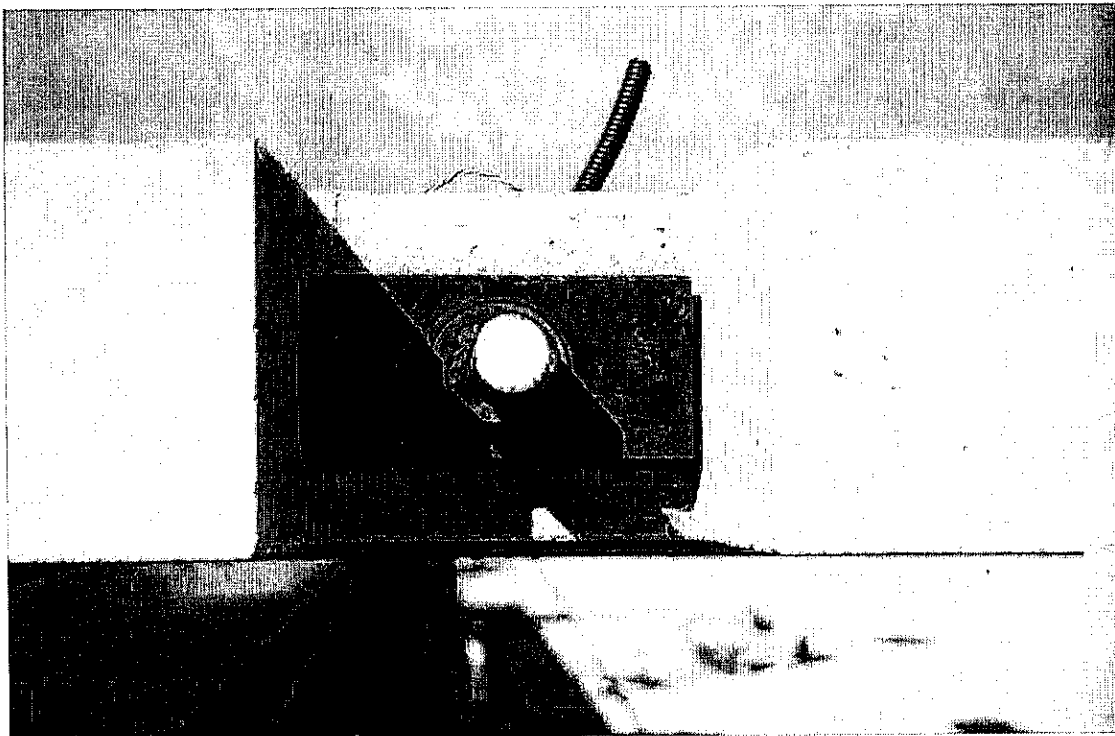
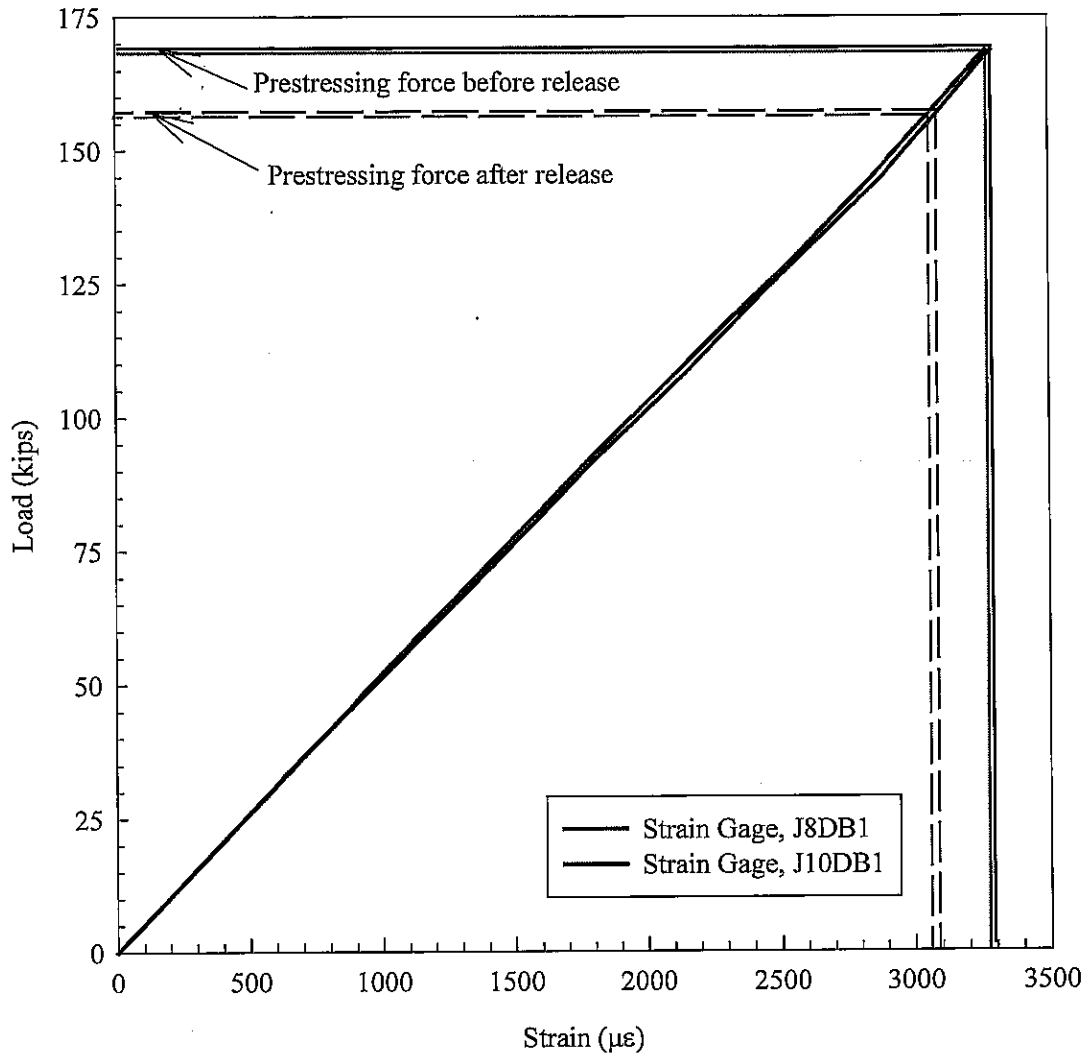


Fig. 6.27 End plates for post-tensioned Dywidag bars



Dywidag bar line (See Figure 6.25)	Strain gage Designation	Strain reading ( $\mu$ -strain)		Strain loss ( $\mu$ -strain)
		Before release	After release	
DBE1 Initial prestressing = 168.5 kips	J4DB4	3324	3260	64
	J8DB1	3270	3079	191
	J10DB1	3290	3090	200
DBE2 Initial prestressing = 168.5 kips	J4DB1	3265	3161	104
	J8DB2	3170	3100	70
	J10DB2	3186	3120	66
DBM1 Initial prestressing = 168.5 kips	J4DB3	3215	3198	17
	J6DB2	3206	3130	76
DBM2 Initial prestressing = 168.5 kips	J4DB2	--	--	--
	J6DB1	--	--	--

Fig. 6.28 Load-strain calibration curves for Post-tensioned Dywidag bars

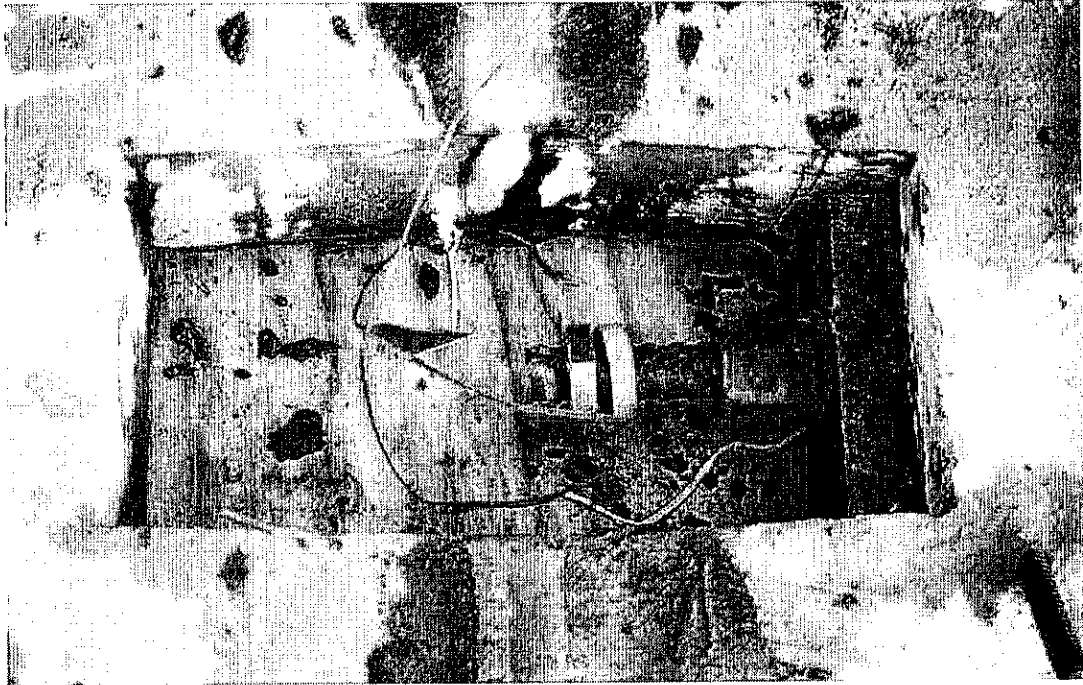


Fig. 6.29 Block-out for coupling of Dywidag bars

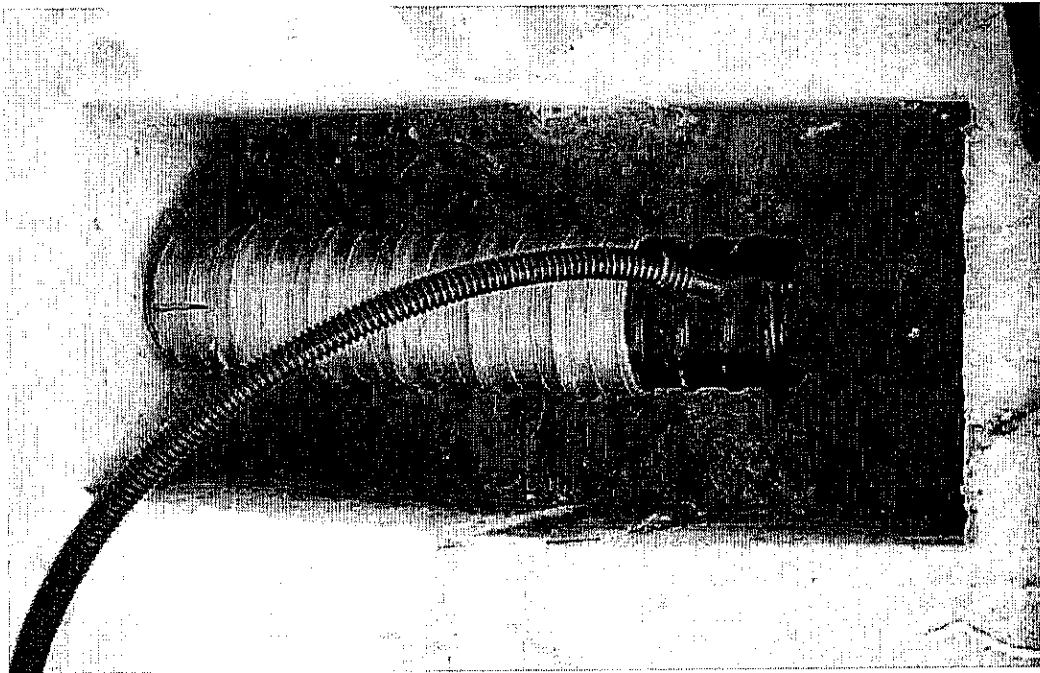


Fig. 6.30 Coupling of Dywidag bars

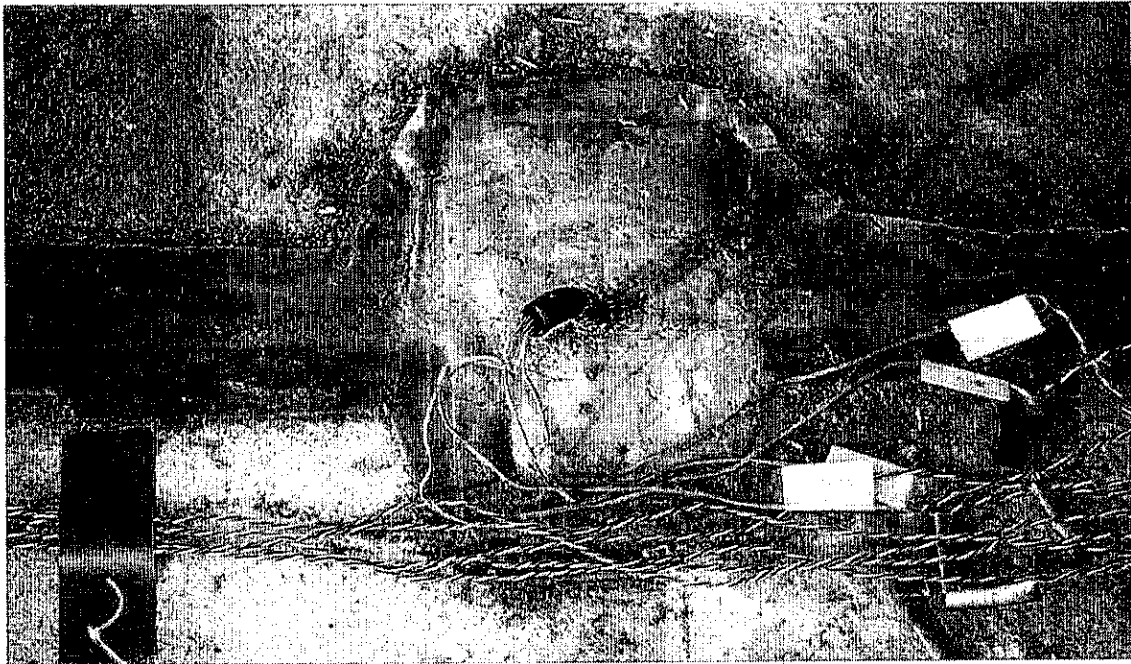


Fig. 6.31 Instrumentation of prestressing strands

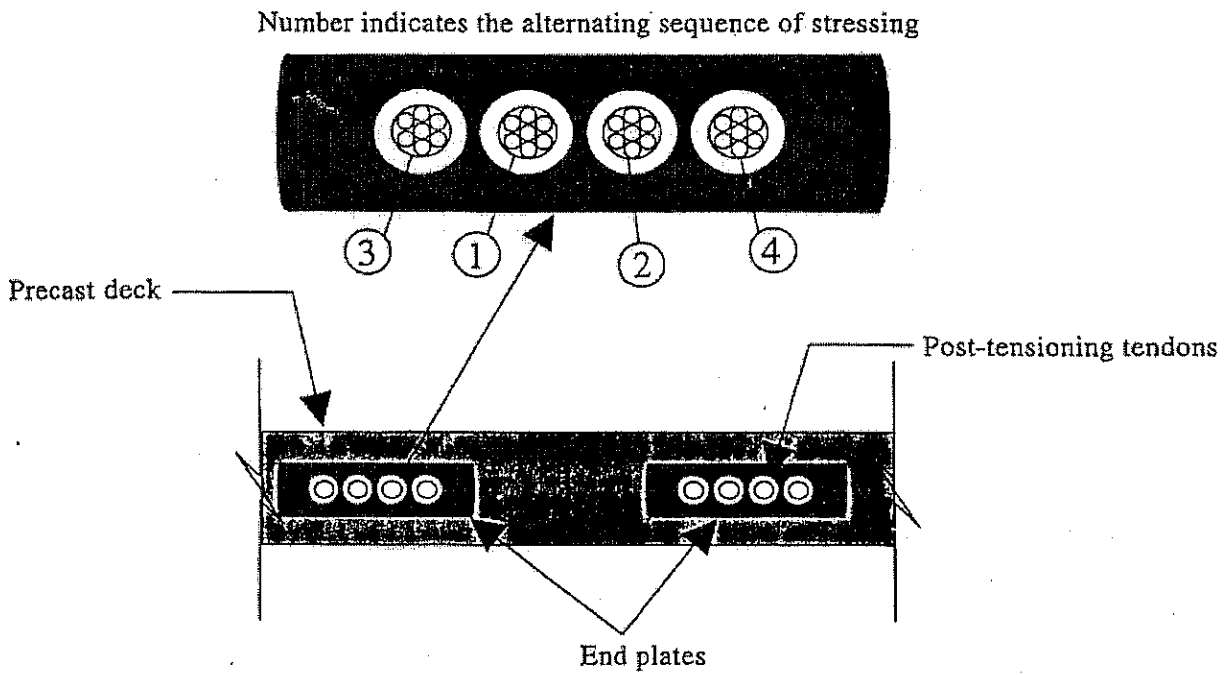


Fig. 6.32 Post-tensioning sequence for strands

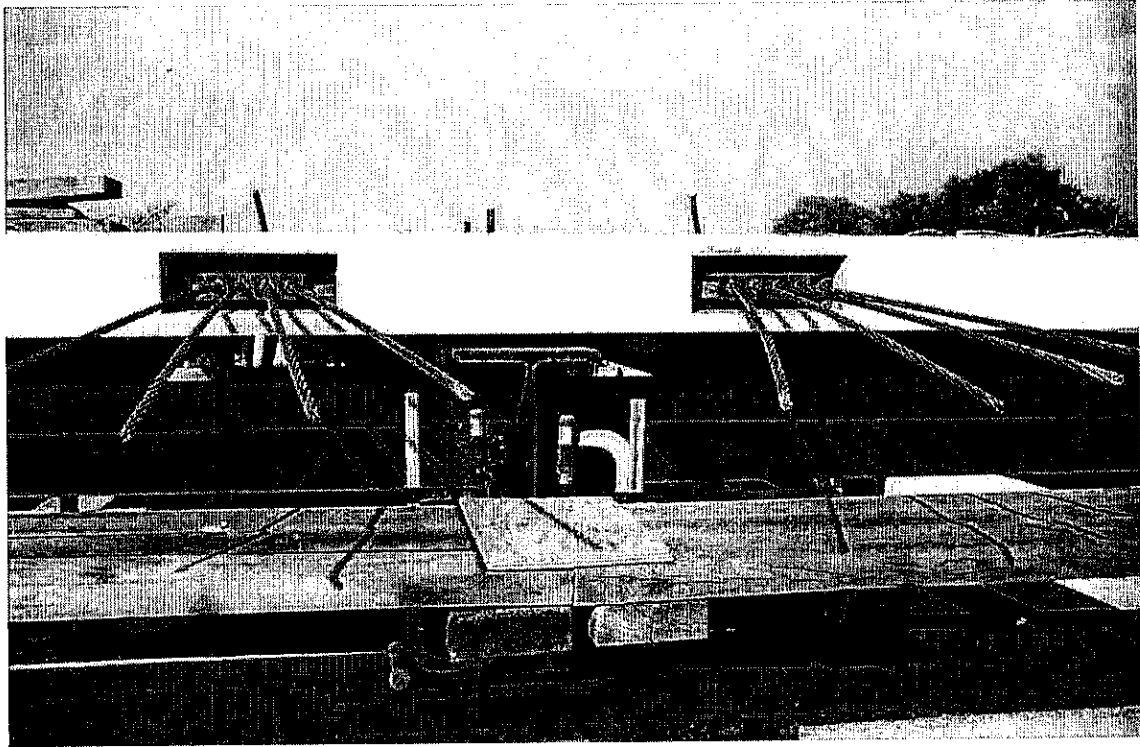
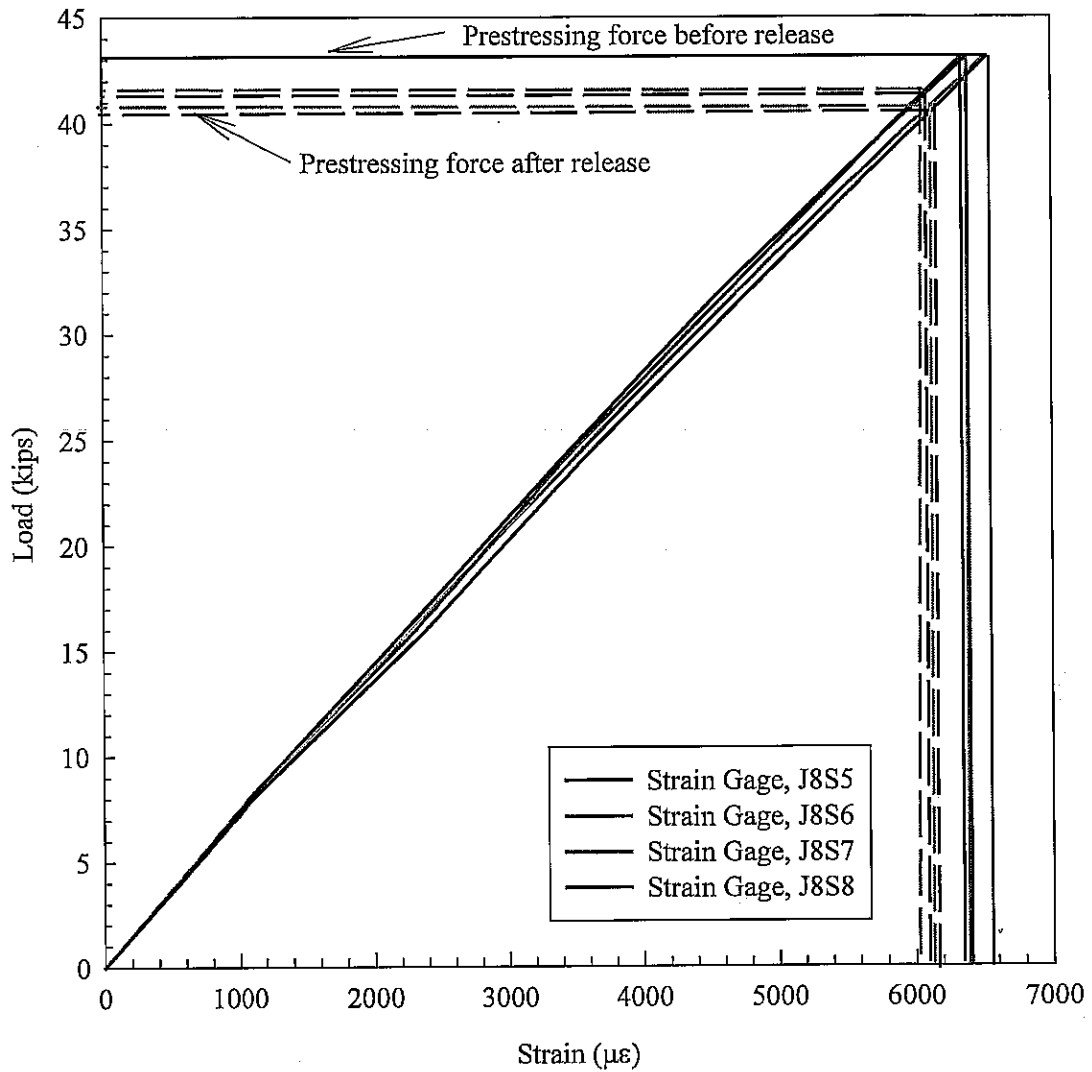


Fig. 6.33 Post-tensioned panels



Strand line (See Figure 6.25)	Strain gage designation	Strain reading ( $\mu$ -strain)		Strain loss ( $\mu$ -strain)
		Before release	After release	
Strand line 1 Initial prestressing = 43.09 kips	J8S1	6792	6535	257
	J8S2	6539	6225	314
	J8S3	6465	6157	308
	J8S4	6077	5791	286
Strand line 2 Initial prestressing = 43.09 kips	J8S5	6389	6040	349
	J8S6	6354	6048	306
	J8S7	6520	6230	290
	J8S8	6539	6272	267

Fig. 6.34 Load-strain calibration curves for prestressing strands

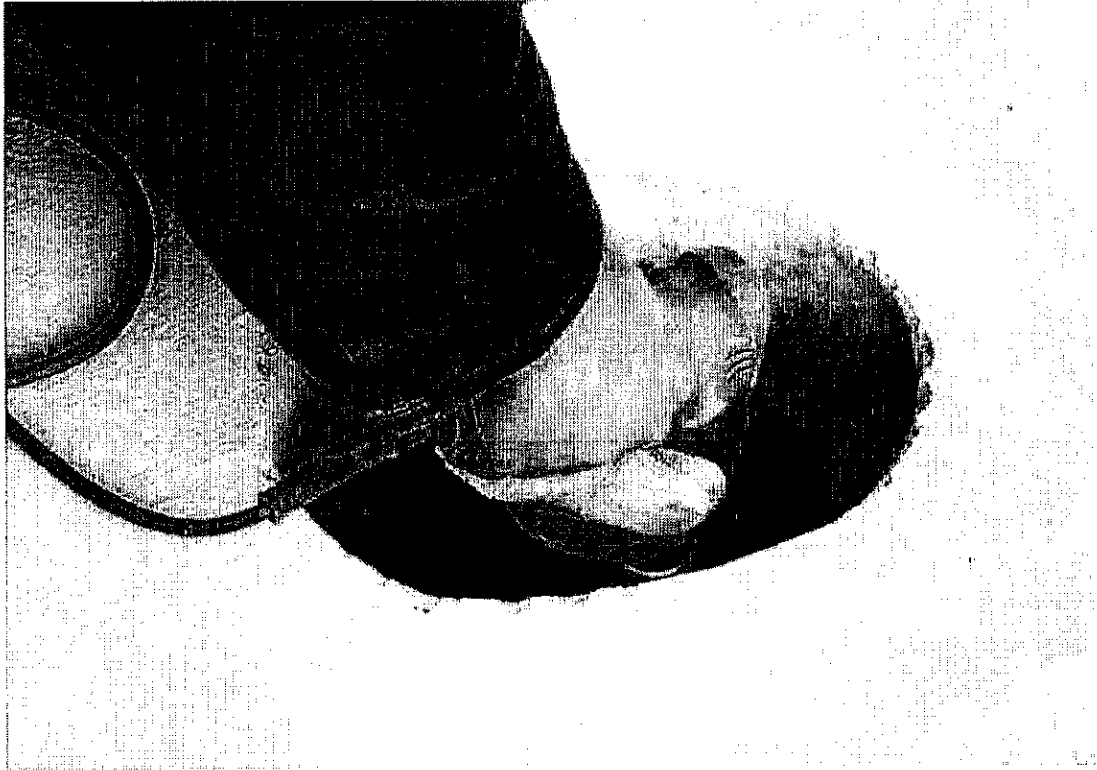


Fig. 6.35 Cleaning of flange tops for stud welding

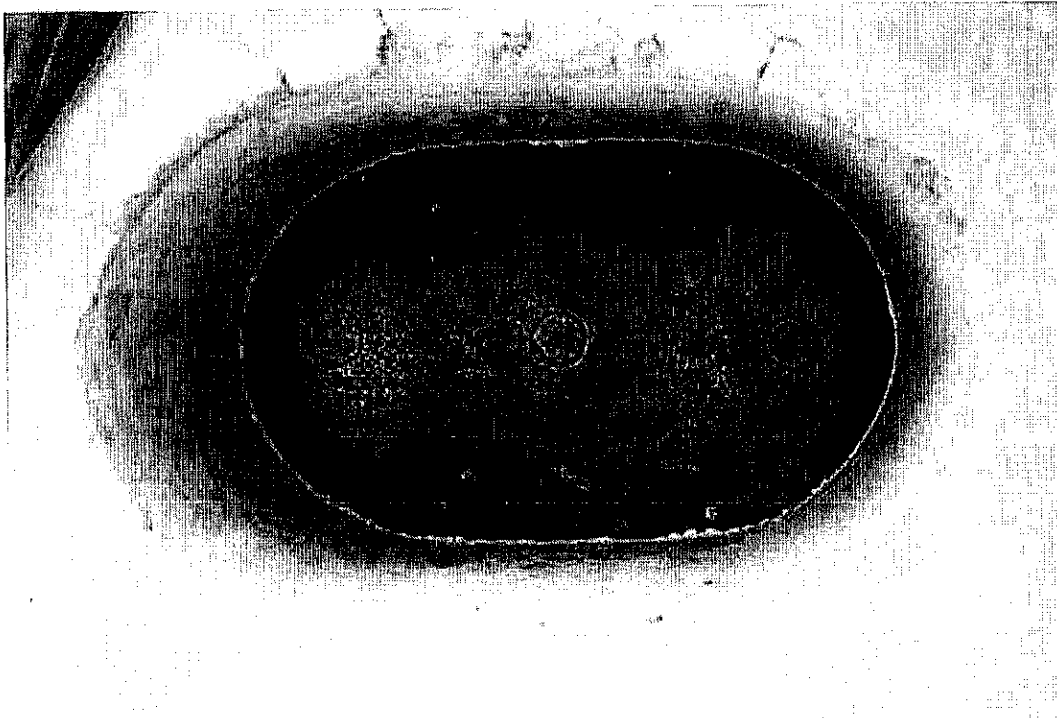


Fig. 6.36 Layout of shear studs in pockets

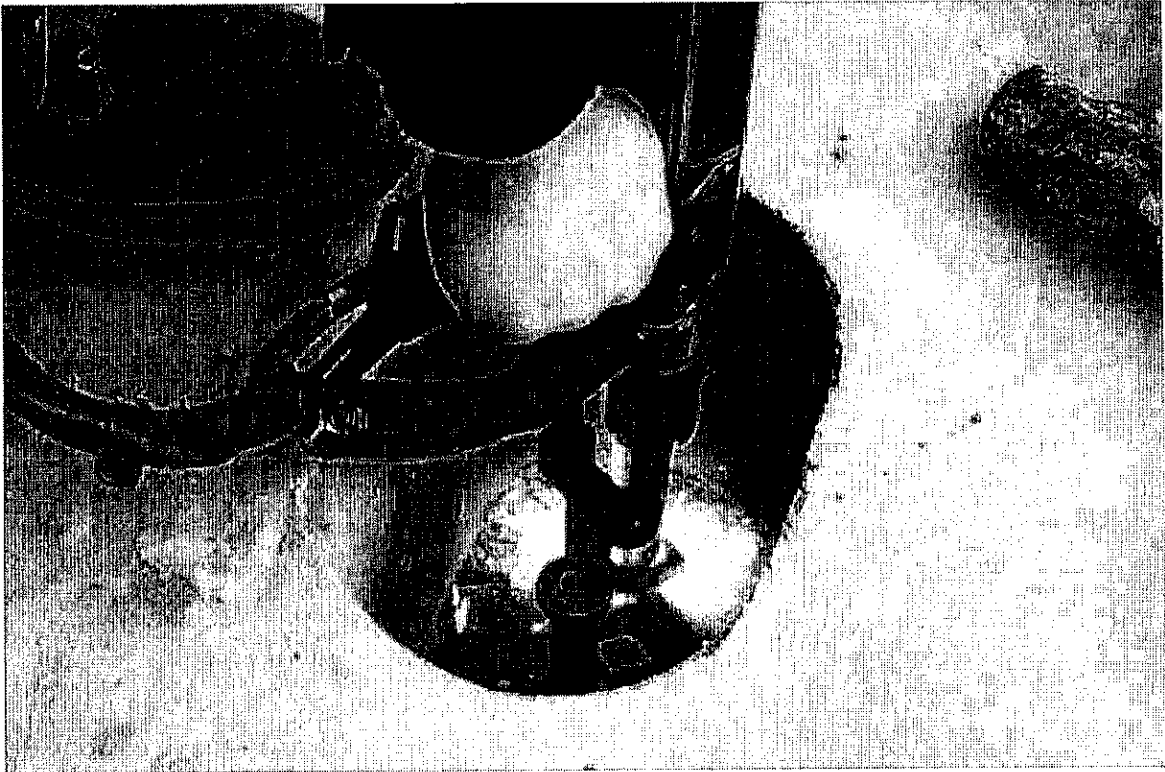


Fig. 6.37 Stud welding

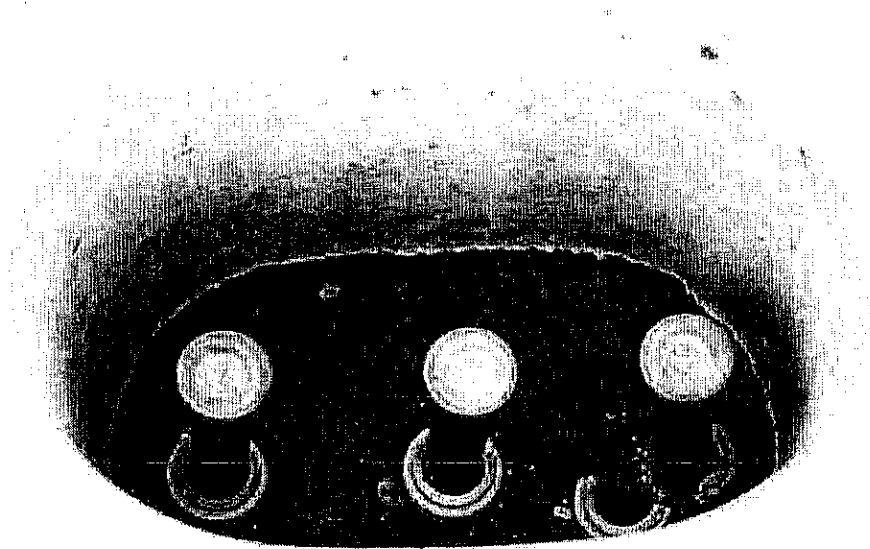


Fig. 6.38 Close-up view of shear pocket with welded stud

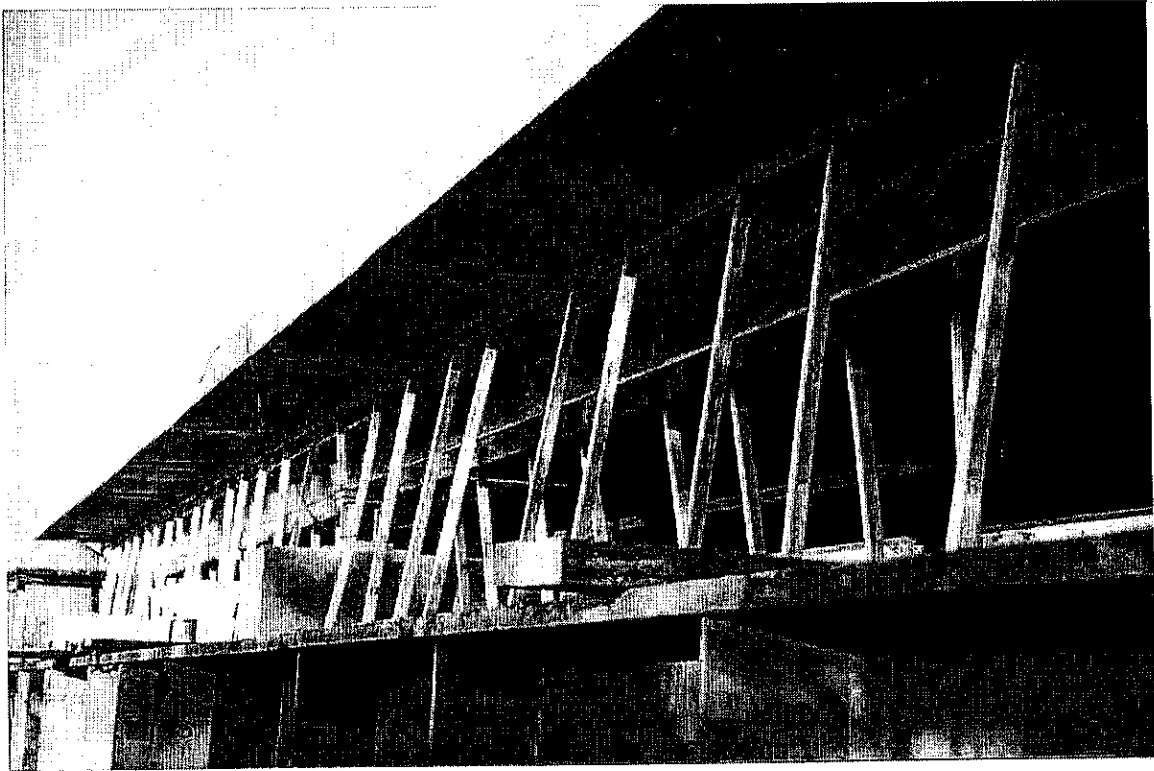


Fig. 6.39 Forming of haunches and shear pockets

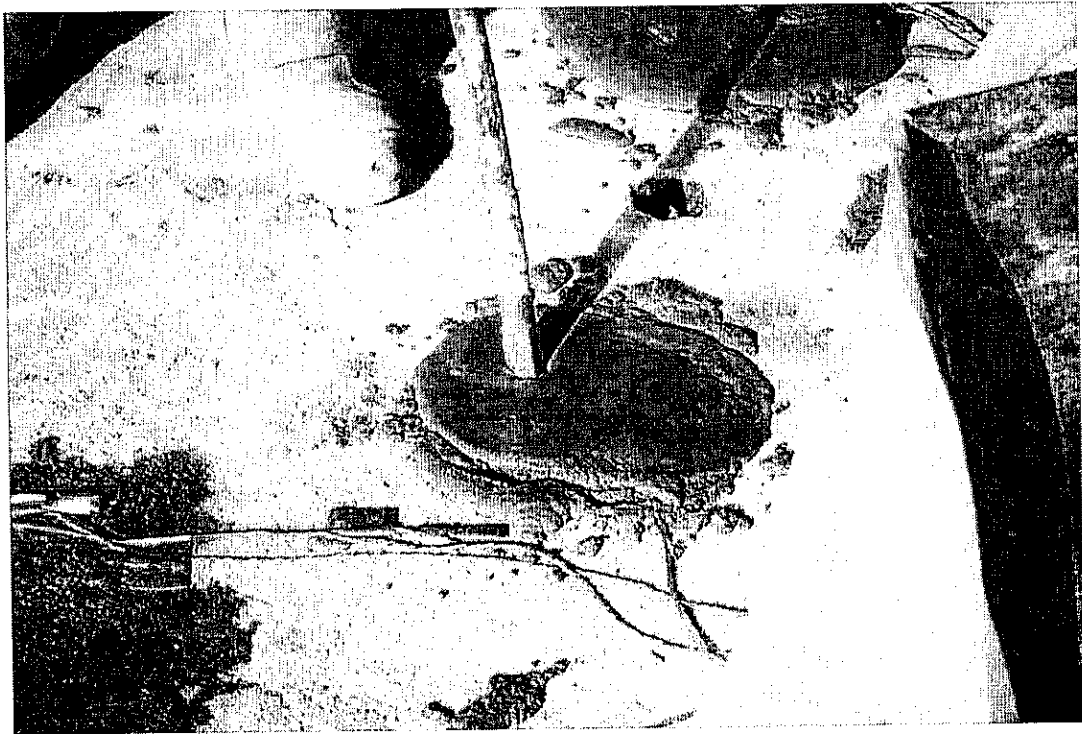


Fig. 6.40 Grouting of shear pockets

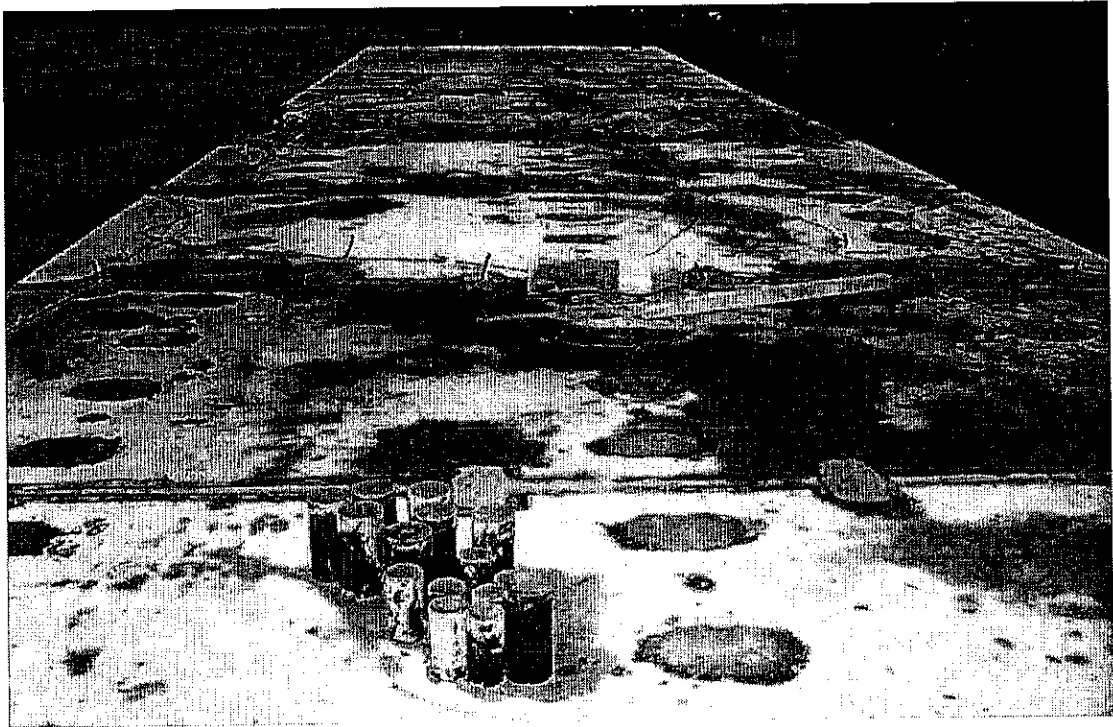


Fig. 6.41 Finished pockets

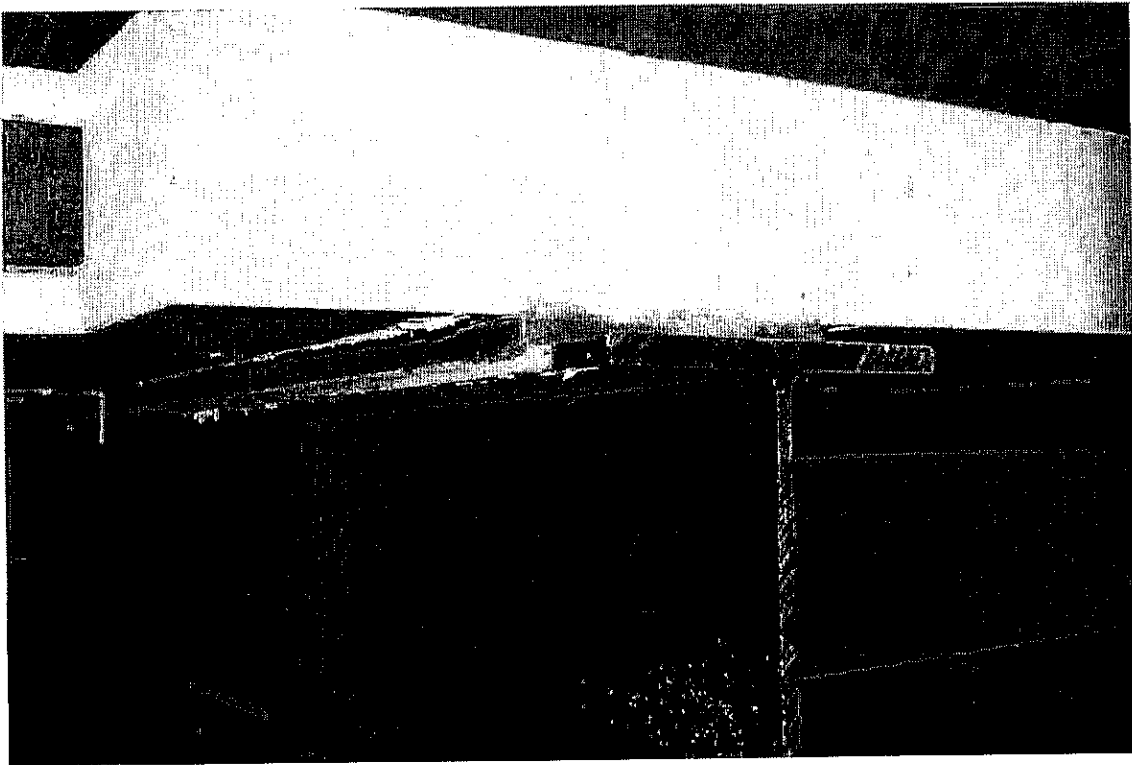


Fig. 6.42 Haunch after grouting

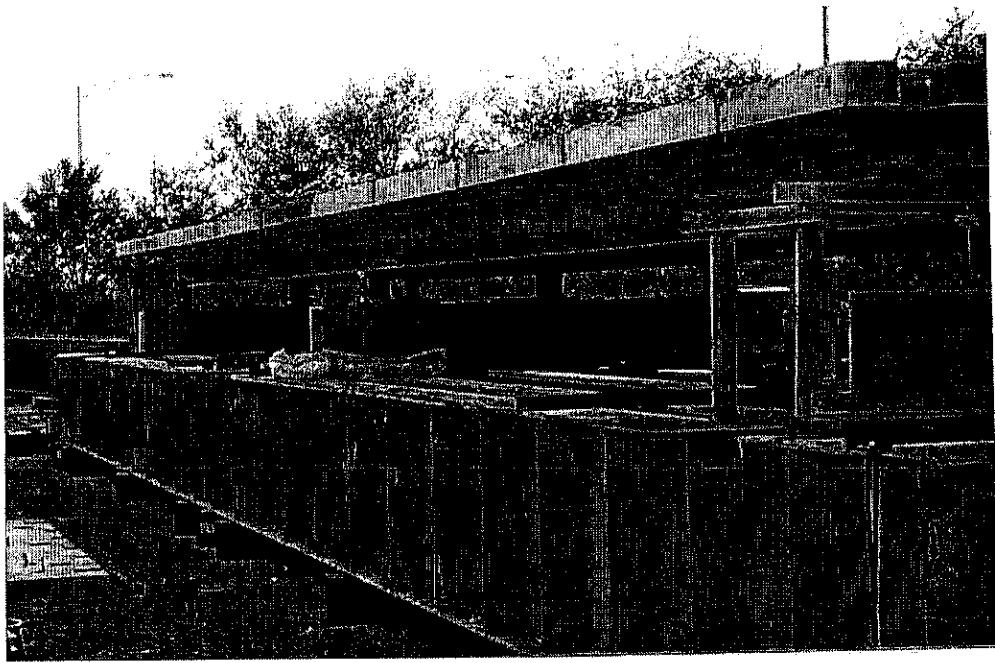


Fig. 6.43 Overview of assembled bridge

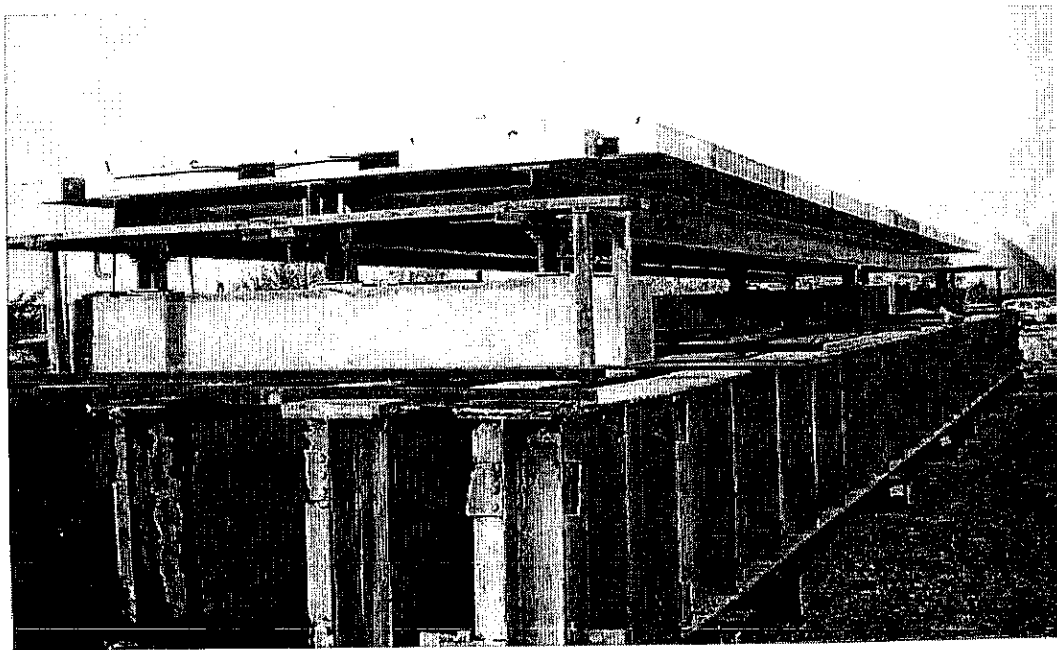


Fig. 6.44 Overview of assembled bridge

## **6.4 Bridge Testing**

### **6.4.1 Test Setup**

The test setup was designed to incorporate the conditions prevalent in the real structure as well as the type of imposed loading. The supports used were pinned at both ends and fixed at the interior support.

#### **6.4.1.1 Loading Frame**

A setup of the loading frames was prepared to simulate the effect of truck loading. A total of four loading frames were fabricated. Two frames were used for maximum positive moment testing, while the other two frames were used for maximum negative moment testing. Each loading frame is composed of four HP14x89 columns and two W24x94 beams as shown in Fig. 6.45. The loading beams were stiffened to guard against any premature failure. The columns were welded to the 5 x 4 ft base plate and the base plate was anchored to the reaction frame by means of bolts. Steel plates of 1 in. thickness were attached to the beam ends and the plates were bolted to the columns. Two hydraulic rams were used to load the bridge. The hydraulic cylinder of the ram was clamped to the beams at mid-span. A spread beam was used to transfer the load from the hydraulic cylinder to two points, 6 ft apart uniformly. An overall sketch of this loading arrangement is shown in Fig. 6.46, while Fig. 6.47 shows an overall view of the loading configuration.

#### **6.4.1.2 Truck Load Simulation**

The prototype bridge was tested for service, cracking, post cracking and ultimate load. AASHTO HS-20 truck loading was simulated by an equivalent load as shown in Fig. 6.48 to study the structural behavior or interaction between the precast panels and the supporting system, e.g., shear pocket connectors, and joint system between adjacent precast panels, in the negative and positive moment regions. Positioning of the truck loading was in accordance with that producing the maximum positive moment in each span and maximum negative moment over the interior support. The simulated truck is a two-axle vehicle, 6 ft wide. The axles are 17 ft and the

wheel loads are applied to the deck by pads, which distribute the load over a contact area of 8 x 20 in. Fig. 6.49 shows a typical simulated single axle configuration, while Fig. 6.50 shows a close-up view of a hydraulic cylinder. An overview of the spread beams used to distribute the load at the contact points is shown in Fig. 6.51.

#### **6.4.1.3 Instrumentation of Bridge**

The bridge deck system was instrumented for strains, deflections, crack openings, etc. Layout of electrical resistance strain gages and vibrating wire strain gages on the top and bottom concrete bridge deck surfaces are shown in Fig. 6.52. Strain gages were mounted at critical locations on steel girders along the depth to monitor the strain distribution as shown in Fig. 6.53. Linear variable displacement transducers (LVDTs) were used to measure the vertical deflection (see Fig. 6.54) and slippage (see Fig. 6.55) between the precast panels and supporting system, i.e., the magnitude of full composite action as shown in Fig. 6.56. In addition, crack displacement transducers were used to monitor any movement in the transverse joint between adjacent precast panels to predict adequacy of the joint configuration as well as the material within the joint (see Fig. 6.57).

#### **6.4.1.4 Data Recording**

The test data was monitored and recorded by a data acquisition system, MEGADAC 5017, with 120 channels and speed of 250,000 samples per second (see Fig. 6.58). This data acquisition system can accurately capture static, dynamic, or transient analog, and a wide range of digital data, e.g., strain, load, displacement, rotation, acceleration, pressure, voltage, temperature, etc. The results obtained from the experimental study were analyzed to determine behavior of the bridge deck system under the prescribed loading.

#### **6.4.2 Load Tests**

The precast, post-tensioned full-depth bridge deck system was tested under service loads, overloads, and ultimate design loads. Positioning of the truck loading was in accordance with that producing the maximum positive moment over the first span and that producing maximum negative moment over the middle support. These locations were obtained following an

investigation of the influence lines for the structure. The equivalent HS20 AASHTO truck was used for maximum positive moment testing (Fig. 6.48). For producing maximum negative moment, the equivalent truck was placed 14 ft apart on either sides of the interior support. The overall view of the loading arrangement for producing maximum positive and negative moment is shown in Figs. 6.59 and 6.60, respectively. The load application sequence was such as to produce maximum positive moments, i.e. applying the loads on one span at the locations shown in Fig. 6.59. After the measurements were collected, loads were released. Loads causing maximum negative moments were then applied by loading the two spans simultaneously shown in Fig. 6.60, and the same process of data collection and load release was performed for overloads and ultimate loads. For ultimate load cases, the deck was loaded in a pattern approximating the design moment envelope diagrams.

The test was conducted in order to study:

- (a) Adequacy of the panel-to-girder and panel-to-panel connections for the development of full composite interaction.
- (b) Relative slip displacement between the precast deck and girders.
- (c) Shear stiffness of the panel-to-girder connection at the interface.
- (d) Performance of the transverse joint between adjacent precast panels.

#### **6.4.2.1 Service Load Tests**

Service level loads were applied in the form of equal concentrated forces applied downward at the critical locations of the bridge models. Two patterns of loading were used, one producing maximum positive moments and the second producing maximum negative moments along the middle support location. To achieve the maximum positive bending moment in the span, the loading frame was positioned above the first span. After data collection was completed for this load case, the hydraulic pumps were released in preparation for the next load case. The loading frame location was then adjusted in order to load the two spans for maximum negative bending moments along the middle support. Loads were then released for the application of the next test case.

#### **6.4.2.2 Overload Tests**

Overloads at 2 times the service loads were applied on the bridge to simulate the response of the structure under design overload conditions. Loads causing maximum positive bending using the same pattern for service loads, and the corresponding response of the deck system was observed and recorded. The frame was then released, and loading was resumed for simulating negative bending moments.

#### **6.4.2.3 Ultimate Load Tests**

The ultimate load test was carried out in order to investigate adequacy of the precast deck to girder connections under ultimate load conditions and to observe the post-cracking behavior and modes of failure. The behavior of the transverse joint was investigated in terms of the effect of post-tensioning on the performance of the joint. The first case was to load the structure to failure under positive bending using the loading pattern shown in Fig. 6.59. Loads were then applied in a pattern approximating design negative moment envelopes using the loading zones of Fig. 6.60.

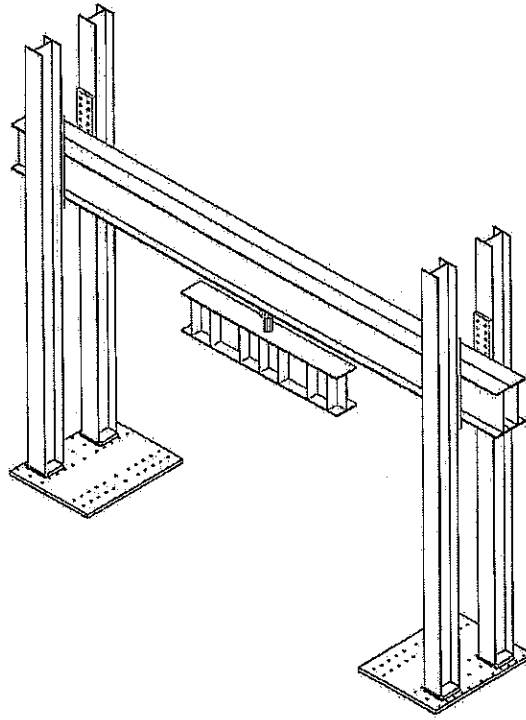


Fig. 6.45 Beam-column connection of loading frame

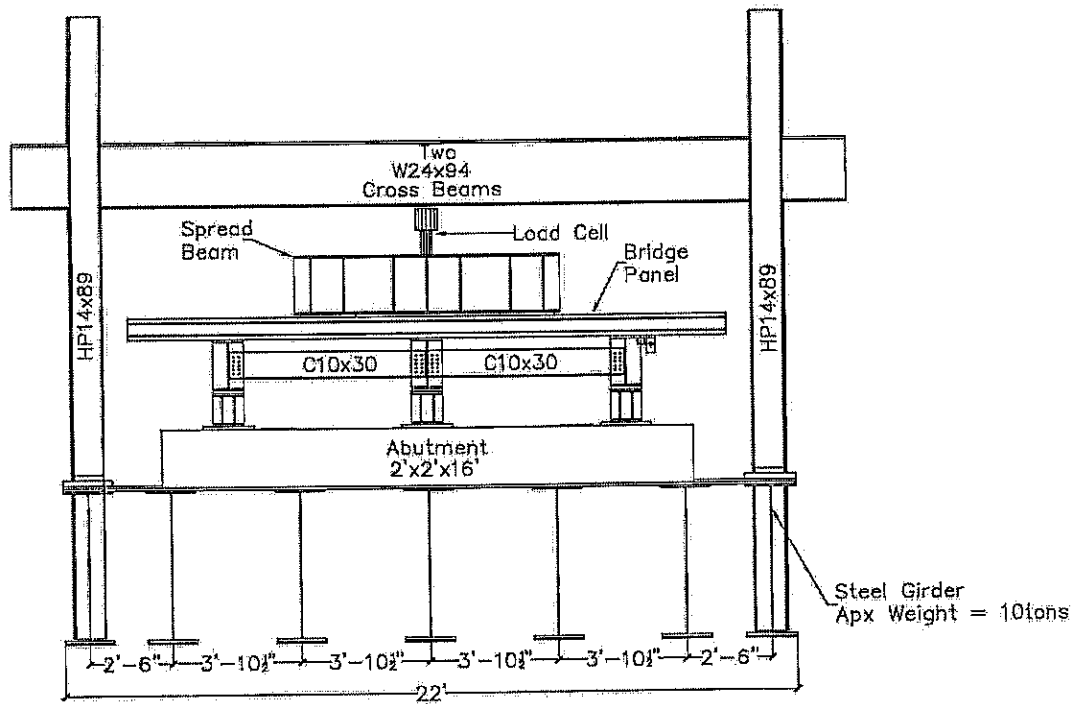


Fig. 6.46 Elevation view of loading frame

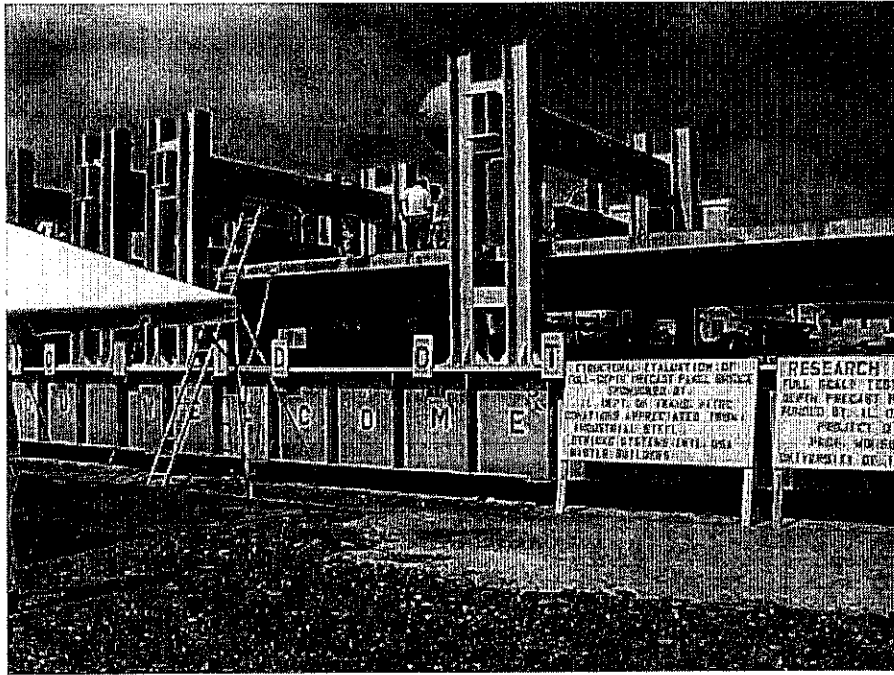
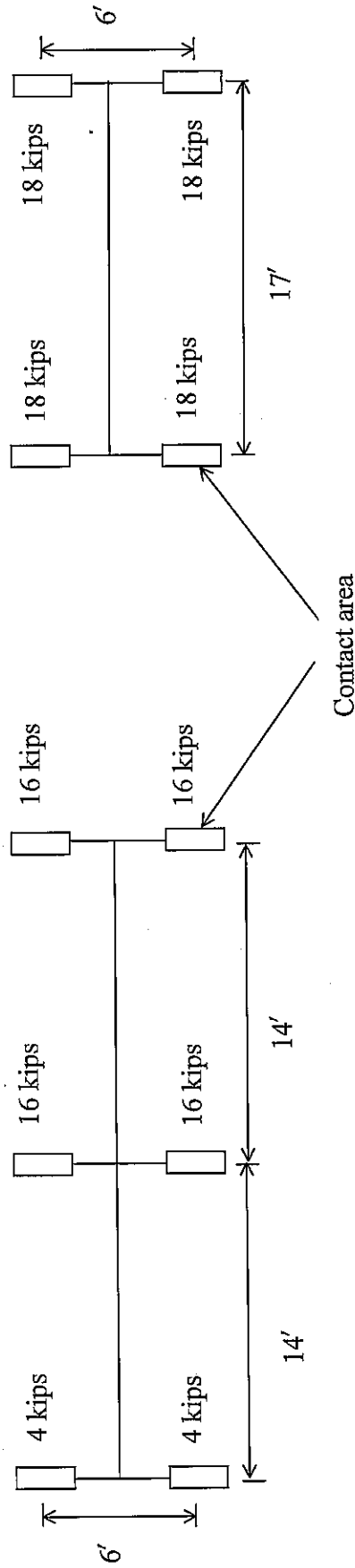


Fig. 6.47 Test Setup



(a) Three-axle loading

(b) Two-axle loading

Area of contact =  $0.10P = 0.1(16000) = 160 \text{ in.}^2$

The length to width ratio of contact are = 2.5:1

If,  $x$  = width of contact point parallel to traffic, total area of contact =  $2.5x^2 = 160$

Hence, width of contact point = 8 in. and length of contact point = 20 in.

Fig. 6.48 Simulated AASHTO truck loading

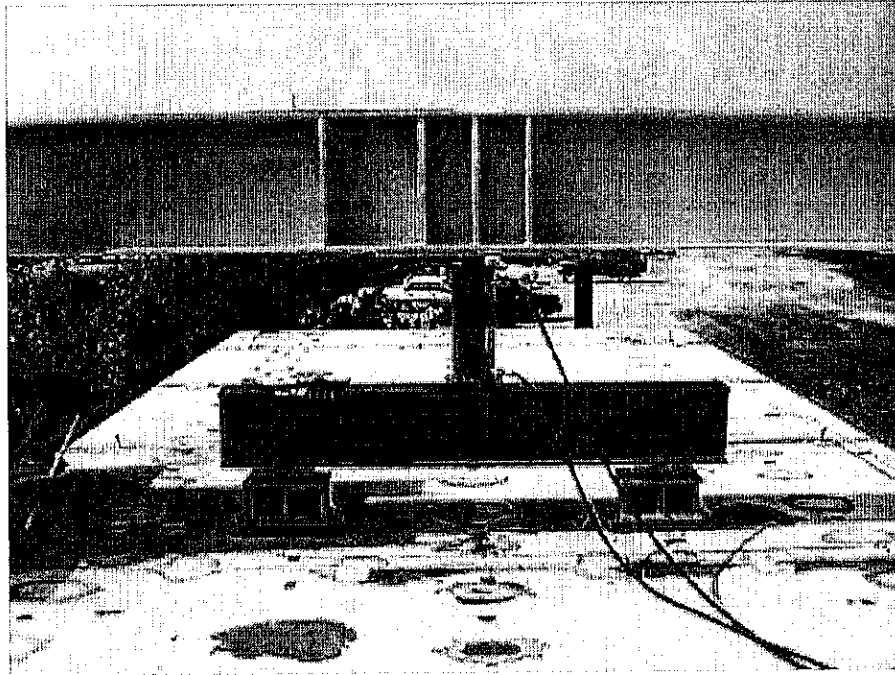


Fig. 6.49 Simulated Single Axle

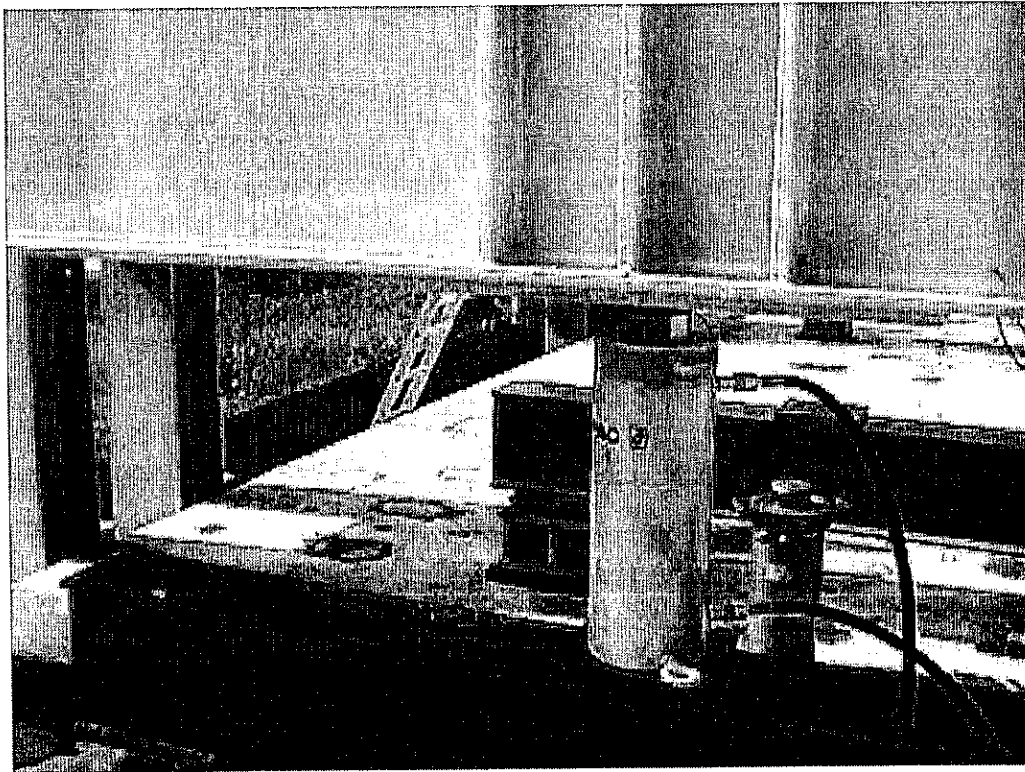


Fig. 6.50 Close-up view of hydraulic cylinder

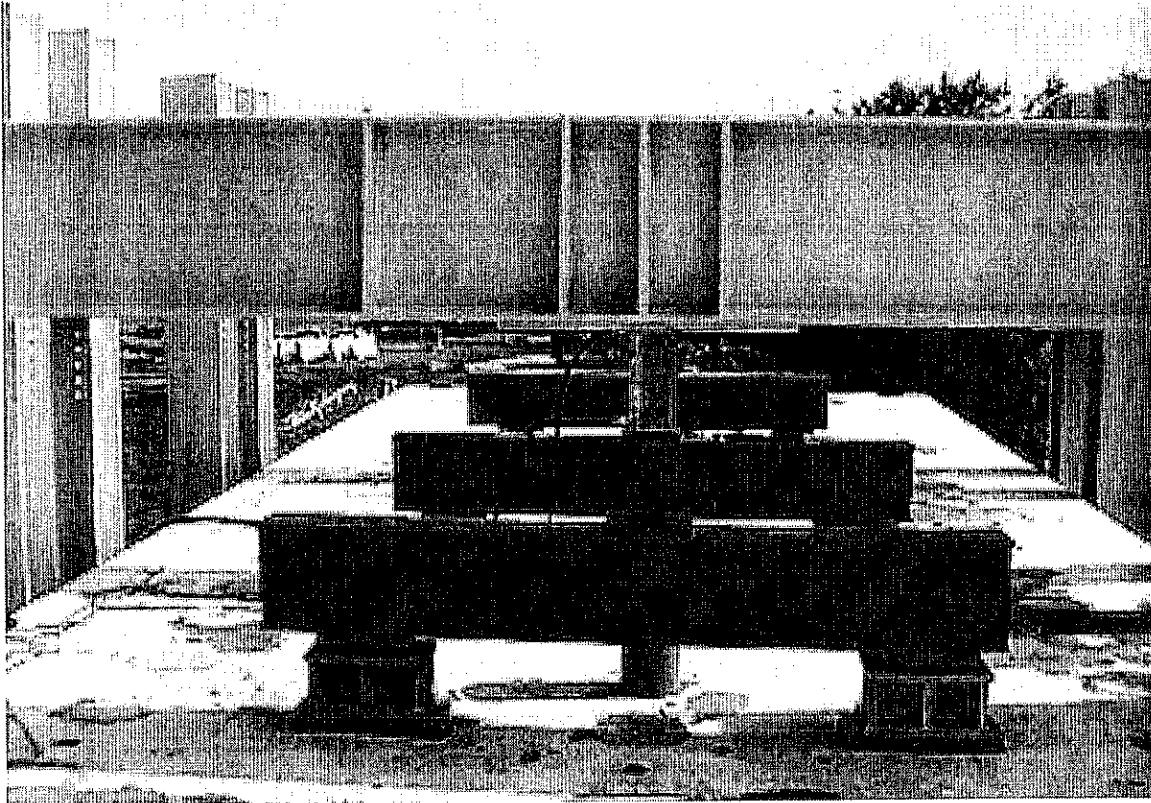


Fig. 6.51 Spread beams used to distribute the load at contact points

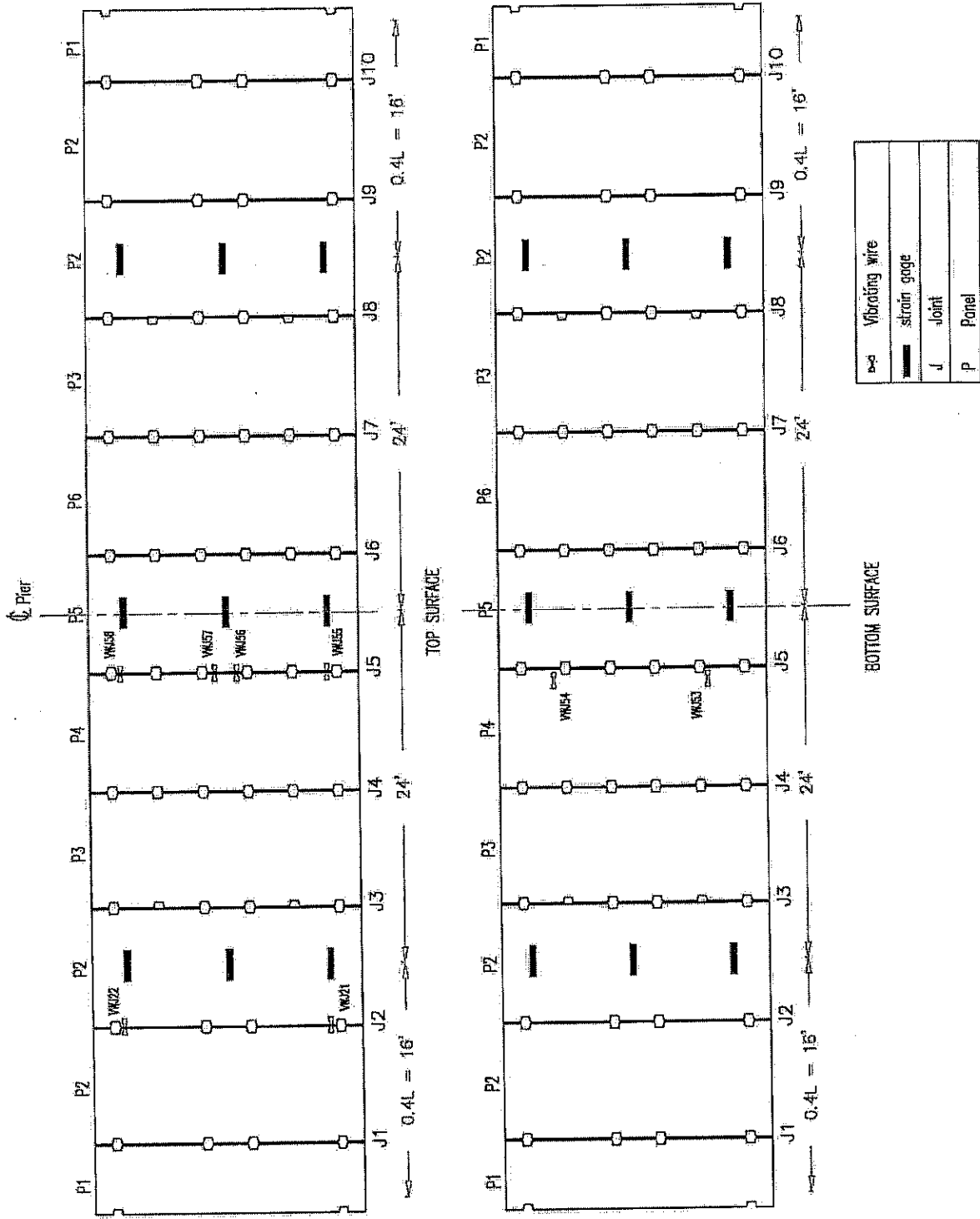


Fig. 6.52 Layout of electrical resistance strain gages and vibrating wire strain gages on concrete bridge deck

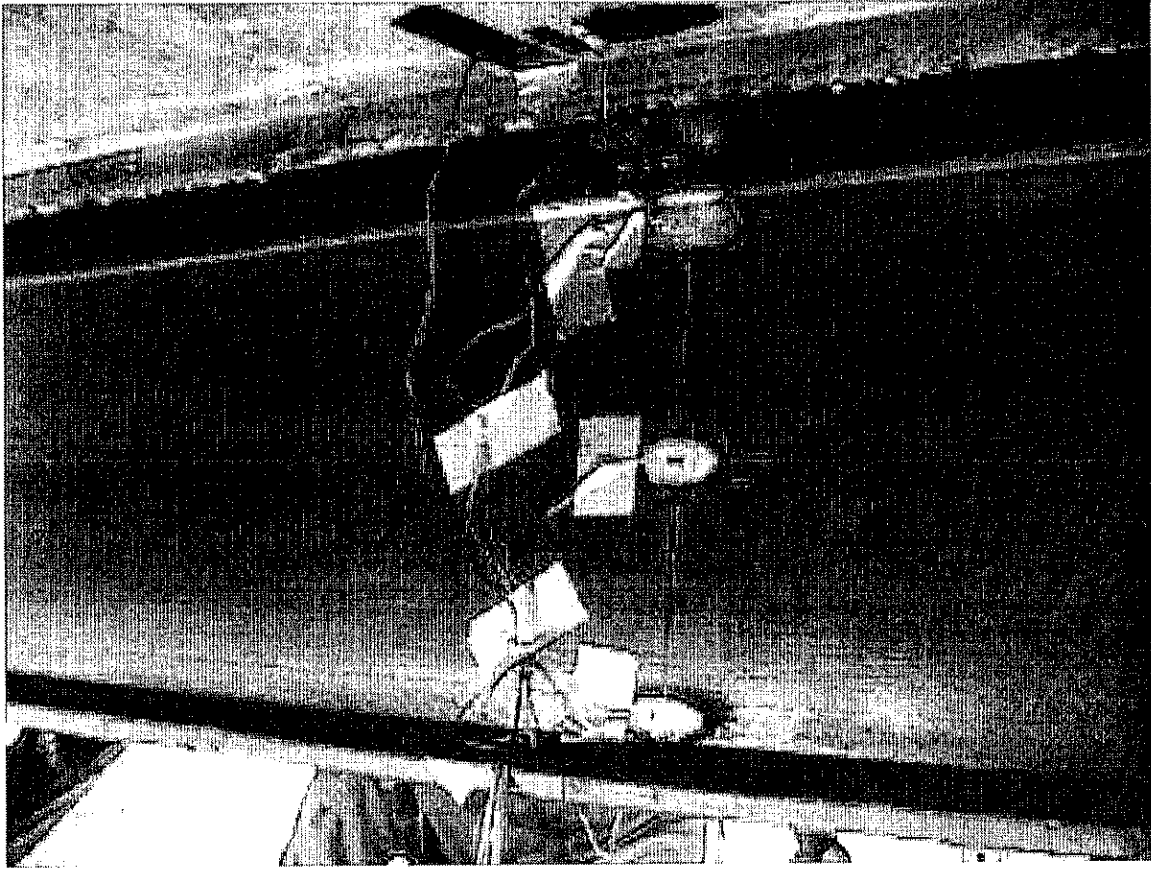


Fig. 6.53 Strain gages across the depth of the steel beam

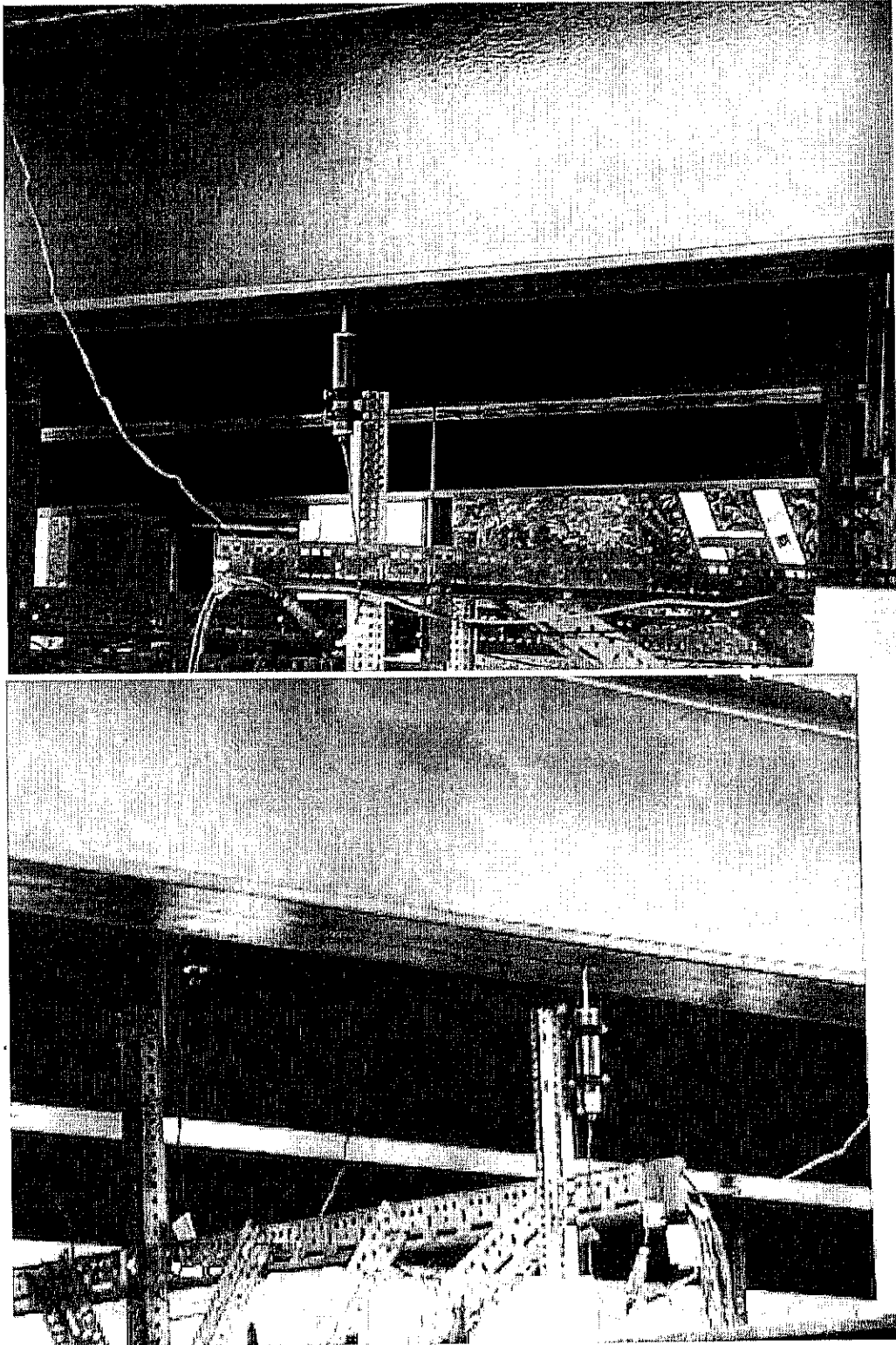


Fig. 6.54 LVDT used to measure the deflection of steel beams and deck

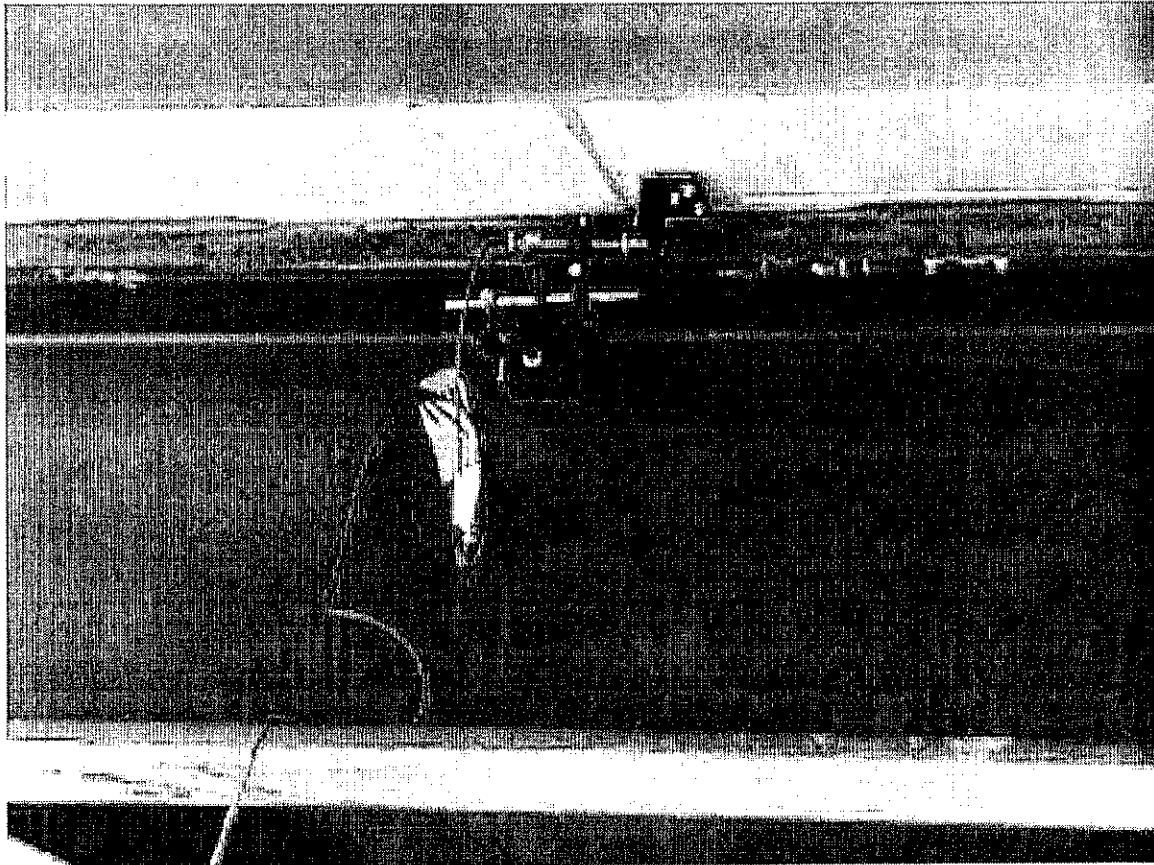
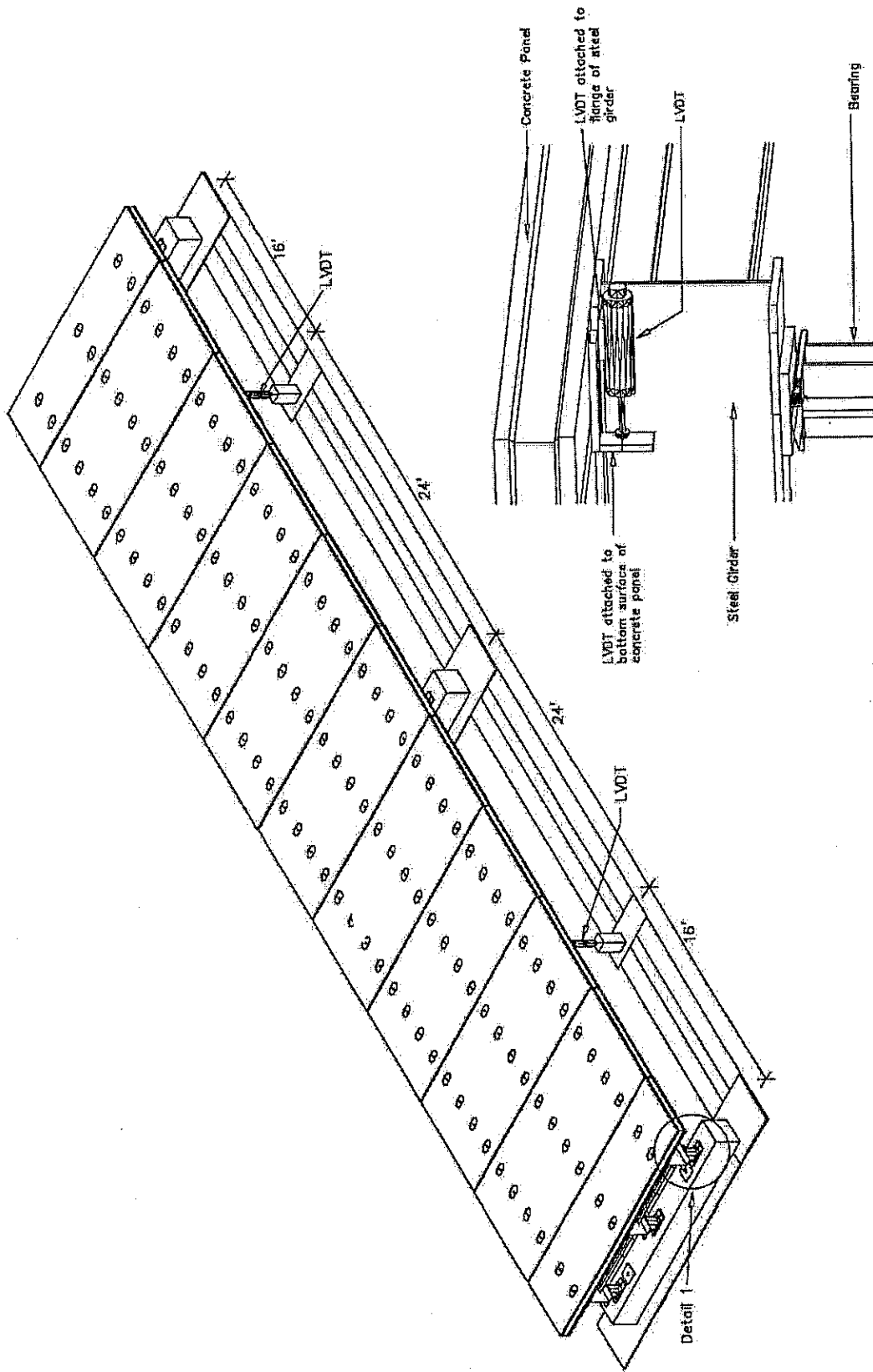


Fig. 6.55 Slippage measurement



Detail 1

Fig. 6.56 Layout of LVDTs for deflection and slip measurement in full-scale bridge

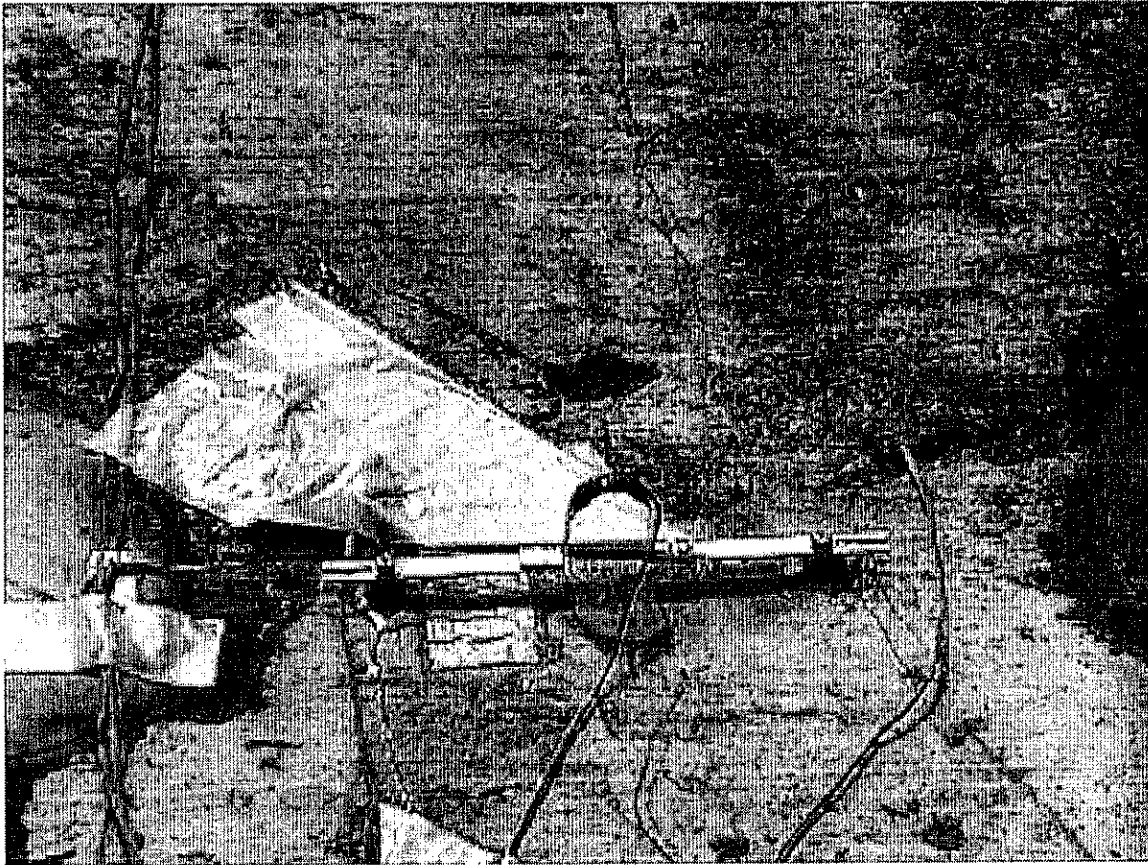


Fig. 6.57 CMOD gage to measure the concrete strain over middle support and transverse joint

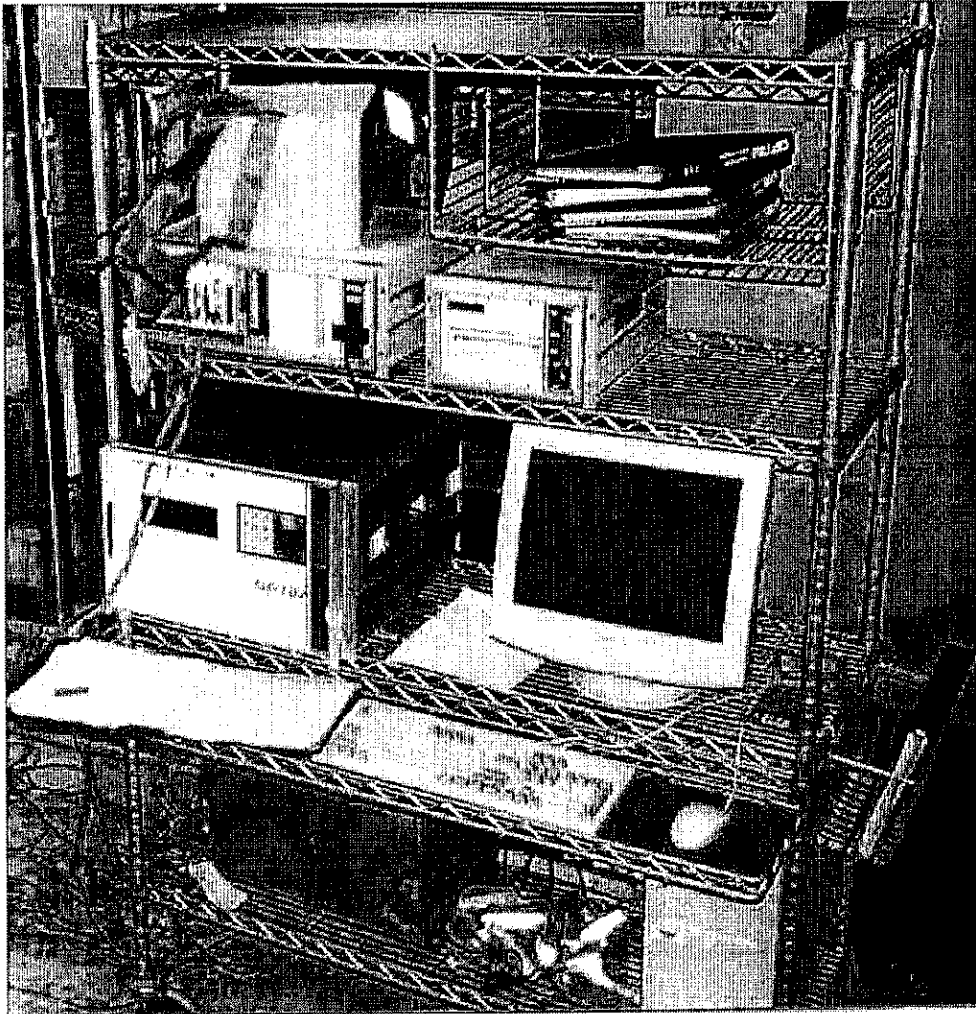


Fig. 6.58 Data acquisition system used in collecting data

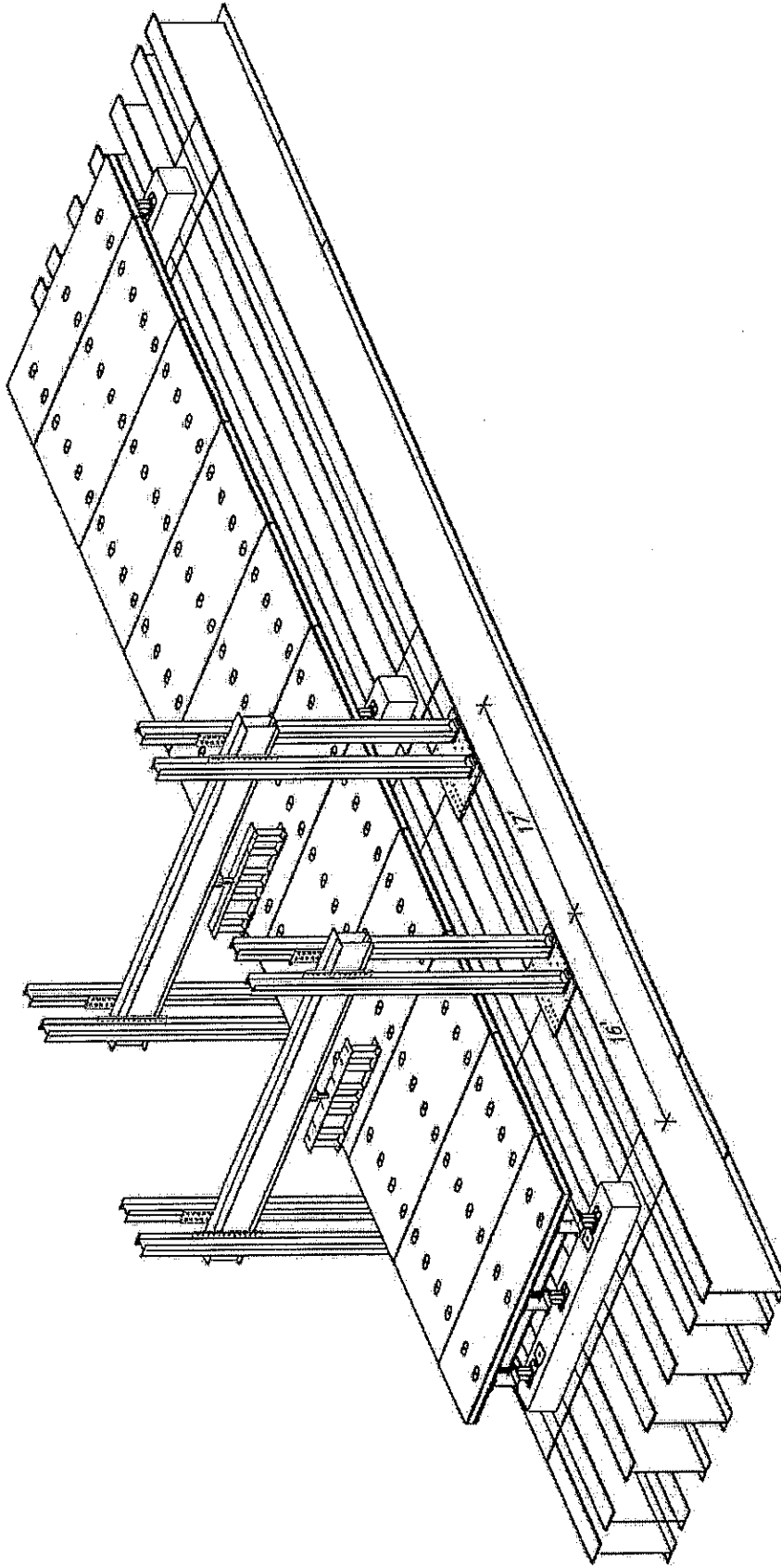


Fig. 6.59 Overall view of the loading arrangement for maximum positive moment

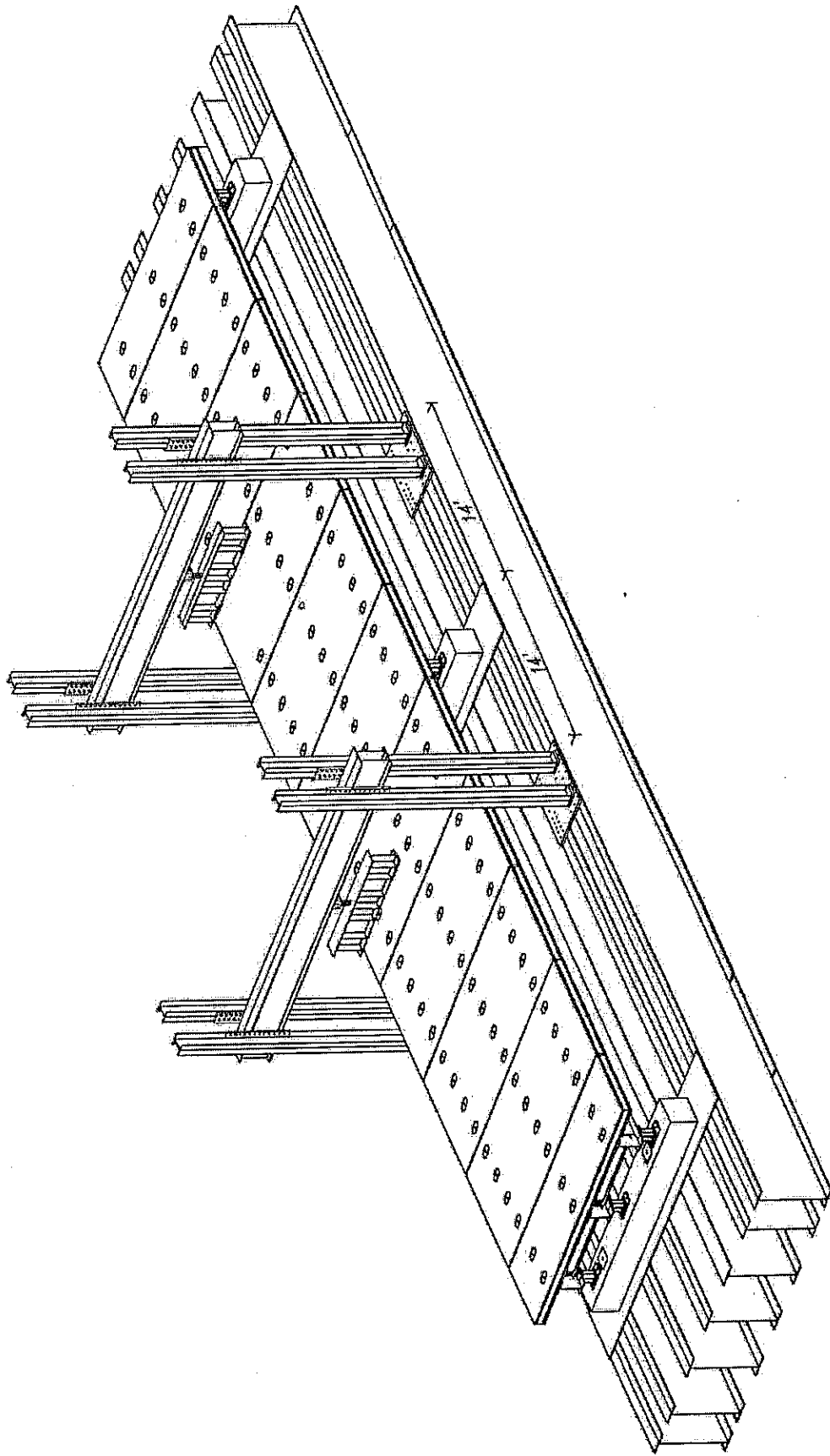


Fig. 6.60 Overall view of the loading arrangement for maximum negative moment



## 7. TEST RESULTS OF FULL-SCALE BRIDGE

### 7.1 Introduction

The full-scale precast bridge deck system was tested under service loads (including 30% impact), overloads (2 times the service loads), and ultimate loads. The first service loading was applied to produce maximum negative moments. Load was applied in an increment of 18.42 kips (300 psi of the hydraulic jack). For each increment, loads, strains, and deflections were recorded and cracks (if any) were identified. After the application of maximum loading and collection of measurements, the loads were released. Loads causing maximum positive service moments were then applied and the same process of data collection and load release was performed for overloads and ultimate loads. The location of concrete strain gages, steel strain gages and LVDTs are shown in Figs. 7.1-7.3.

### 7.2 Test Results

#### 7.2.1 Service Loads

Service loads were applied to produce a maximum negative moment over the middle support and a maximum positive moment in the bridge span. Loading was applied in 5 stages in increments of 18.42 kips. The overall behavior of the precast deck system was outstanding under service loads since no cracks were detected.

##### 7.2.1.1 Maximum Negative Service Load Test

Load-deflection response at the critical location is depicted in Fig. 7.4. A maximum deflection of 0.08 in. was observed. Fig. 7.5 demonstrates the load-slippage behavior of the composite section (deck-steel beam) where a maximum slippage of 0.007 in. was recorded. No cracks were observed at the final stage of this loading. The load-strain response of central steel beam is shown in Fig. 7.6.

##### 7.2.1.2 Maximum Positive Service Load Test

The load-deflection curve at 0.4L from the left support is shown in Fig. 7.7. It can be seen that the load-deflection curve is almost linear. Under positive bending, a maximum

deflection of 0.22 in. was observed. This deflection corresponds to  $L/2182$ , which is less than the specified AASHTO limit of  $L/800$  for continuous spans. The deflection obtained from the finite element analysis was 0.25 in., which is comparable to the experimental results. A maximum slippage of 0.02 in. was recorded as shown in Fig. 7.8. The load-strain response of the central steel beam is shown in Fig. 7.9. Fig. 7.10 shows the variation of strain along the depth of the composite section. No transverse joint separation was observed. Overall, the system performed well under design service loads in both positive and negative bending.

## **7.2.2 Overloads**

Overload corresponding to two service trucks and impact loading was applied for maximum positive and negative moments. Overall, the system performed well under both overload cases.

### **7.2.2.1 Maximum Positive Over Load Test**

The load-deflection diagrams were almost linear as shown in Fig. 7.11. A maximum deflection of 0.44 in. was reported. A maximum slippage of 0.04 in. was observed as shown in Fig. 7.12. The load-strain response of the central steel beam is shown in Fig. 7.13. Fig. 7.14 shows the variation of strain along the depth of the composite section. No cracks were reported until the last stage of overloads for positive loading. At a maximum load of 184 kips, hairline longitudinal transverse cracks were reported in the bottom of the slabs directly under the load contact points as shown in Fig. 7.15. However, no transverse joint separation and haunch-slab separation were observed.

### **7.2.2.2 Maximum Negative Over Load Test**

Under negative bending, a maximum deflection of 0.13 in. and a maximum slippage of 0.013 in. were observed as shown in Figs. 7.16 and 7.17, respectively. The load-strain response of the central steel beam is shown in Fig. 7.18. Similar to the positive bending case, at a maximum load of 184 kips, longitudinal cracks were reported in the bottom of the slabs right under the load contact points. However, no transverse joint separation and haunch-slab separation were observed.

### 7.2.3 Ultimate Positive Load Test

A total load of 553 kips was gradually applied in 30 stages in increments of 18.42 kips causing positive bending in the left span. The load-deflection curve at 0.4L from the left support is shown in Fig. 7.19. Longitudinal hairline cracks were observed on the bottom surface of the panels at 0.4L after reached a load of 203 kips. Afterwards, for each load increment, new hairline cracks initiated and propagated. At a load of 294 kips, a 20 in. long longitudinal crack was reported at the bottom deck under the loading contact point. A deflection of 1.67 in. was reported at this ultimate loading. A maximum slippage of 0.14 in. was observed at the ultimate loading as shown in Fig. 7.20.

The load-strain response of the central steel beam is shown in Fig. 7.21. The load-strain response of the concrete at 0.4L from the left support is shown in Fig. 7.22. Fig. 7.23 shows the variation of strain along the depth of the composite section. Hairline cracking was observed in the haunch at 386 kips as shown in Fig. 7.24. Cracking of bottom deck at ultimate loading is shown in Fig. 7.25. At a load of 490 kips, an uplift of  $\frac{1}{2}$  to 1 in. was observed at the right support of the right span as shown in Fig. 7.26. At this stage, a continuous transverse crack was noticed in the deck above the central support. A close-up view of the deflected steel beam at ultimate loading is shown in Fig. 7.27. No cracking was reported at the transverse joints. The steel girder reached a maximum tensile strain of 905 micro-strain and a maximum compressive strain of 1976 micro-strain at the ultimate load. However, no failure due to positive bending moments was detected up to the maximum load. This maximum load was 7.7 times the service live load and at this stage the capacity of the hydraulic jacks was reached. Deflection profiles of the loaded span due to service, overloads, and ultimate loading are shown in Fig. 7.28. It can be concluded that the design of this deck was satisfactory based on the applied loading and excellent behavior of the system.

### 7.2.4 Ultimate Negative Load Test

A total load of 571 kips was gradually applied in 31 stages in increments of 18.42 kips causing negative bending over the central support. A total deflection of 0.63 in. was reported (Fig. 7.29) at this maximum applied loading. The deflection obtained from the finite element

analysis was 0.65 in., which is comparable to the experimental results. A maximum slippage of 0.058 in. was observed at the ultimate loading as shown in Fig. 7.30.

Load-strain response of the central beam is shown in Fig. 7.31. The strains in the concrete at critical locations are shown in Fig. 7.32. Longitudinal hairline cracks were observed on the bottom surface of the panels under the loading contact points after it reached a load of 184 kips. Afterwards, for each load increment, new cracks initiated and propagated on the deck top over the central support. Strain in the transverse joint near the central support is shown in Fig. 7.33. Cracks at the bottom of the deck at 14 ft from central support at a load of 552 kips are shown in Fig. 7.34. Crack openings were measured as shown in Fig. 7.35. No failure due to negative bending moments was detected up to the maximum load. This maximum load was 7.9 times the service live load and at this stage the capacity of the hydraulic jacks were reached. The steel girder reached a maximum tensile strain of 1862 micro-strain and a maximum compressive strain of 2762 micro-strain at the ultimate load. It was observed that the deck system maintained its integrity even at the 7.9 multiple of service loads.

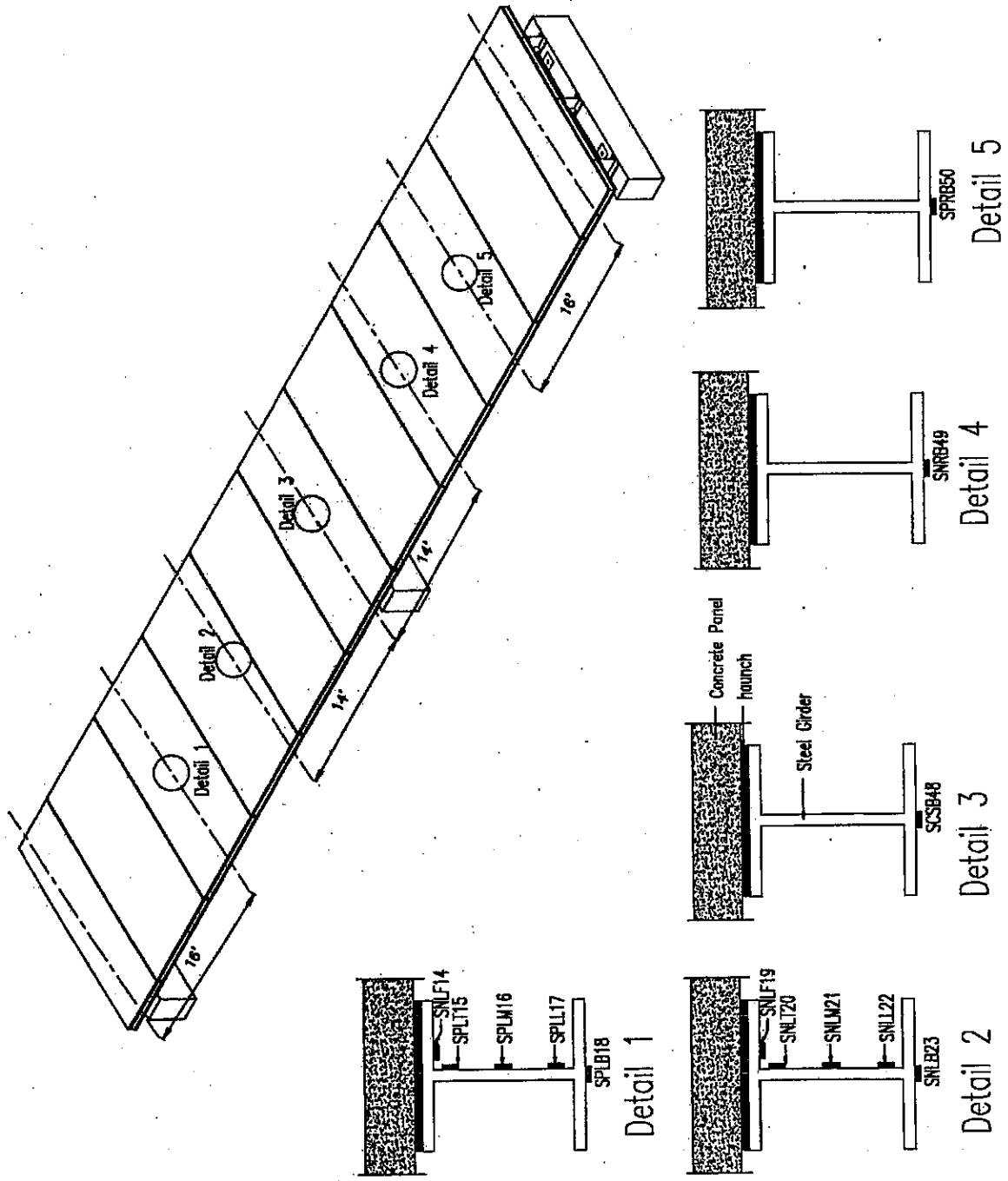


Fig. 7.2 Location of steel strain gages

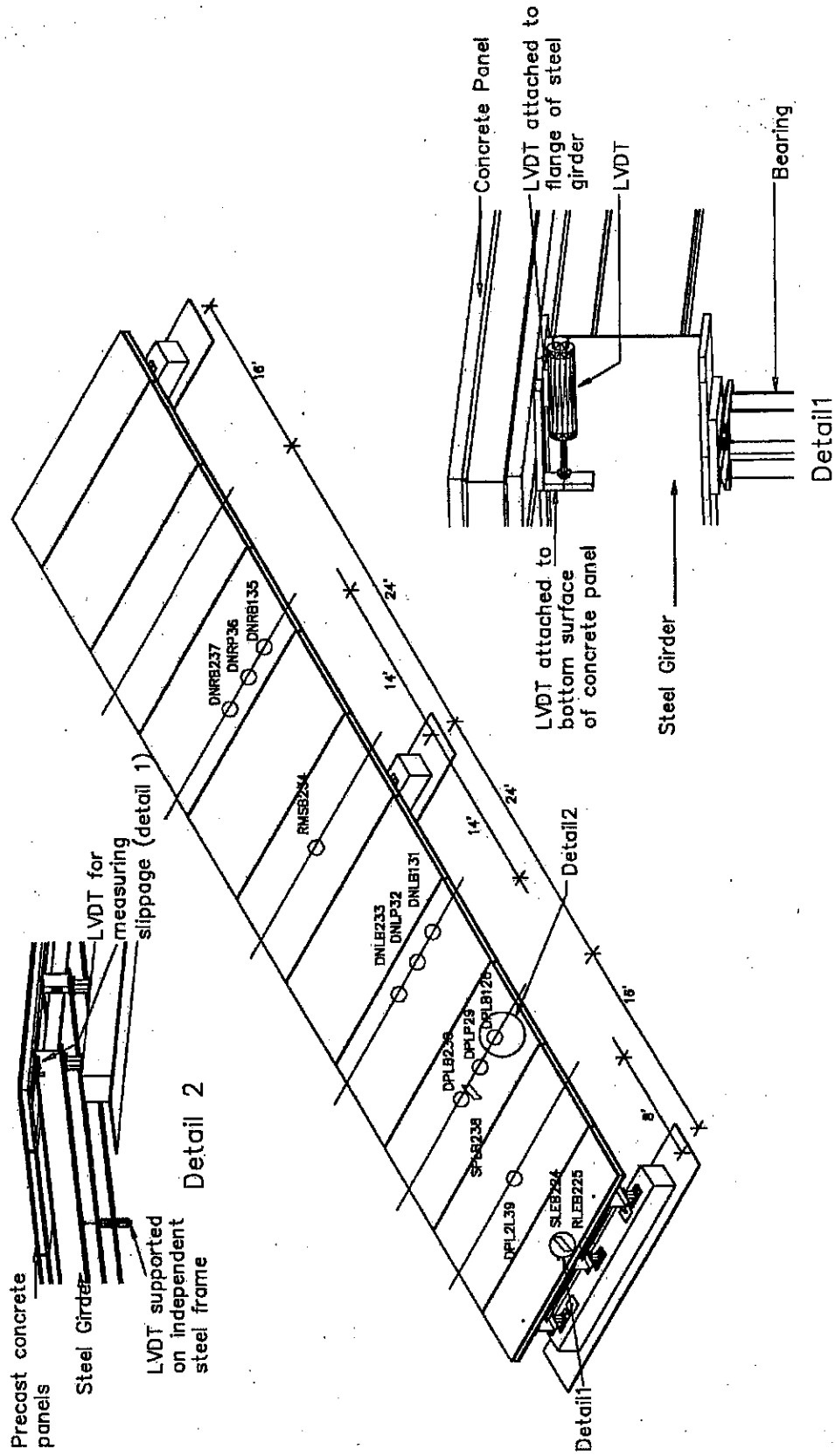


Fig. 7.3 Location of LVDTs for deflection and slippage measurement

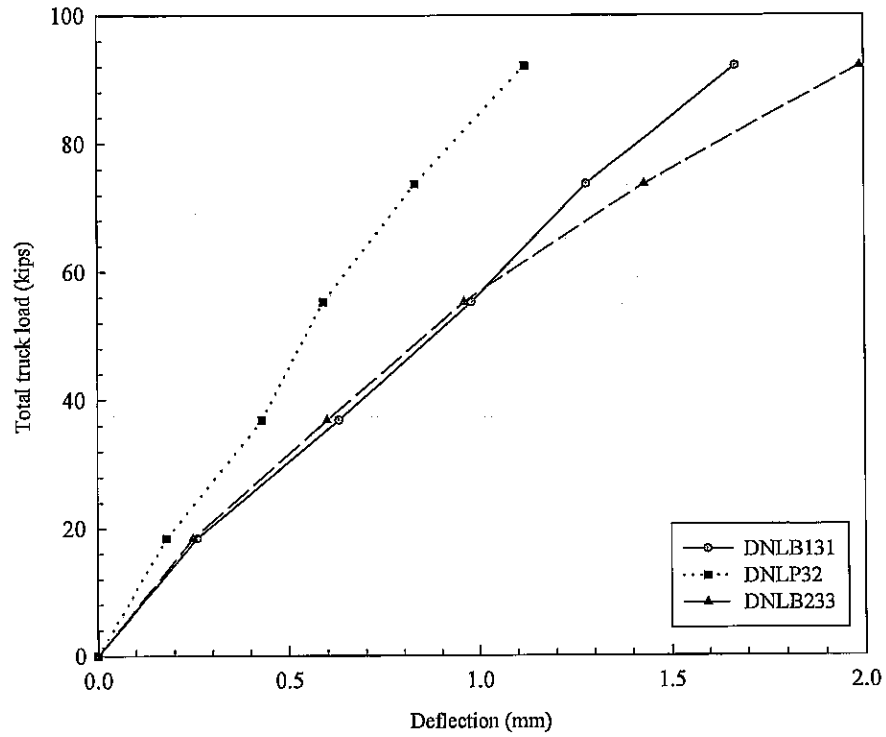


Fig. 7.4 Load-deflection response at 14 ft from middle support for service negative loading

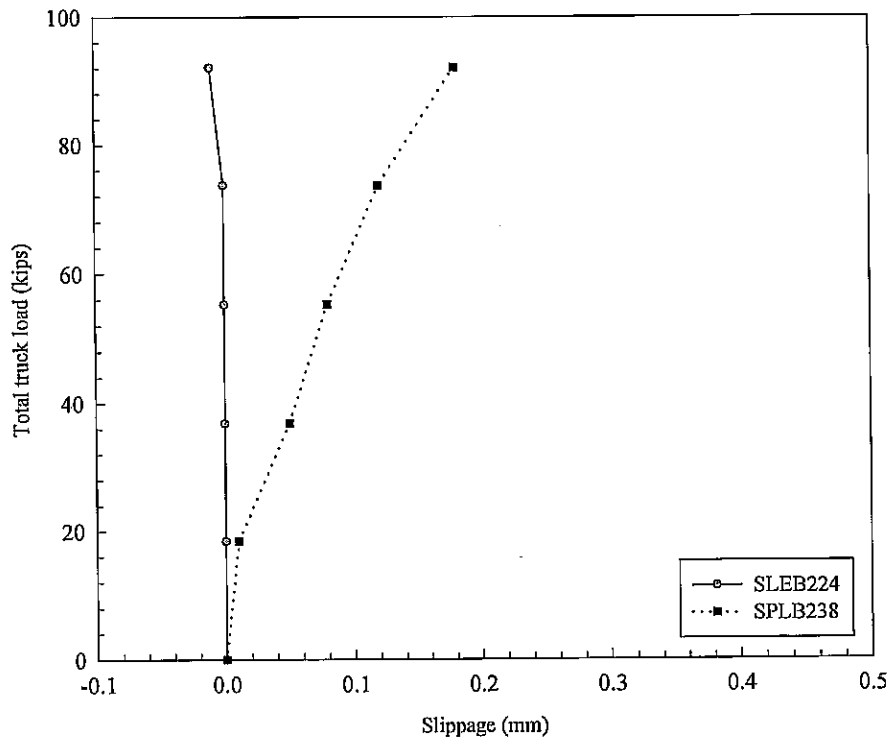


Fig. 7.5 Load-slippage response of the composite section for service negative loading

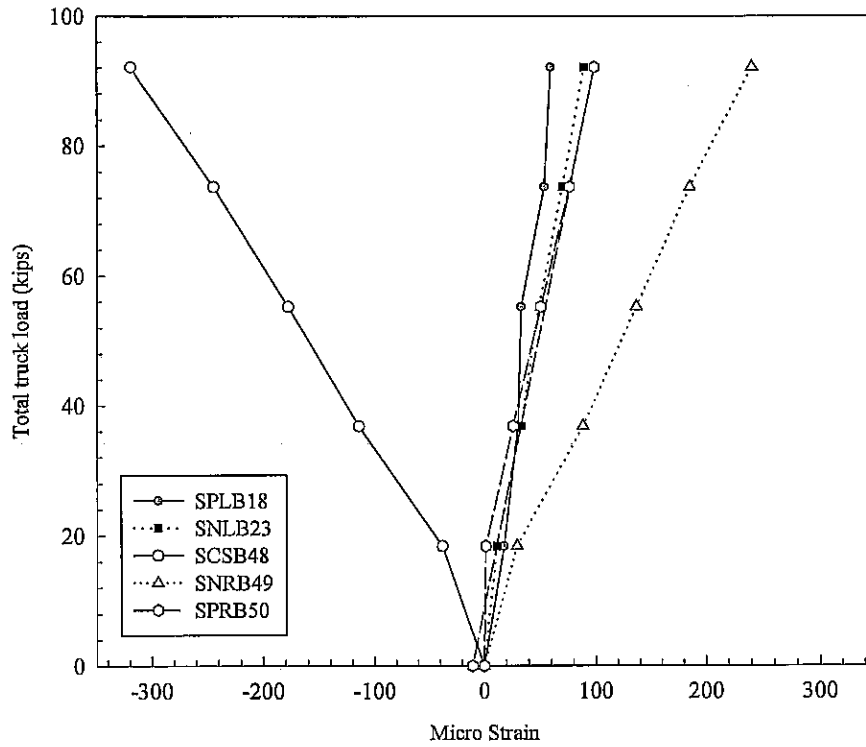


Fig. 7.6 Load-strain response of central steel beam (bottom) for service negative loading

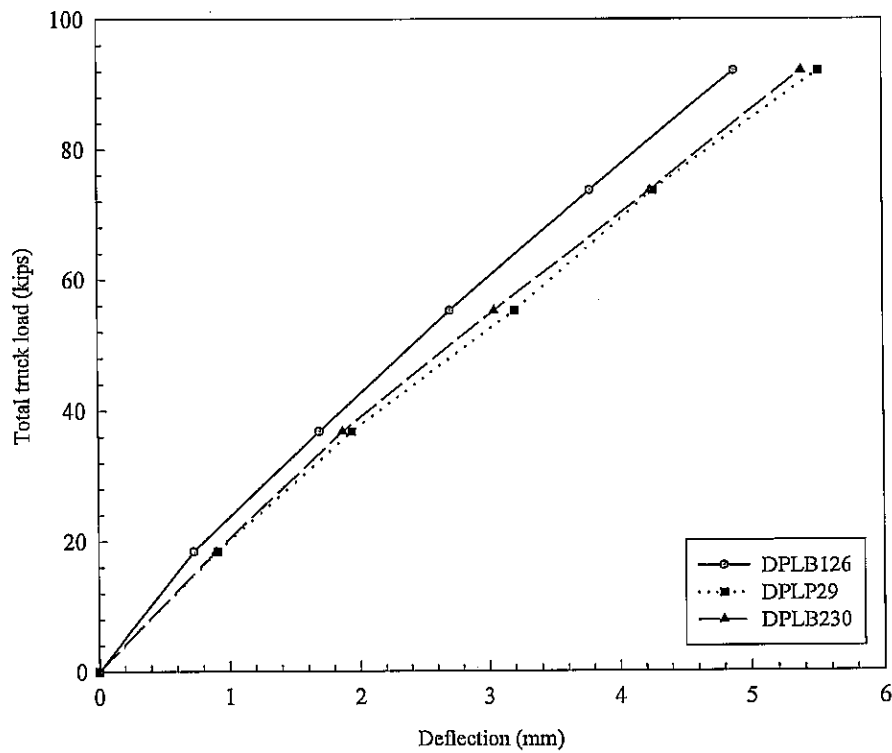


Fig. 7.7 Load-deflection response at 0.4L from left support for service positive loading

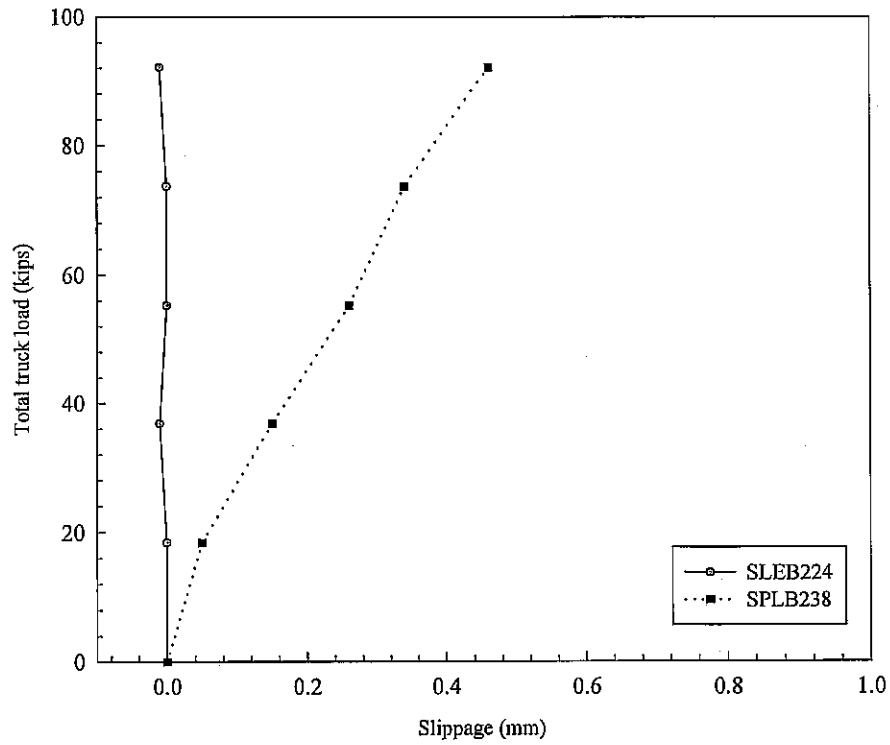


Fig. 7.8 Load-slippage response of composite section for service positive loading

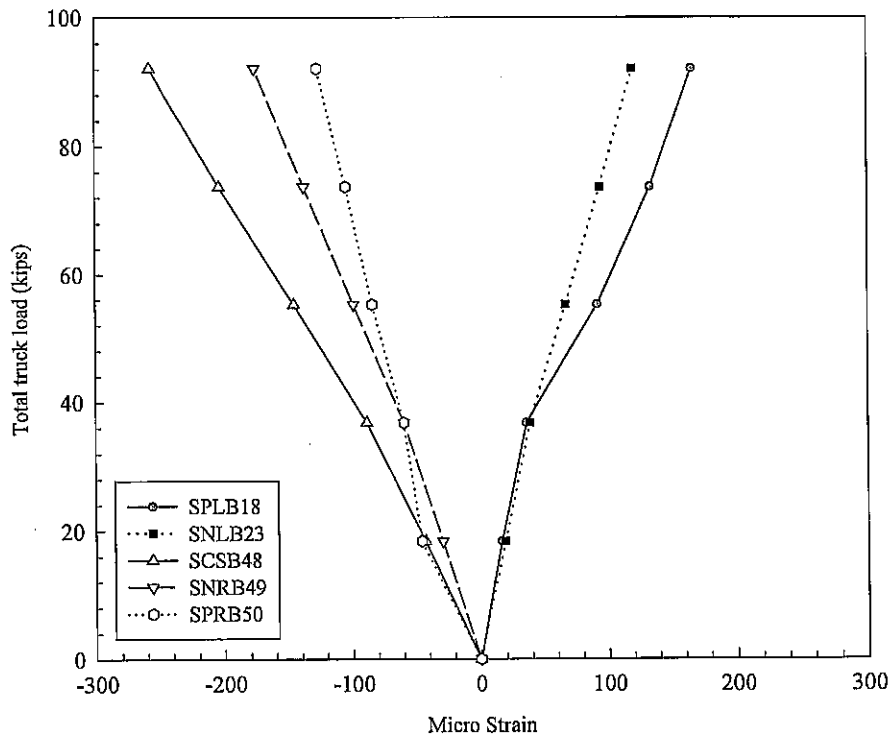


Fig. 7.9 Load-strain response of central steel beam (bottom) for service positive loading

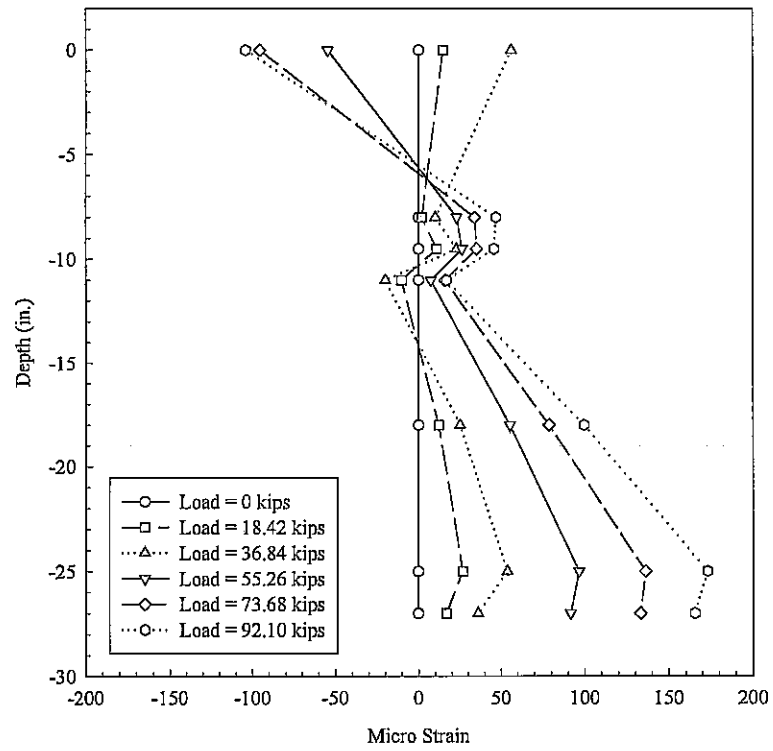


Fig. 7.10 Variation of strain along depth of composite section for positive service loading

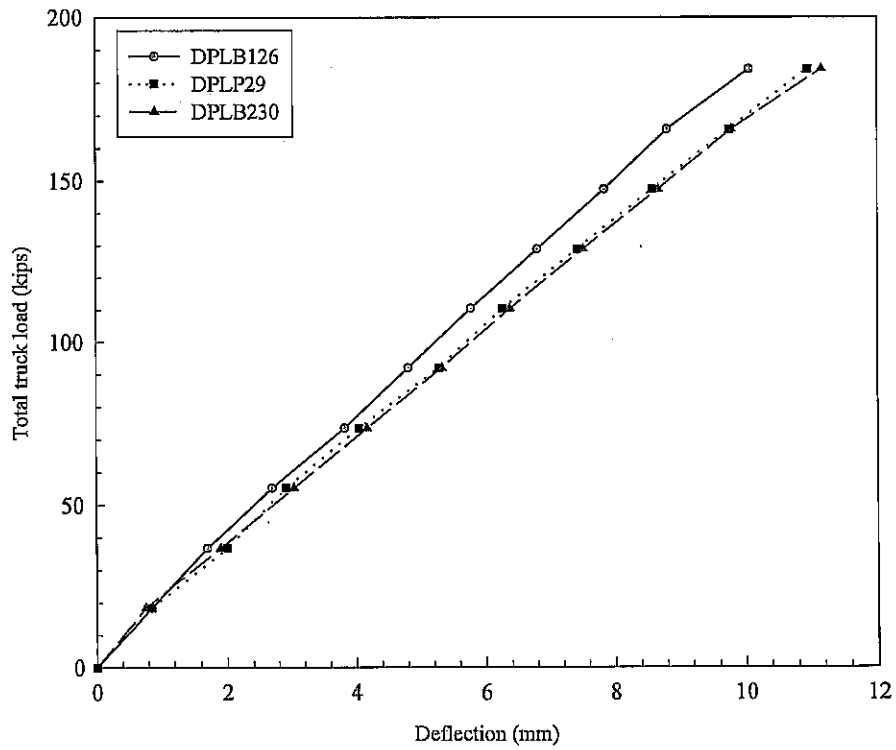


Fig. 7.11 Load-deflection response at 0.4L from left support for positive overloading

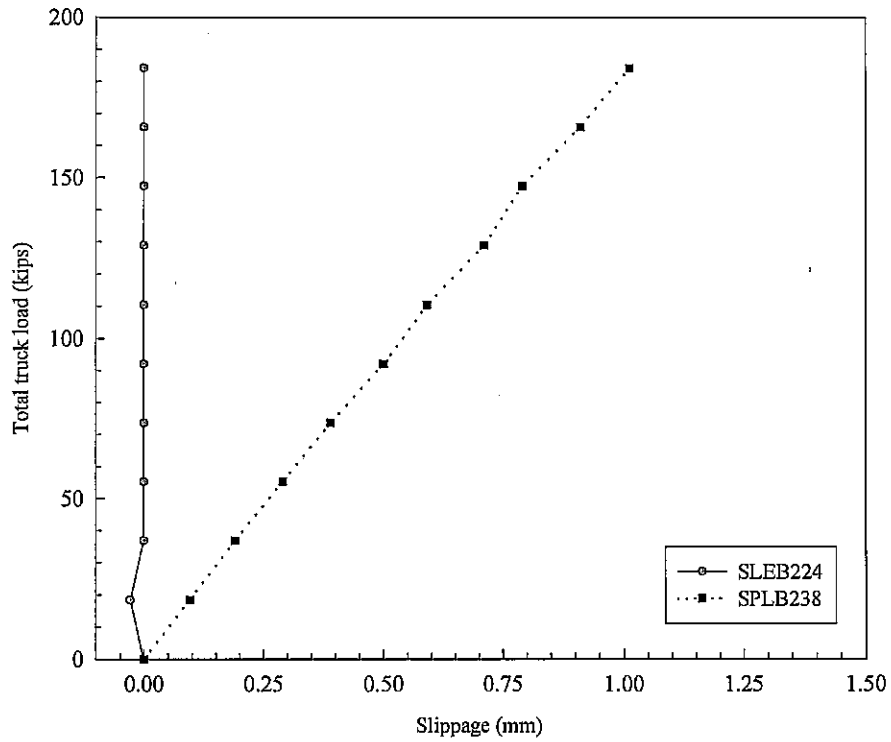


Fig. 7.12 Load-slippage response of composite section for positive overloading

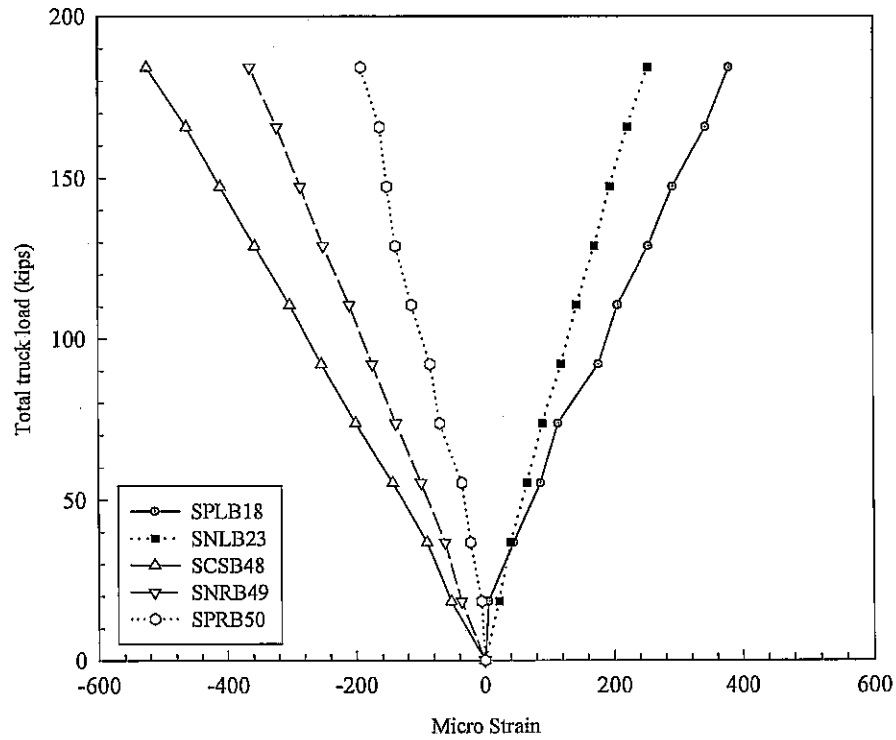


Fig. 7.13 Load-strain response of central steel beam (bottom) for positive overloading

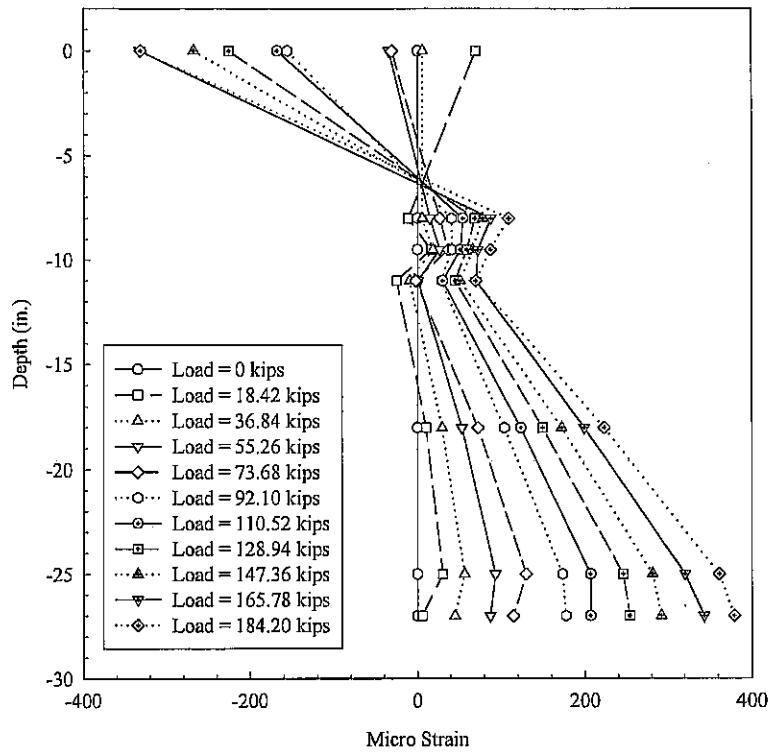


Fig. 7.14 Variation of strain along depth of composite section for positive overloading

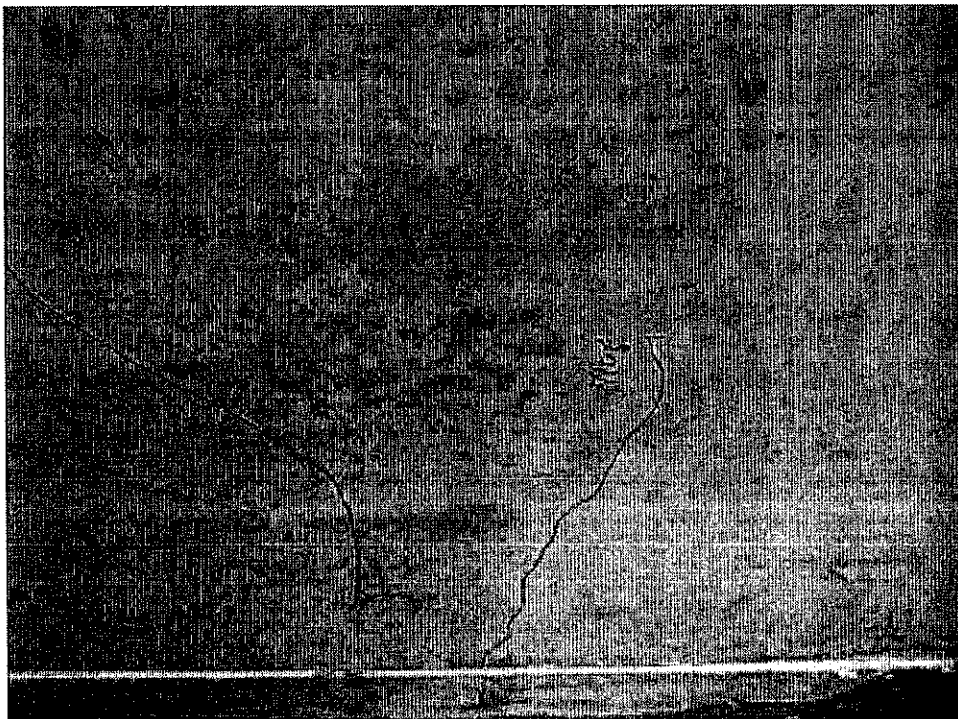


Fig. 7.15 Cracks underneath deck during positive overloading

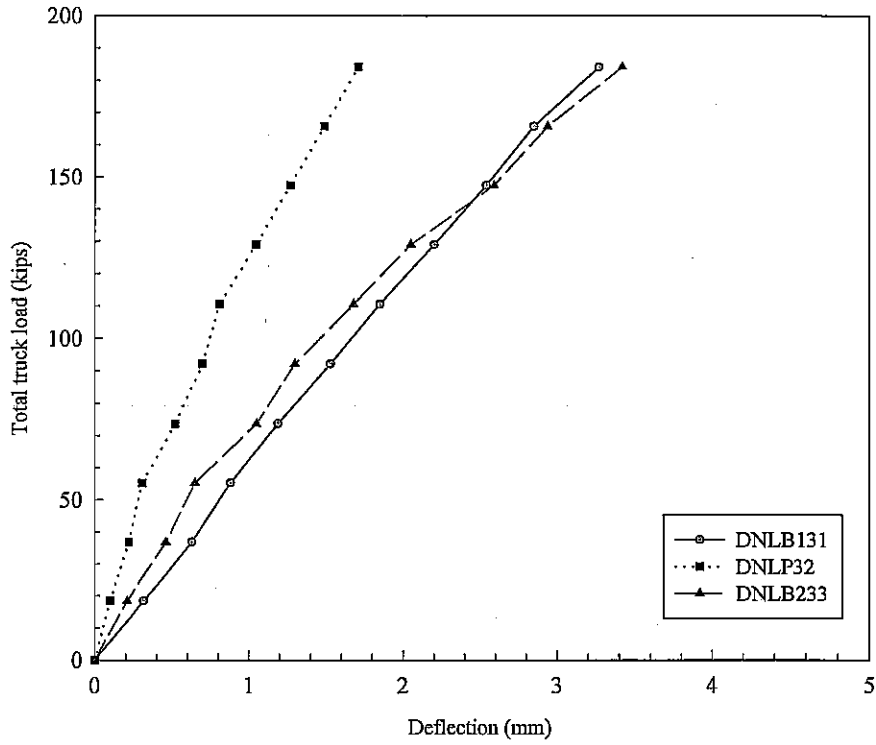


Fig. 7.16 Load-deflection response at 14 ft from middle support for negative overloading

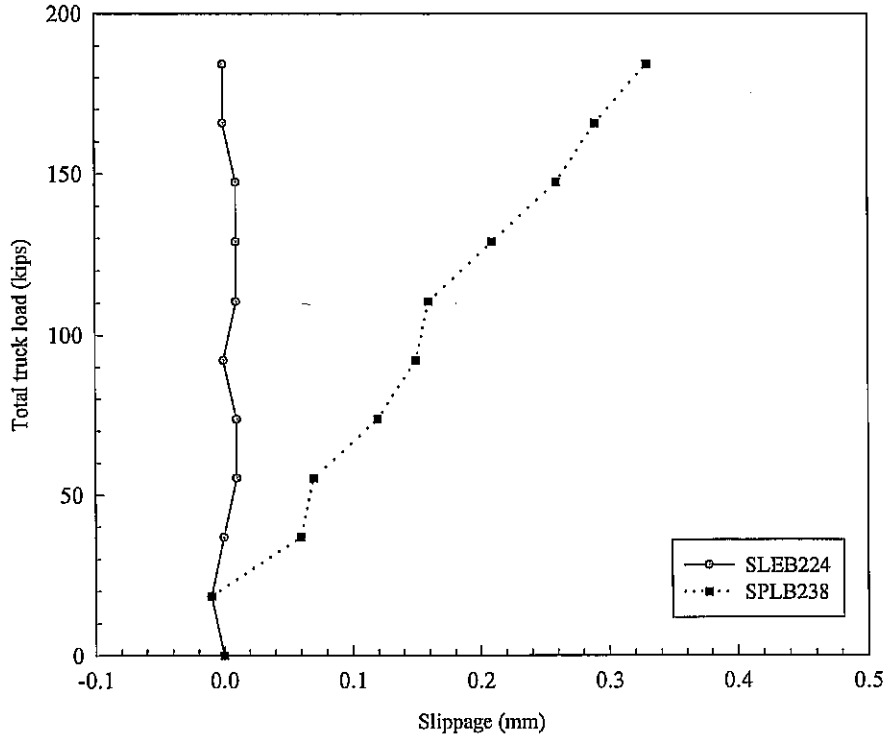


Fig. 7.17 Load-slippage response of composite section for negative overloading

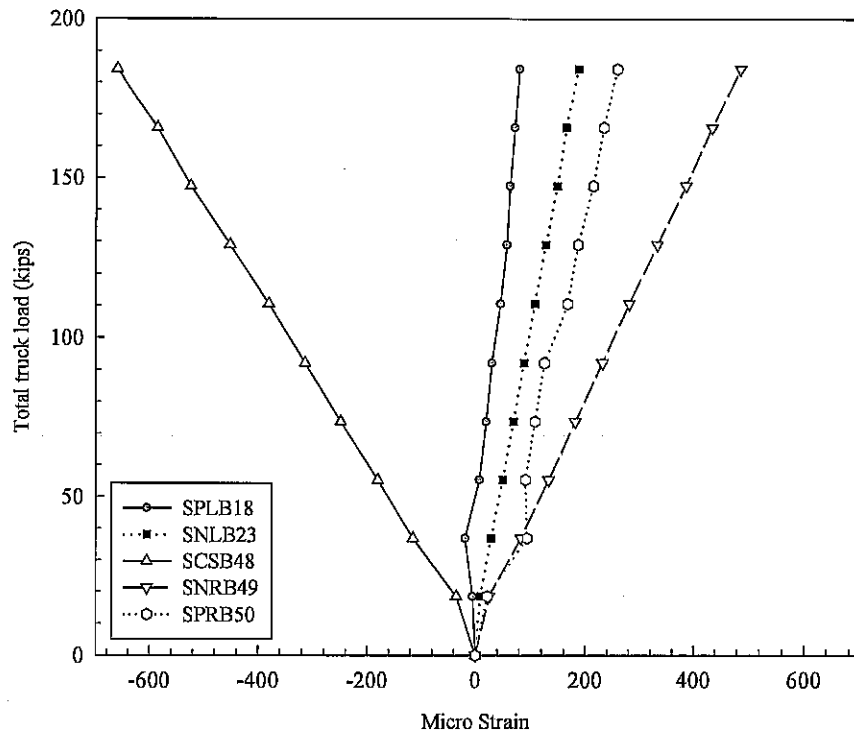


Fig. 7.18 Load-strain response of central steel beam (bottom) for negative overloading

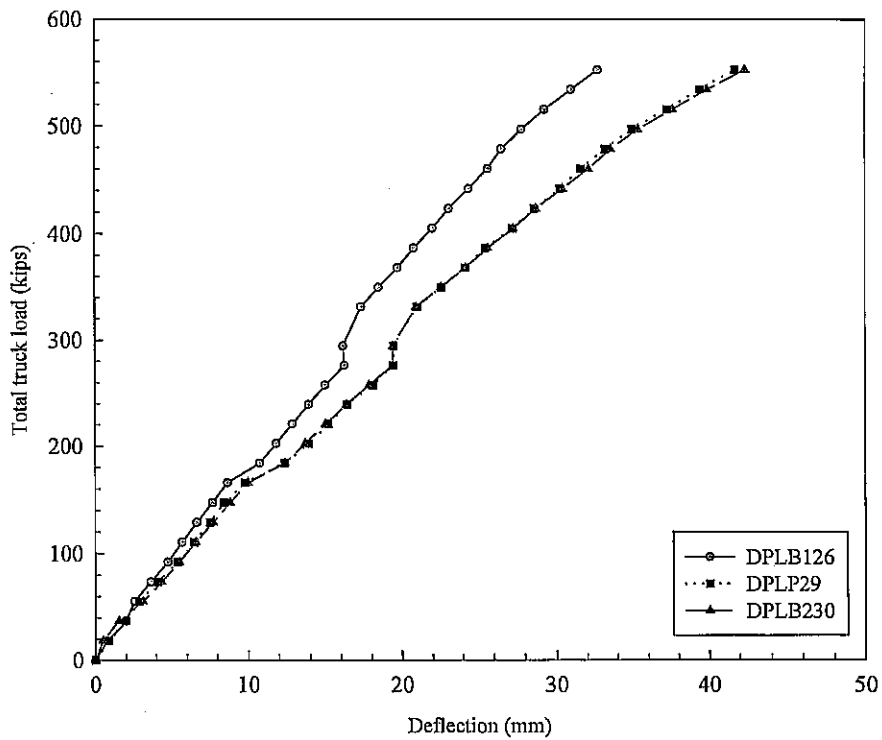


Fig. 7.19 Load-deflection response at 0.4L from left support for ultimate positive loading

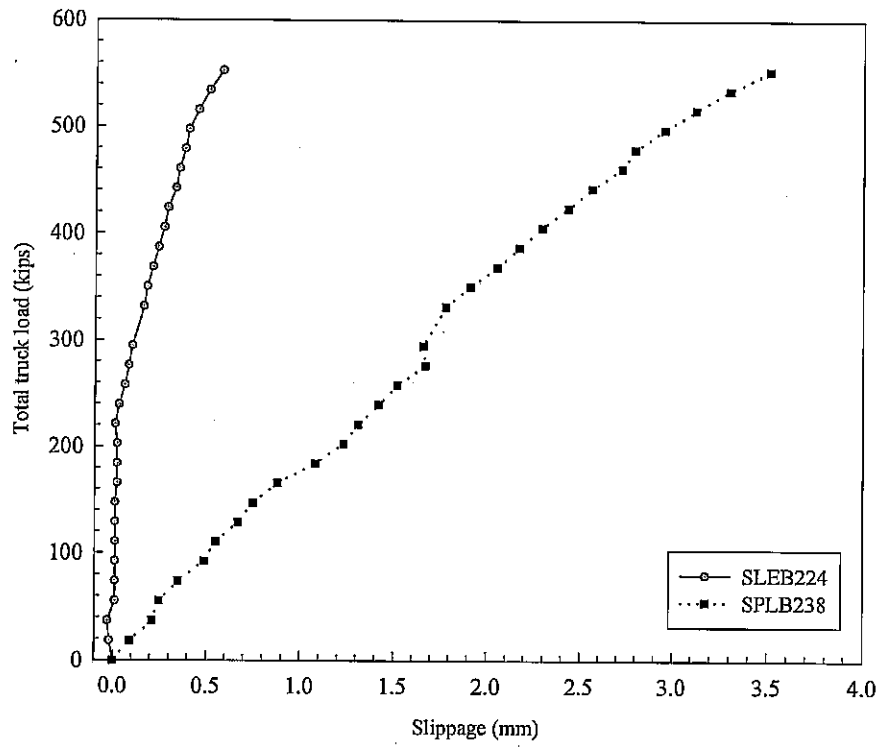


Fig. 7.20 Load-slippage response of composite section for ultimate positive loading

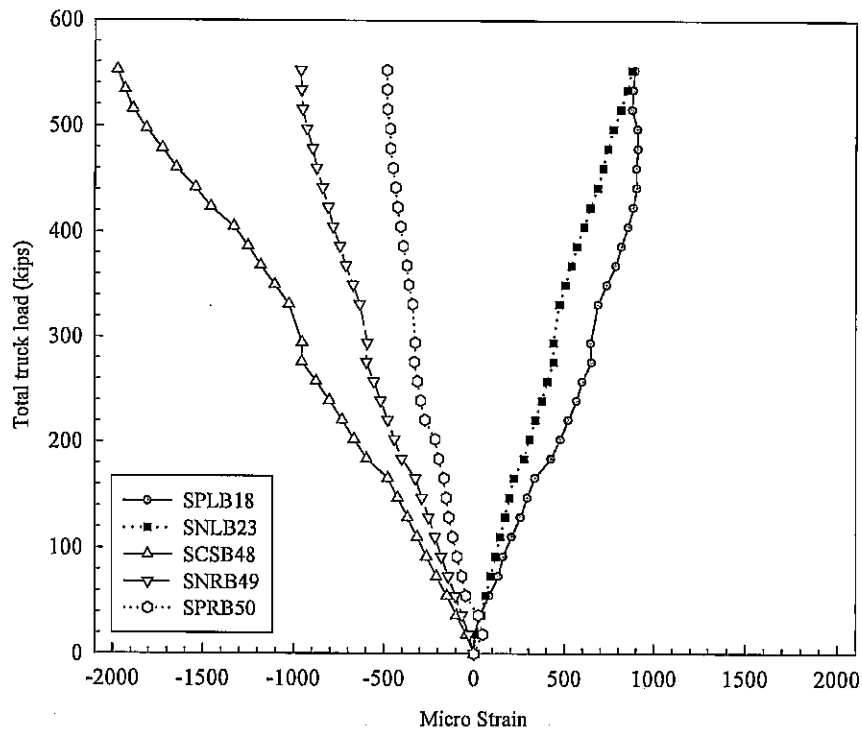


Fig. 7.21 Load-strain response of central steel beam (bottom) for ultimate positive loading

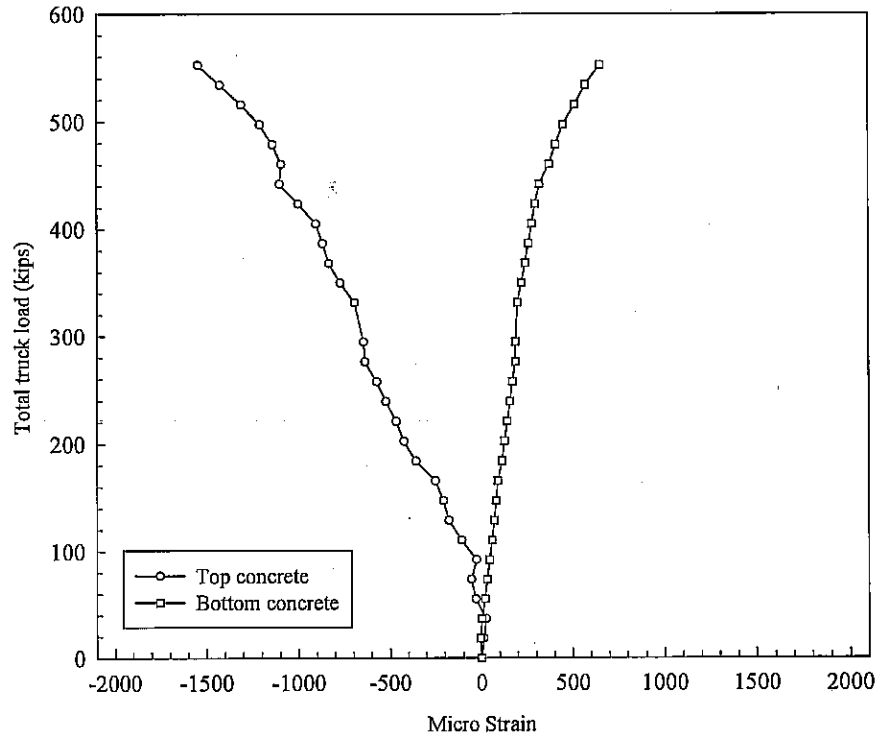


Fig. 7.22 Load-strain response of concrete at 0.4L from left support for ultimate positive loading

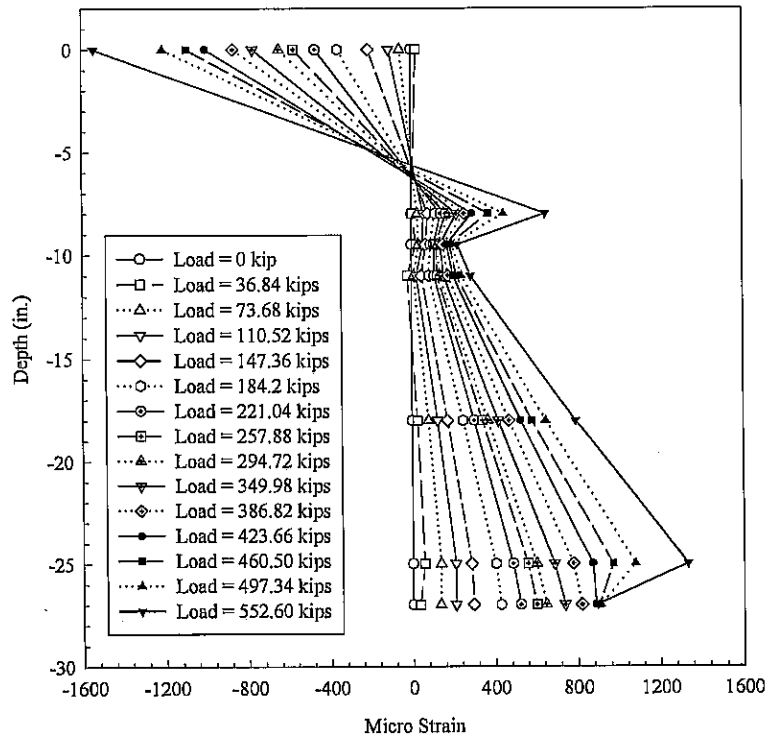


Fig. 7.23 Variation of strain along depth of composite section for ultimate positive loading

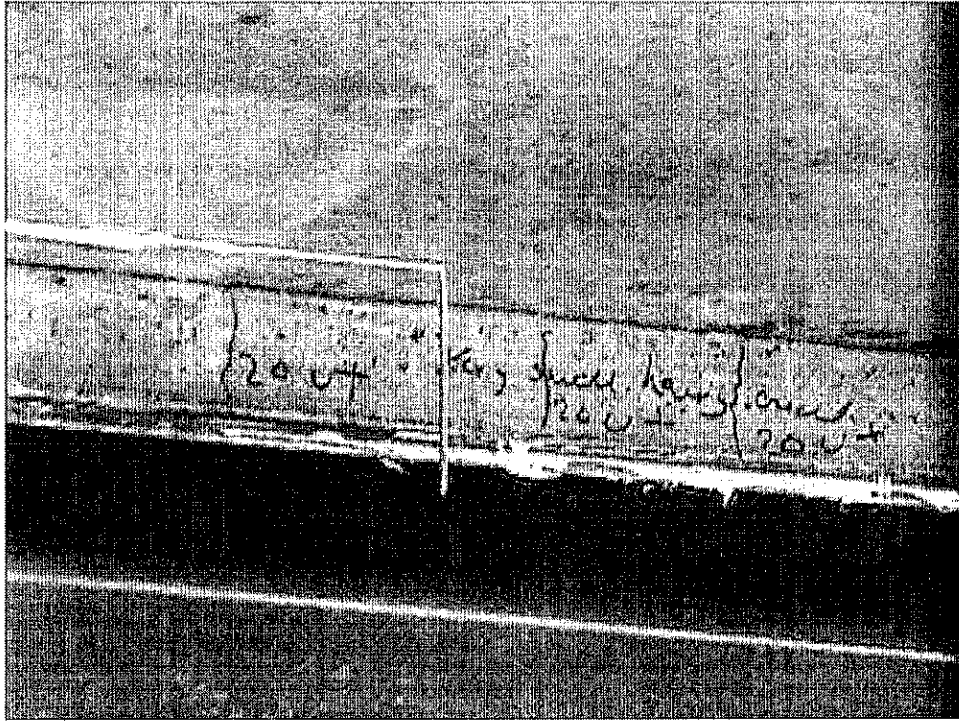


Fig. 7.24 Close-up view of hairline cracking at haunch at 386 kips load for positive bending

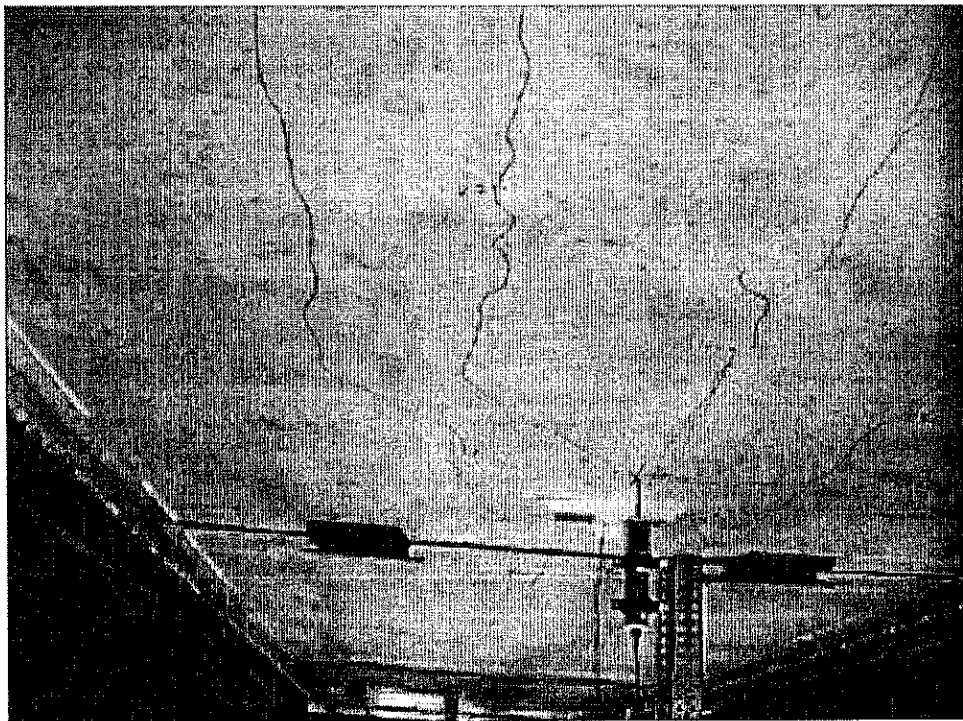


Fig. 7.25 Cracking of bottom deck at ultimate positive loading



Fig. 7.26 Uplift of steel beam due to positive bending of other span

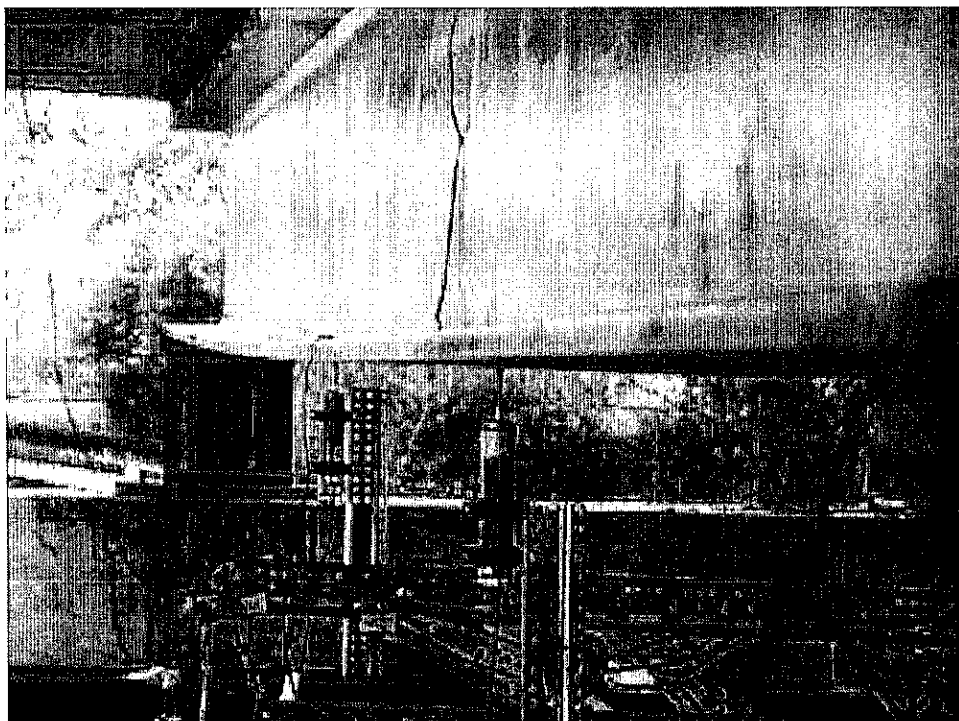


Fig. 7.27 Close-up view of steel beam deflection for ultimate positive bending

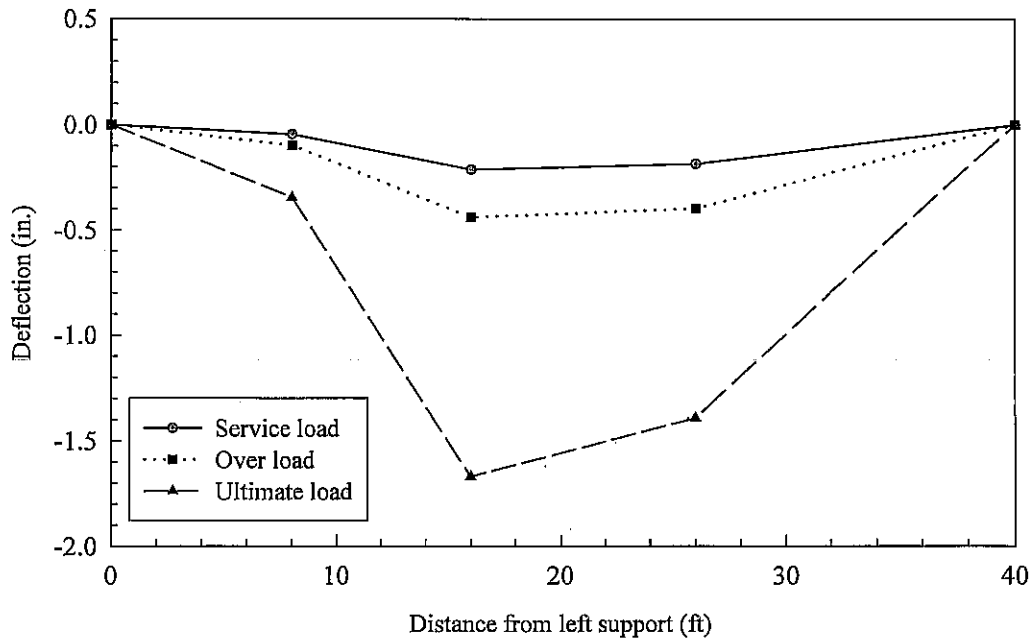


Fig. 7.28 Comparison of deflections for positive loading at different load levels

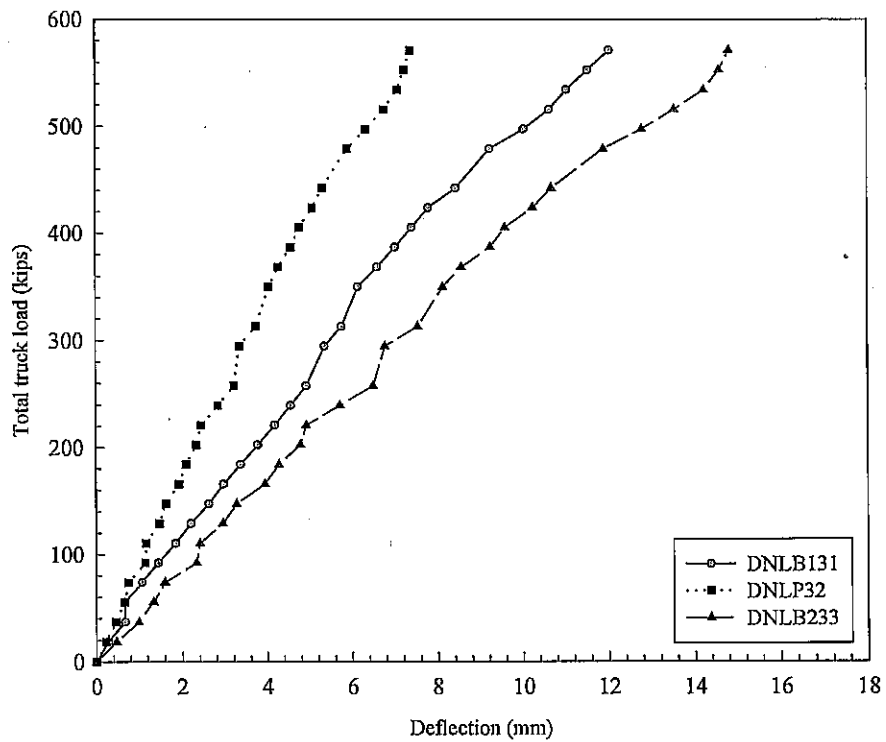


Fig. 7.29 Load-deflection response at 14 ft from middle support for ultimate negative loading

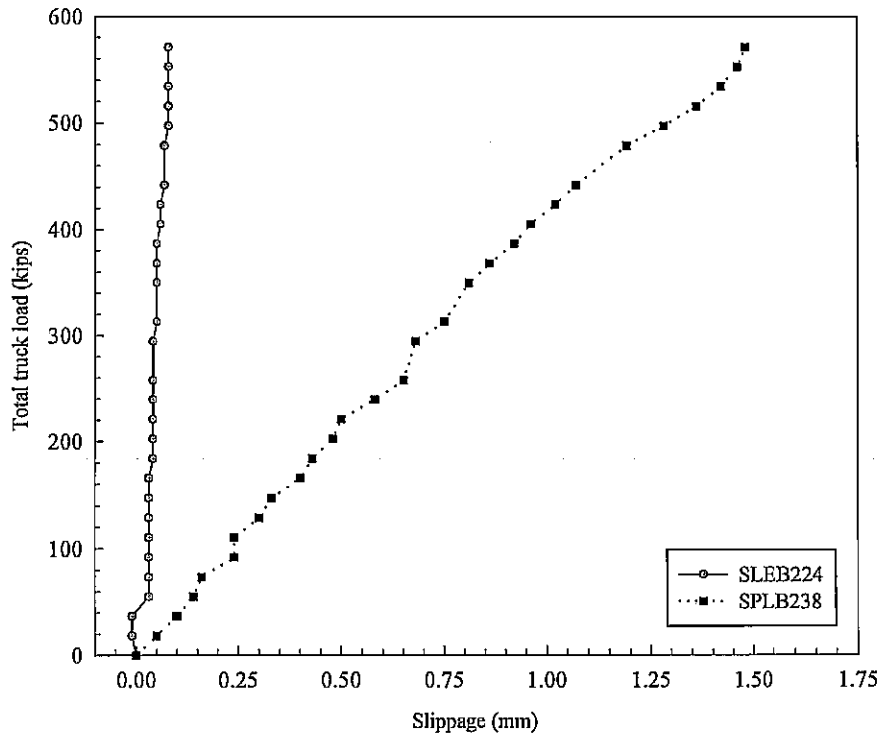


Fig. 7.30 Load-slippage response of composite section for ultimate negative loading

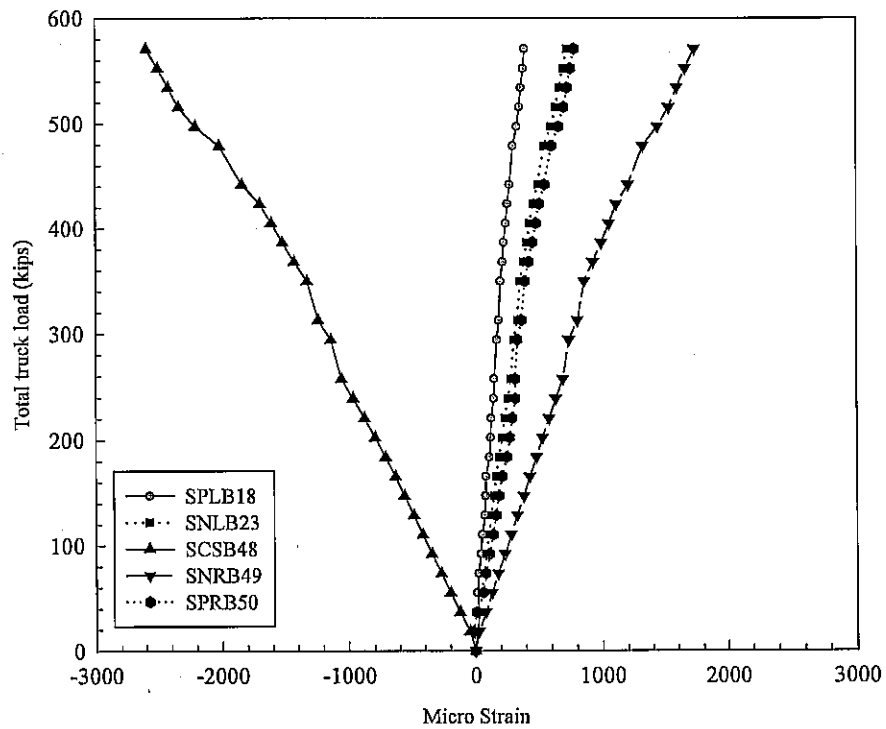


Fig. 7.31 Load-strain response of central steel beam (bottom) for ultimate negative loading

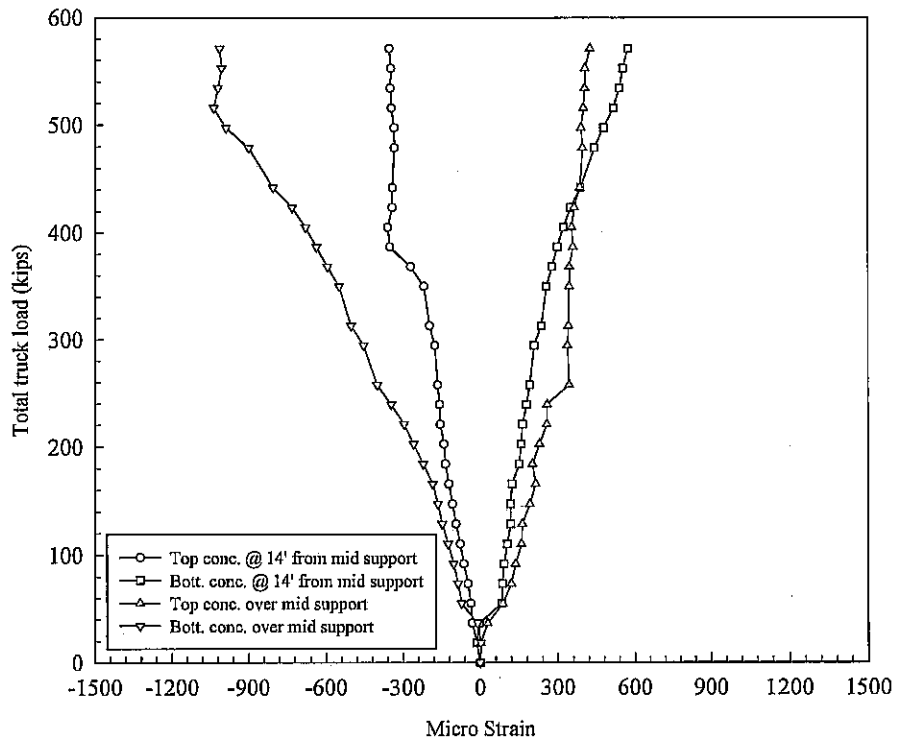


Fig. 7.32 Load-strain response of concrete at critical locations for ultimate negative loading

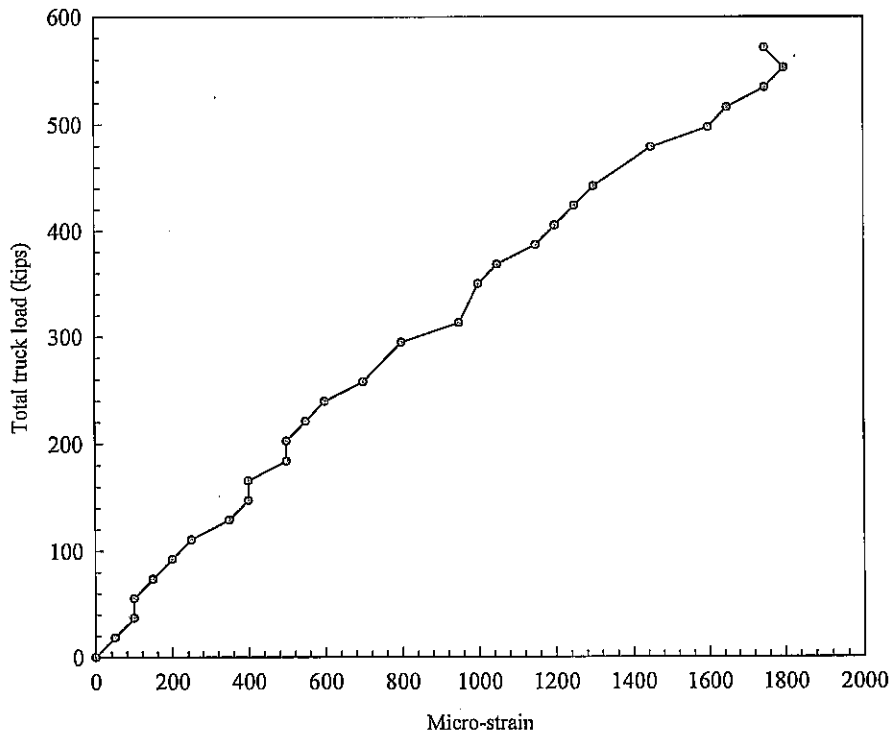


Fig. 7.33 Opening of transverse joint near central support during ultimate negative loading

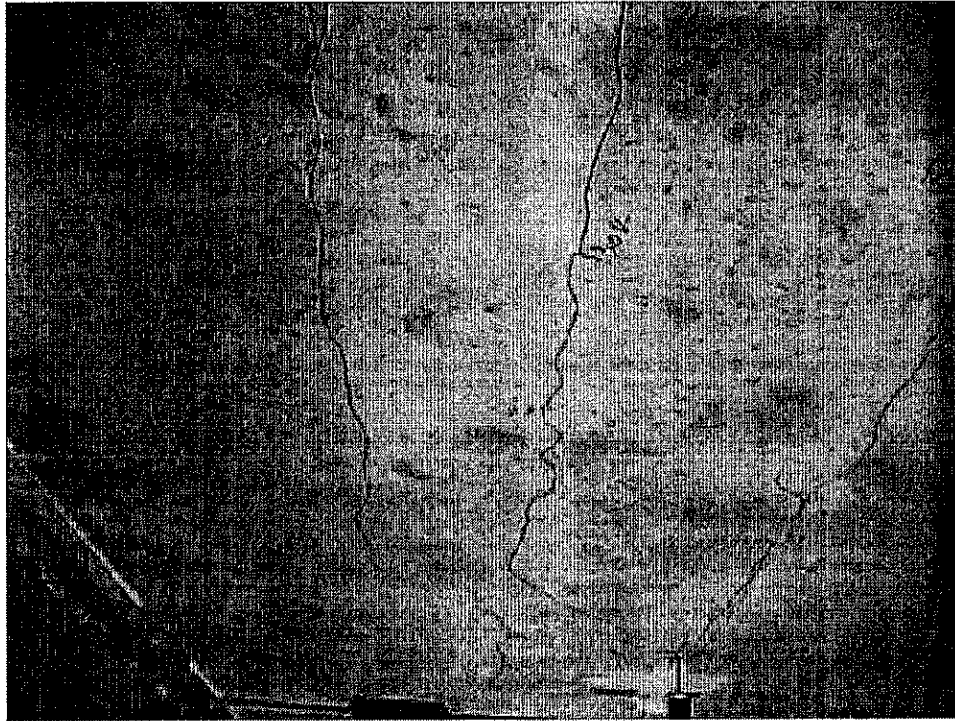


Fig. 7.34 Cracks at bottom of deck at 14 ft from central support at load of 552 kips during negative bending



Fig. 7.35 Measuring of crack width after ultimate negative loading



## 8. SPECIFICATIONS FOR PRECAST CONCRETE BRIDGE DECK PANELS

### 8.1 Introduction

The proposed system provides a very effective and economic design concept, and can be implemented for the rehabilitation of existing highway bridges as well as new bridge construction in order to shorten the time of reconstruction and bridge closures, and to minimize interference with traffic flow. This system combines high strength tendons and good quality concrete to produce durable deck panels that are effective in aggressive environments. The panels are connected to the steel stringers through shear pockets to provide composite action. The deck panels can either be precast or precast prestressed, and post-tensioned in the longitudinal direction to provide continuity and secure tightness in the joints between adjacent precast elements. In this type of construction, the entire bridge deck is of precast concrete to enable the rapid replacement of deteriorated decks, and render the rehabilitation process extremely cost effective. There is no additional field cast-in-place concrete acting structurally, except that used in the connections and slab closures.

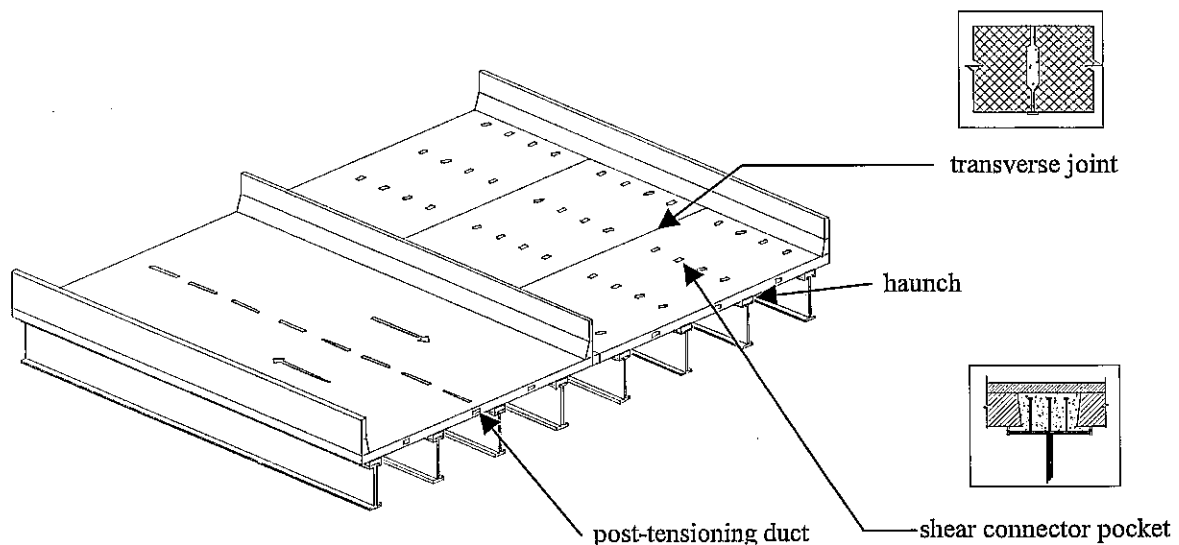


Fig. 8.1 Typical Layout of Precast Slab on Steel Stringers

The following are comprehensive specifications pertaining to the system:

1. Precast concrete bridge deck panels may be used for replacement of existing deck slabs or for new construction. Fig. 8.1 presents a layout of the precast deck on steel stringers. The supporting system may also be precast or precast prestressed concrete girders.
2. The panels may be designed for transverse flexure (main reinforcement perpendicular to traffic) with mild reinforcement, prestressing strands, bonded post-tensioning strands, or combination of each.
3. Depending on the width of the precast panels, the panels must have a sufficient amount of transverse prestress to avoid cracking during handling and erection of the slab units.
4. Leveling bolts should be used to adjust the grade of the precast slab units during placement. Each bolt should be torqued to insure that there is approximately equal bearing on each leveling bolt providing proper dead load distribution to each girder. There should be a minimum of two leveling bolts over each girder. Fig. 8.2 presents the leveling device.

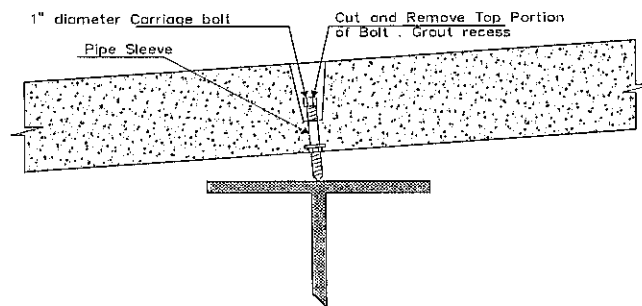


Fig. 8.2 Leveling Device

5. The transverse joints between the precast panels should be of female to female type and have a nominal width of  $1\frac{1}{4}$  inch at the top and  $\frac{1}{2}$  inch at the bottom as shown in Fig. 8.3. The width of this joint may be adjusted in the field by  $\pm\frac{1}{4}$  inch to account for casting tolerances. Any minor dimensional growth can be accounted for in the closure pours at the ends of the spans. The opening shall be enlarged through the entire depth of the panel as shown in Fig. 8.3 to allow for securing the ducts once the strands are run through. The ducts shall be wrapped with duct tape to secure the duct.

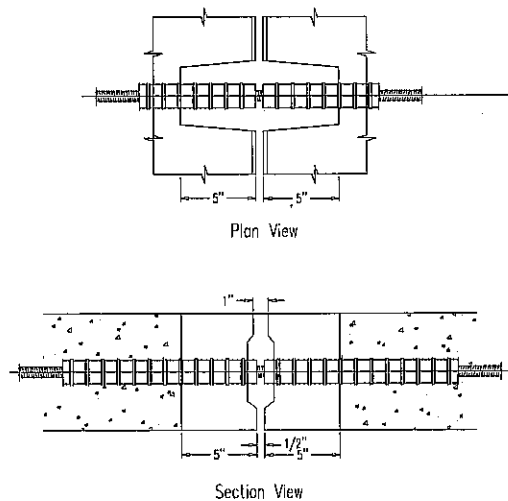


Fig. 8.3 Typical Transverse Joint

6. A minimum 1 inch haunch shall be provided between the precast panels and the steel stringers to allow for any misalignment or irregularity. Forming for the haunch shall be made at the bottom of the panel so that grout can flow through the depth of the deck.
7. The mix design for precast/prestressed panels permits a wide latitude in the use of aggregate and cement. The coarse aggregate gradations permitted are CA-7, CA-11, and

CA-14 or CA-7 and CA-16. The 28-day compressive strength of the concrete element must be 34.5 MPa (5,000 psi) minimum. The units can be shipped and used if their compressive strength has attained 30 MPa (4,500 psi) after 4 days. The amount of cement in the mix design can range from 335 to 418 kg/m<sup>3</sup> (565 to 705 lbs/yd<sup>3</sup>). The maximum water-to-cement ratio is 0.4. The air content of the concrete mix must be within 5 % to 8% total air. Typical slumps are between 2.5 and 7.5 cm (1 to 3 in.) with water-reducing admixtures permissible at the discretion of the engineer or designated representative. Set retarding admixtures are also permissible for use when concrete temperatures are 20°C (68°F) or higher.

8. The grout used within the transverse joints should be high early strength polymer grout to allow for post-tensioning of the precast slab units approximately one hour later. The process of applying the polymer concrete consists of priming concrete surfaces and furnishing, mixing, and placing polymer concrete for closure of transverse roadway joints between precast deck panels. Alternatively, set grout can be used within the transverse joints, if the post-tensioning is not required immediately after casting.
9. The sequence of construction for the precast concrete deck panels should be such that the longitudinal post-tensioning is accomplished after the transverse joints between precast panels have been grouted and before the slab is made fully composite with the girders in order to avoid inducing unusual stresses in the girders.
10. The grout for the post-tensioning metal conduit shall consist of a mixture of Portland cement, water, and expansive admixture. The grout shall conform to the following requirements:
  - a. The grout mix shall have an unrestrained volumetric expansion of not less than 3 percent nor more than 8 percent.
  - b. The grout mix shall have a minimum 28 day compressive strength of 4,500 psi, when tested by methods conforming to the requirements of ASTM C-109.
  - c. The water content of the grout shall be kept as low as possible for proper grouting. However, it shall not exceed 5 gallons per sack of cement.

Chlorides, fluorides, sulfates, and nitrates shall not be used. The water shall be potable. Portland cement for the grout shall be Type I or Type II cement. Non-shrink grout for the girder haunches and shear connector blockouts shall have a one hour compressive strength of 500 psi.

11. The grout shall be applied so that all voids to be filled are completely filled. Haunches between the top of stringers and the bottom of deck panels shall be grouted through the grouting voids in sequence so that the grout shall be observed to be entering the grouting void and be at an elevation above the bottom of the next void prior to beginning grout application through the next void.
12. The fabrication and placement of the slabs shall include:
  - a. Details shall outline the method of stressing sequence, jacking force, strain due to jacking and effective force for each tendon, and give complete specifications and details of the prestressing steel and anchorage devices and other data pertaining to the post-tensioning operation.
  - b. Complete details of the method, materials, and equipment used in the grouting operation, including the manner of mixing, the equipment to be used, step by step procedure to be followed and the sequence for grouting of the conduits.
  - c. The size of the anchorage assemblies and pockets shall be detailed.
  - d. The details for splicing the post-tensioning ducts at the transverse precast slab joints.
  - e. The manner of securing the conduit and other components into place.
  - f. Type and location of lifting inserts or devices.
  - g. Details of vertical adjusting hardware.
13. Longitudinal post-tensioning should be provided for continuity between precast panels. The post-tensioning should be located at mid-depth in the slab units and shall run the entire length of the bridge or between closure pours. The post-tensioning shall transmit a prestress force of 150 psi minimum after all losses and after dead loads have been applied

to the structure. The engineer must design for additional prestress to overcome the tensile stress due to negative composite dead load moments in continuous spans. A minimum prestress force of 300 psi may be used for the continuous spans. The post-tensioning sequence is shown in Fig. 8.4.

The post-tensioning ducts shall be made continuous between precast slabs with watertight sleeves. After all slabs in a span or one post-tensioning segment of the span are set, the grade of the slabs shall be checked and adjusted to provide the required elevations. No construction equipment, or vehicles in excess of 5,000 pounds will be allowed on the precast deck slabs until the post-tensioning process is complete.

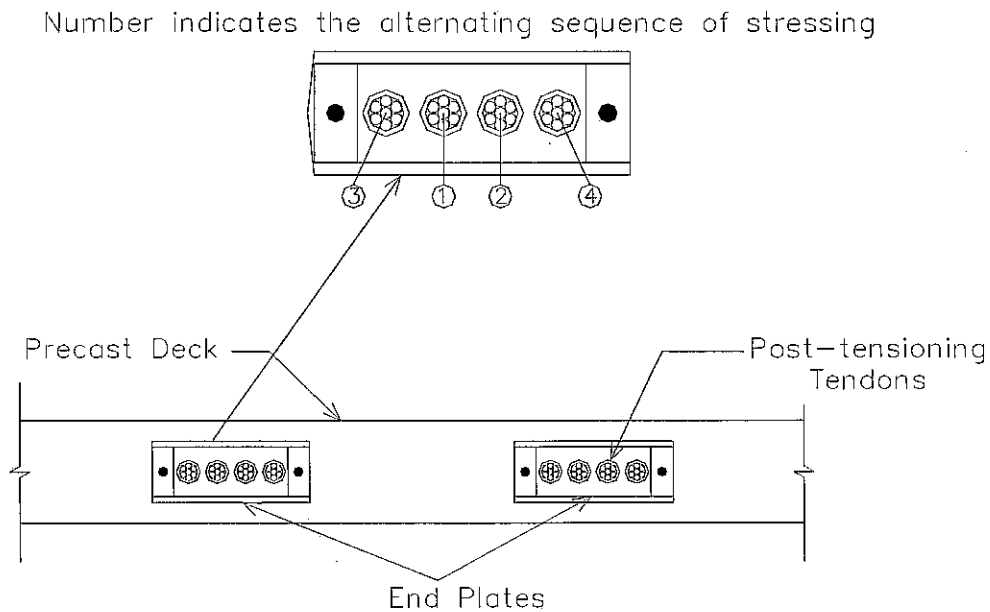


Fig. 8.4 Sequence of Post-tensioning

14. After the post-tensioning is completed, the shear studs shall be installed and the haunches formed. The shear stud blockout and formed haunch shall be grouted using non-shrink grout. The shear stud blockout details are presented in Fig. 8.5. The method for installation of the grout shall be such that no voids in the haunches and shear connector blockouts will occur. No superimposed dead loads or live loads shall be applied to the

precast slabs until the non-shrink grout in the shear stud blockouts and the haunch has been in place for two hours.

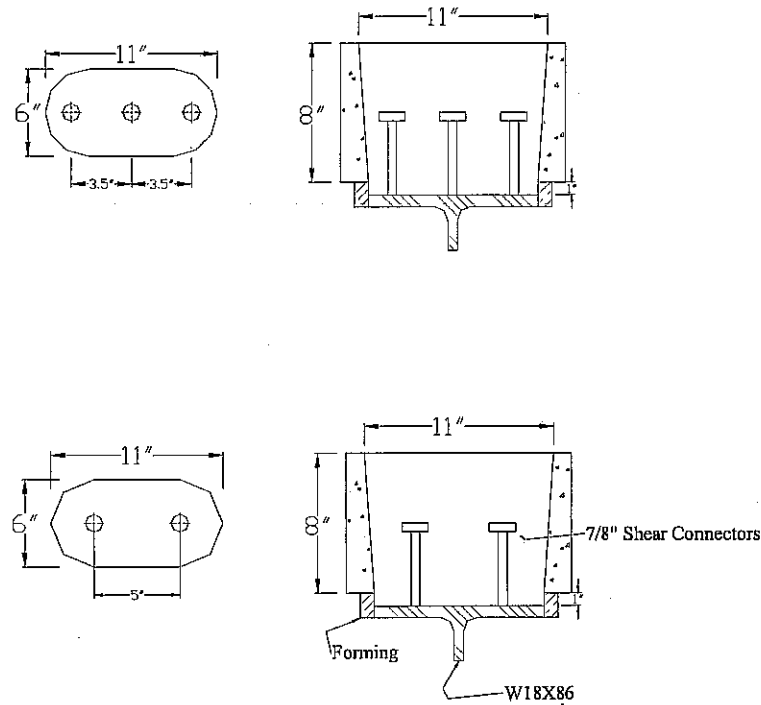


Fig. 8.5 Shear Stud Blockout Details

15. In making the slab units and the supporting system fully composite, the spacing of shear connector blockouts should be kept at two feet on center where possible. The design for variable horizontal shear can be accommodated by varying the number of shear connectors per blockout. The configuration of the shear connector blockouts should be of beveled shape to avoid any stress concentration at the corners.
  
16. The use of precast concrete panels on curved structures is also acceptable. The slab units shall be cast in a trapezoidal shape with the longitudinal post-tensioning running along the curve. The design of the longitudinal post-tensioning should take into account the losses due to friction in the post-tensioning ducts.

17. Several types of overlays are being utilized throughout the nation including the following:
  - a. Epoxy Concrete
  - b. Concrete Containing Silica Fume
  - c. Latex Modified Concrete
  - d. Class O Dense Concrete
  - e. Bituminous Wearing Surface

A waterproofing membrane system is installed followed by two layers of a bituminous wearing surface.

18. A corrosion inhibitor admixture may be incorporated into the concrete used to fabricate the precast panels, cast-in-place closure pours, concrete parapets, and the concrete used to fill the shear connector pockets in the precast slabs. The corrosion inhibitor shall be a solution of 29 to 32 percent by weight of calcium nitrite and water with a unit weight of at least 10½ pounds per gallon.

## 9. CONCLUSIONS

Laboratory investigation on the composite behavior of shear connection for bridge deck system was performed. In addition, performance of grouting materials was investigated. Conclusions pertaining to this study are reported here. The adopted construction procedures were very effective in terms of scheduling, materials, and actual work techniques. The test results were compared with the finite element analysis results.

A total of twenty-six push-out specimens were fabricated with different number of pockets and studs as well as configuration. Specimens consisted of full-scale and quarter-scale sets. These composite systems were subjected to static loading and measurements were made with respect to the load and slip. A total of thirty-six full-scale specimens were fabricated and tested for vertical shear, direct tension, and flexure. The joints were cast using four different materials; set grout, set 45 at normal temperatures, set 45 at hot weather, and polymer concrete. Observed strengths and modes of failure were compared.

The following conclusions can be drawn from the full-scale and quarter-scale shear connection studies:

1. The addition of studs did not increase the load capacity in proportion, i.e., the load carried by two studs was not double that carried by only one stud. This was also true in the case of 3 and 4 stud systems.
2. The load capacity increased almost linearly as the number of studs in each respective pocket was increased.
3. Arrangement configuration of the studs is an important factor in composite performance. The load necessary to induce slippage is affected by both the configuration and number of studs.
4. The push-out test specimens with one and two pockets are a reliable source to determine the behavior of precast concrete deck systems. Based on these results, extrapolation is possible to a greater number of pockets and ultimately to the overall behavior of the deck system.

5. The test results of quarter-scale specimens can be used to predict the ultimate shear connection capacity of full-scale specimens. In most of the cases, the observed and the predicted values were very close.

The following conclusions can be drawn from the transverse joint study:

1. Polymer concrete is the best material for transverse joints based on the tests performed in terms of strength, bond, and mode of failure.
2. The set 45 material has a better mode of failure than set grout. This conclusion is based on the observation that the failure for the set 45 occurred through the joint, while failure for the set grout occurred through both the concrete and joint.
3. Set 45 requires a more technically precise approach than set grout since procedures for mixing and preparing the surface considerably affects the performance of the set 45 material.
4. The set grout is easy to apply and has a satisfactory performance. Although the performance of set grout is inferior to that of polymer concrete, it is easier to work with and economically advantageous.

The following conclusions can be drawn from the full-scale bridge testing:

1. The overall behavior of the precast deck system was outstanding under service loads in both positive and negative bending since no cracks were detected.
2. At a maximum load of 184 kips, hairline longitudinal transverse cracks were reported in the bottom of the slab units directly under the load contact points for both positive and negative bending overload, however, no transverse joint separation and haunch-slab separation were observed.
3. During the ultimate positive load testing, longitudinal hairline cracks were observed on the bottom surface of the panels at 0.4L after reaching a load of 203 kips, however, no cracking was observed in the transverse joints and shear pockets.
4. The measured deflection was within AASHTO limits. However, the deflection was somewhat significant in observing the steel girder curvature, while the transverse joints remained free of cracking.

5. The maximum load reached due to hydraulic jack capacity was approximately 8 times the service live load (570 kips), while the deck system maintained its integrity.
6. No losses were observed in the prestressing strands.
7. Deflection of the deck and steel girders was within the allowable limits.

The full-scale testing of the bridge along with the component testing of the shear connections and transverse joints proved to be instrumental in verifying that the full-depth precast prestressed concrete bridge deck replacement and reconstruction system is ideal for bridge rehabilitation. The system proved its effectiveness in withstanding the applied loading that exceeded 8 times truck loading in addition to the maximum negative and positive moment application. Only hairline cracking was observed in the deck at the maximum loading applied. Of most significance, was the fact that full composite action was achieved between the precast panels and the steel supporting system, and the exceptional performance of the transverse joint between adjacent precast panels.



## REFERENCES

- Abendroth, R.E., "Nominal Strength of Composite Prestressed Concrete Bridge Deck Panels," *Journal of Structural Engineering*, ASCE, Vol. 121, No. 2, February 1995, pp. 307-318.
- Barker, J.M., "Research, Application, and Experience with Precast Prestressed Bridge Deck Panels," *PCI JOURNAL*, V. 20, No. 6, November-December 1975, pp. 66-85.
- Berger, R.H., "Full Depth Modular Precast Prestressed Bridge Decks," *Transportation Research Record 903, Bridges and Culverts*, Transportation Research Board, Washington, D.C., 1983, pp. 52-59.
- Biswas, M., "Precast Bridge Deck Design Systems," *PCI JOURNAL*, V. 31, No. 2, March-April 1986, pp. 40-94.
- Culmo, M.P., "Bridge Deck Rehabilitation Using Precast Concrete Slabs," Paper Number IBC-91-55, Eighth Annual International Bridge Conference, Pittsburgh, Pennsylvania, June 10-12, 1991.
- Dedic, D.J., "Push-Out and Composite Beam Tests of Shear Connectors," *Iowa State University. Thesis*, 1983.
- Fagundo, F.E., Tabatabai, H., Soongswang, K., Richardson, J.M., and Callis, E.G., "Precast Panel Composite Bridge Decks," *Concrete International*, V. 7, No. 5, May 1985, pp. 59-65.
- Farago, B., Agarwal, A.C., Brown, J., and Bassi, K.G., "Precast Concrete Deck Panels for Girder Bridges," Ministry of Transportation of Ontario, Downsview, Canada, M3M 1J8, 1993.
- Gulyas, R.J., Wirthlin, G.J., and Champa, J.T., "Evaluation of Keyway Grout Test Methods for Precast Concrete Bridges," *PCI Journal*, January-February 1995.
- Issa, M.A., Idriss, A.T., Kaspar, I.I., and Khayyat, S.Y., "Full Depth Precast and Precast, Prestressed Concrete Bridge Deck Panels," *PCI JOURNAL*, Vol. 40, No. 1, January-February 1995a, pp. 59-80.
- Issa, M.A., Yousif, A.A., and Issa, M.A., "Construction Procedures for Rapid Replacement of Deteriorated Bridge Decks," *Concrete International*, Vol. 17, No. 2, February 1995b, pp. 49-52.

- Issa, M.A., Yousif, A.A., and Issa, M.A., "Structural Behavior of Full Depth Precast Prestressed Concrete Bridge Deck Replacement," Final Report, Illinois Department of Transportation, October 1995c.
- Issa, M.A., Yousif, A.A., Issa, M.A., Kaspar, I.I., and Khayyat, S.Y., "Field Performance of Full Depth Precast Panels in Bridge Deck Reconstruction," PCI JOURNAL, Vol. 40, No. 3, May-June 1995d, pp. 82-108.
- Issa, M.A., Yousif, A.A., Issa, M.A., Kaspar, I.I., and Khayyat, S.Y., "Analysis of Full Depth Precast Concrete Bridge Deck Panels," Precast/Prestress Concrete Institute Journal, Vol. 43, No. 1, January-February 1998, pp. 74-85.
- Issa, M.A., Yousif, A.A., and Issa, M.A., "Experimental Behavior of Full-Depth Precast Concrete Panels for Bridge Rehabilitation," ACI Structural Journal, Vol. 97, No. 3, May-June 2000, pp. 397-407.
- King, D.C., Slutter, R.G., and Driscoll, G.C., "Fatigue Strength of ½-inch Diameter Stud Shear Connectors," *Highway Research Record*, No. 103, 1963, pp. 78-106.
- Kluge, R.W., and Sawyer, H.A. "Interacting Pretensioned Concrete Form Panels for Bridge Decks," PCI JOURNAL, V. 20, No. 3, May-June 1975, pp. 34-61.
- Knudsen, C.V., "Re-decking of a Bridge With Precast Concrete," Civil Engineering, American Society of Civil Engineers, New York, V. 50, No. 4, April 1980, pp. 75-77.
- Lehman, H.G., Lew, H.S., and Toprac, A.A., "Fatigue Strength of ¾ -inch Studs in Lightweight Concrete," *Center For Highway Research University of Texas*, May 1965.
- Maher, T.K., "Rapid Replacement of Bridge Decks," Final Report, 12-41, National Cooperative Highway Research Program, Transportation Research Board, July 1997.
- Mainstone, R.J. and Menzies, J.B., "Shear Connectors in Steel-Concrete Composite Beams for Bridges," Part 1: *Static and Fatigue Tests on Push-Out Specimens*. Concrete. Vol. 1, No 9, September 1967.
- Osegueda, R.A. and Noel, J.S., "Positive Moment Tests for Precast Concrete Panel-Decked Composite Bridges," Report, Research Report 324-1, Texas Transportation Institute, 1987.

- Osegueda, R.A. and Noel, J.S., "Rapid Bridge Deck Replacement: A Field Demonstration and Load Test," Final Report, Research Report 324-5F, Texas Transportation Institute, May 1988.
- PCI Committee on Bridges, "Precast Prestressed Concrete Bridge Deck Panels," PCI JOURNAL, V. 32, No. 2, March-April 1987, pp. 26-45.
- Rabbat, B.G. and Hanson, N.W., "Fatigue Tests of Bolted Connections Designed by Shear Friction," *Research and Development Bulletin*, RD064.01E, 1979.
- Salmon, C.G. and Johnson, J.E., "Steel Structures: Design and Behavior," *Harper Collins College Publishers* 1996.
- Sinclair, G.M., "Fatigue Strength of ¾-inch Welded Stud Shear Connectors," Nelson Stud Welding, Lorain, Ohio, Engineering Test Data, September 1955.
- Slavis, C., "Precast Concrete Deck Reconstruction," PCI JOURNAL, V. 28, No. 4., July-August 1983, pp. 120-135.
- Slutter, R.G. and Driscoll, G.C., "Flexural Strength of Steel-Concrete Composite Beams," *Proceedings of the American Society of Civil Engineers: Journal of the Structural Division*. April 1965, pp. 71-99.
- Toprac, A.A., "Fatigue Strength of ¾-inch Stud Shear Connectors," *Highway Research Record*, No. 103, 1965, pp. 53-77.

